

**SYNTHESIS AND IDENTIFICATION OF NOVEL ARYLNAPHTHALENE
V-ATPASE INHIBITORS AS SELECTIVE ANTI-FILOVIRAL AGENTS**

by

Aaron Lindstrom

A Dissertation

Submitted to the Faculty of Purdue University

In Partial Fulfillment of the Requirements for the degree of

Doctor of Philosophy



Department of Medicinal Chemistry and Molecular Pharmacology

West Lafayette, Indiana

December 2018

THE PURDUE UNIVERSITY GRADUATE SCHOOL
STATEMENT OF COMMITTEE APPROVAL

Dr. Vincent Jo Davisson, Chair

Department of Medicinal Chemistry and Molecular Pharmacology

Dr. Douglas J. LaCount

Department of Medicinal Chemistry and Molecular Pharmacology

Dr. Tony R. Hazbun

Department of Medicinal Chemistry and Molecular Pharmacology

Dr. Zhao-Qing Luo

Department of Biological Sciences

Dr. Mingji Dai

Department of Chemistry

Approved by:

Dr. Zhong-Yin Zhang

Head of the Graduate Program

*To my family who have provided the immense support that allowed me to complete this project,
especially my parents who have always provided the resources to reach for my dreams*

ACKNOWLEDGMENTS

This work required an immense amount of personal investment but would not have been possible without the aid of many people. The past five years have required a level of work that I would not have believed before undertaking this project and I am very thankful for all of those who helped to complete the project. The amazing group of graduate students, undergraduate students, post-doctoral researchers, professors, technicians, and support staff that I have had the privilege to work alongside were integral to the complete of this project.

First, I would like to thank my mentor Dr. Davisson for the countless hours of guidance that he provided over the past couple years and for providing the arena in which I could develop new skills. Dr. Davisson provided a stimulating environment that challenged me to reach beyond my envisioned limits and achieve my goals. I consider it to have been a great honor to have had a brilliant mentor. I want to acknowledge my graduate committee of Dr. Douglas LaCount, Dr. Tony Hazbun, Dr. Mingji Dai, and Dr. Zhao-Qing Luo for their invaluable guidance during the course of this project. I especially want to thank Dr. LaCount for the extensive experience that I was able to gain during my year in his lab.

I would also like to thank Dr. Susan Holladay and Dr. Animesh Aditya for their invaluable assistance in forming my teaching skills that immeasurably aided in growth as a researcher. I would like to acknowledge Dr. Matt Bartolowits, Dr. Dino Petrov, and Jonathon Gast (soon to be Dr.) for the great work environment that they provided during my time in the Davisson lab. I would also like to thank all the undergraduate students who worked directly or indirectly on this project over the past years and wish them the best of luck in their studies and careers: Ryan DiFalco, Logan Baker, Rebecca Tso, Madison McAteer, Christopher Blackwell, Andrew Kim, Kasey Martineau, Jacob Riedel, Anqi Shao, Lauren Orr, Renee Oles, Ashlee Hasler, Drew Thieme, and Rani Bendersky. I would also like to thank Dr. Sudip Khadka, Dr. Patrick Dolan, and Dr. Bikash Shakya for their help during my time in the LaCount lab.

A large number of other researchers for many disciplines assisted in the completion of this work and I would like to recognize their contributions. Dr. Manu Anantpadma in Dr. Robert Davey's lab at Boston University (formerly of the Texas Biomedical Research Institute) was instrumental in completing this work through the contribution of all ebolavirus antiviral testing. Kelsey Lubin, Monika Lavan, and Mark Joseph Schopper in Dr. Greg Knipp's lab at Purdue

University completed the formulation, stability testing, toxicity testing in mice, and pharmacokinetic testing in rats. Dr. Jason Ray Nielson in Dr. Randall Peterson's lab at the University of Utah completed the toxicity testing in zebrafish. I would also like to thank Kyle Harvey for his assistance with confocal microscopy. I would like to thank all the other graduate and undergraduate students that were not individually mentioned but were necessary for the completion of this project.

To all my family and friends who joined me in this long journey, I would like to express the deepest gratitude for accompanying me along this path. I would never have been able to complete my dreams without their assistance.

Financial support for this work was provided by the Purdue Research Foundation and Purdue University Graduate School.

“A single dream is more powerful than a thousand realities.”

- J.R.R. Tolkien

TABLE OF CONTENTS

LIST OF TABLES	x
LIST OF SCHEMES.....	xi
LIST OF FIGURES	xii
LIST OF ABBREVIATIONS.....	xiv
ABSTRACT.....	xvi
CHAPTER 1. INTRODUCTION	15
1.1 The Filoviridae family of viruses are the causative agents of severe hemorrhagic disease and death in humans.....	15
1.1.1 Filoviridae Taxonomy	15
1.1.2 Filovirus Structure	15
1.1.3 Ebolavirus Cellular Lifecycle (Fig. 1.1).....	17
1.1.4 Ebolavirus Antagonism of the Immune System allows for Increased Infection	22
1.1.5 Filovirus Pathogenesis	23
1.1.6 Filovirus Epidemiology	25
1.1.7 Therapies for EBOV	25
1.1.7.1 Vaccines.....	25
1.1.7.2 Therapeutics for EBOV infection.....	28
1.1.7.2.1 EBOV Inhibitors in Clinical Trials	28
1.1.7.2.2 EBOV Entry Inhibitors.....	30
1.1.8 Requirements of Vesicular Acidification During the Entry of Filoviruses and Other Viral Families	31
1.2 Vacuolar-ATPase is responsible for cellular endosomal acidification	33
1.2.1 V-ATPase Background.....	33
1.2.2 V-ATPase Structure.....	33
1.2.3 V-ATPase Isoforms	35
1.2.4 V-ATPase Regulation	36
1.2.5 Cellular roles of V-ATPase	37
1.2.6 V-ATPase and Disease	38
1.2.7 V-ATPase Inhibitors	39

1.2.8 Natural Products Inhibitors.....	39
1.2.9 Synthetic Inhibitors.....	43
1.2.10 Diphyllin and Related Lignans.....	46
1.3 Research Focus	47
CHAPTER 2. PHENOTYPIC PRIORITIZATION OF DIPHYLLIN DERIVATIVES THAT BLOCK FILOVIRAL CELLULAR ENTRY BY VACUOLAR (H ⁺)-ATPASE INHIBITION .	48
2.1 Abstract.....	48
2.2 Introduction.....	48
2.3 Experimental Methodology	50
2.3.1 Biological Assays	50
2.3.2 Chemistry.....	56
2.4 Results.....	72
2.5 Discussion.....	90
CHAPTER 3. SYNTHESIS AND EVALUATION OF NOVEL, HETEROCYCLIC DIPHYLLIN ETHERS <i>IN VITRO</i> AND THEIR SAFETY PROFILES <i>IN VIVO</i>	91
3.1 Abstract.....	91
3.2 Introduction.....	91
3.3 Experimental Methodology	94
3.3.1 Biological Assays	94
3.3.2 Chemistry.....	98
3.4 Results.....	113
3.5 Discussion.....	131
3.6 Conclusions.....	132
CHAPTER 4. FUTURE DIRECTIONS	133
4.1 Introduction.....	133
4.2 Structural Optimization of the Diphyllin Chemotype.....	133
4.3 Identification of the Diphyllin Binding Site	140
4.4 Novel therapeutic Targets for the use of selective V-ATPase inhibitors.....	143
APPENDIX A- ADDITIONAL DATA.....	146
aAPPENDIX B- SPECTRAL CHARACTERIZATION OF SELECT CHAPTER 2 DERIVATIVES	148

APPENDIX C- SPECTRAL CHARACTERIZATION OF SELECT CHAPTER 3

DERIVATIVES	158
LIST OF REFERENCES	187
VITA	223

LIST OF TABLES

Table 1.1. Summary of EBOV Genes and Their Functions.	16
Table 1.2 Summary of V-ATPase subunits, isoforms, and their functions within the complex. .	34
Table 2.1. SwissADME LogP and PAINS Information for Compounds in Chapter 2	75
Table 2.2. Activity of diphyllin and derivatives against EBOV infection, endosomal acidification and cytotoxicity.....	76
Table 2.3. Inhibition of endosomal acidification, Cytotoxicity and SI data for A549	82
Table 2.4. Inhibitory Activity of Derivatives against Isolated Human V-ATPase.....	84
Table 2.5. Anti-Filoviral activity of Diphyllin and Top Derivatives in HeLa and Primary Human Macrophages.	88
Table 3.1. Activity of basic alkyl phenol ethers against V-ATPase in biochemical and cell-based assays, in addition to inhibitor cytotoxicity.	112
Table 3.2. Physicochemical properties of alkyl and acetamide derivatives in Chapter 3.....	114
Table 3.3. Activity of acetamide phenol ethers against V-ATPase in biochemical and cell-based assays, in addition to inhibitor cytotoxicity.	115
Table 3.4. LD50 values 5dpf zebrafish embryos treated with inhibitors. ^a	127
Table 3.5. Formulation Stability and gastrointestinal permeability of derivatives. ^a	127

LIST OF SCHEMES

Scheme 2.1. Synthesis of Diphyllin Derivatives.	73
Scheme 3.1. Synthesis of diphyllin phenol derivatives with alkyl linkers.	112
Scheme 3.2. Synthesis of diphyllin acetamide series of derivatives.....	115
Scheme 4.1. Synthesis of novel C-ring analogs.....	134
Scheme 4.2. Synthesis of diphyllin lactam and potential alkylated derivatives.	134
Scheme 4.3. Synthesis of novel alkylated phenol derivatives.	136
Scheme 4.4. Synthesis of A- and D-ring derivatives of the diphyllin core structure.	139

LIST OF FIGURES

Figure 1.1. Cellular Lifecycle of EBOV Infection.	20
Figure 1.2. Inhibitors of EBOV infection that have entered clinical trials.	29
Figure 1.3 Identified Inhibitors of EBOV entry. Inhibitors of NPC-1 are shown in green. Protease inhibitors are shown in purple. Inhibitors of phosphatidylinositol-3-phosphate 5-kinase are shown in orange. Proposed inhibitors of EBOV GP are shown in blue. Inhibitors of calcium channels are shown in red.	32
Figure 1.4 Natural Product V-ATPase inhibitors	41
Figure 1.5 Synthetic V-ATPase inhibitors.....	44
Figure 2.1. Antiviral Screening of Ebolavirus (EBOV) infection at 12.5 μ M in HeLa cells.	73
Figure 2.2. Screening of hit compounds with HEK-293 cells for activity against endosomal acidification.....	77
Figure 2.3. Selectivity Indices (CC50/IC50) graphs of compound hits in HEK-293 cells.....	78
Figure 2.4. Diphyllin derivatives cause an increase in intracellular vesicle pH but no corresponding change in cytosolic pH.	82
Figure 2.5. Dose-response curves of the inhibition of V-ATPase mediated proton-translocation by diphyllin and derivatives.....	83
Figure 2.6. 1 μ M screening of compound hits with HEK-293 vesicles for ATPase activity.	84
Figure 2.7. Inhibition of Cellular Endosomal Acidification is not Time-Dependent in HEK-293 cells.	85
Figure 2.8. Inhibition of V-ATPase mediated acridine orange quenching is not time-dependent.	85
Figure 2.9. Stability of select compounds under assay conditions.	86
Figure 2.10. Example chromatographs from the isolation of select inhibitors from treated HEK-293 cells.	86
Figure 3.1. Selectivity Indices (CC50/IC50) graphs of compound hits in HEK-293 cells.....	117
Figure 3.2. Dose-response curves of the inhibition of V-ATPase mediated inhibition of proton translocation by diphyllin alkyl and acetamide derivatives.....	119
Figure 3.3. Stability of 1c and top acetamide derivatives in cell culture media over 48h.	123

Figure 3.4. Figure 3.4. Example chromatographs from the isolation of select inhibitors from treated HEK-293 cells.....	123
Figure 3.5. Blood chemistry mice treated with diphyllin and derivatives.....	130
Figure 4.1. Structure of diphyllin with labeled rings.....	134
Figure 4.2. Incorporation of amide bioisosteres into the linker of diphyllin ethers.....	136
Figure 4.3. Amino-termini with an increased number of basic groups.	136
Figure 4.4. Ring derivatives for the synthesis diphyllin derivatives.....	139
Figure 4.5. Molecules to be used in the determination of diphyllin's binding site.....	141
Figure 4.6. Recovery of HEK-293 cells that were treated with diphyllin, 2g/1b , and bafilomycin A1.....	144

LIST OF ABBREVIATIONS

AO-	Acridine Orange
ATP-	Adenosine Triphosphate
Baf-	Bafilomycin A1
BzATP-	2'(3')-O-(4-Benzoylbenzoyl)adenosine 5'-triphosphate triethylammonium salt
CC ₅₀ -	50% cytotoxicity concentration
DCM-	Dichloromethane
DMEM-	Dulbecco's modified eagle media
EA-	cellular endosomal acidification
EBOV-	Ebolavirus
EGTA-	Ethylene glycol-bis(β-aminoethyl ether)-N,N,N',N'-tetraacetic acid
ESI-	Electrospray ionization
EVD-	Ebolavirus disease
FBS-	Fetal bovine serum
GFP-	Green fluorescent protein
GP-	Glycoprotein
HCl-	Hydrochloric acid
HCTU-	2-(6-Chloro-1H-benzotriazole-1-yl)-1,1,3,3-tetramethylammonium hexafluorophosphate
HEPES-	4-(2-hydroxyethyl)-1-piperazineethanesulfonic acid
HEK-293-	Human embryonic kidney cell line
HeLa-	Human cervical cancer cell line
HPLC-	High Performance Liquid Chromatography
IC ₅₀ -	Half maximal inhibitory concentration
IL-	interleukin
IMDM-	Iscoe modified Dulbecco medium
L protein-	Large protein, RNA-dependent RNA polymerase
MARV-	Marburgvirus
Mda5-	Melanoma Differentiation-Associated protein 5
MeOH-	Methanol
MTT-	3-(4,5-Dimethylthiazol-2-yl)-2,5-Diphenyltetrazolium Bromide

NLys- tert-butyl (4-aminobutyl)carbamate
NP- Nucleoprotein
NPC1- Niemann-Pick C1 protein
PBS- Phosphate-buffered saline
PHM- Primary human macrophage
P_i- Phosphate ions
RIG-1- Retinoic acid-inducible gene I
RNA- Ribonucleic acid
RNP- Ribonucleoprotein complex
sGP- soluble Glycoprotein
ssGP- short, soluble Glycoprotein
STAT1- Signal transducer and activator of transcription 1
TAM- Tyro3 protein kinase
TFA- Trifluoroacetic acid
THF- Tetrahydrofuran
TIM- T-cell immunoglobulin mucin domain
TLC- Thin layer chromatography
TNF α - Tumor necrosis factor alpha
V-ATPase- Vacuolar (H⁺)-ATPase
VLP- virus-like particle
VP24- Viral protein 24
VP30- Viral protein 30
VP35- Viral protein 35
VP40- Viral protein 40

ABSTRACT

Author: Lindstrom, Aaron, R. Ph.D.

Institution: Purdue University

Degree Received: December 2018

Title: Synthesis and Identification of Novel Arylnaphthalene V-ATPase Inhibitors as Selective Anti-Filoviral Agents

Committee Chair: Vincent Jo Davisson

Ebolavirus, a genus of filoviruses, are responsible for outbreaks that cause up to 90% fatality, including the recent outbreak in West Africa that has resulted in over 28,603 reported cases and 11,301 deaths according to the WHO. Inhibitors of vacuolar-ATPase (V-ATPase), a key protein complex that is responsible for endosomal acidification and represents a unique method to block this common viral pathway. V-ATPase inhibitors have previously been explored as therapies for many diseases but have failed due to high toxicity. Diphyllin is a natural, arynaphthalene lignan that represents a novel structural class of V-ATPase inhibitors with a greater selectivity index than previous V-ATPase inhibitors. Diphyllin has shown promising anti-tumor and anti-osteoclast activity, as well as strong anti-viral activity against Influenza and Dengue viruses.

Herein, novel modifications of the lactone and phenol functional groups of diphyllin were explored for the ability to enhance the potency or therapeutic selectivity of the diphyllin core. Four initial sets of derivatives were synthesized and assayed for activity against ebolavirus infection, inhibition of cellular endosomal acidification, cytotoxicity and biochemical inhibition of isolated V-ATPase. Modification of diphyllin's lactone functional group reduced both activity and selectivity, while alkylation of the phenol groups significantly enhanced activity. The incorporation of basic heterocycles to the alkyl group created an alkylamino series of derivatives that exhibited significantly improved therapeutic selectivity compared to diphyllin. Further investigation of the alkylamino class indicated that they retained activity against Marburgvirus infection, a filovirus related to Ebolavirus. Alkylamino derivatives inhibited ebolavirus infection of human macrophages at low micromolar levels with no apparent cytotoxicity.

Further investigation of the alkylamino class of diphyllin derivatives was conducted to determine if potency and/or therapeutic selectivity could be optimized. The addition of a 1-methylpiperazine moiety to the end of the alkyl chain improved potency 1260-fold over diphyllin, though therapeutic selectivity was not improved. The modification of the alkylamino linker to an

acetamide eliminated cytotoxicity but decreased derivative activity against V-ATPase activity. To evaluate if the cytotoxicity evidenced by the alkylamino derivatives was evidenced in organisms, the derivative toxicity was assessed in zebrafish and mouse models. Derivatives displayed toxicity in a zebrafish developmental model but were all at least 10-fold less toxic than the known V-ATPase inhibitor bafilomycin A1. Three derivatives were well tolerated in CD-1 mice when administered at therapeutically relevant concentrations and caused no abnormal changes in their blood chemistry. Overall, these results demonstrate that the alkylamino and acetamide diphyllin phenol derivatives should be further studied as therapies for ebolavirus infection in addition to other V-ATPase mediated diseases.

CHAPTER 1. INTRODUCTION

1.1 The Filoviridae family of viruses are the causative agents of severe hemorrhagic disease and death in humans.

1.1.1 Filoviridae Taxonomy

The *Filoviridae* family consists of enveloped, negative-sense RNA viruses of large, filamentous size that have caused severe hemorrhagic fevers in humans.¹⁻⁸ The *Filoviridae* family is part of the order *Mononegavirales* and contains three genera (*Ebolavirus*, *Marburgvirus*, and *Cuevavirus*) with seven total viral species.⁷ Four species of *Ebolavirus* (EBOV) exhibit acute disease in humans (*Zaire*, *Sudan*, *Bundibugyo*, *Tai Forest*), and one with fatality in non-human primates and pigs but no pathology in humans (*Reston*).⁸ Three *Ebolavirus* species (*Zaire*, *Sudan*, *Bundibugyo*) are responsible for Ebola virus disease (EVD) and have caused recurrent and severe epidemics in humans with fatalities of 25-90%.⁹ The *Marburgvirus* genus consists of one viral species with two subspecies, Marburg (MARV) and Ravn viruses, and is responsible for deadly outbreaks in Germany and Africa with fatality rates of 25 and 90% respectively. MARV is the causative agent of Marburg virus disease while Ravn virus was more recently identified and studies are ongoing. The *Cuevavirus* genus was identified by analysis of bat tissues from northern Spain and consists of one species, Lloviu virus, of unknown pathogenicity to humans.¹⁰

1.1.2 Filovirus Structure

The filovirus genome consists of one single-stranded, negative-sense, 19kb RNA strand that encodes seven genes that produce seven structural and three non-structural protein products. These genes encode proteins known as nucleoprotein (NP), viral protein 35 (VP35), viral protein 40 (VP40), glycoprotein (GP), viral protein 30 (VP30), viral protein 24 (VP24), and the large protein (L) (**Table 1.1**).^{11,12} The genes are transcribed by viral RNA-dependent RNA polymerase into nine discrete mRNA transcripts that are capped and polyadenylated by the same protein.¹¹ While six of the genes are transcribed normally, slippage during transcription of the GP gene results in the production of three different mRNA transcripts. An internal stretch of seven uridines within the GP gene causes the viral polymerase to slip and results in frameshift changes to the transcript.¹³ The polymerase slippage is also controlled by the stretches of genomic RNA around the repeat

Table 1.1. Summary of EBOV Genes and Their Functions.

Viral Protein	Function	References
Nucleoprotein (NP)	RNA Encapsulation/ Stabilization, Transcription/ replication cofactor	14–16
VP35	Replication/Transcription essential cofactor, mediates the interaction of L and NP; Inhibition of RIG-1 and IRF3 signaling	17–21
VP40	Matrix Protein, aids in localization of nucleocapsid to the host plasma membrane, responsible for budding	22,23
Glycoprotein (GP)	Surface glycoprotein, responsible for attachment, trafficking, and release of the virus from endolysosome system	24–28
Soluble Glycoprotein (sGP)	Truncated, soluble form of GP; aids immune evasion through interaction with host antibodies for GP	13,29
Short, Soluble Glycoprotein (ssGP)	Shorter form of sGP, function is poorly understood but may be similar to sGP	13
Delta peptide	Viroporin, aids in EBOV virion release and the prevention of further EBOV infection of	30
VP30	Initiation of transcription cofactor, switch between transcription and genome replication	31,32
VP24	Integral to the formation of viral nucleocapsid; interferes with nuclear translocation of immune factors	33–35
L	Three domains with 1. RNA-dependent RNA polymerase activity, 2. 5' mRNA cap-methyltransferase, 3. 3'-mRNA polyadenylation; responsible for genome replication and mRNA transcription	36,37

and between the GP and VP30 genes.³⁸ The GP gene can encode for three separate mRNA products (pre-sGP, pre-GP, and ssGP) that are transcribed with an approximate ratio of 14:5:1.^{13,38}

The seven structural proteins of filoviruses (NP, VP35, VP40, GP, VP30, VP24, L) form the infectious viral particle. The outer envelope of the virus contains only GP, a transmembrane protein that is sufficient for attachment and entry of the virion into cells. VP40 forms a matrix on the inside of the plasma membrane that forms the structure of the virion and allows for attachment of the nucleocapsid.³⁹ The nucleocapsid consists mainly of genomic RNA coated with NP and takes a rigid coiled structure upon interaction with VP24, VP35 and VP40.⁴⁰ L and VP30 are also bound to the genomic RNA and packaged in the nucleocapsid of the virion to allow for transcription upon release of the virion.

1.1.3 Ebolavirus Cellular Lifecycle (**Fig. 1.1**)

Cellular infection begins as EBOV begins to interact with the receptors present on the plasma membrane of a host cell. The viral glycoprotein has been demonstrated to bind to the Tyro3 protein kinase (TAM) family of receptors, C-type lectin family members, and the T-cell immunoglobulin mucin domain (TIM) receptors TIM-1 and TIM-4.^{27,41,42} However, entry of the virus has also been shown to be independent of each these receptors in different systems, which demonstrates the flexibility of the virus for entry into numerous cell types. The phosphatidylserine-rich viral envelope can interact with TAM, TIM-1 and TIM-4 which may explain some of the ambiguity in EBOV attachment.⁴³ The binding of the virus is believed to elicit a signal cascade that induces macropinocytosis in the region of the virus.^{24,44}

Internalization of the virus-containing macropinosome is trafficked into the endolysosome system where the virion can release its contents into the host cytoplasm prior to it is degraded in the lysosome. As the EBOV virion is routed through the pathway from endosome to lysosome, decreasing pH within the endosomal lumen activates host cathepsin proteases present in the lumen. Cathepsins B and L sequentially process GP into a fusion-competent form by removing the glycan cap responsible for stabilization of buried fusion sequence.⁴⁵ Although some processing is necessary to activate the filoviral GP, the requirement of cathepsins varies amongst between EBOV and MARV and between the EBOV species.^{46,47} The exposed sequences of GP allow for binding with host Niemann-Pick C1 protein (NPC1), an integral membrane protein responsible for cholesterol handling in the late endosome.^{48,49} NPC1 has been identified as an integral protein for

filovirus entry and may be responsible for the species-specific effects of the virus.^{50,51} NPC1 has been proposed to stabilize GP as it undergoes the conformational shift necessary for the insertion of the GP fusion peptide into the endosomal membrane. A conformational shift in GP is triggered by protonation of histidine residues present on the fusion loop of GP.⁵² The role of pH in the fusion of GP with the endosomal membrane has been questioned by recent work in *in vitro* systems but the requirement of low pH for protease activity still necessitates its role in EBOV entry.⁵³ Further work on EBOV entry has also identified calcium channels as important to the entry of EBOV but their activities in the pathway are not fully understood.⁵⁴

Upon fusion between viral and endosomal membranes, the EBOV ribonucleoprotein is released into the cytoplasm of the host cell to begin replication. mRNA transcription by filoviruses requires the combined activities of NP, VP30, VP35, and L protein for mRNA transcript production. The binding of VP30 to a hairpin loop in the 3'UTR (untranslated region) of the EBOV genomic RNA signals the initiation of transcription by preventing polymerase pausing at the loop.⁵⁵ Transcription proceeds sequentially from the 3' to 5' ends of the genome as the polymerase pauses transcription at each gene ending sequence for polyadenylation of each transcript before reinitiating at a transcription start sequence.⁵⁶⁻⁵⁸ Addition of the 5'cap by the L protein occurs during transcription and may be important for transcript elongation if the process is similar to other related viral polymerases.^{37,59} The dissociation of the polymerase during the addition of the polyadenylated tails to each mRNA transcript may be responsible for the decreasing number of transcripts observed in infected cells for later genes.⁵⁷ Switching between viral transcription and genome replication depends on the phosphorylation state of VP30. Phosphorylation of VP30 increases its affinity for NP and aids in the packaging of the VP30 within the virion but also inhibits the interaction with VP30 and L that is necessary for transcription.³¹ The dephosphorylation of VP30 by host protein phosphatases 1 and 2A allows for VP30 oligomerization and initiation of transcription.³² The production of new VP30 after transcription results in more copies of phosphorylated and dephosphorylated protein and likely aids in the switching between transcription and replication through mechanisms still to be defined.

Ebolavirus genome replication requires the coordination of NP, VP35 and L to produce genomic and anti-genomic RNA. The 3' end of the filoviral genome and anti-genome contain promoters necessary for polymerase binding and contain stem-loop structures thought to be used in replication initiation.⁶⁰ VP35 forms an essential cofactor in this process and participates in a

number of roles. VP35 interacts with both NP and L and is proposed to act as a bridge between the two proteins and regulate their interaction.^{18,19} An intrinsically-disordered region of the VP35 N-terminus is responsible for inhibiting NP oligomerization with RNA and likely releases it for interaction with the polymerase.⁶¹

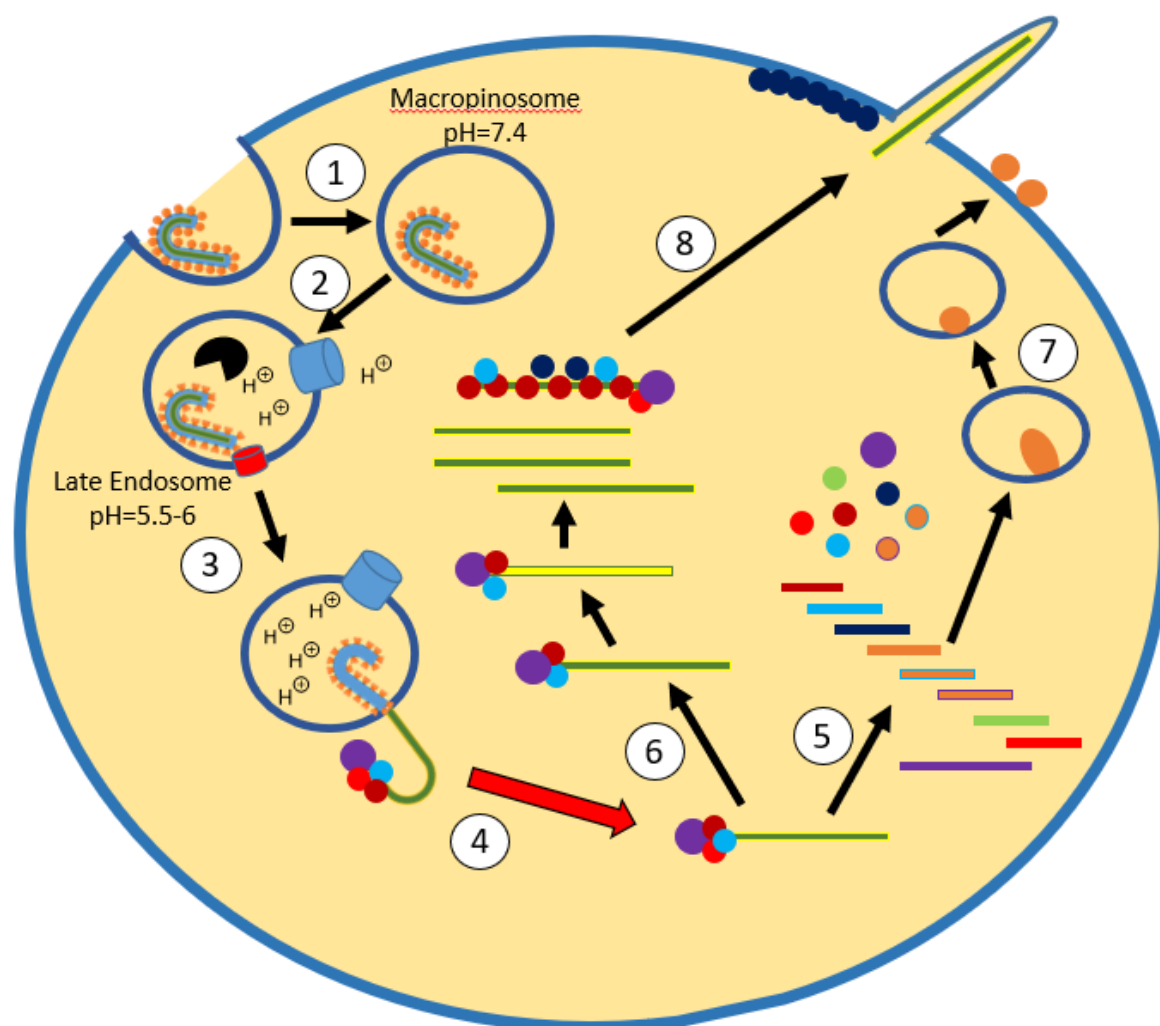
Virion assembly is initiated upon the synthesis of new EBOV genomes during replication and transitions from nucleocapsid to full virion formation through interaction with VP40. The switch from replication/transcription to assembly is poorly understood but may be caused by phosphorylation events on NP.¹⁵ NP likely encapsulates newly formed EBOV genomes soon after synthesis, as it oligomerizes in the presence of RNA when VP35 is not present. As NP coats RNA, it forms into helical tubes that interact with VP35 and VP24, which are necessary and sufficient for the formation of the viral nucleocapsid.¹⁶ Loss of VP24 results in a reduction of virions release, though its role in the process is poorly understood.³⁵ The polymerase becomes locked to the 3' end of the genome upon formation of the nucleocapsid to allow immediate activity once the nucleocapsid is released into a new host cell.⁶² VP40 acts as the shuttle of the nucleocapsid to the plasma membrane and is integral in the packaging and budding of the virion. Post-translational phosphorylation and ubiquitination of VP40 allows it to mediate the trafficking of nucleocapsids to the plasma membrane of infected cells by hijacking the host exocytosis machinery.^{63,64} NP interaction with VP40 allows this transport to the membrane where VP40 dimers become anchored to the plasma membrane through hydrophobic interactions within phosphatidylserine rich area of the membrane.^{14,23}

While genome replication and assembly of the virion is ongoing, GP is processed and becomes localized to lipid rafts on the plasma membrane. The pre-GP mRNA encodes the GP₀ protein that is expressed in the ER and Golgi of infected cells. GP₀ is cleaved into two separate proteins (GP₁, GP₂) by furin-like proteases in the Golgi that remain associated by disulfide bonds and form a trimeric structure of three GP₁ proteins (extracellular exposed) and three GP₂ (membrane-bound).²⁵ GP₁ is divided into three domains the exposed glycan cap, the head which stabilizes the pre-fusion protein, and the base attached to GP₂. GP₂ contains the solvophobic fusion peptide in an unstable state that is maintained by the presence of GP₁. GP₁ is heavily glycosylated (believed to prevent immune recognition) and formed into a chalice-like structure that protects the fusion peptide of GP₂.²⁵ Transport of GP_{1,2} to lipid raft domains on the plasma membrane allow it to associate with VP40.²⁶ Remarkably, the presence of GP and VP40 at the plasma membrane

Figure 1.1. Cellular Lifecycle of EBOV Infection.

(1) EBOV virion binds to cell surface and is taken into cells by macropinocytosis. (2) The virion-containing macropinosome is trafficked into the endolysosomal pathway where decreasing pH activates cathepsin proteases that modify GP into a fusion-competent state. (3) The combination of decreasing pH and interaction with endosomal proteins allow the fusion of the viral and endosomal membranes. (4) Fusion allows the release of the viral RNP into the cytoplasm and the initiation of cellular infection. (5) Sequential transcription of individual mRNA transcripts from the viral genome results in production of viral proteins. (6) Genome replication occurs through the synthesis of anti-genomes and new genomes. (7) pre-GP is expressed in the Golgi and is modified by furin proteases into the mature GP_{1,2} and transited to the plasma membrane. (8) Interaction of VP40 with NP and other proteins bound to new viral genomes allows for the transit of the genome to the plasma membrane for the budding of new virions.

Figure 1.1 (cont.)



Legend

EBOV RNA		VP40	
EBOV virion		GP	
Cathepsin		sGP	
V-ATPase		ssGP	
NPC1		VP30	
Furin		VP24	
NP		L	
VP35			

alone is sufficient for the release of virus-like particles with similar morphology to infectious virions.²² VP40 binding to lipids at the plasma membrane is integral to its oligomerization as hexamers and formation of a long lattice-like structure on the inner surface of the plasma membrane.^{65,66} The budding that follows the change in VP40 oligomerization occurs as the nucleocapsid becomes wrapped in the plasma membrane and is pushed through protrusions in the plasma membrane to form new viral particle.⁶⁷

1.1.4 Ebolavirus Antagonism of the Immune System allows for Increased Infection

To survive in hosts and specifically host cells, EBOV inhibits the immune response to infection through numerous methods. EBOV begins an early and extensive subversion of the host immune response soon after the initiation of infection. VP24 blocks the nuclear translocation of phosphorylated signal transducer and activator of transcription 1 (STAT1) to the nucleus by interfering with its interaction to karyopherin $\alpha 1$.^{34,68} In addition, VP24 also blocks host interferon response by inhibiting the phosphorylation of p38- α and JAK-STAT signaling.⁶⁹ Through these activities, VP24 antagonizes the interferon response by host cells and integral to EBOV's immunosuppression.³³ VP35 also obstructs the host interferon response by binding to viral double-stranded RNA and preventing its interaction with host retinoic acid-inducible gene-1 (RIG-1) and melanoma differentiation-associated gene-5 (MDA-5).^{17,20} Combining this activity with the inhibition of interferon-regulatory factor (IRF3), VP35 antagonizes type 1 interferon expression by infected cells.¹⁷ VP35 interference in the RIG-1 signaling pathway also blocks antigen presentation and maturation of dendritic cells.²¹

The expression of GP isoforms is also implicated in EBOV evasion of immune response by host cells and immune system. sGP mRNA encodes a 60kDa protein that is cleaved by furin protease into sGP and the delta peptide.⁷⁰ The sGP (soluble glycoprotein) is lacking the transmembrane portion of the protein and is believed to act in both an anti-inflammatory and anti-cytotoxicity factor. Secretion of the sGP protein is proposed as an immune system decoy because it shares the same epitope with GP that interacts with neutralizing antibodies and likely prevents antibody recognition of GP on host cells.⁷¹ The delta peptide is highly post-translationally modified and is believed to regulate further infection of EBOV-infected cells by new virions and may act as a viroporin to facilitate the exit of virions from infected cells.³⁰ The ssGP mRNA

encodes a 36kDa protein (short, soluble glycoprotein) that exists as a dimer and is also secreted but the function of this protein is not fully known.¹³

Despite EBOV subversion of the immune response in host cells, tissue damage caused by the host response to viral infection can be severe. The release of proinflammatory cytokines (tumor necrosis factor- α (TNF- α), interleukin (IL)-1 β , IL-6, and IL8 amongst many others) contribute to organ damage and are associated with increased severity and death in EVD.^{72–74} Vascular permeability and hypotensive shock is induced by the release of nitric oxide and other pro-inflammatory cytokines from EBOV-infected endothelial cells and macrophages.^{75,76} Impairment of coagulation through increased tissue factor expression, increased TNF- α expression, and liver injury lead to conjunctival and gingival hemorrhages indicative of EVD.^{77–79}

1.1.5 Filovirus Pathogenesis

Filoviruses are zoonotic viruses that cause severe outbreaks when transmitted to humans and non-human primates. Reservoirs of Ebola and Marburg viruses are known to be in fruit bats but other mammalian species (squirrels, mice, and rats) have also been proposed to harbor the virus asymptotically in enzootic cycles.⁸⁰ Infections of humans and non-human primates are epizootic as these hosts are dead-end reservoirs for the virus given the high mortality and poor intraspecies transmission of the virus through them. The natural cycle of the virus within the ecosystem appears complex and the method of its recurrence in the human population is currently unknown.^{81,82} Anecdotally, epidemics of the virus in the human populations are preceded by outbreaks in non-human primates and other species closely associated with humans but the evidence is limited.⁸¹

EBOV infections spread through contact with infectious fluids and affects all parts of a population. The virus can be found from infancy to old-age, though the apparent higher prevalence in adults is likely due to their activity as caregivers.⁸³ The virus is transmitted between humans, and between other species and humans by contact with blood or bodily fluids of an infected individual.^{80,84} Humans can transmit the virus to other individuals from the beginning of fever symptoms until after death.^{85,86} During the 2014 outbreak in Sierra Leone, 74% of viral transmissions were within extended family groups.⁸⁷ Another major mechanism of transmission is contact with infected remains and regulation of burial practices is recognized as an important epidemic control.⁸⁸ Infectious particles also remain viable on exposed surfaces for weeks and

longer in climate-controlled hospitals which has contributed to outbreaks of the virus amongst healthcare workers.⁸⁹ While airborne spread of the virus has been stated anecdotally and reported in non-human primate models, thorough studies have not identified it as an effective mode of transmission.^{90,91}

Filoviruses are not restricted to specific tissue types which results in a rapid spreading infection that hits many organs in quick succession.⁷⁷ Upon contact of infectious material with host mucous membranes or breaks in the skin, filoviruses gain entry to the bloodstream and initially target macrophages and dendritic cells.⁹² These early viral reservoirs provide transport from the site of infection to the lymphatic system, and the virus is disseminated throughout the body from there.^{92,93} The wide tissue tropism of EBOV is likely caused by the broad variety of host cellular receptors found to interact with the virus. The ability of the virus to penetrate organs is also be related to the transition of infected macrophages into tissues or the transmission of the virus to tissue-specific monocyte-derived cells like Kupffer cells and fibroblastic reticular cells.

Clinical signs of infection progress from flu-like symptoms into multi-organ failure and death within three weeks of the first sign of symptoms. Early non-specific symptoms are indistinguishable from those presented by malaria, bacterial, and other viral infections but progress into nausea/vomiting, abdominal pain, and diarrhea within a week.⁸⁰ Rashes and mucosal bleeding begin during the first week and become more severe as the disease progresses.^{94,95} During the second week, severe symptoms of the disease present in multiple organs (including the central nervous system, kidneys, liver, lungs, and heart) and death follows within 16 days of symptom onset.^{80,86} Recurrence of the disease has been reported months after recovery and symptoms like fatigue and hearing loss can persists for over a year.^{96,97}

Filovirus infection can be identified by two principle methods at steps early during infection and other tests have been identified in the aftermath of the 2014-2016 outbreak. After the onset of fever symptoms, viral RNA can be detected by qRT-PCR (quantitative reverse transcriptase polymerase chain reaction) though viral RNA levels are not predictive of disease severity.⁹⁸ ELISA (Antigen-capture enzyme-linked immunosorbent assay) can be used to detect IgM antibodies within several days of fever presentation and IgG antibodies can be identified within a week.⁹⁹ Both assays have been implemented in field laboratories to rapidly diagnose EBOV infection.⁸⁶ Serum transaminases, hemoglobin, and hematocrit blood levels are all elevated early during infection and higher levels are correlated with increasingly severe illness.¹⁰⁰

1.1.6 Filovirus Epidemiology

Since 1967, there have been 22 outbreaks of EBOV and 11 outbreaks of MARV that have resulted in severe disease in humans and 11 have resulted in >100 cases.^{7,101,102} Most outbreaks of filovirus have occurred in central Africa with only sporadic occurrences of the virus in south and west Africa before the major outbreak in 2014.⁹ The first filovirus outbreak occurred in Germany and Yugoslavia in 1967, when researchers exposed to green monkeys from Uganda exhibited an unknown hemorrhagic fever that was eventually diagnosed as MVD.^{103,104} In 1976, central Africa experienced the first known outbreaks of Zaire and Sudan species of EBOV, which resulted in fatality rates of 88 and 53%, respectively.^{105,106} While sporadic outbreaks of the virus have continued to cause severe mortality in rural areas of central Africa, the spread of the virus appeared to be curtailed by its limited ability for transmission and high fatality. This situation changed with the outbreak of Zaire ebolavirus in west Africa early in 2014.

The 2014-2016 outbreak of Zaire ebolavirus in west Africa (mainly in Guinea, Liberia and Sierra Leone though cases were identified in several adjoining countries) was the largest filovirus outbreak in history.¹⁰⁷ Although case identification was difficult due to poor surveillance and weak public health infrastructure, 28,639 cases of infection were reported with a 39% fatality rate. Lack of infrastructure, cultural norms, and the transition of the virus from rural area into urban settings are amongst the factors implicated in the widespread occurrence of the virus.¹⁰⁸ The imposition of proper quarantine procedures, measures of infection prevention and expanded healthcare facilities in affected communities are believed to have aided in the containment of the virus. By the declared end of the outbreak, significant interest in the virus had been aroused and research has continued to be a priority to prevent further outbreaks.¹⁰⁸ However, new outbreaks of Zaire ebolavirus have occurred in the Democratic Republic of the Congo but these have been considerably smaller in number of infected individuals (<100 cases).

1.1.7 Therapies for EBOV

1.1.7.1 Vaccines

The best option for prevention of widespread EBOV infection is through vaccination programs. There is no FDA approved filoviral vaccine, but the development of a vaccine has been prioritized since the 2014-2016 outbreak of EBOV in west Africa. Several clinical trials have been attempted during and after the outbreak to assess the efficacy of vaccines. Multiple strategies are

being pursued including inactivated viruses, DNA vaccines, virus-like particles, and vector-based vaccines.

The first EBOV vaccine was produced in 1980 using heat-inactivated EBOV particles and demonstrated effective protection from EBOV challenge in guinea pigs.¹⁰⁹ However, the overall results from conventionally inactivated viruses have resulted in varying results in multiple infection models, including non-human primates.¹¹⁰ Safety concerns about the demonstrated retention of virulence have also contributed to the failure of these traditional approaches.¹¹⁰

DNA vaccines are being pursued that allow for the selective expression of the antigenic EBOV GP and NP genes are being pursued. These plasmids can be injected into a host, taken up by host cells, and used to produce the antigenic protein from the host cells. GP DNA vaccines using sequences from the Zaire and Sudan species and Marburg virus have shown protection of mice up to 100% from EBOV challenge.^{111–113} A phase 1 trial utilizing plasmids containing GP sequences from Zaire and Sudan species and the NP sequence of the Zaire species were well tolerated in healthy adults. This vaccine resulted in CD4⁺ T-cell responses in all individuals and CD8⁺ T cell responses in the cohort administered with higher vaccine load.¹¹⁴ Further clinical trials using EBOV and MARV GPs have been well tolerated in wider populations and produced humoral and cellular immunogenic responses.^{115,116}

Virus-like particles (VLPs) are under study due their lack of a viral genome and the self-assembling ability of the filoviral VP40 matrix protein. Expression of VP40 alone in cells will cause virion formation and budding from cells and the inclusion of GP induces the proper viral morphology.²² VLPs have demonstrated efficacy at protection against EBOV challenge in murine models, even in the absence of detectable anti-EBOV antibodies.^{117–119} Production of VLPs has been hampered by their production from human cell culture which is costly and hard to scale to industrial levels. Currently, production from insect cells and specialized mammalian cells is being studied as a method to produce more VLPs for further study and potential clinical trials.^{119–121}

Recombinant viral vaccines are the most popular method of developing EBOV vaccines and have achieved significant success. Replication competent or deficient options are available, but both have down sides. Replication-deficient vaccines are safe and cheap to produce but are weakly immunogenic and require multiple dosing to achieve immunity. Replication-deficient vaccines incorporating the EBOV GP are being developed using vaccinia virus, Venezuelan equine

encephalitis virus, adenovirus, or Kunjin virus expression systems. All of these systems have shown efficacy for prevention of EBOV infection in rodents and non-human primates.^{122–125} Recombinant human adenovirus 5 (rAd5) expressing GP from Zaire or Sudan viral species have proved protective in mice and non-human primates and induced CD8⁺ T-cell and antibody responses in non-human primates.^{126,127} Phase 1 trials with rAd5 encoding GP from the Zaire and Sudan viral species did not elicit severe side effects and patients developed humoral and cellular immune responses to the antigens presented.¹²⁸ Pre-existing immunity to rAd5 has shifted focus to a vector based on the recombinant chimpanzee adenovirus type 3-vectored vaccine (ChAd3) using GP from the Zaire and/or the Sudan viral species. Non-human primates exposed to this vaccine exhibited complete immunity to EBOV challenge but the immunity was not long-lasting.¹²⁹ The addition of a modified vaccinia Ankara (MVA) expressing the same GPs to the ChAd3 vaccine enhanced the durability of the vaccine.¹²⁹ Clinical trials of the ChAd3 vaccine indicated that the vaccine was safe to use and conferred high-level protection and the addition of an MVA booster added long-term expression of protective antibodies.^{130,131}

Replication-competent EBOV vaccines, especially those using the vesicular stomatitis virus (VSV), have demonstrated efficient strategies for the prevention of ebolavirus infection. Studies on a VSV vector containing the EBOV GP (rVSVΔG/EBOVGP) showed non-human primates exposed to the vaccine had completely protective immune responses to EBOV challenge.^{132–134} Clinical studies with the vaccine have shown that a single vaccine dose was enough to elicit anti-EBOV antibody responses and was generally well-tolerated and safe to use, though minor side effects were reported.^{135–137} A second VSV vaccine in phase II/III clinical trials (rVSV-ZEBOV, expresses the GP from the Zaire viral species) has demonstrated protection in multiple mammalian species and a single dose is completely protective in non-human primates challenged >7 days after receiving the vaccine (partly protective when challenged <3days after receiving the vaccine).^{134,138–140} A phase III trial conducted in Guinea and Sierra Leone with the rVSV-ZEBOV vaccine found complete protection from EBOV infection 10 days after vaccine administration.¹⁴⁰ A study utilizing a vaccine (GamEvac-Combi) combining live-attenuated recombinant VSV expressing the EBOV GP from the recent west African outbreak (Ebola virus/H.sapiens-wt/GIN/2014/Makona-C15 strain) and recombinant Ad5 expressing the same GP induced humoral and cellular immune responses in all patients who received the vaccine.¹⁴¹

1.1.7.2 Therapeutics for EBOV infection

While vaccine development is prioritized and necessary for the prevention of EBOV outbreaks, there are no therapeutics for the treatment of infected individuals. The current treatments for EBOV infection are limited to basic care and hydration with some use of interferon-gamma in severe cases. Numerous studies have been designed to identify novel inhibitors of EBOV from existing drugs and novel chemical entities. Multiple drugs that are being developed for other viral infections have been repurposed to potentially treat EBOV infection. The following is a short review of drugs undergoing therapeutic trials for EBOV infection (**Fig. 1.2**) or agents that hold promise as options to prevent EBOV entry as a therapeutic strategy (**Fig. 1.3**).

1.1.7.2.1 EBOV Inhibitors in Clinical Trials

Favipiravir is a viral polymerase inhibitor that has demonstrated efficacy against EBOV infection *in vitro* and in mouse models of EBOV infection. Favipiravir is an inhibitor of the RNA-dependent RNA polymerase of influenza virus that has shown efficacy against many RNA viruses (flaviviruses, noroviruses, alphaviruses, picornaviruses, paramyxoviruses).¹⁴² Favipiravir treatment was 100% successful at preventing death in several mouse studies and was believed to be a potential therapy for EBOV infection.^{143,144} A proof-of-concept study with 126 patients during the EBOV outbreak in west Africa did not demonstrate efficacy and toleration was not conclusive but further studies are planned.¹⁴⁵

Gilead Sciences has pushed the development of another broad-spectrum RNA-dependent RNA polymerase inhibitor, Remdesivir (GS-5734), into clinical trials for EBOV infection. Remdesivir is an ester prodrug of a 1'-cyano substituted adenine C-nucleoside that is metabolized into the active nucleotide triphosphate within host cells.^{146,147} Remdesivir has also demonstrated activity against respiratory syncytial virus, Junin virus, Lassa fever virus and Middle East respiratory syndrome virus.¹⁴⁸ Remdesivir was found to be 100% protective in non-human primates even when administered three days post infection.¹⁴⁸ Remdesivir has begun Phase 1 clinical trials to treat EBOV infection in two compassionate therapy cases in the United Kingdom and Guinea made use of this drug.^{97,149}

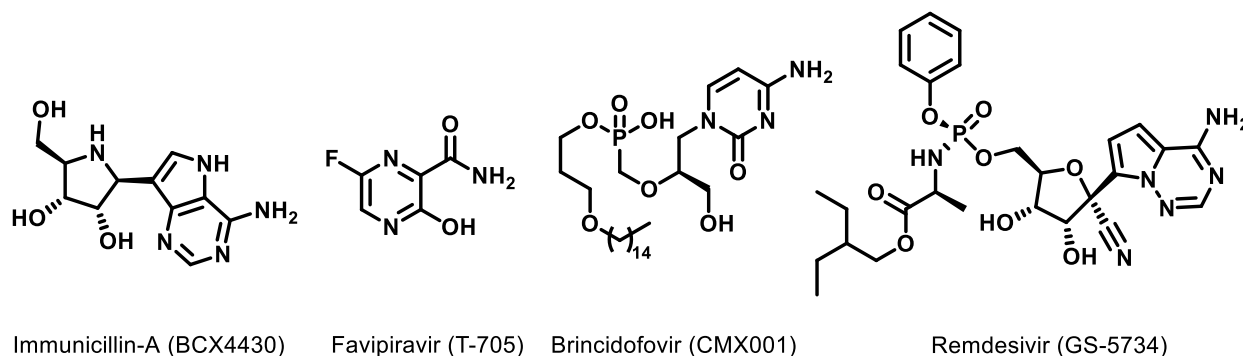


Figure 1.2. Inhibitors of EBOV infection that have entered clinical trials.

BCX4430 is an adenosine analog developed by BioCryst Pharmaceuticals as a novel inhibitor of EBOV RNA-dependent RNA polymerase. BCX4430 was identified as a terminator of viral RNA polymerase function from a small molecule library and subsequently demonstrated potent activity against EBOV and MARV infection in rodent and non-human primate models.¹⁵⁰ BCX4430 has also shown broad-spectrum efficacy against bunyaviruses, arenaviruses, paramyxoviruses, flaviviruses, and coronaviruses.^{150,151} Phase 1 clinical trials of BCX4430 are currently ongoing.¹⁵²

Brincidofovir is a broad-spectrum inhibitor of DNA virus infection developed by Chimerix used during the 2014-2016 EBOV outbreak in west Africa. It is a hexadecylpropyl prodrug of the nucleotide analog cidofovir that has shown potency against poxviruses, herpesviruses, adenoviruses, and polyomaviruses.¹⁵³ Interestingly, the hexadecylpropyl tail is required for activity against EBOV, while it needs to be cleaved for activity against DNA viruses.¹⁵⁴ Brincidofovir was removed from human trials during the 2014-2016 epidemic by Chimerix and it was subsequently reported that the prodrug is metabolized quickly in non-human primate serum, which may limit the bioavailability of the drug.^{154,155}

Several nucleic acid-based therapies have been studied for activity against EBOV infection and several have transitioned into clinical trials. TKM-Ebola is a combination of two siRNA molecules (targeting the RNA-dependent RNA polymerase and VP35) and entered Phase 1 clinical trials in early 2014 but they were terminated by the FDA.^{156,157} A second siRNA product, siEbola-3 was derived from TKM-Ebola by adapting the siRNA for the Makona strain responsible for the 2014-2016 outbreak.¹⁵⁸ A Phase 2 clinical trial of siEbola-3 started in 2015 but was terminated

due to limited efficacy.¹⁵⁹ An antisense phosphorodiamidate morpholino oligomer called AVI-6002 targeting VP35 and VP24 protected a majority of non-human primates from EBOV challenge.^{160,161} Phase 1 clinical trials of AVI-6002 indicated that it was well tolerated but no further information is available.¹⁶²

The use of antibodies to target EBOV infection gained considerable attention during the 2014-2016 outbreak though there is little precedent for the treatments. Treatment of infected patients with plasma donated by EVD survivors was used in a large-scale effort during the 2014-2016 outbreak.¹⁶³ In the end, there was no significant difference in survival rate between the treated and untreated groups.¹⁶⁴ Using non-human primates, concentrated polyclonal IgG antibodies from primates who survived EBOV challenge were able to protect 100% of a second group treated with the antibody.¹⁶⁵ However, the production of enough antibody to treat an outbreak would require supplies that are currently unobtainable. Lastly, ZMapp (a combination of monoclonal antibodies produced from the plant species *Nicotiana benthamiana*) was used to treat two patients who were transferred to the United States.¹⁶⁶ A Phase I clinical trial of ZMapp in west Africa reduced mortality by 15% between the treated and control groups but was not deemed significantly different than the control group.¹⁶⁷

1.1.7.2.2 EBOV Entry Inhibitors

The identification of novel EBOV inhibitors has been accelerated since the 2014-2016 outbreak of the virus and has involved both cutting edge technologies and old-school medicinal chemistry and screening. Inhibitors of ebolavirus infection come in many forms but can be divided into two main classes: those directly targeting the virus/viral proteins and those targeting host factors that engage the virus. Screening for novel inhibitors has occurred through computer-aided approaches and high throughput screening. Targeting EBOV entry pathways is a major area of research yielding a wealth of information about EBOV and multiple novel approaches to target the virus.

While several EBOV proteins have been targets of viral entry inhibitors, inhibition of GP activity has been the main target. The conformational shift in the EBOV GP have been the focus of many studies and several novel and FDA-approved inhibitors can bind in a novel binding pocket. Toremifene and Ibuprofen were found to bind to GP in a cavity between the GP1 and GP2 subunits and destabilized the GP, which may be the mechanism of inhibition by these compounds.¹⁶⁸

Multiple FDA approved drugs (benztropine, bepridil, sertraline, paroxetine, imipramine, clomipramine, thioridazine) have all been shown as weak binders of GP in a thermal shift assay though the binding constant is significantly higher than the activity of the compounds against EBOV infection.^{169,170} All of these compounds bound in the same cavity as toremifene and destabilized the glycoprotein though the interaction was weaker than toremifene.

Host entry inhibitors-A large number of host processes are necessary for ebolavirus infection of cells and many inhibitors have been identified that block viral entry at numerous steps. Phosphatidylinositol-(3,5)-bisphosphate production is important for the maturation of endosomes and is critical for the entry of EBOV.¹⁷¹ Apilimod, an inhibitor of phosphatidylinositol-3-phosphate 5-kinase (a producer of phosphatidylinositol-(3,5)-bisphosphate), was identified as a 10 nM inhibitor of EBOV infection of primary human macrophages.¹⁷² An adamantane dipeptide piperazine inhibitor of EBOV entry through the antagonism of the interaction between NPC1 and EBOV GP was identified through the screening of a small molecule inlibrary.⁵⁰ A derivative of this inhibitor, (-)-3-25 was combined with the anti-HIV compound ritonavir to achieve blood concentrations in mice high enough to match *in vitro* inhibitory concentrations.¹⁷³ Inhibition of NPC1 cholesterol transport with U18666A was also shown to inhibit EBOV infection, though there was no antagonistic interaction between the inhibitor and EBOV GP.¹⁷⁴ The antifungal agent posaconazole is also an antagonist of NPC1 activity and was identified as an inhibitor of EBOV entry in combination with toremifene and clarithromycin, an inhibitor of lysosomal calcium release.¹⁷⁵ Inhibitors of L-type calcium channel blockers (tetrandrine, verapamil, bepridil) have also been identified through screening as inhibitors of EBOV infection *in vitro* and *in vivo* and are believed to block the trafficking of EBOV-containing endosomes within cells.^{54,176,177} Nafamostat mesylate, an inhibitor of the protease cathepsin B, was found to block EBOV entry and is a candidate for treating disseminated intravascular coagulation caused by EVD.¹⁷⁸

1.1.8 Requirements of Vesicular Acidification During the Entry of Filoviruses and Other Viral Families

A potential target for new anti-EBOV therapies is the endosomal acidification responsible for protease activation and fusion between the viral and endosomal membranes. Targeting acidification has previously been used to inhibit influenza virus infection with M2 channel

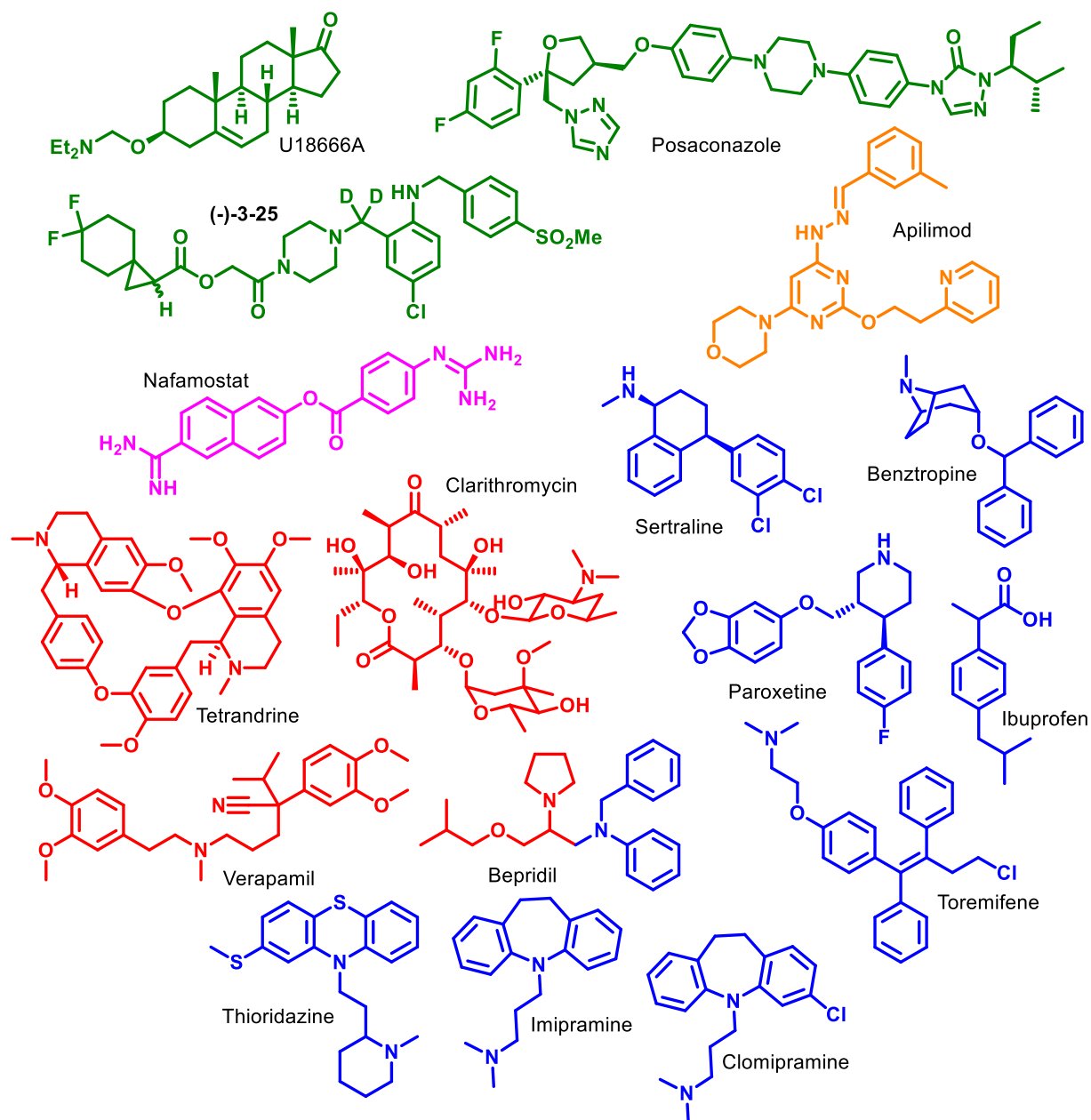


Figure 1.3 Identified Inhibitors of EBOV entry.

Inhibitors of NPC-1 are shown in green. Protease inhibitors are shown in purple. Inhibitors of phosphatidylinositol-3-phosphate 5-kinase are shown in orange. Proposed inhibitors of EBOV GP are shown in blue. Inhibitors of calcium channels are shown in red.

inhibitors and has been shown to be important in the lifecycles of numerous viruses.¹⁷⁹ Viruses from diverse families like flaviviridae, togaviridae, orthomyxoviridae, papillomaviridae, and coronaviridae all require the endosomal acidification to commence cellular infection in addition to numerous others.^{180–185} Flaviviridae, togaviridae, herpesviridae, and many other viruses also require acidic activation of furin proteases to process their glycoproteins into infection-competent forms.^{186,187} Thus, targeting the host factors responsible for the acidification of cellular vesicles may represent novel targets for antiviral drug development.

1.2 Vacuolar-ATPase is responsible for cellular endosomal acidification

1.2.1 V-ATPase Background

Vacuolar-ATPase (V-ATPase) is a ~1MDa multi-subunit, transmembrane complex that is responsible for the maintenance of endosomal and lysosomal pH environments within cells.^{188,189} V-ATPase is evolutionarily related to the F and A-type ATPases but has acquired a distinct activity profile and wider variety of cellular functions from the other types.^{188–191} The main activity of V-ATPase is to couple the energy released in ATP hydrolysis to the transport of protons across a lipid membrane.^{192,193} V-ATPase is found in all eukaryotic organisms, along with multiple species of archaea and bacteria that express related homologs of the enzyme.^{188,191} V-ATPase can be found in a variety of locations with cells including endosomes, lysosomes, Golgi vesicles, secretory vesicles and at the plasma membrane of certain specialized cells.¹⁹⁴ Given the important and varied activities of the complex, exquisite regulation of V-ATPase is required to direct its activities and dysregulation is associated with a wide variety of diseases.^{188,194}

1.2.2 V-ATPase Structure

V-ATPase consists of fourteen proteins organized into the integral membrane bound V_0 domain and the cytosolic V_1 domain. The V_0 domain acts as the transmembrane proton channel composed of subunits a, d, e, c, c' (found in yeast), c'', Ac45 (found in higher eukaryotes) (**Table 1.2**).^{195–197} The c, c', and c'' subunits make up an integral proteolipid ring in the endosomal membrane and their interaction with the a subunit allows for the formation of a proton conduit through the membrane.^{191,197} The a subunit is an integral membrane protein that interacts with the outside of the proteolipid ring and interacts with the d subunit and the central stalk of the V_1 domain.^{192,198} Protons are moved through the V_0 domain when two half channels in the a subunit

Table 1.2 Summary of V-ATPase subunits, isoforms, and their functions within the complex.

V-ATPase Subunit	Human Gene(s) (Tissue expression)	Subunit Function	References
A	ATP6V1A	ATP Hydrolysis, Interacts with V-ATPase regulators	192,199–201
B	ATP6V1B1 (renal, epididymis), ATP6V1B2 (ubiquitous)	Non-catalytic ATP binding site, Interacts with V-ATPase regulators	192,200,202,203
C	ATP6V1C1 (ubiquitous), ATP6V1C2 (lung, renal, epididymis)	Portion of peripheral stator, Interacts with V-ATPase regulators, C2 has 2 splice variants	192,204,205
D	ATP6V1D	Member of Central Stalk	192,206
E	ATP6V1E1 (testis), ATP6V1E2 (ubiquitous)	Portion of peripheral stator, Interacts with V-ATPase regulators	192,207
F	ATP6V1F	Member of Central Stalk	192,208
G	ATP6V1G1 (ubiquitous), ATP6V1G2 (neural), ATP6V1G3 (renal, epididymis)	Portion of peripheral stator, Interacts with V-ATPase regulators	192,206,209
H	ATP6V1H	ATP hydrolysis regulation, Interacts with V-ATPase regulators, has 2 splice variants	192,210,211
a	ATP6V0A1 (neural), ATP6V0A2 (ubiquitous), ATP6V0A3 (osteoclasts), ATP6V0A4 (renal, epididymis)	Proton hemichannel, Subcellular targeting	192
c	ATP6V0C	Proton hemichannel, Proteolipid rotor	192
c'	ATP6V0B	Proton hemichannel, Proteolipid rotor	192
d	ATP6V0D1 (ubiquitous), ATP6V0D2 (renal, epididymis)	Coupling V0 domain with V1, Member of central stalk	192,212–214
e	ATP6V0E1	Function unknown, Interacts with subunit a	215
Ac45	ATP6AP1	V-ATPase assembly and trafficking	216,217

and the proteolipid ring line up and allow the conserved glutamate and arginine residues to move protons through the channel at a ratio of 10 protons for every 3 hydrolyzed ATP molecules.²¹⁸ The location and activity of subunit e is not entirely known but believed to interact with subunit a.²¹⁵ The V₁ domain is composed of subunits A-H and is responsible for ATP hydrolysis. Subunits A and B form a heterohexamer of the composition A₃B₃ and form three ATP binding domains.¹⁹² ATP hydrolysis in the hexamer energizes the rotation of the central stalk (composed of subunits D, F and d) which rotates the proteolipid ring of the V₀ domain.¹⁹² Three heterodimers of subunits E and G form around the hexamer while subunits C and H each interact with a single heterodimer to provide stabilization as stators and interaction surfaces for V-ATPase regulatory proteins.²¹⁸ Subunit H is also involved in the regulation of ATP hydrolysis and coupling of proton transport with ATP hydrolysis.^{210,211} The activity of different subunits can vary due to the existence of multiple isoforms of many V-ATPase subunits.

1.2.3 V-ATPase Isoforms

Higher eukaryotes carry multiple genes of some V-ATPase subunits and are expressed as different isoforms. Isoforms of subunits a, d, B, C, E, and G have been identified within cells and their expression is generally tissue-specific with one isoform being ubiquitously expressed and another being expressed in a specific location like renal intercalated cells. Subunits B2, C1, E2, G1, and d1 are all found ubiquitously in cells while specific combinations of the isoforms tend to be found in discreet tissues and cell types.¹⁹⁴ Examples of these are: Subunits a4, B2, C2, G3, and d2 are highly expressed in renal and epididymal cells, a1 and G2 are mainly found in the brain, a3 and d2 are highly expressed in osteoclasts, and B1 and E1 are highly expressed in the olfactory epithelium.^{194,202,219,220} Understanding of V-ATPase isoforms and the activities of the various isoforms is still growing but isoforms of subunit a are the most well-studied due to their importance in a number of diseases.

Isoforms of subunit a are the most characterized and understood of V-ATPase isoforms since they are responsible for the localization of V-ATPase within cells. There are four isoforms of the a subunit (a1-4) and they share 47-61% amino acid sequence identity, though most of the variation occurs in the cytosolic-exposed N-terminal domain.¹⁹⁴ Though certain isoforms of a are specifically expressed in certain cell types, they may not be the only isoform found within those cells. Subunit a1 can be found in the endosomes of many cells types but is most highly expressed

within neuronal cells, where it is responsible for the targeting of V-ATPase to synaptic vesicles.^{196,221} Isoform a2 expression is also widespread and is mainly found within the intracellular endosomal system.²²² Also, the a2 isoform can specifically be found in endosomes near the apical membrane of renal proximal tubule cells.²²³ In healthy cells, subunit a3 is found in osteoclasts, the adrenal, parathyroid, thyroid and pituitary glands, and pancreatic islet cells. The a3 subunit becomes localized to the plasma membrane of mature osteoclasts and aids in the secretion of insulin and other hormones.^{222,224} The a3 subunit is also heavily expressed in many cancer types, especially those with more invasive and metastatic phenotypes.^{225,226} The a4 isoform is found in renal and epididymal clear cells and is responsible for the translocation of V-ATPase to the apical membranes of these cells.²²⁷

1.2.4 V-ATPase Regulation

Cellular energy status is closely linked to V-ATPase function, as expected for a complex able to consume large amounts of cellular energy stores, and V-ATPase activity appears to be highly tunable depending on cellular status and metabolic priority. The most well-understood cellular method for controlling V-ATPase activity is to regulate the assembly of the complex. Other regulation through signaling pathways and interacting partners have been identified with more knowledge still to be learned about the complex.

The dissociation of V_1 from the V_0 domain during glucose depletion in insects and yeast is likely done to conserve ATP but regulation appears to be much more complex than initially thought.²²⁸ V-ATPase assembly in mammalian cells is upregulated in response to increased cellular glucose concentrations and decreased amino acid concentrations.^{229,230} Glucose-dependent activation of V-ATPase is traditionally believed to occur through both protein kinase A (PKA) and phosphatidylinositol-3-kinase (PI3K) dependent pathways. The activation of PKA by glucose is believed to increase V-ATPase assembly and activity to maintain cytosolic pH that is decreased during elevated glycolysis that occurs during high glucose conditions.²³⁰ PI3K signaling is important in the assembly and localization of V-ATPase to the plasma membrane in osteoclasts and renal cells.^{231,232} During the maturation of dendritic cells, PI3K and mTOR signals increase the assembly of V-ATPase to aid in antigen processing.²³³ Recently, adenosine monophosphate-activated protein kinase (AMPK) was found to increase V-ATPase assembly and activity in human cells during glucose starvation.²³⁴ Epidermal growth factor stimulation of V-ATPase assembly is

related to increased lysosomal protein degradation and the increase of amino acid levels.²³⁵ Interestingly, PI3K and extracellular signal-regulated kinase (ERK) signaling induced by influenza virus infection cause V-ATPase assembly to aid in the release of virus into the cytosol.²³⁶

V-ATPase activity is also regulated by intracellular trafficking, phosphorylation, and through its interacting partners. The density of plasma membrane pumps in renal cells is controlled by a soluble, bicarbonate-sensitive adenylyl cyclase.²³⁷ The adenylyl cyclase increases cytosolic cyclic-AMP levels in response to decreased cytosolic pH, which increases PKA activity. PKA directly phosphorylates the A subunit of V-ATPase at S175 which promotes the transition of V-ATPase from endosomal vesicles to the plasma membrane. Phosphorylation of S384 on the A subunit by AMPK reduces V-ATPase activity in renal intercalated cells.²³⁸ Interaction with the actin cytoskeleton and microtubule network allows the correct localization of V-ATPase and tightly controls V-ATPase activity at the plasma membrane.²³⁹

1.2.5 Cellular roles of V-ATPase

V-ATPase is a major enzyme responsible for the maintenance of cellular homeostasis and the endosome/lysosome system in all cells. While V-ATPase is known for its maintenance of the pH homeostasis observed in the endosomal system, it is also responsible for numerous other activities. Receptor recycling relies upon the acidification of early endosomes to dissociate ligands from their receptors. For example, the Wnt and Notch signaling pathways rely upon V-ATPase mediated endosomal acidification to activate receptors for their proper function in cells.^{240–242} V-ATPase also regulates metabolic signaling through amino acid sensing that can cause the upregulation of mechanistic target of rapamycin complex 1 (mTORC1). Amino acid sensing by V-ATPase is dependent upon its interaction with Ragulator (a heteropentameric complex of RagGTPases), which is strengthened upon amino acid starvation.²⁴³ Proteases in the endolysosome and secretory systems require acidification of their compartments before they are able to modify host receptors and other proteins into their active forms.^{244–246} Trafficking of endosomes and their fusion with lysosomes or phagosomes is also dependent upon the activity of V-ATPase although the mechanism is not acidification dependent and still under investigation.^{247,248}

In addition to the general activities of V-ATPase, V-ATPase also has integral activities in many specialized cells. The loading of secretory vesicles with neurotransmitters requires V-ATPase driven acidification of the vesicles to work a proton-neurotransmitter antiporter to move

neurotransmitters into the vesicle.²⁴⁹ Hormones like insulin and thyroxine require V-ATPase activity for their processing and secretion from cells.^{250,251} Localization of V-ATPase to the plasma membrane is integral for V-ATPase activity in a number of cells including osteoclasts, renal intercalated cells, and epididymal clear cells. Osteoclasts move V-ATPase to the plasma membrane to aid in the catabolism of bone through the extrusion of protons into the extracellular matrix of bone.²⁵² Renal intercalated cells utilize plasma membrane V-ATPase to maintain proper blood pH through the secretion of acid into the urine.^{253,254} Epididymal clear cells utilize plasma membrane V-ATPase to maintain low pH in the seminal fluid that is used for sperm maturation and storage.^{253,254}

1.2.6 V-ATPase and Disease

As might be expected for a complex intimately involved in many integral function, dysregulation of V-ATPase is associated with a host of diseases. Mutations in the a4 and B1 subunits have defective acid secretion from renal intercalated cells that results in renal tubular acidosis.²⁵⁵ Knockouts of the a4 isoform in mice result in deafness and enlarged endolymphatic fluid compartments.²⁵⁶ Mutations in the E1 isoform can lead to defects in sperm maturation, though mutations in the B1 subunit can be covered by increased B2 isoform expression.^{207,257} Defects in bone resorption due to mutations in the a3 and d2 subunits are known causes of osteopetrosis in humans and rodents.^{214,258} Mice with knockouts of the a3 gene are also defective in insulin secretion, though cells are still able to process insulin into its active form.²⁵¹ Mutations in Ac45 have been identified in patients with immunodeficiency with hepatopathy and neurocognitive impairment.²¹⁶ Defects in the H subunit result in osteoporosis and short stature in humans caused by the upregulation of matrix metalloproteases and by upregulation of V-ATPase activity.²⁵⁹

Plasma membrane localization of V-ATPase can be the cause of severe disease phenotypes when specifically dysregulated during osteoporosis and metastatic cancer. Upregulation of the V-ATPase at the plasma membrane in osteoclasts causes increased bone resorption and remodeling and subsequent loss of bone mass that leads to frailty.²⁶⁰ The involvement of V-ATPase in metastatic cancer is multifaceted. Increased glycolysis within tumor cells causes a concomitant decrease in cellular pH, which V-ATPase is able to ameliorate by pumping protons into the extracellular space.²⁶¹ The decrease in extracellular pH causes the degradation of the extracellular matrix through destabilization of protein stability in low pH and the activation of secreted

proteases that degrade the matrix.²⁶² Cancer metastasis is tied to the localization of V-ATPase to the plasma membrane in several models though conflicting data also exists.^{196,225,226} The upregulation of plasma membrane localization in non-metastatic cells increases the metastatic nature of the cells.²⁶³ This activity is also entwined with the epithelial-mesenchymal transition of cancer cells, though the exact mechanism of this activity is still under investigation with the archazolid class of V-ATPase inhibitors.²⁶⁴ V-ATPase subunits have been identified as integral in the infection of influenza viruses, flaviviruses, and human immunodeficiency virus (HIV) through siRNA screening.^{265,266} Subunit c has been identified as integral for infection of all three types of viruses and subunits b, d, A, and B have been identified as necessary in various contexts.

1.2.7 V-ATPase Inhibitors

Multiple classes of V-ATPase inhibitors have been identified with both natural product (**Fig. 1.4**) and synthetic inhibitors (**Fig. 1.5**) demonstrating a variety of interesting activities. V-ATPase appears to be a common target of secondary metabolites developed by bacteria and other organisms and likely plays a defensive role for these species. For example, modulation of host defenses by V-ATPase inhibitors like the protein SidK in *L. pneumonia* also appear to function in a protective role for intracellularly-oriented parasites.²⁶⁷ The development of synthetic derivatives of these natural products has led to the identification of novel selectivity between different V-ATPase isoforms that is not found in nature. Furthermore, several inhibitors have demonstrated the ability to separate on-target activity against V-ATPase from the associated cytotoxicity. No discussion of V-ATPase inhibitors can begin without mentioning the bafilomycin A1, which is the most recognized member of the plecomacrolide class of inhibitors.

1.2.8 Natural Products Inhibitors

The most well-known V-ATPase inhibitor class is the plecomacrolides, of which bafilomycin A1 and concanamycin A are the most prominent members. Plecomacrolides are have 16-18 member macrolactone rings with conjugated diene units and a hemiacetal sidechain.²⁶⁸ Bafilomycin A1 is the standard-bearer used for all types of V-ATPase related studies and was the first specific inhibitor of V-ATPase identified.²⁶⁹ Bafilomycin A1 and concanamycin A interact with the c subunit of V-ATPase in the proteolipid ring and bind at the interface of two of the c subunits and the a subunit.^{270,271} Binding at this site blocks the proton channel formed by the

subunits and inhibit proton flux. Bafilomycin is used widely to interrogate the necessity of V-ATPase and endosomal acidification to pathways in cancer, viral infection, osteoporosis, autophagy, in addition to many others.^{272–275} Bafilomycin A1 has been used to inhibit alphaviruses, influenza virus, flaviviruses, filoviruses, and picornaviruses amongst numerous other viruses.^{180–184} Bafilomycin A1 has been evaluated as a potential therapeutic numerous times but has failed due to high toxicity in *in vivo* models and off-target effects.^{276,277}

The archazolid class are another identified macrolactone class of V-ATPase inhibitor that has been studied mainly as a novel inhibitor of cancer metastasis. Archazolid A and B are myxobacterial products with a similar macrolactone core seen in the plecomacrolides that differ by the presence or absence of a methyl group.^{278,279} The archazolids and binds to a similar region of the c subunit of V-ATPase proteolipid ring though they to bind on the lipid face of a single c subunit instead of between subunits.^{279–281} The archazolids have been used as inhibitors of cancer cell metastasis through interference with signaling pathways dependent upon membrane-related Ras and Rac activity.^{264,282,283} Archazolid treatment of M1 macrophages increases the secretion of tumor necrosis factor α through NF κ B and SAPK/JNK activation that can lead to the suppression of tumor cell viability.²⁸⁴ Archazolid B also potently inhibits Influenza virus infection but the selectivity index is 3-8 and not very different from the activity demonstrated by the plecomacrolide class.¹⁸⁰

The iejimalides are another class of macrolide V-ATPase inhibitors but has represented a slightly different activity profile from the plecomacrolides.^{285,286} Iejimalides are derived from marine microorganisms and have demonstrated potent activity against both V-ATPase and actin polymerization, though these activities may be intertwined.²⁸⁷ Iejimalides have demonstrated picomolar activities against V-ATPase activity and causes cancer cell apoptosis through S phase arrest, though this mechanism appears to vary by cell type.^{288,289} Modification of the iejimalide framework has indicated that modification of the core macrocyclic structure is not tolerated but the *N*-formyl-L-serine tail can be modified to enhance potency and cell line selectivity.^{290–292} While a wealth of anticancer data is available for the compound, no antiviral work has been done with the iejimalide class. Iejimalides would likely produce similar antiviral profiles to those of the plecomacrolide and archazolid classes.

Benzolactone enamides contain a significantly different macrolactone superstructure from the previously discussed V-ATPase inhibitors and have demonstrated novel activities. The natural

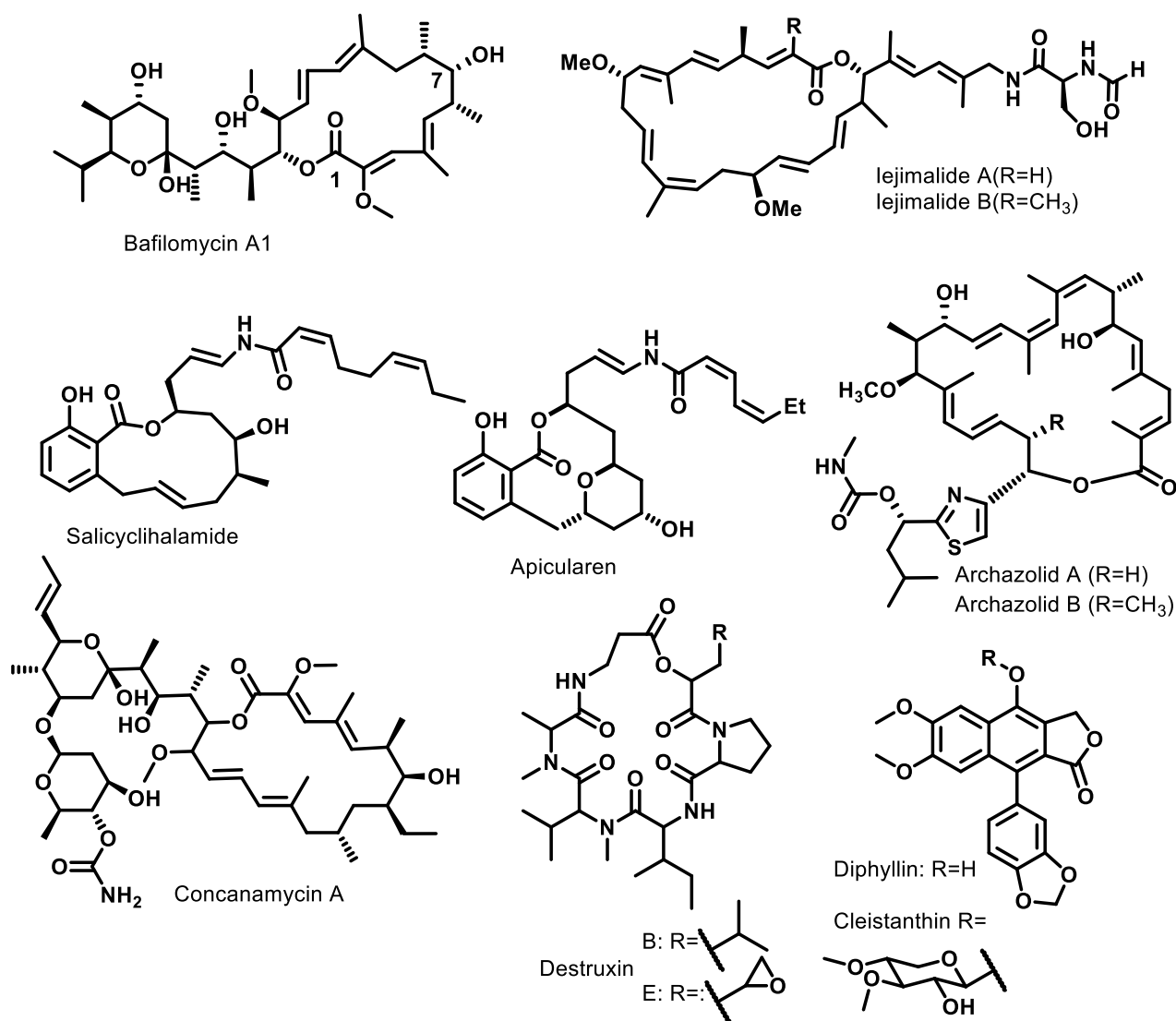


Figure 1.4 Natural Product V-ATPase inhibitors

products salicylihalamide A, apicularen, oximidines I and II, lobatamides A-f and, and cruentaren A are structurally different benzolactone enamide V-ATPase inhibitors isolated from separate marine sources.²⁹³ All benzolactone enamides demonstrate unprecedented selectivity for V-ATPase from mammalian sources and are ineffective against V-ATPase from yeast and insects.²⁹⁴ The two most well characterized benzolactone enamides are salicylihalamide and apicularen. Both of these compounds bind to the V_0 domain of V-ATPase at a different site from those occupied by other macrolactone inhibitors.^{279,295,296} Apicularen has been used as an anticancer agent in human colon cancer models where it induces caspase-independent apoptosis through destabilization of the microtubule network.^{297,298} Apicularen also changes to response of lipopolysaccharide treated monocytes through repression of cytokine secretion in a mechanism similar to that of bafilomycin and archazolid.²⁹⁹ Salicylihalamide has also demonstrated potent anticancer activity though more focus has been paid to its synthetic analogs.³⁰⁰

Destruxins are a class of cyclodepsipeptides isolated from fungi that have a wide-range of functions including potent and specific V-ATPase activity. Destruxin B was initially identified as an inhibitor of EGF and insulin response in a mechanism similar to bafilomycin A1 and subsequently identified as a V-ATPase inhibitor.³⁰¹ Destruxins B and E disrupt actin organization and V-ATPase localization in polarized osteoclasts.^{302,303} Destruxin B has been identified as an inhibitor of *E. Hirae* V-ATPase with a 5 μ M IC_{50} value.^{304,305} Multiple destruxins were identified as inhibitors of yeast V-ATPase and destruxin E had an IC_{50} value of 400 nM.^{305,306}

Several proteins identified in bacteria and plants have been identified as inhibitors of V-ATPase with modes of inhibition and selectivity different from small molecule inhibitors. The *Legionella pneumophila* effect protein SidK is an inhibitor of V-ATPase induced acidification in human macrophages and binds to the A subunit.^{267,307} V-ATPase activity is not entirely inhibited by SidK but it does reduce the affinity of subunit A for ATP.^{267,307} A second *L. pneumophila* WipB was identified as interacting with V-ATPase subunits B and d1 and inhibited cellular lysosomal function.³⁰⁸ Pea Albumin 1 subunit b is a novel peptide inhibitor of V-ATPase isolated from pea seeds that is insect-specific.³⁰⁹ It is also the first known inhibitor to bind to subunit e, through which it interacts with c subunits and prevents the rotation of the proteolipid ring.³¹⁰

1.2.9 Synthetic Inhibitors

Extensive structure-activity relationships have been conducted on bafilomycin A to identify the key structural features necessary for V-ATPase inhibition. A main problem with small-molecule, natural product V-ATPase inhibitors was their lack of specificity for specific isoforms of the complex. Exploration of the structure-activity relationships between bafilomycin A1 and its V-ATPase activity led to the identification of a core area of the structure that was eventually modified into several classes of indolyl inhibitors.²⁷⁵ The C1-C7 subunit was deemed critical to bafilomycin's V-ATPase activity and became the focus of studies that resulted in the derivative SB242784. SB242784 is the first identified selective V-ATPase inhibitor, with 40-fold greater potency against V-ATPase isolated from human osteoclasts over V-ATPase isolated from human kidneys.^{311,312} The binding site of SB242784 has been studied by classical competition and novel spin-labelling technique and is very similar to that of bafilomycin A1 and concanamycin A.³¹³ However, these studies have not identified the interactions that lead to the selectivity of SB242784 though they claim their understanding of the a subunit contributions are incomplete. Interestingly, *in vivo* studies of SB242784 in an ovariectomized rat osteoporosis model indicated the inhibitor was as effective as estrogen therapy at preventing bone loss.³¹⁴ SB242784 was also 1,000-fold more potent against V-ATPase isolated from rat osteoclasts than V-ATPase isolated from liver or kidney cells.³¹⁴ Further studies comparing the V-ATPase inhibition in human osteoclast and other cell models have not demonstrated the same isoform preference though this may be due to compensation of other isoforms present in osteoclasts lysosomes (a1 instead of a3) for the inhibited enzyme.³¹⁵ Unfortunately, SB242784 has been reported to cause body weight decrease, increase plasma total cholesterol, and decrease blood glucose in another rat osteoporosis model.²⁶²

Further derivatization of the SB242784 class of indolyl inhibitors identified NiK-12192 as a novel derivative of SB242784 with a more rigid linker between the indole and amide groups.³¹⁶ NiK-12192 is a potent inhibitor of V-ATPase activity in bovine chromaffin granules and human osteoclasts.³¹⁷ NiK-12192 can also block cancer cell proliferation and synergize with topoisomerase inhibitors to potentiate their effects in colorectal carcinoma models.^{318–321}

Several other synthetic V-ATPase inhibitors have been identified with isoform selectivity and interesting properties that are still under investigation. FR167356 was identified by random screening of a chemical library using chicken osteoclasts as a selective inhibitor of V-ATPase activity. FR167356 inhibited osteoclast V-ATPase activity (170 nM) 7-fold more than lysosomal

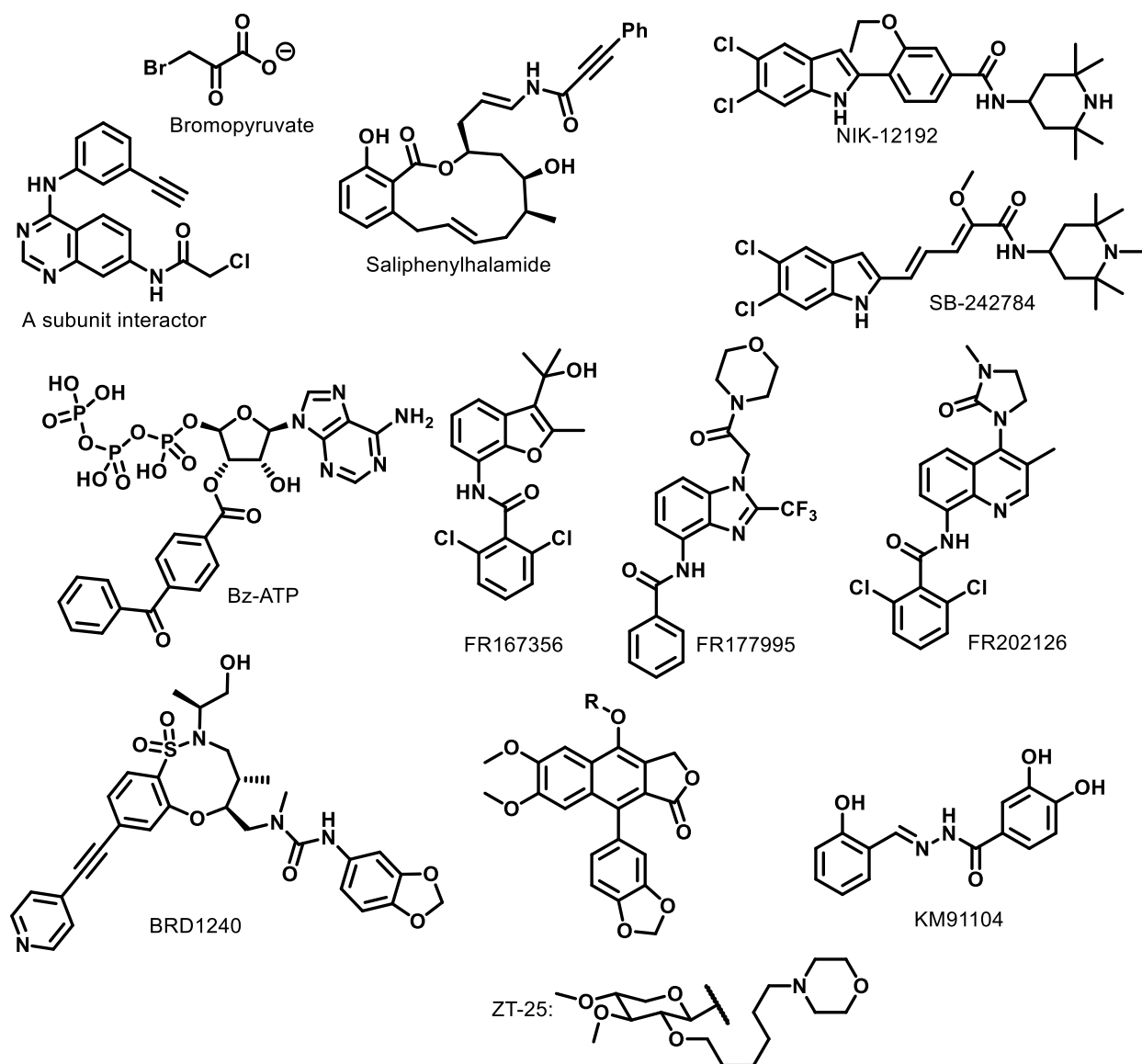


Figure 1.5 Synthetic V-ATPase inhibitors

V-ATPase (1200 nM) though it demonstrated similar activities against V-ATPase isolated from macrophages (220 nM) and kidneys (370 nM).³²² Studies in ovariectomized rat osteoporosis models have indicated that FR167356 restored bone mineral density and had none of the adverse side effects observed in SB242784-treated rats.²⁶² FR167356 has also been used to inhibit distant metastasis of mouse B16-F10 melanoma cells that express plasma membrane localized $\alpha 3$ V-ATPase isoforms in a mouse model.³²³ FR177995 inhibits V-ATPase activity, blocks bone loss, and ameliorates adjuvant-induced arthritis in rats.³²⁴ FR202126 was identified as a V-ATPase inhibitor and used to prevent osteoclast-mediated alveolar bone destruction in rat models and bone loss in a mouse breast cancer model.^{325–327} A benzohydrazide inhibitor of the interaction between $\alpha 3$ and B2 isoforms, KM91104, was identified by library screening library and blocked osteoclast bone resorption *in vitro*.³²⁸ KM91104 treatment of primary human hepatic stellate cells downregulates the fibrogenic profile through activation of AMPK.³²⁹

Saliphenylhalamide (Saliphe) is derived from the benzolactone enamide salicylhalamide and has shown potent V-ATPase activity and an improved selectivity index not before seen. Saliphe was selected from synthetic derivatives of salicylhalamide A because of ease of synthesis, activity against V-ATPase similar to salicylhalamide, and differential effects on tumorigenic and human cells lines.³⁰⁰ Saliphe has been used as a probe to interrogate the role of V-ATPase in trafficking of endosomal and synaptic vesicle exocytosis pathways in normal cells and neurons.^{330,331} Saliphe has potent activity against influenza virus infection and separated its anti-influenza activity from the cytotoxicity up to 61-fold, as opposed to a factor of 0-8 for the plecomacrolides and archazolid.^{180,332} Saliphe also protected 62.5% of mice from influenza virus challenge while bafilomycin showed no protection. In addition to activity against influenza viruses, Saliphe has demonstrated activity against Zika virus and human papilloma virus infection.^{333,334} Unfortunately, Saliphe impairs innate immune responses by influenza virus infected macrophages and thus may prevent immune responses to infection *in vivo*.³³⁵

Several covalent inhibitors of V-ATPase have been identified that bind to new pockets on V₁ domain of V-ATPase. The anticancer agent 3-bromopyruvate was found to inhibit V-ATPase-induced dye uptake that was dependent on the modification of a cysteine residue on V-ATPase, supporting the idea that it was covalently modifying the enzyme.³³⁶ The photoactivated nucleotide analog 3'-O-(4-benzoyl)benzoyl-adenosine 5'-triphosphate (BzATP) can inhibit V-ATPase by covalent modification of a non-catalytic nucleotide binding site on the B subunit.²⁰⁰ Most

interestingly, a screen of a library of covalent kinase inhibitors identified a molecule that covalently bound to the non-homologous region of the A subunit of the V₁ domain.²⁰¹ The binding of the inhibitor appeared to be specific to Cys138 and dependent upon electrophile and scaffold.²⁰¹ The compound was demonstrated to inhibit cellular acidification driven by V-ATPase in a roundabout way and more information is eagerly awaited.²⁰¹ BRD1240 was recently identified as a putative inhibitor of V-ATPase from a screen of autophagy modulators.³³⁷ The mechanism of inhibition is unknown but involved different kinetics than bafilomycin A1.³³⁷

1.2.10 Diphyllin and Related Lignans

Diphyllin is an aryl-naphthalene lignan isolated from plant species that have demonstrated a wide range of bioactivities. Natural extracts of plants like *C. collinus*, *J. procumbens*, *H. bucharicum*, and numerous others that contain diphyllin have been used as therapeutic and toxic mixtures for thousands of years. Diphyllin from natural sources possesses antiviral, anticancer, and antileishmanial activity in addition to general cytotoxicity.^{338–341} Eleven years ago, the mechanism for much of this activity was explained in diphyllin's potent inhibition of V-ATPase activity in an osteoclast model of bone resorption.³⁴² Diphyllin represents a significantly different chemotype than previous inhibitors of V-ATPase activity and has generated renewed interest in the compound. Diphyllin has been shown to reduce the proliferation of gastric adenocarcinoma and esophageal cancer cells through antagonism of the mTORC1/HIF-1 α /VEGF pathway (which is caused by V-ATPase inhibition).^{343,344} Most interestingly, diphyllin has also been identified as an inhibitor of influenza, dengue and feline coronavirus infection in cellular models.^{345,346}

Diphyllin glycosides have also demonstrated a wide range of biological activities and are being investigated for multiple types of therapies. The natural product cleistanthin is xylopyranose glycoside derivative of diphyllin at the phenol position that has demonstrated potent V-ATPase inhibition in biochemical assays and cytotoxicity in a number of cancer cell lines.^{347–349} Several natural derivatives of cleistanthin have also been identified as V-ATPase inhibitors with antiproliferative activity.^{348,350} Several groups have worked to modify the glycoside moiety of cleistanthin and have identified an alkylamino derivative of the diphyllin glycoside, ZT-25, with improved potency against V-ATPase activity and antiproliferative effects in the HepG2 liver cancer cell model.^{351,352} Further work with ZT-25 demonstrates that the observed selective cytotoxicity in cancer cells occurs through mitochondrial-associated mechanisms.³⁵³ A class of

arabinopyranosyl diphyllin glycosides (phyllanthusmins) isolated from *P. poilanei* have demonstrated potent cytotoxicity toward HT-29 human colon cancer cells though the mechanism of toxicity was not entirely identified.³⁵⁴ Derivatives of the phyllanthusmin glycoside and lactone moieties have recently shown improved antiproliferative effects against colon, breast, and ovarian cancer cell lines though the mechanism of action is still poorly understood.³⁵⁵

1.3 Research Focus

V-ATPase inhibitors have not entered the clinic for the treatment of any disease, especially viral diseases. The lack of clinical treatments for EBOV infection represents a new possible avenue for the use of V-ATPase inhibitors in the clinic if selectivity can be added to the potent inhibition of V-ATPase by current inhibitors. The novel selectivity between V-ATPase activity and cytotoxicity identified for diphyllin represents a never-before-seen opportunity for the development of a selective V-ATPase inhibitor and could be useful in the treatment of EVD. However, little work has been done to identify areas of diphyllin's structure that are important for its interactions with V-ATPase (its V-ATPase pharmacophore). Due to the size and complexity of V-ATPase, ligand-based drug design was determined to be the best method for identifying which areas of the diphyllin scaffold define the pharmacophore. Therefore, the goal of this work was to create novel derivatives of diphyllin that improve both the potency and therapeutic selectivity of the structure. To accomplish the objective, a set of novel assays were designed to identify diphyllin derivatives that selectively inhibited EBOV infection through activity against V-ATPase. These assays identified modification of the phenol moiety as being highly tolerant of additional groups while the lactone ring was not. Further derivatization of the phenol group allowed for increases in selectivity and potency that have not been seen in previous V-ATPase inhibitors. Therefore, modification of the phenol ring may be the best method to introduce modification of the diphyllin pharmacophore and the development of novel EBOV therapies.

CHAPTER 2. PHENOTYPIC PRIORITIZATION OF DIPHYLLIN DERIVATIVES THAT BLOCK FILOVIRAL CELLULAR ENTRY BY VACUOLAR (H⁺)-ATPASE INHIBITION

2.1 Abstract

Many viruses utilize endosomal pathways to gain entry to cells and propagate infection. Sensing of endosomal acidification is a trigger for release of many virus cores into the cell cytosol. Previous efforts with natural product inhibitors of the V-ATPase have been shown to block endosomal acidification and affect viral entry albeit with limited selectivity. Herein, four series of novel derivatives of the V-ATPase inhibitor diphyllin were synthesized to assess their potential for enhancing potency and selectivity toward filoviral entry inhibition. Derivatives that suitably blocked Ebola virus entry were further evaluated for inhibition of endosomal acidification and cytotoxicity in human cell models, as well as inhibition of isolated human V-ATPase activity. Finally, three compounds showed significant selectivity indices for the inhibition of infection of primary human macrophages by wild-type Ebola virus.

2.2 Introduction

The *Filoviridae* family of viruses are highly contagious, lethal viruses that cause severe hemorrhagic fever in humans and primates.¹⁻³ The *Filoviridae* family consists of large, filamentous, negative-strand RNA viruses that are grouped into *Ebolavirus* (EBOV), *Marburgvirus* (MARV), and *Cuevavirus* genera. Viruses from the EBOV and MARV genera are responsible for outbreaks that have up to 90% fatality, including the recent outbreak in West Africa that resulted in over 28,000 reported cases and 11,317 deaths.³⁵⁶ Efforts are underway to develop novel EBOV therapies, including discovery of small molecule inhibitors,³⁵⁷⁻³⁶² repurposed drugs,³⁶³⁻³⁶⁸ and vaccines.³⁶⁹⁻³⁷² Currently, there are no approved therapeutic measures for the treatment of filovirus infections but the development of a vaccine is being prioritized by the FDA and a promising viral polymerase inhibitor has also recently advanced in development.³⁷³

Filoviruses, like many other viruses, utilize the acidification of endosomes during their maturation to facilitate cellular entry.^{180,374-376} Many cellular infections begin when individual virions are taken into cells by one of several mechanisms of endocytosis. As the virion-containing

endosomes mature toward lysosomes, the luminal pH of the endosome decreases. EBOV requires this acidification to trigger penetration of the endosomal membrane by the filoviral glycoprotein to release the virus capsid into the cytosol and initiate replication. For enveloped viruses, penetration involves fusion of the virion's membrane with that of the endosome. Additionally, for filoviruses, pH-dependent endosomal proteases need to cleave the membrane glycoprotein into a fusion-capable form that interacts with the endosomal receptor NPC1.³⁷⁷ Inhibitors of endosomal acidification are therefore potentially anti-filoviral and broad-spectrum anti-viral compounds.

A primary host factor responsible for endosomal acidification is the multi-subunit enzyme vacuolar (H⁺)-ATPase (V-ATPase), whose role is to couple proton transport across cellular membranes with the hydrolysis of ATP.¹⁸⁸ In addition to endosomal acidification, many cellular and physiological processes are associated with V-ATPase function, including roles in renal pH homeostasis, osteoclast bone remodeling, and sperm maturation.^{188,284,378} Different forms of V-ATPase are present in renal, neuronal, osteoclast and cancer cells along with the V-ATPase found in the endosomal membranes.³⁷⁹ Dysregulation of specific isoforms have been associated with diseases, including osteoporosis, metastatic cancers, male infertility and renal acidosis.³⁸⁰ Disease indications such as Ebola infection where treatment for acute conditions could justify the pursuit of V-ATPase inhibition. This case would be valid if useful therapeutic selectivity can be exhibited through structural modifications of the inhibitor chemotype.

Many natural product inhibitors of V-ATPase have been identified with a majority being macrocyclic lactones. Most of these natural inhibitors, such as bafilomycin A1 (Baf), have historic utility as cellular probes but lack the needed therapeutic selectivity to serve as drug leads due to off-target effects.^{277,293} Diphyllin is an aryl-naphthalene lignan and represents the only known phenylpropanoid-derived V-ATPase inhibitor to date.⁶

Cellular activities established for diphyllin have shown useful anti-tumor and anti-osteoclastic activity,^{6,343} as well as anti-viral activity in early testing using influenza and Dengue virus models.^{265,381} The inhibition of pH-dependent virus infection and lack of cytotoxicity in tested cell lines prompted a feasibility study of diphyllin as a scaffold for a medicinal chemistry approach to develop selective V-ATPase inhibitors as potential broad-spectrum anti-viral agents. Two major questions about the diphyllin scaffold are addressed in this initial structure-activity work: a) if the biochemical and endosomal pH inhibition can be predictive of filoviral entry

inhibition, and b) is there potential for enhancing V-ATPase inhibition without increasing risks of cytotoxicity?

There are advantages and disadvantages to host-specific anti-viral agents and an initial challenge is to establish therapeutic selectivity.²² Herein, we report the identification of several novel diphyllin derivatives that are potent inhibitors of V-ATPase and EBOV infection of macrophages by phenotypic screening of a small library of diphyllin derivatives. The compounds were screened as inhibitors of EBOV pseudotype virus entry and endosomal acidification. Compounds selected from these screens were ranked by their potency against EBOV entry and dose selectivity of cellular endosomal acidification versus cytotoxicity. The positive hits were further assayed for the ability to inhibit V-ATPase activities in isolated vesicles. Three compounds were then evaluated on their ability to inhibit MARV cellular entry and replication-competent EBOV infection of primary human macrophages (PHMs) due to their importance as a site of filovirus infection.³⁸² Overall, this approach demonstrates the use of phenotypic screening to identify more selective V-ATPase inhibitors that block filoviral infection with reduced cytotoxicity.

2.3 Experimental Methodology

2.3.1 Biological Assays

Cells- 293FT cells (catalog number R700-07; Thermo), HEK-293 cells (ATCC® CRL-1573™), Vero cells and HeLa cells were maintained in Dulbecco modified Eagle medium (Fisher Scientific) supplemented with 10% fetal bovine serum (Atlanta Biologicals) (referred to here as complete medium). Primary human macrophages were differentiated from the buffy coat fraction of human blood (from the South Texas Blood and Tissue Center) according to previously published protocols.³⁵⁷ Briefly, mononuclear lymphocytes were isolated using LeucoSep tubes (Fisher Scientific), resuspended in Iscove modified Dulbecco medium (IMDM, Fisher Scientific), and plated in 96-well plates (50,000 cells per well). After the cells were allowed to adhere for 1 h, unattached cells were washed off using IMDM. Attached monocytes were allowed to differentiate into macrophages for 7 to 8 days in IMDM containing 2% heat-inactivated human serum (Corning Inc.), 100 U/ml penicillin, 100 µg/ml streptomycin, 1× nonessential amino acids (Fisher Scientific), 50 µM 2-mercaptoethanol (Fisher Scientific), and 800 U/ml human macrophage colony-stimulating factor (BioLegend). Adherent monocytes (PHMs) were washed, and the medium was

replaced on days 2 and 6 while the cells were differentiating. All cells were kept at 37°C in a humidified incubator with 5% CO₂.

Pseudovirus assays- This work was completed by Manu Anantpadma in the Davey lab at Boston University. Recombinant VSV pseudovirions expressing Zaire EBOV GP were produced as described previously.^{238,357} Briefly, virions expressing the EBOV GP were formed in HEK-293T cells by transfection of cells with the EBOV GP-expressing plasmid 24 h before transduction with VSVΔG-EGFP virions. Supernatant was collected from 48-72 h and filtered through a 0.45 μm filter to yield new pseudotyped virions. Viral titer was determined by exposure of HEK-293T cells to the new pseudotyped virions and analyzing EGFP expression 24 h later by flow cytometry. HeLa cells were seeded in a 384-well plate (4000 cells/well) and allowed to adhere overnight in complete medium at 37°C with 5% CO₂. Cells were treated with inhibitors at varying concentrations (<1% DMSO) for 1 h before the cells were infected with EBOV or MARV pseudovirus. After 24 h, cells were fixed with formalin and washed three times with phosphate-buffered saline. Nuclei were then stained with Hoechst stain at a concentration of 1:10,000. Cells were imaged using a Nikon Ti eclipse robotic microscope and analyzed with CellProfiler software. The number of infected cells (GFP-expressing cells) was divided by the total number of cells (Hoechst-stained nuclei) to determine the rate of infection. The infection rate in vehicle-treated cells was used to determine the ratio of infection in the drug-treated cells. IC₅₀ data are reported as the concentration at which 50% of the viral infection was inhibited relative to the vehicle-treated cells with the standard deviation for 6 individual experiments.

Filovirus-GFP infection- This work was completed by Manu Anantpadma in the Davey lab at Boston University. Live EBOV were produced as previously described.³⁵⁷ In brief, Zaire Ebola virus Mayinga strain with an insertion of green fluorescent protein (GFP) between the nucleoprotein (NP) and VP35, a kind gift of Heinz Feldmann (NIH, Rocky Mountain Laboratory, Hamilton, MT). All work was done in a biosafety level 4 (BSL4; protection level 4) lab at the Texas Biomedical Research Institute.

PHMs were treated with inhibitors at varying concentrations (<1% DMSO) for 1 h before the cells were infected with EBOV-GFP. After 24 h, cells were fixed with formalin and washed three times with phosphate-buffered saline. Nuclei were then stained with Hoechst stain at a concentration of

1:10,000. Cells were imaged using a Nikon Ti eclipse robotic microscope and analyzed with CellProfiler software. The number of infected cells (GFP-expressing cells) was divided by the total number of cells (Hoechst-stained nuclei) to determine the rate of infection. The infection rate in vehicle-treated cells was used to determine the ratio of infection in the drug-treated cells. IC₅₀ data are reported as the concentration at which 50% of the viral infection was inhibited relative to the controls with the standard deviation for 6 individual experiments.

Inhibition of cellular vesicle acidification- HEK-293 cells were seeded into clear 96-well plates (Falcon) at 10,000 cells/well and allowed to grow for 18-20 h at 37°C and 5% CO₂ in complete medium. Cells were treated with inhibitors at varying concentrations (<2% DMSO) for 4 h before the addition of 1 µg/ml acridine orange in DMEM for 10min before media is removed and cells washed twice with 1x PBS. Fluorescent readings were taken with a Biotek Synergy 4 microplate reader using the following filter pairings: 485/20 nm-530/30 nm and 485/20 nm-665/7 nm. Data are shown the 665 nm/530 nm emission ratio for 12 individual experiments. IC₅₀ data are reported as the concentration at which 50% of the 665 nm/ 530 nm ratio was inhibited relative to the vehicle-treated control with the standard deviation. All compounds were also assayed without the acridine orange dye to determine if background fluorescence was interfering with the assay. This background fluorescence was determined by washing cells with 1x PBS twice and reading in both fluorescence wavelengths and subtracted from the total fluorescence in both channels before determining the fluorescent ratio after dye treatment.

Aggregation screening for cellular endosomal acidification- All hits from the cellular endosomal acidification assay were further screened at 10µM under two different conditions to eliminate any compounds that inhibit the assay by aggregation. The first condition was the addition of 0.1% Triton X-100 as inhibitors were added to HEK-293 cells. The assay was run for 4h before 1 µg/ml acridine orange in DMEM was added with 0.1% Triton X-100 to additionally inhibit any aggregation between dye and inhibitors. The second condition was to add inhibitors to assay media and centrifuge them for 10min at 14,000xg to remove aggregates before adding inhibitors to HEK-293 cells. The assay was conducted as above.

Time-dependent inhibition of cellular vesicle acidification- HEK-293 cells were seeded into clear 96-well plates (Falcon) at 10,000 cells/well and allowed to grow for 18-20 h at 37°C and 5% CO₂ in complete medium. Cells were then treated with a dilution series of diphyllin and incubated at 37°C and 5%CO₂ until 1 µg/ml acridine orange was added at 2, 4, and 8h. After 10min incubation the dye, cells were washed with 1x PBS twice and 100µl of PBS was added. Fluorescent readings were taken with a Biotek Synergy 4 microplate reader using the following filter pairings: 485/20 nm-530/30 nm and 485/20 nm-665/7 nm. Data are shown as mean± standard error of the mean of the 665 nm/530 nm emission ratio for 4 individual experiments.

Measurement of intracellular endosomal pH- HEK-293 cells were seeded into clear 96-well plates (Falcon) at 10,000 cells/well and allowed to grow for 18-20 h at 37°C and 5% CO₂ in complete medium. Cells were then incubated with 0.5 mg/ml FITC-dextran for 3 h. The dextran was then removed and the cells washed once with 1x PBS before the addition of inhibitors (<2% DMSO) in DMEM for 4 h. Cell were then washed 1x with PBS and read with a Biotek Synergy 4 microplate reader with the 485/20 nm and 380/20nm excitation filters and the 530/30 nm emission filter. The 380 nm induced emission was subtracted from the 485 nm induced emission to normalize the results for dye concentration. Data are shown as mean± standard error of the mean of the normalized 530nm emission for 12 individual experiments. FITC-dextran fluorescence was standardized in vehicle-treated cells using HEPES-phosphate buffers with 10 µg/ml of nigericin at pH values from 4-8 for a standard curve. The ionophore nigericin was added to equilibrate the cell's internal pH with the external buffer pH.

Measurement of cytosolic pH- HEK-293 cells were seeded into clear 96-well plates (Falcon) at 10,000 cells/well and allowed to grow for 18-20 h at 37°C and 5% CO₂ in complete medium. Cells were then treated with inhibitors at varying concentrations (<2% DMSO) for 3.5 h before the addition of 10 µg/ml of BCECF-AM. After 30 min, cells were washed twice with 1xPBS before reading the plate with a Biotek Synergy 4 microplate reader with the 485/20 nm and 380/20nm excitation filters and the 530/30 nm emission filter. The 380 nm induced emission was subtracted from the 485 nm induced emission to normalize the results for dye concentration. Data are shown as mean± standard error of the mean of the normalized 530 nm emission for 12 individual experiments. BCECF-AM fluorescence was standardized in vehicle-treated cells using HEPES-

phosphate buffers with 10 µg/ml of nigericin at pH values from 4-8 for a standard curve. The ionophore nigericin was added to equilibrate the cell's internal pH with the external buffer pH.

Determination of cytotoxicity- HEK-293 cells were seeded into clear 96-well plates (Falcon) at 10,000 cells/well and allowed to grow for 18-20 h at 37°C and 5% CO₂ in complete medium. Cells were then treated with inhibitors at varying concentrations (<2%DMSO) for 72 h. 0.5 mg/ml 3-(4,5-Dimethylthiazol-2-yl)-2,5-Diphenyltetrazolium Bromide (MTT) was added to cells for 4 h before quenching the reaction with acidic isopropanol (10% Triton, 0.1 M HCl). After incubation for 24 h at room temperature, the absorbance at 570 nm and 650 nm was measured using a Biotek Synergy 4 microplate reader. The absorbance at 650 nm subtracted from the 570 nm to normalize data to any residual media fluorescence. Data are shown as mean± standard error of the mean of the normalized 570nm absorbance. CC₅₀ data are reported as the concentration at which cell viability was 50% relative to the controls with the standard deviation for 12 individual experiments. HeLa cytotoxicity was determined as shown previously.³⁵⁷ In brief, HeLa cells plated in 96-well plates (20,000 cells/well) were treated with the compounds at different concentrations in a 100 µl final volume. After 24 h of incubation with the compounds, cytotoxicity was measured using a CytoTox-Fluor cytotoxicity assay (Promega) per the manufacturer's protocol.

PHM cytotoxicity was determined as shown previously.³⁵⁷ In brief, PHMs were treated with the top three diphyllin derivatives at varying concentrations (<1% DMSO). After 24 h of incubation with the compounds, cytotoxicity was measured using a CytoTox-Fluor cytotoxicity assay (Promega) per the manufacturer's protocol for 3 individual experiments.

HEK-293 vesicle isolation- The following isolation and assays were performed similar to that previously described.^{383,384} In brief, cells were grown to confluency with complete medium in a 175 cm² flask (Corning) before growth media was removed and replaced with serum-free DMEM for 2 h. 1 µM FCCP in DMEM was then added for 15 min before cells were scrapped from the plate and pelleted at 1000xg for 5min. The media was discarded and cells were re-suspended in HEK assay buffer (20 mM HEPES, 5 mM Glucose, 50 mM Sucrose, 50 mM potassium chloride, 90 mM potassium gluconate, 1 mM EGTA, PierceTM protease inhibitor Mini tablet, pH=7.4) were then lysed by passage through a 22g needle 10-15 times. Lysates were then centrifuged at 10,000xg for 30 s with a Beckman Coulter Microfuge 22R centrifuge. The supernatant was removed and

centrifuged at 14,500xg for 20 min. The remaining supernatant was discarded and the pellet was resuspended in HEK assay buffer.

Inhibition of acridine orange quenching assay-The vesicle mixture was resuspended in HEK assay buffer+1%BSA+6 μ M acridine orange and split into fractions with the protein concentration being 100 μ g/mL and transferred to a clear 96-well plate. The isolated vesicles were pretreated with inhibitors for 60 min at 37°C. Fluorescent readings were taken with a Biotek Synergy 4 microplate reader with the 485/20 nm excitation filter and the 530/30 nm emission filter. Plates were read at 1 min intervals for 2 min to measure baseline fluorescence before 5 mM ATP and 5 mM MgCl_2 were added to initiate V-ATPase activity. Readings were taken at 1 min intervals for 60 min before the addition of 1 μ g/ml nigericin (Tocris) and further reading for 15 min at 1 min intervals. The change in fluorescence between the 60-minute timepoint after ATP addition and the reading 2 min after nigericin was added were used to quantify the activity of V-ATPase in each sample. Data are shown as mean \pm standard deviation of nine individual experiments for each compound and concentration.

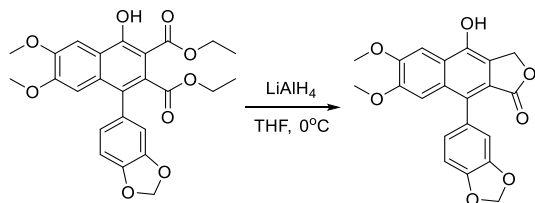
Inhibition of ATPase activity- The vesicle mixture was resuspended in HEK assay buffer and split into fractions with the protein concentration being 300 μ g/mL in 97.5 μ l of buffer and transferred to a clear 96-well plate. Vesicles were pretreated with inhibitors (DMSO<1%) for 1hr at 37°C in the presence of 2 mM NaN_3 and 100 μ M sodium orthovanadate. The reaction was initiated by the addition of 2.5 μ l of 100 mM ATP+100 mM MgCl_2 (5 mM ATP+5 mM MgCl_2 in solution). 10 μ l aliquots of the reaction were added to 90 μ l of P_i detection mixture (0.0135% malachite green, 0.954% ammonium molybdate, 0.387% polyvinyl alcohol, 1 M HCl in water) after 60 minutes. After 2 minutes, 10 μ l of 34% sodium citrate was added to quench the reaction. After a 30min incubation at room temperature, the absorbance at 620 nm was read using a Biotek Synergy 4 microplate reader. Data are shown as mean \pm standard error of the mean of the 620nm absorbance for nine individual experiments per compound.

Stability in cell media assessment- Compounds were suspended in DMEM+10%FBS at 100mM concentration and aliquots were removed at 0, 4, 24, 48h while incubating 37°C with 5% CO_2 . 100 μ L of sample media was suspended in 900 μ L of acetonitrile+0.1%trifluoroacetic acid and

cooled to 4°C for 30min. Samples were then centrifuged at 14,000xg and the supernatant was removed and analyzed by HPLC using a Phenomenex Kromasil C18 HPLC column. The percentage of the original sample peak was used to determine the amount of compound remaining at each time point in comparison with phenol standard. Data shown are the mean \pm standard error of the mean for five individual experiments.

Stability in HEK-293 cells- HEK-293 cells were seeded into Corning 6-well plates at a concentration of 5×10^5 cells/well in DMEM+10% FBS and incubated overnight at 37°C with 5% CO₂. The media was then removed and replaced with DMEM+10% FBS containing 100mM of select inhibitors and allowed to incubate for 24h at 37°C with 5% CO₂. Media was then collected and cells were washed three times with cold PBS before being allowed to dry for 15min. 1.5ml of a 1:1:0.0005 mixture of acetonitrile: methanol: trifluoroacetic acid was then added to each well and incubated at 4°C for 16h. The supernatant was then removed and centrifuged at 14,000xg for 10min to remove cellular debris. The new supernatant was then concentrated to 500uL and analyzed by HPLC using Phenomenex Kromasil C18 HPLC column. Data shown are the average of 3 independent experiments.

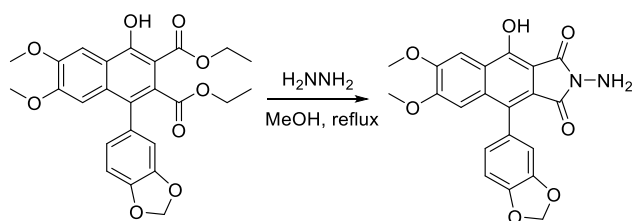
2.3.2 Chemistry



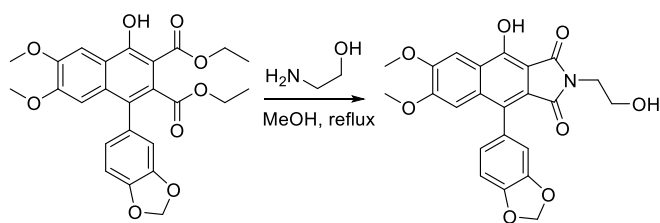
9-(benzo[d][1,3]dioxol-5-yl)-4-hydroxy-6,7-dimethoxynaphtho[2,3-*c*]furan-1(3*H*)-one (2a)-diethyl 1-(benzo[d][1,3]dioxol-5-yl)-4-hydroxy-6,7-dimethoxynaphthalene-2,3-dicarboxylate (1a) (511 mg, 1.05 mmol, 1 eq.) was dissolved in 20 mL of tetrahydrofuran (THF) and cooled to 0°C in an ice bath. This solution was added dropwise to a stirring solution of 50mL of lithium aluminum hydride (79.7mg, 2.10 mmol, 2 eq.). After 1h at 0°C, the reaction was quenched with saturated sodium sulfate, filtered through celite, and concentrated under reduced pressure. The crude mixture was extracted with ethyl acetate (3x50 mL) and washed with water (50 mL) and brine (50 mL). The water layers were combined and acidified with 1M HCl. The resulting precipitate was filtered to yield a yellow solid (368 mg, 92%, Purity: 97.5%). ¹H NMR (500 MHz, DMSO-*d*₆) δ 10.39 (s,

1H), 7.61 (s, 1H), 7.00 (d, $J = 7.8$ Hz, 1H), 6.94 (s, 1H), 6.85 (d, $J = 1.6$ Hz, 1H), 6.74 (dd, $J = 7.9$, 1.7 Hz, 1H), 6.10 (d, $J = 1.3$ Hz, 2H), 5.35 (s, 2H), 3.93 (s, 3H), 3.64 (s, 3H). ^{13}C NMR (126 MHz, DMSO- d_6) δ 169.98, 150.79, 150.02, 147.16, 146.91, 145.20, 129.78, 129.09, 124.09, 123.59, 121.98, 119.01, 111.39, 108.18, 105.73, 101.35, 101.04, 66.94, 56.34, 55.93, 55.43. ^{13}C NMR (126 MHz, DMSO- d_6) δ 169.98, 150.79, 150.02, 147.16, 146.91, 145.20, 129.78, 129.09, 124.09, 123.59, 121.98, 119.01, 111.39, 108.18, 105.73, 101.35, 101.04, 66.94, 56.34, 55.93, 55.43. ESI-MS (ESI+) m/z : calculated for $\text{C}_{21}\text{H}_{16}\text{O}_7 + \text{H}^+$, 381.0969 $[\text{M} + \text{H}]^+$, found 381.0964 $[\text{M} + \text{H}]^+$.

Synthesis of Imide Derivatives:

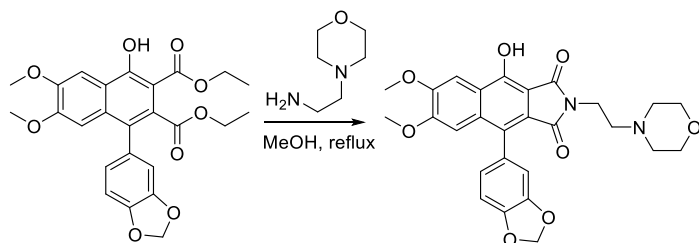


2-amino-4-(benzo[d][1,3]dioxol-5-yl)-9-hydroxy-6,7-dimethoxy-1H-benzo[f]isoindole-1,3(2H)-dione (**1b**) - **1a** (148 mg, 0.316mmol) was dissolved in methanol (5 mL) and heated to reflux. Hydrazine hydrate (500ul, ~60% solution) was added dropwise and the reaction was refluxed overnight. Precipitate formed upon cooling the mixture to -20°C and was filtered off to yield a pure, yellow solid (121mg, 93%, Purity: 99.3%). ^1H NMR (500MHz, DMSO- d_6): 8.53 (s, 1H), 7.68 (s, 1H), 7.11 (s, 1H), 6.97 (d, $J=10\text{Hz}$, 1H), 6.86 (s, 1H), 6.85 (d, 1.5Hz, 1H), 6.09 (d, $J=20\text{Hz}$, 2H), 4.08 (s, 3H), 4.07 (s, 2H), 3.83 (s, 3H). LC-MS m/z : calculated for $\text{C}_{21}\text{H}_{16}\text{N}_2\text{O}_7 + \text{H}^+$, 409.1 $[\text{M} + \text{H}]^+$, found 409.2 $[\text{M} + \text{H}]^+$.

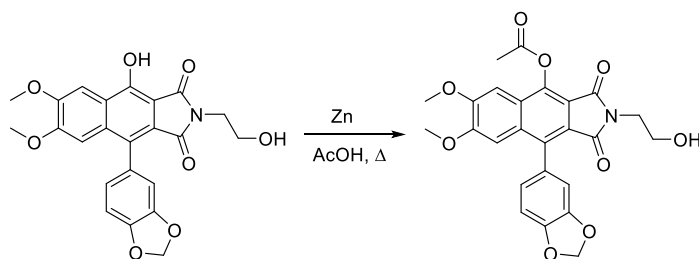


4-(benzo[d][1,3]dioxol-5-yl)-9-hydroxy-2-(2-hydroxyethyl)-6,7-dimethoxy-1H-benzo[f]isoindole-1,3(2H)-dione (**1c**) - **1a** (150mg, 0.320mmol) was dissolved in methanol (5ml) and heated to reflux. Ethanolamine (1ml, 1.012g, 16.6mmol) was added dropwise and the reaction was allowed to react overnight. The reaction was cooled, and methanol was removed by rotary evaporation. The remaining liquid was acidified by 1M HCl and the resulting precipitate was collected by vacuum filtration. The precipitate was recrystallized from toluene and methanol to

yield 120mg (85%, Purity: 95.1%) of yellow solid. ^1H NMR (500MHz, DMSO- d_6): 7.78(s, 1H), 7.03 (s, 1H), 6.93 (d, $J=10\text{Hz}$, 1H), 6.82 (s, 1H), 6.80 (d, $J=10\text{Hz}$, 1H), 6.02 (d, $J=5\text{Hz}$, 2H), 4.59 (s, 2H), 3.97 (s, 3H), 3.72 (s, 3H), 3.68 (s, 4H). LC-MS m/z : calculated for $\text{C}_{23}\text{H}_{19}\text{NO}_8+\text{H}^+$, 438.1 $[\text{M}+\text{H}]^+$, found 438.1 $[\text{M}+\text{H}]^+$.



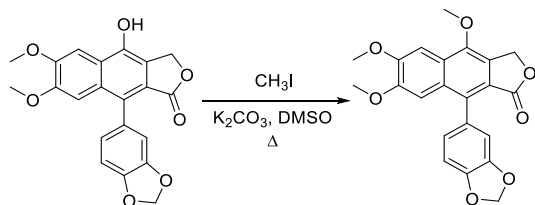
4-(benzo[d][1,3]dioxol-5-yl)-9-hydroxy-6,7-dimethoxy-2-(2-morpholinoethyl)-1H-benzo[f]isoindole-1,3(2H)-dione (**1d**)- **1a** (102mg, 0.218mmol) and was dissolved in methanol (5ml) and heated to reflux. 4-(2-aminoethyl)morpholine (1ml, 0.992g, 7.62mmol) was added dropwise and the reaction proceeded overnight. The reaction was cooled, and methanol was concentrated under reduced pressure. The crude mixture was extracted with ethyl acetate (3x20ml) and the organic layers were combined and washed with distilled water (20mL) and brine (20mL). The organic layer was dried with anhydrous sodium sulfate and concentrated by under reduced pressure. The crude solid was recrystallized from toluene and methanol to yield an amorphous, yellow solid (61mg, 57%, Purity: 95.3%). ^1H NMR (500 MHz, DMSO- d_6) δ 10.96 (s, 1H), 9.56 (s, 1H), 7.74 (s, 1H), 7.04 – 6.97 (m, 2H), 6.90 (d, $J = 1.7$ Hz, 1H), 6.79 (dd, $J = 7.9, 1.7$ Hz, 1H), 6.09 (d, $J = 7.5$ Hz, 2H), 4.01 – 3.95 (m, 2H), 3.93 (s, 3H), 3.87 – 3.83 (m, 2H), 3.66 (s, 3H), 3.56 (d, $J = 12.4$ Hz, 4H), 3.10 (d, $J = 11.0$ Hz, 2H). LC-MS m/z : calculated for $\text{C}_{27}\text{H}_{26}\text{N}_2\text{O}_8+\text{H}^+$, 507.2 $[\text{M}+\text{H}]^+$, found 507.1 $[\text{M}+\text{H}]^+$.



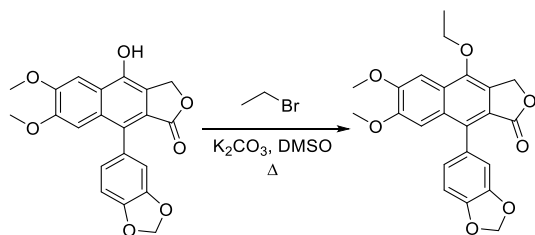
9-(benzo[d][1,3]dioxol-5-yl)-2-(2-hydroxyethyl)-6,7-dimethoxy-1,3-dioxo-2,3-dihydro-1H-benzo[f]isoindol-4-yl acetate (**1e**)- Imide **1c** (110 mg, 0.252mmol), activated zinc dust (200 mg), and acetic acid (20mL) were added to a reaction flask and heated to reflux overnight. The reaction was cooled to room temperature and the precipitate was filtered off and the filtrate was washed

with methanol until only a black precipitate remained. The filtrate was condensed under reduced pressure and the crude product was separated by silica gel column chromatography (hexanes: ethyl acetate 5:5 to 0:100) to yield a fluorescent, green solid (64 mg, 53%, Purity: 97.5%). ^1H NMR (500 MHz, $\text{DMSO}-d_6$) δ 7.70 (s, 1H), 7.03 – 6.93 (m, 2H), 6.90 (d, J = 1.7 Hz, 1H), 6.80 – 6.74 (m, 1H), 6.09 (d, J = 2.9 Hz, 2H), 4.14 (t, J = 5.5 Hz, 2H), 3.92 (s, 3H), 3.64 (s, 3H), 1.90 (s, 3H), 1.00 (s, 1H). ESI-MS (ESI+) m/z : calculated for $\text{C}_{25}\text{H}_{21}\text{NO}_9 + \text{H}^+$, 480.1295 $[\text{M} + \text{H}]^+$, found 480.1289 $[\text{M} + \text{H}]^+$.

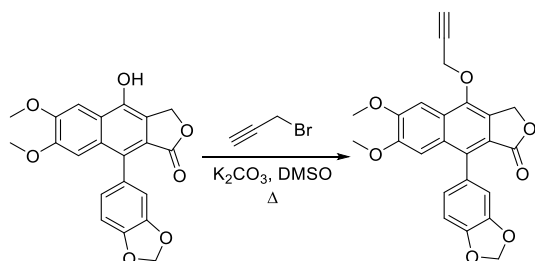
General synthetic procedure for hydrophobic phenol ether derivatives: 2a (1eq), haloalkane (2eq), and potassium carbonate (5eq) were dissolved in dimethyl sulfoxide (6mL). The reaction was heated to reflux overnight. The reaction was then cooled to room temperature and 20mL of distilled water was added to the flask. The mixture was added to a separatory funnel and extracted with dichloromethane (3x20mL). The organic layers were combined and washed with distilled water (30mL) and brine (30mL) before concentrating the organic layers under reduced pressure. The crude product was purified with normal phase silica gel chromatography (Hexanes/EtOAc 100/0 to 80/100) to yield the pure solid.



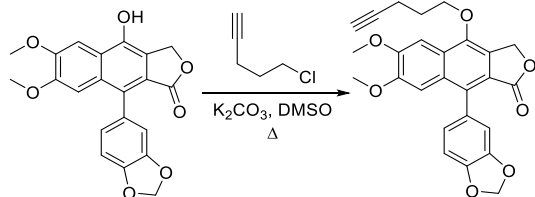
9-(benzo[d][1,3]dioxol-5-yl)-4,6,7-trimethoxynaphtho[2,3-c]furan-1(3H)-one (**2b**)- **2a** (50mg, 0.131mmol, 1eq), methyl iodide (20 μ l, 22.8mg, 2.5eq), and potassium carbonate (91mg, 0.655mmol, 5eq) were dissolved in dimethyl sulfoxide (6mL). The reaction was heated to reflux overnight. The reaction was worked up and purified as above to yield a white solid (yield: 46mg, 91%, Purity: 98.0%). ^1H NMR (500 MHz, $\text{DMSO}-d_6$) δ 7.49 (s, 1H), 7.00 (d, J = 7.9 Hz, 1H), 6.92 (s, 1H), 6.84 (d, J = 1.6 Hz, 1H), 6.72 (dd, J = 7.9, 1.7 Hz, 1H), 6.09 (s, 2H), 5.69 (s, 2H), 4.11 (s, 3H), 3.92 (s, 3H), 3.62 (s, 3H). ^{13}C NMR (201 MHz, $\text{DMSO}-d_6$) δ 169.45, 151.65, 150.41, 147.65, 147.37, 147.23, 133.00, 129.89, 128.91, 125.31, 124.16, 124.05, 119.47, 111.30, 108.38, 105.94, 101.56, 101.02, 67.24, 59.54, 56.12, 55.65, 21.23. ESI-MS (ESI+) m/z : calculated for $\text{C}_{22}\text{H}_{18}\text{O}_7 + \text{H}^+$, 395.1125 $[\text{M} + \text{H}]^+$, found 395.1125 $[\text{M} + \text{H}]^+$.



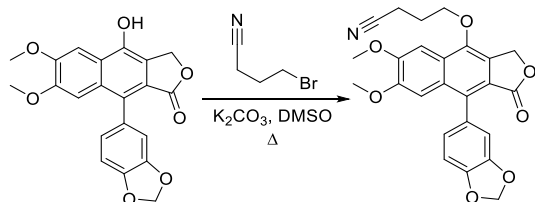
9-(benzo[d][1,3]dioxol-5-yl)-4-ethoxy-6,7-dimethoxynaphtho[2,3-c]furan-1(3H)-one (**2c**)- **2a** (51mg, 0.134mmol, 1eq), ethyl bromide (20 μ l, 29.2mg, 2eq), and potassium carbonate (90mg, 0.651mmol, 5eq) were dissolved in dimethyl sulfoxide (6mL). The reaction was heated to reflux overnight. The reaction was worked up and purified as above to yield an off-white/yellow solid (yield: 40mg, 74%, Purity: 99.1%). ^1H NMR (500 MHz, DMSO- d_6) δ 7.48 (s, 1H), 6.99 (d, J = 7.9 Hz, 1H), 6.92 (s, 1H), 6.84 (d, J = 1.7 Hz, 1H), 6.72 (dd, J = 7.9, 1.7 Hz, 1H), 6.09 (s, 2H), 5.72 (s, 2H), 5.57 (s, 2H), 4.29 (q, J = 7.0 Hz, 2H), 3.91 (s, 3H), 3.62 (s, 3H), 1.42 (t, J = 7.0 Hz, 3H). ^{13}C NMR (201 MHz, DMSO- d_6) δ 169.51, 151.68, 150.40, 147.36, 147.23, 146.86, 133.29, 129.94, 128.85, 126.10, 125.82, 124.05, 119.41, 111.30, 108.38, 105.98, 101.54, 101.06, 68.03, 67.11, 56.04, 55.65, 31.14, 16.14. ESI-MS (ESI+) m/z : calculated for $\text{C}_{23}\text{H}_{20}\text{O}_7 + \text{H}^+$, 409.1281 $[\text{M}+\text{H}]^+$, found 409.1276 $[\text{M}+\text{H}]^+$.



9-(benzo[d][1,3]dioxol-5-yl)-6,7-dimethoxy-4-(prop-2-yn-1-yloxy)naphtho[2,3-c]furan-1(3H)-one (**2d**)- **2a** (50mg, 0.131mmol, 1eq), propargyl bromide (30 μ l of 80 wt.% solution in toluene, 2eq), and potassium carbonate (85mg, 0.615mmol, 5eq) were dissolved in dimethyl sulfoxide (6mL). The reaction was heated to reflux overnight. The reaction was worked up and purified as above to yield a light brown solid (yield: 31mg, 56%, Purity: 95.8%). ^1H NMR (500 MHz, DMSO- d_6) δ 7.52 (d, J = 1.9 Hz, 1H), 7.01 (dd, J = 7.9, 1.9 Hz, 1H), 6.95 (d, J = 1.9 Hz, 1H), 6.87 (d, J = 1.8 Hz, 1H), 6.74 (dd, J = 7.9, 1.8 Hz, 1H), 6.10 (d, J = 1.9 Hz, 2H), 5.59 (s, 2H), 5.00 (d, J = 2.4 Hz, 2H), 3.93 (s, 3H), 3.70 (t, J = 2.4 Hz, 1H), 3.63 (s, 3H). ^{13}C NMR (201 MHz, DMSO- d_6) δ 169.35, 151.81, 150.46, 147.39, 147.34, 145.97, 134.58, 130.07, 128.60, 127.61, 126.61, 124.03, 119.20, 111.25, 108.40, 106.03, 101.58, 101.20, 80.08, 79.84, 66.93, 60.44, 56.09, 55.68. ESI-MS (ESI+) m/z : calculated for $\text{C}_{24}\text{H}_{18}\text{O}_7 + \text{H}^+$, 419.1125 $[\text{M}+\text{H}]^+$, found 419.1129 $[\text{M}+\text{H}]^+$.

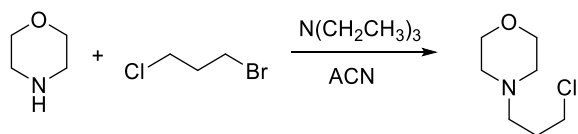


9-(benzo[d][1,3]dioxol-5-yl)-6,7-dimethoxy-4-(pent-4-yn-1-yloxy)naphtho[2,3-c]furan-1(3H)-one (**2e**)- **2a** (49mg, 0.129mmol, 1eq), 5-chloro-1-pentyne (28μl, 26.9mg, 2eq), and potassium carbonate (89mg, 0.644mmol, 5eq) were dissolved in dimethyl sulfoxide (6mL). The reaction was heated to reflux overnight. The reaction was worked up and purified as above to yield a white solid (yield: 36mg, 61%, Purity: 98%). ¹H NMR (500 MHz, DMSO-*d*₆) δ 7.48 (s, 1H), 7.02 – 6.91 (m, 2H), 6.85 (d, *J* = 1.6 Hz, 1H), 6.73 (dd, *J* = 7.8, 1.7 Hz, 1H), 6.09 (s, 2H), 5.56 (s, 2H), 4.28 (t, *J* = 5.9 Hz, 2H), 3.92 (s, 3H), 3.62 (s, 3H), 2.86 (t, *J* = 2.7 Hz, 1H), 2.50 – 2.48 (m, 2H), 2.00 (q, *J* = 6.5 Hz, 2H). ¹³C NMR (126 MHz, DMSO-*d*₆) δ 169.35, 151.58, 150.25, 147.23, 147.13, 146.51, 133.45, 129.82, 128.64, 126.08, 125.95, 123.92, 119.25, 111.17, 108.25, 105.84, 101.43, 100.70, 83.97, 72.30, 70.57, 66.85, 55.90, 55.51, 28.85, 14.95. ESI-MS (ESI+) *m/z*: calculated for C₂₆H₂₂O₇ + H⁺, 447.1438 [M+H]⁺, found 447.1432 [M+H]⁺.

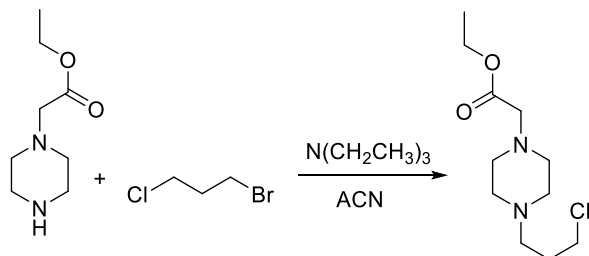


4-((9-(benzo[d][1,3]dioxol-5-yl)-6,7-dimethoxy-1-oxo-1,3-dihydronaphtho[2,3-c]furan-4-yl)oxy)butanenitrile (**2f**)- **2a** (51mg, 0.134mmol, 1eq), 4-bromobutyronitrile (27μl, 38.8mg, 2eq), and potassium carbonate (89mg, 0.644mmol, 5eq) were dissolved in dimethyl sulfoxide (6mL). The reaction was heated to reflux overnight. The reaction was worked up and purified as above to yield a white solid (yield: 21mg, 36%, Purity: 95.1%). ¹H NMR (500 MHz, DMSO-*d*₆) δ 7.54 (s, 1H), 7.03 – 6.91 (m, 2H), 6.86 (d, *J* = 1.7 Hz, 1H), 6.73 (dd, *J* = 7.9, 1.7 Hz, 1H), 6.09 (s, 2H), 5.61 (s, 2H), 4.33 (t, *J* = 5.8 Hz, 2H), 3.94 (s, 3H), 3.63 (s, 3H), 2.80 (t, *J* = 7.0 Hz, 2H), 2.13 (q, *J* = 6.5 Hz, 2H). ¹³C NMR (201 MHz, DMSO-*d*₆) δ 169.41, 151.80, 150.44, 147.37, 147.26, 146.51, 133.58, 129.96, 128.79, 125.84, 125.62, 124.03, 121.02, 119.40, 111.26, 108.38, 105.99, 101.54, 101.10, 70.55, 67.07, 56.19, 55.66, 25.99, 14.09. ESI-MS (ESI+) *m/z*: calculated for C₂₅H₂₁NO₇ + H⁺, 448.1390 [M+H]⁺, found 448.1287 [M+H]⁺.

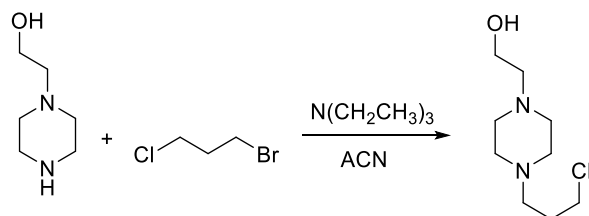
General Procedure for synthesis of chloro-alkene precursors: of 1-bromo-3-chloropropane (1.1mL, 1.72g, 11mmol; 1.5equiv.) and amine component (1eq) were dissolved in acetonitrile (40mL) at room temperature while stirring. triethylamine (3.1 mL, 2.2g, 2eq) of was added dropwise and the reaction mixture was stirred at room temperature for 24-48 hours. When reaction was deemed complete by thin-layer chromatography, the solvent was removed under reduced pressure to yield a crude oil. The crude oil was purified by normal phase silica gel chromatography (DCM/MeOH 100/0 to 50/50) to yield the pure oil.



4-(3-chloropropyl)morpholine (2ga)- 1-bromo-3-chloropropane (1.1mL, 1.72g, 11mmol; 1.5equiv.) of 1-bromo-3-chloropropane and amine component (641μl, 639mg, 1eq) were dissolved in acetonitrile (40mL) at room temperature while stirring. triethylamine (3.1mL, 2.2g, 2eq) was then added dropwise, the reaction mixture was stirred at room temperature for 24h and purified as above to yield a yellow oil (yield: 351mg, 30%). LC-MS *m/z*: calculated for C₇H₁₄ClNO+H⁺, 164.1 [M+H]⁺, found 164.1 [M+H]⁺.

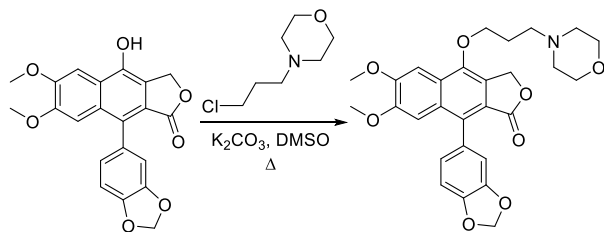


ethyl 2-(4-(3-chloropropyl)piperazin-1-yl)acetate (2ha)- 1-bromo-3-chloropropane (1.1mL, 1.72g, 11mmol; 1.5equiv.) of 1-bromo-3-chloropropane and ethyl 2-(piperazin-1-yl)acetate (1.16g, 1eq) were dissolved in acetonitrile (40mL) at room temperature while stirring. triethylamine (3.1mL, 2.2g, 2eq) was then added dropwise, the reaction mixture was stirred at room temperature for 24h and purified as above to yield a yellow oil (yield: 654mg, 36%). LC-MS *m/z*: calculated for C₁₁H₂₁ClN₂O₂+H⁺, 248.1 [M+H]⁺, found 248.2 [M+H]⁺.

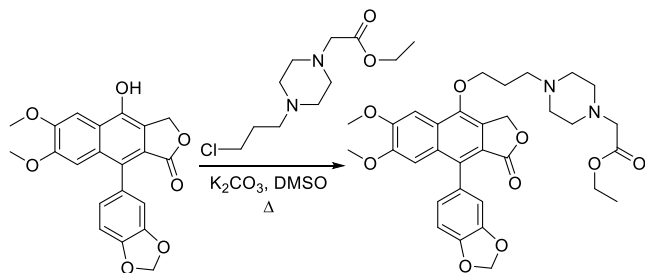


2-(4-(3-chloropropyl)piperazin-1-yl)ethan-1-ol (2ia)- 1-bromo-3-chloropropane (1.1mL, 1.72g, 11mmol; 1.5equiv.) of 1-bromo-3-chloropropane and 2-(piperazin-1-yl)ethanol (0.952g, 1eq) were dissolved in acetonitrile (40mL) at room temperature while stirring. triethylamine (3.1mL, 2.2g, 2eq) was then added dropwise, the reaction mixture was stirred at room temperature for 24h and purified as above to yield a yellow oil (yield: 551mg, 36%). LC-MS m/z : calculated for $C_9H_{19}ClN_2O+H^+$, 207.1 $[M+H]^+$, found 207.1 $[M+H]^+$.

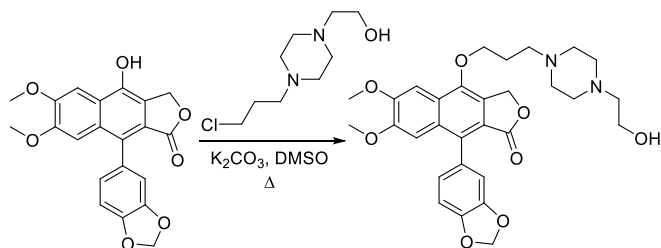
General synthetic procedure for hydrophilic phenol ether derivatives: 2a (50mg, 0.131mmol, 1eq), the chloropropylamine linker (2eq), and potassium carbonate (91mg, 0.655mmol, 5eq) were dissolved in dimethyl sulfoxide (6mL). The reaction was heated to reflux overnight (16-20h). The reaction was then cooled to room temperature and 20mL of distilled water was added to the flask. The mixture was added to a separatory funnel and extracted with ethyl acetate (5x30mL). The organic layers were combined and washed with brine (30mL) before concentrating the organic layers under reduced pressure. The crude product was purified with normal phase silica gel chromatography (DCM/MeOH 100/0 to 80/20) to yield the pure solid.



9-(benzo[d][1,3]dioxol-5-yl)-6,7-dimethoxy-4-(3-morpholinopropoxy)naphtho[2,3-c]furan-1(3H)-one (2g)- **2a** (50mg, 0.131mmol, 1eq), **2ga** (43mg, 2eq), and potassium carbonate (80mg, 0.579mmol, 5eq) were dissolved in dimethyl sulfoxide (6mL). The reaction was heated to reflux overnight and purified as above to give a yellow solid (yield: 45mg, 67%, Purity: 99.3%). 1H NMR (500 MHz, DMSO- d_6) δ 7.49 (s, 1H), 7.00 (d, J = 7.9 Hz, 1H), 6.93 (s, 1H), 6.85 (d, J = 1.6 Hz, 1H), 6.73 (dd, J = 7.9, 1.7 Hz, 1H), 6.09 (s, 2H), 5.58 (s, 2H), 4.27 (t, J = 6.1 Hz, 2H), 3.92 (s, 3H), 3.63 (s, 3H), 3.55 (t, J = 4.5 Hz, 4H), 2.53 (t, J = 7.3 Hz, 2H), 2.36 (s, 4H), 1.97 (p, J = 6.6 Hz, 2H). ^{13}C NMR (201 MHz, DMSO- d_6) δ 169.49, 151.68, 150.40, 147.36, 147.25, 146.88, 133.33, 129.95, 128.82, 126.01, 125.84, 124.05, 119.44, 111.29, 108.38, 106.02, 101.55, 100.95, 70.42, 67.06, 66.66, 56.02, 55.66, 55.36, 53.89, 27.25. ESI-MS (ESI+) m/z : calculated for $C_{28}H_{29}NO_8+H^+$, 508.1966 $[M+H]^+$, found 508.1967 $[M+H]^+$.



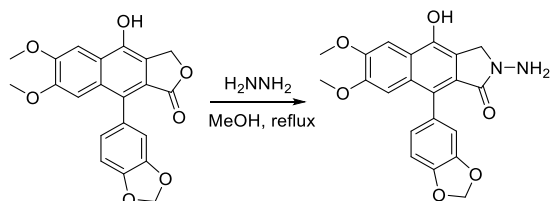
Ethyl 2-(4-(3-((9-(benzo[d][1,3]dioxol-5-yl)-6,7-dimethoxy-1-oxo-1,3-dihydronaphtho[2,3-*c*]furan-4-yl)oxy)propyl)piperazin-1-yl)acetate (**2h**)- **2a** (51mg, 0.134mmol, 1eq), **2ha** (66mg, 2eq), and potassium carbonate (90mg, 0.655mmol, 5eq) were dissolved in dimethyl sulfoxide (6mL). The reaction was heated to reflux overnight and purified as above to give an off-white, amorphous solid (yield: 36mg, 46%, Purity: 97.1%). ¹H NMR (500 MHz, DMSO-*d*₆) δ 7.47 (s, 1H), 6.99 (d, *J* = 7.9 Hz, 1H), 6.92 (s, 1H), 6.84 (d, *J* = 1.6 Hz, 1H), 6.72 (dd, *J* = 8.0, 1.7 Hz, 1H), 6.09 (s, 2H), 5.56 (s, 2H), 4.24 (t, *J* = 6.1 Hz, 2H), 4.04 (q, *J* = 7.1 Hz, 2H), 3.91 (s, 3H), 3.62 (s, 3H), 3.15 (s, 2H), 2.59 – 2.53 (m, 2H), 2.50 (s, 8H), 1.96 (p, *J* = 6.6 Hz, 2H), 1.14 (t, *J* = 7.1 Hz, 3H). ¹³C NMR (126 MHz, DMSO-*d*₆) δ 170.24, 169.37, 151.51, 147.22, 147.11, 146.71, 133.19, 129.78, 128.67, 125.85, 125.71, 123.91, 119.27, 111.17, 108.24, 105.81, 101.43, 100.75, 70.26, 66.92, 60.12, 58.75, 55.87, 55.50, 53.06, 52.25, 40.73, 27.34, 14.46. ESI-MS (ESI+) *m/z*: calculated for C₃₂H₃₆N₂O₉+H⁺, 593.2493 [M+H]⁺, found 593.2491 [M+H]⁺.



9-(benzo[d][1,3]dioxol-5-yl)-4-(3-(4-(2-hydroxyethyl)piperazin-1-yl)propoxy)-6,7-dimethoxynaphtho[2,3-*c*]furan-1(3*H*)-one (**2i**)- **2a** (51mg, 0.134mmol, 1eq), **2ia** (54mg, 2eq), and potassium carbonate (90mg, 0.655mmol, 5eq) were dissolved in dimethyl sulfoxide (6mL). The reaction was heated to reflux overnight and purified as above to give a yellow, amorphous solid (Yield: 32mg, 44%, Purity: 95.1%). ¹H NMR (500 MHz, DMSO-*d*₆) δ 7.48 (s, 1H), 7.00 (d, *J* = 7.9 Hz, 1H), 6.93 (s, 1H), 6.73 (dd, *J* = 7.9, 1.7 Hz, 1H), 6.09 (s, 2H), 5.57 (s, 2H), 4.42 (s, 1H), 4.26 (t, *J* = 6.0 Hz, 2H), 3.92 (s, 3H), 3.62 (s, 3H), 3.46 (t, *J* = 6.3 Hz, 2H), 2.57 – 2.48 (m, 4H), 2.38 (s, 8H), 1.96 (p, *J* = 6.6 Hz, 2H). ¹³C NMR (126 MHz, Chloroform-*d*) δ 169.38, 151.52, 150.24, 147.23, 147.11, 146.73, 133.19, 129.80, 128.67, 125.87, 125.74, 123.92, 119.29, 111.17,

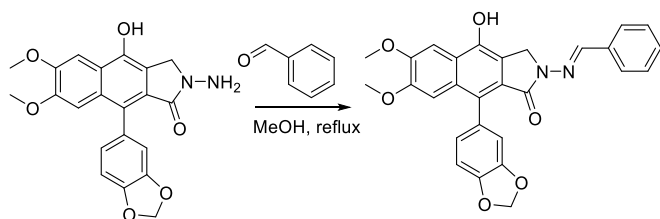
108.26, 105.83, 101.43, 100.78, 70.29, 66.94, 60.46, 58.62, 55.89, 55.52, 54.75, 53.41, 53.00, 27.37. ESI-MS (ESI+) m/z : calculated for $C_{30}H_{34}N_2O_7+H^+$, 551.2388 $[M+H]^+$, found 551.2383 $[M+H]^+$.

Diphyllin Hydrazone Synthesis:



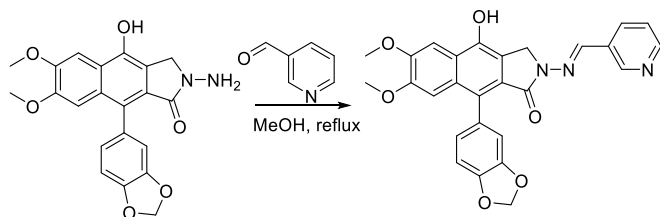
2-amino-9-(benzo[d][1,3]dioxol-5-yl)-4-hydroxy-6,7-dimethoxy-2,3-dihydro-1H-benzo[f]isoindol-1-one (3a)- **2a** (200mg, 0.526mmol, 1eq) and hydrazine hydrate (0.5mL) were dissolved in 50mL of methanol. The reaction was heated to reflux overnight (16-20h). The solution was cooled to -20°C and the precipitate that formed was collected. The crude product was recrystallized with ethanol to yield 136mg (66%, Purity: 96.1%) of **3a** as a yellow solid. ^1H NMR (500 MHz, $\text{DMSO}-d_6$) δ 9.98 (s, 1H), 7.56 (s, 1H), 6.93 (d, $J = 7.8$ Hz, 1H), 6.88 (s, 1H), 6.75 (d, $J = 1.7$ Hz, 1H), 6.66 (dd, $J = 7.9, 1.6$ Hz, 1H), 6.06 (d, $J = 1.9$ Hz, 2H), 4.78 (s, 2H), 4.42 (s, 2H), 3.88 (s, 3H), 3.59 (s, 3H). ESI-MS (ESI+) m/z : calculated for $C_{21}H_{18}N_2O_6+H^+$, 395.1237 $[M+H]^+$, found 395.1240 $[M+H]^+$.

General Procedure for Hydrazone synthesis: **3a** (50mg, 0.126mmol, 1eq) and the select aromatic aldehyde (1.2eq) were dissolved in methanol (10mL). The reaction was heated to reflux overnight (16-20h). The reaction was then cooled to room temperature and concentrated under reduced pressure. The residual solution was then cooled to -20°C to precipitate the crude product from solution. The crude precipitate was collected and recrystallized with ethanol to yield the final product.

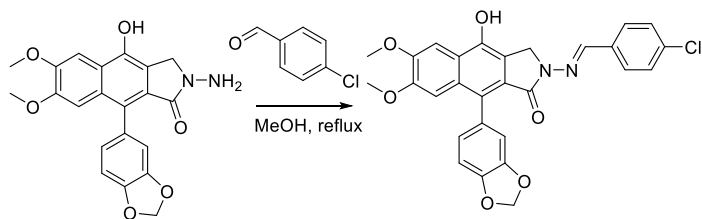


(E)-9-(benzo[d][1,3]dioxol-5-yl)-2-(benzylideneamino)-4-hydroxy-6,7-dimethoxy-2,3-dihydro-1H-benzo[f]isoindol-1-one (3b)- **3a** (50mg, 0.126mmol, 1eq) and benzaldehyde (15 μ l 16mg,

1.2eq) were dissolved in methanol (10mL). The reaction was heated to reflux overnight, and the final product was purified as above to give a yellow solid (yield: 52mg, 85%, Purity: 96.2%). ^1H NMR (500 MHz, $\text{DMSO-}d_6$) δ 10.22 (s, 1H), 8.65 – 8.61 (m, 2H), 8.10 (s, 1H), 7.64 (d, J = 5.2 Hz, 4H), 6.98 (d, J = 8.0 Hz, 1H), 6.92 (s, 1H), 6.83 (s, 1H), 6.72 (d, J = 8.0 Hz, 1H), 6.09 (s, 2H), 4.84 (s, 2H), 3.90 (s, 3H), 3.61 (s, 3H). ESI-MS (ESI+) m/z : calculated for $\text{C}_{28}\text{H}_{22}\text{N}_2\text{O}_6 + \text{H}^+$, 483.1551 $[\text{M}+\text{H}]^+$, found 483.1547 $[\text{M}+\text{H}]^+$.

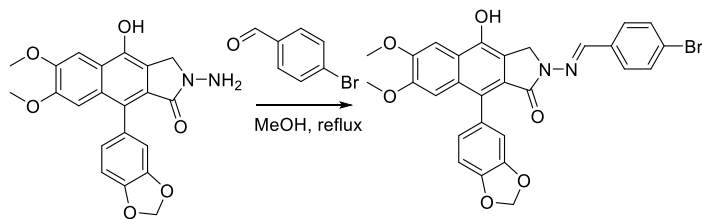


(*E*)-9-(benzo[*d*][1,3]dioxol-5-yl)-4-hydroxy-6,7-dimethoxy-2-((pyridin-3-ylmethylene)amino)-2,3-dihydro-1H-benzo[*f*]isoindol-1-one (**3c**)- **3a** (50mg, 0.126mmol, 1eq) and nicotinaldehyde (14 μ l, 16mg, 1.2eq) were dissolved in methanol (10mL). The reaction was heated to reflux overnight, and the final product was purified as above to give a yellow solid (yield: 45mg, 74%, Purity: 95.5%). ^1H NMR (300 MHz, $\text{DMSO-}d_6$) δ 10.24 (s, 1H), 8.90 (s, 1H), 8.60 (s, 1H), 8.23 (s, 1H), 8.13 (d, J = 8.1 Hz, 1H), 7.67 (s, 1H), 7.56 – 7.45 (m, 1H), 7.06 – 6.91 (m, 2H), 6.86 (d, J = 1.6 Hz, 1H), 6.75 (d, J = 8.1 Hz, 1H), 6.11 (s, 2H), 4.88 (s, 2H), 3.93 (s, 3H), 3.64 (s, 3H), 1.90 (s, 1H). ^{13}C NMR (201 MHz, $\text{DMSO-}d_6$) δ 164.01, 150.86, 150.45, 149.88, 149.23, 147.16, 146.83, 146.02, 140.67, 133.66, 131.17, 130.05, 129.72, 129.10, 124.53, 124.21, 123.23, 115.80, 111.72, 108.13, 106.01, 101.47, 101.39, 56.04, 55.54, 45.53, 21.50. ESI-MS (ESI+) m/z : calculated for $\text{C}_{27}\text{H}_{21}\text{N}_3\text{O}_6 + \text{H}^+$, 483.1503 $[\text{M}+\text{H}]^+$, found 483.1500 $[\text{M}+\text{H}]^+$.

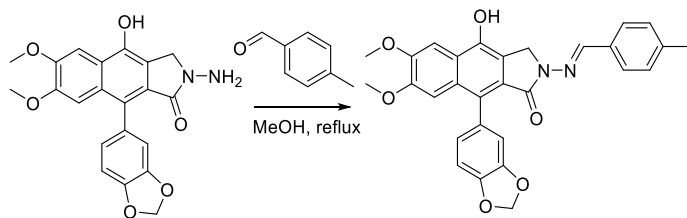


(*E*)-9-(benzo[*d*][1,3]dioxol-5-yl)-2-((4-chlorobenzylidene)amino)-4-hydroxy-6,7-dimethoxy-2,3-dihydro-1H-benzo[*f*]isoindol-1-one (**3d**)- **3a** (49mg, 0.124mmol, 1eq) and 4-chlorobenzaldehyde (21mg, 1.2eq) were dissolved in methanol (10mL). The reaction was heated to reflux overnight, and the final product was purified as above to give a yellow solid (yield: 51mg, 77%, Purity: 99.2%). ^1H NMR (500 MHz, $\text{DMSO-}d_6$) δ 10.19 (s, 1H), 8.16 (s, 1H), 7.75 (d, J = 8.6 Hz, 2H), 7.64 (s, 1H), 7.55 – 7.48 (m, 2H), 6.98 (d, J = 7.9 Hz, 1H), 6.91 (s, 1H), 6.82 (d, J = 1.7 Hz, 1H),

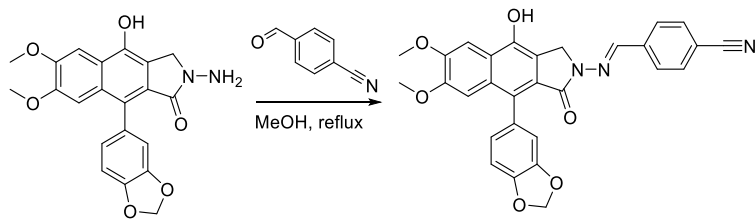
6.72 (dd, $J = 7.9, 1.7$ Hz, 1H), 6.08 (s, 2H), 4.84 (s, 2H), 3.91 (s, 3H), 3.61 (s, 3H). ESI-MS (ESI+) m/z : calculated for $C_{28}H_{21}ClN_2O_6 + H^+$, 517.1161 $[M+H]^+$, found 517.1156 $[M+H]^+$.



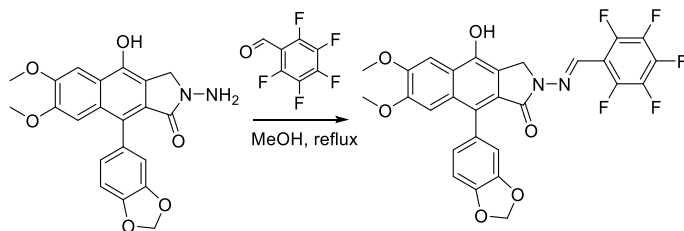
(*E*)-9-(benzo[*d*][1,3]dioxol-5-yl)-2-((4-bromobenzylidene)amino)-4-hydroxy-6,7-dimethoxy-2,3-dihydro-1H-benzo[*f*]isoindol-1-one (**3e**) - **3a** (50mg, 0.126mmol, 1eq) and 4-bromobenzaldehyde (28mg, 1.2eq) were dissolved in methanol (10mL). The reaction was heated to reflux overnight, and the final product was purified as above to give a yellow solid (yield: 55mg, 76%, Purity: 97.9%). 1H NMR (300 MHz, DMSO- d_6) δ 10.23 (s, 1H), 8.16 (s, 1H), 7.68 (dd, $J = 5.8, 2.9$ Hz, 5H), 7.05 – 6.89 (m, 2H), 6.88 – 6.69 (m, 2H), 6.11 (s, 2H), 4.86 (s, 2H), 3.93 (s, 3H), 3.63 (s, 3H). LC-MS m/z : calculated for $C_{28}H_{21}BrN_2O_6 + H^+$, 561.1 $[M+H]^+$, found 561.4 $[M+H]^+$.



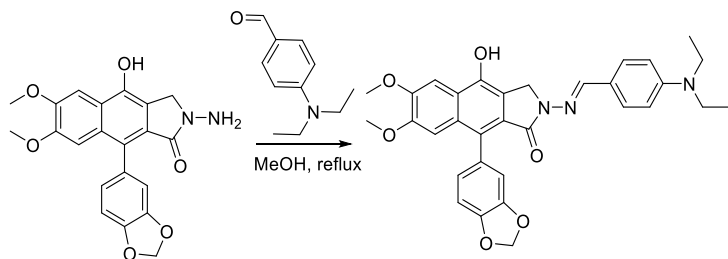
(*E*)-9-(benzo[*d*][1,3]dioxol-5-yl)-4-hydroxy-6,7-dimethoxy-2-((4-methylbenzylidene)amino)-2,3-dihydro-1H-benzo[*f*]isoindol-1-one (**3f**) - **3a** (49mg, 0.124mmol, 1eq) and 4-methylbenzaldehyde (18 μ l, 18mg, 1.2eq) were dissolved in methanol (10mL). The reaction was heated to reflux overnight, and the final product was purified as above to give a yellow solid (yield: 39mg, 62%, Purity: 97.3%). 1H NMR (500 MHz, DMSO- d_6) δ 10.17 (s, 1H), 8.10 (s, 1H), 7.61 (d, $J = 6.9$ Hz, 3H), 7.24 (d, $J = 7.7$ Hz, 2H), 6.98 (d, $J = 7.9$ Hz, 1H), 6.91 (s, 1H), 6.82 (s, 1H), 6.71 (d, $J = 7.9$ Hz, 1H), 6.08 (s, 2H), 4.80 (s, 2H), 3.90 (s, 3H), 3.60 (s, 3H), 2.30 (s, 3H). LC-MS m/z : calculated for $C_{29}H_{24}N_2O_6 + H^+$, 497.2 $[M+H]^+$, found 497.3 $[M+H]^+$.



(*E*)-4-(((9-(benzo[d][1,3]dioxol-5-yl)-4-hydroxy-6,7-dimethoxy-1-oxo-1,3-dihydro-2*H*-benzo[f]isoindol-2-yl)imino)methyl)benzonitrile (**3g**)- **3a** (51mg, 0.129mmol, 1eq) and 4-formylbenzonitrile (17mg, 1.2eq) were dissolved in methanol (10mL). The reaction was heated to reflux overnight, and the final product was purified as above to give a yellow solid (yield: 30mg, 47%, Purity: 98.1%). ¹H NMR (300 MHz, DMSO-*d*₆) δ 10.22 (s, 1H), 8.17 (s, 1H), 7.65 (s, 1H), 7.01 (d, *J* = 7.9 Hz, 1H), 6.93 (s, 1H), 6.90 – 6.84 (m, 1H), 6.80 – 6.70 (m, 1H), 6.12 (s, 2H), 4.83 (s, 2H), 3.92 (s, 3H), 3.64 (s, 3H). ¹³C NMR (201 MHz, DMSO-*d*₆) δ 164.08, 150.46, 149.86, 147.15, 146.82, 145.99, 141.27, 139.71, 133.18, 130.01, 129.69, 129.17, 127.85, 124.29, 124.21, 123.28, 119.17, 115.78, 111.90, 111.70, 108.13, 105.99, 101.42, 101.38, 56.01, 55.52, 45.54. ESI-MS (ESI+) *m/z*: calculated for C₂₉H₂₃N₃O₆+H⁺, 508.1500 [M+H]⁺, found 508.1503 [M+H]⁺.

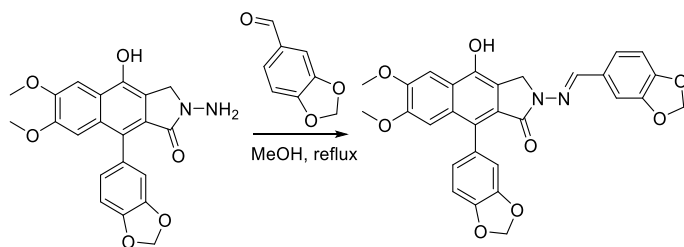


(*E*)-9-(benzo[d][1,3]dioxol-5-yl)-4-hydroxy-6,7-dimethoxy-2-(((perfluorophenyl)methylene)amino)-2,3-dihydro-1*H*-benzo[f]isoindol-1-one (**3h**)- **3a** (51mg, 0.129mmol, 1eq) and 2,3,4,5,6-pentafluorobenzaldehyde (19μl, 30mg, 1.2eq) were dissolved in methanol (10mL). The reaction was heated to reflux overnight, and the final product was purified as above to give a white solid (yield: 64mg, 88%, Purity: 98.9%). ¹H NMR (300 MHz, DMSO-*d*₆) δ 10.41 (s, 1H), 7.65 (s, 1H), 7.12 – 6.57 (m, 5H), 6.12 (s, 2H), 3.94 (s, 3H), 3.65 (s, 3H), 3.17 (s, 2H). ESI-MS (ESI+) *m/z*: calculated for C₂₈H₁₇F₅N₂O₆+H⁺, 573.1079 [M+H]⁺, found 573.1077 [M+H]⁺.

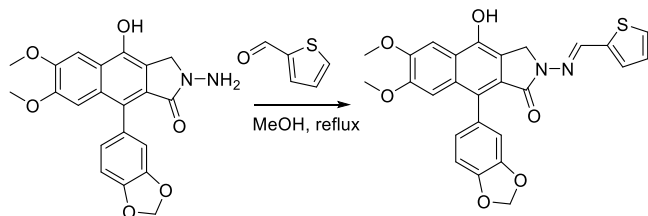


(*E*)-9-(benzo[d][1,3]dioxol-5-yl)-2-((4-(diethylamino)benzylidene)amino)-4-hydroxy-6,7-dimethoxy-2,3-dihydro-1*H*-benzo[f]isoindol-1-one (**3i**)- **3a** (50mg, 0.126mmol, 1eq) and 4-(diethylamino)benzaldehyde (27mg, 1.2eq) were dissolved in methanol (10mL). The reaction was heated to reflux overnight, and the final product was purified as above to give a bright yellow solid

(yield: 45mg, 64%, Purity: 94.9%). ^1H NMR (300 MHz, DMSO- d_6) δ 10.15 (s, 1H), 8.07 (s, 1H), 7.64 (s, 1H), 7.54 (d, J = 8.7 Hz, 2H), 7.04 – 6.90 (m, 2H), 6.83 (d, J = 1.6 Hz, 1H), 6.78 – 6.67 (m, 3H), 6.10 (s, 2H), 4.81 (s, 2H), 3.92 (s, 3H), 3.63 (s, 3H), 3.38 (d, J = 7.0 Hz, 4H), 2.53 (s, 11H), 1.10 (t, J = 6.9 Hz, 7H). LC-MS m/z : calculated for $\text{C}_{32}\text{H}_{31}\text{N}_3\text{O}_6 + \text{H}^+$, calculated 554.2 $[\text{M} + \text{H}]^+$, found 554.4 $[\text{M} + \text{H}]^+$.

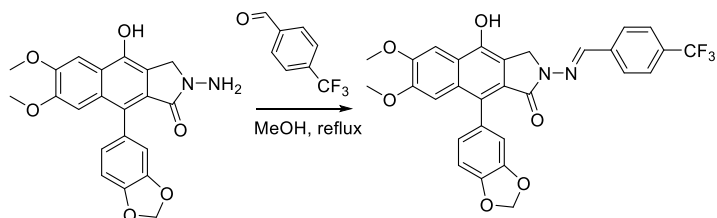


(*E*)-9-(benzo[*d*][1,3]dioxol-5-yl)-2-((benzo[*d*][1,3]dioxol-5-ylmethylene)amino)-4-hydroxy-6,7-dimethoxy-2,3-dihydro-1H-benzo[*f*]isoindol-1-one (**3j**)- **3a** (50mg, 0.126mmol, 1eq) and piperonal (23mg, 1.2eq) were dissolved in methanol (10mL). The reaction was heated to reflux overnight, and the final product was purified as above to give a beige solid (yield: 55mg, 82%, Purity: 96.1%). ^1H NMR (300 MHz, DMSO- d_6) δ 8.11 (s, 1H), 7.65 (d, J = 4.2 Hz, 1H), 7.29 (d, J = 1.6 Hz, 1H), 7.22 (d, J = 8.3 Hz, 1H), 7.00 (dd, J = 7.9, 1.7 Hz, 2H), 6.93 (d, J = 3.4 Hz, 1H), 6.84 (d, J = 1.6 Hz, 1H), 6.73 (dd, J = 7.8, 1.7 Hz, 1H), 6.09 (d, J = 8.0 Hz, 4H), 4.81 (s, 2H), 3.92 (s, 3H), 3.63 (s, 3H). LC-MS m/z : calculated for $\text{C}_{29}\text{H}_{22}\text{N}_2\text{O}_8 + \text{H}^+$, 527.1 $[\text{M} + \text{H}]^+$, found 527.4 $[\text{M} + \text{H}]^+$.



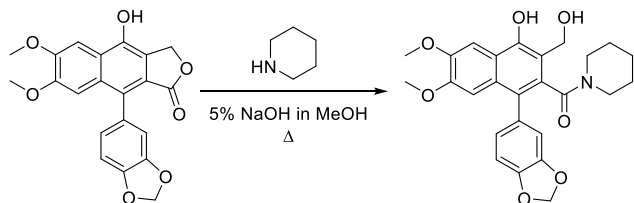
(*E*)-9-(benzo[*d*][1,3]dioxol-5-yl)-4-hydroxy-6,7-dimethoxy-2-((thiophen-2-ylmethylene)amino)-2,3-dihydro-1H-benzo[*f*]isoindol-1-one (**3k**)- **3a** (50mg, 0.126mmol, 1eq) and 2-thiophenecarboxaldehyde (14 μ l, 17mg, 1.2eq) were dissolved in methanol (10mL). The reaction was heated to reflux overnight, and the final product was purified as above to give a beige solid (yield: 43mg, 69%, Purity: 96.7%). ^1H NMR (500 MHz, DMSO- d_6) δ 8.23 (s, 1H), 7.89 (dd, J = 2.9, 1.2 Hz, 1H), 7.69 – 7.56 (m, 2H), 7.43 (dd, J = 5.1, 1.2 Hz, 1H), 6.97 (d, J = 7.9 Hz, 1H), 6.92 (s, 1H), 6.81 (d, J = 1.7 Hz, 1H), 6.71 (dd, J = 7.9, 1.7 Hz, 1H), 6.08 (dd, J = 3.9, 1.0 Hz, 2H), 4.80

(s, 2H), 3.90 (s, 3H), 3.61 (s, 3H). LC-MS m/z : calculated for $C_{26}H_{20}N_2O_6S+H^+$, 489.1 $[M+H]^+$, found 489.1 $[M+H]^+$.



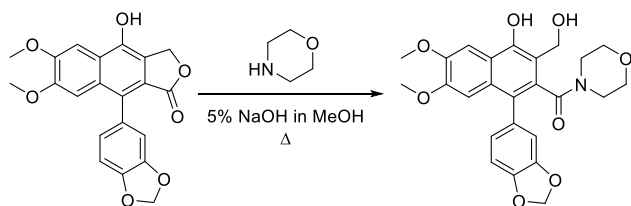
(*E*)-9-(benzo[d][1,3]dioxol-5-yl)-4-hydroxy-6,7-dimethoxy-2-((4-(trifluoromethyl)benzylidene)amino)-2,3-dihydro-1H-benzo[f]isoindol-1-one (**3l**)- **3a** (50mg, 0.126mmol, 1eq) and 4-(trifluoromethyl)benzaldehyde (21 μ l, 26mg, 1.2eq) were dissolved in methanol (10mL). The reaction was heated to reflux overnight, and the final product was purified as above to give a yellow solid (yield: 61mg, 87%, Purity: 99.4%). 1H NMR (500 MHz, DMSO- d_6) δ 10.22 (s, 1H), 8.22 (s, 1H), 7.93 (t, J = 9.0 Hz, 2H), 7.82 (d, J = 8.1 Hz, 2H), 7.65 (s, 1H), 6.99 (d, J = 7.7 Hz, 1H), 6.92 (s, 1H), 6.82 (d, J = 11.5 Hz, 1H), 6.72 (d, J = 8.0 Hz, 1H), 6.09 (s, 2H), 4.87 (s, 1H), 3.91 (s, 3H), 3.61 (s, 3H). LC-MS: m/z : calculated for $C_{29}H_{21}F_3N_2O_6+H^+$, 551.2 $[M+H]^+$, found 551.2 $[M+H]^+$.

General synthesis of ring-opened diphyllin amide synthesis- **2a** (50mg, .131mmol, 1eq) and the amine component (2eq) were dissolved in a 0.5M NaOH in MeOH solution (5mL). The reaction was heated to reflux overnight (16-20h). The reaction was then cooled to room temperature and the solvent was removed under reduced pressure. The reaction was then suspended in 10mL of distilled water and the pH was adjusted to 7. The solution was then added to a separatory funnel and extracted with ethyl acetate (3x30mL). The organic layers were combined and washed with distilled water (30mL) and brine (30mL) before being concentrated under reduced pressure. The crude product was purified using normal phase silica gel chromatography (DCM/MeOH 100/0 to 80/20) to yield the final product.

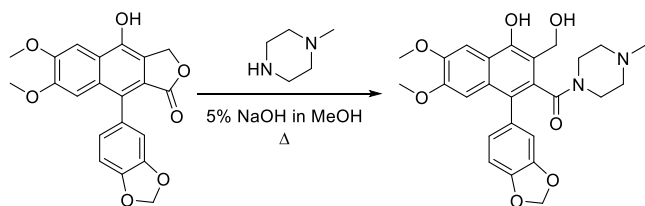


(1-(benzo[d][1,3]dioxol-5-yl)-4-hydroxy-3-(hydroxymethyl)-6,7-dimethoxynaphthalen-2-yl)(piperidin-1-yl)methanone (**4a**)- **2a** (50mg, .131mmol, 1eq) and the piperidine (26 μ l, 22mg, 2eq)

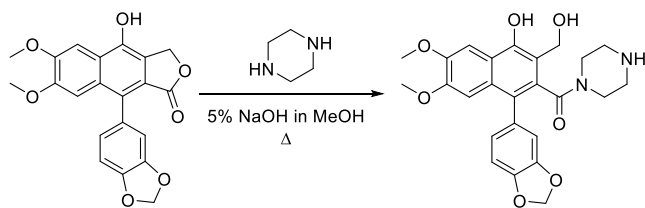
were dissolved in a 0.5M NaOH in MeOH solution (5mL). The reaction was heated to reflux overnight and purified as shown above to yield a yellow solid (yield: 35mg, 57%, Purity: 95.1%). ^1H NMR (500 MHz, DMSO- d_6) δ 7.41 – 7.37 (m, 1H), 7.13 (d, J = 1.7 Hz, 1H), 7.00 (d, J = 8.2 Hz, 1H), 6.89 (d, J = 8.1 Hz, 1H), 6.80 (s, 1H), 6.13 – 6.05 (m, 2H), 3.82 (s, 3H), 3.75 (s, 3H), 3.59 (d, J = 18.3 Hz, 2H), 2.86 – 2.69 (m, 10H). LC-MS m/z : calculated for $\text{C}_{23}\text{H}_{20}\text{O}_7 + \text{H}^+$, 466.2 $[\text{M}+\text{H}]^+$, found 466.3 $[\text{M}+\text{H}]^+$.



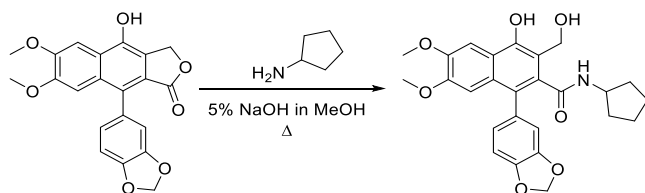
(1-(benzo[d][1,3]dioxol-5-yl)-4-hydroxy-3-(hydroxymethyl)-6,7-dimethoxynaphthalen-2-yl)(morpholino)methanone (**4b**)- **2a** (50mg, .131mmol, 1eq) and morpholine (23 μ l, 23mg, 2eq) were dissolved in a 0.5M NaOH in MeOH solution (5mL). The reaction was heated to reflux overnight and purified as shown above to yield a yellow solid (yield: 26mg, 43%, Purity: 95.4%). ^1H NMR (500 MHz, DMSO- d_6) δ 7.52 (s, 1H), 6.92 – 6.78 (m, 2H), 5.98 (s, 1H), 5.93 (s, 1H), 5.11 (s, 2H), 3.92 (s, 3H), 3.66 (s, 3H), 3.15 – 3.11 (m, 4H), 2.62 (s, 4H), 2.55 (s, 2H). LC-MS m/z : calculated for $\text{C}_{25}\text{H}_{25}\text{NO}_8 + \text{H}^+$, 468.2 $[\text{M}+\text{H}]^+$, found 468.2 $[\text{M}+\text{H}]^+$.



(1-(benzo[d][1,3]dioxol-5-yl)-4-hydroxy-3-(hydroxymethyl)-6,7-dimethoxynaphthalen-2-yl)(4-methylpiperazin-1-yl)methanone (**4c**)- **2a** (50mg, .131mmol, 1eq) and N-methylpiperazine (24 μ l, 21mg, 2eq) were dissolved in a 0.5M NaOH in MeOH solution (5mL). The reaction was heated to reflux overnight and purified as shown above to yield a yellow solid (yield: 10mg, 16%, Purity: 94.6%). ^1H NMR (500 MHz, DMSO- d_6) δ 8.52 (s, 1H), 7.43 (s, 1H), 7.14 (s, 1H), 6.96 (s, 1H), 6.82 (s, 1H), 6.74 (d, J = 8.7 Hz, 1H), 5.94 – 5.84 (m, 2H), 4.98 (s, 2H), 4.06 (s, 1H), 3.74 (s, 3H), 3.20 (s, 3H), 3.03 (s, 8H), 1.20 (s, 3H). LC-MS m/z : calculated for $\text{C}_{26}\text{H}_{28}\text{N}_2\text{O}_7 + \text{H}^+$, 517.1161 $[\text{M}+\text{H}]^+$, found 481.2 $[\text{M}+\text{H}]^+$.



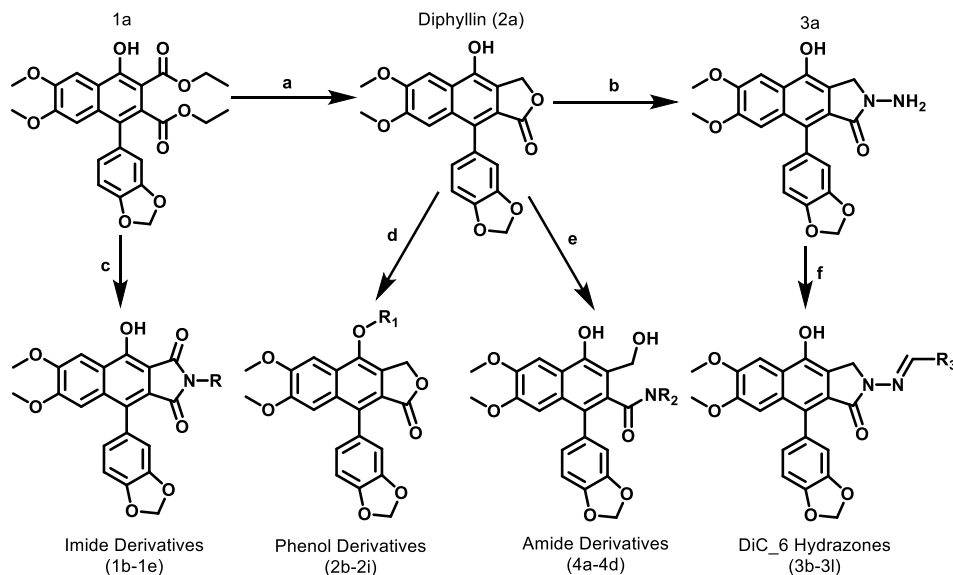
1-(benzo[d][1,3]dioxol-5-yl)-4-hydroxy-3-(hydroxymethyl)-6,7-dimethoxynaphthalen-2-yl(piperazin-1-yl)methanone (4d)- **2a** (50mg, .131mmol, 1eq) and piperazine (23mg, 2eq) were dissolved in a 0.5M NaOH in MeOH solution (5mL). The reaction was heated to reflux overnight and purified as shown above to yield a yellow solid (yield: 12mg, 20%, Purity: 93.2%). ¹H NMR (500 MHz, DMSO-*d*₆) δ 7.65 (s, 1H), 7.09 (s, 1H), 6.97 (d, *J* = 8.7 Hz, 1H), 6.84 (s, 1H), 6.73 (d, *J* = 8.7 Hz, 1H), 6.10 (s, 2H), 5.35 (s, 2H), 3.91 (s, 3H), 3.55 (s, 3H), 2.69 (s, 6H). LC-MS *m/z*: calculated for C₂₅H₂₆N₂O₇+H⁺, 467.2 [M+H]⁺, found 467.1 [M+H]⁺.



1-(benzo[d][1,3]dioxol-5-yl)-N-cyclopentyl-4-hydroxy-3-(hydroxymethyl)-6,7-dimethoxy-2-naphthamide (4e)- **2a** (50mg, .131mmol, 1eq) and cyclopentylamine (26μl, 23mg, 2eq) were dissolved in a 0.5M NaOH in MeOH solution (5mL). The reaction was heated to reflux overnight and purified as shown above to yield an off-white solid (yield: 21mg, 19%, Purity: 96.7%). ¹H NMR (500MHz, DMSO- *d*₆) 7.50(s, 1H), 6.91(s, 1H), 6.75(s, 1H), 6.73(s, 1H), 6.675(d, *J*=5Hz, 1H), 6.03(d, *J*=20Hz, 2H), 4.03(s, 2H), 3.84(s, 3H), 3.56 (s, 3H), 3.31(b, 1H), 3.21(s, b,1H), 1.84(m, 2H), 1.64(m, 2H), 1.5(m, 4H). LC-MS *m/z*: calculated for C₂₆H₂₇NO₇+H⁺, 466.2 [M+H]⁺, found 466.1 [M+H]⁺.

2.4 Results

Four series of diphyllin-related compounds were synthesized to determine the tolerance of modifications of the lactone ring and alkylation of the phenol functional group (**Scheme 1**). Synthesis of intermediate **1a** was completed using modified procedures from Charlton et al.³⁸⁵ A set of imide derivatives were synthesized by condensation of primary amines with **1a** (Scheme 1). Diphyllin (**2a**) was synthesized from **1a** by selective reduction with lithium aluminum hydride and the final three series were synthesized with **2a** as the starting material. A set of propyl ether



Scheme 2.1. Synthesis of Diphyllin Derivatives.

Reagents and Conditions. (a) LiAlH_4 , THF, 0°C , 1h (92%); (b) H_2NNH_2 , MeOH, reflux, 12h (66%); (c) RNH_2 , MeOH, reflux, 2-12h (57-93%); (d) RX , K_2CO_3 , DMSO, 60°C , 1-48h (36-91%); (e) R_2NH , 0.5 M NaOH in MeOH, reflux, 12-18h (16-57%); (f) R_3CHO , MeOH, reflux, 6-12h (47-88%).

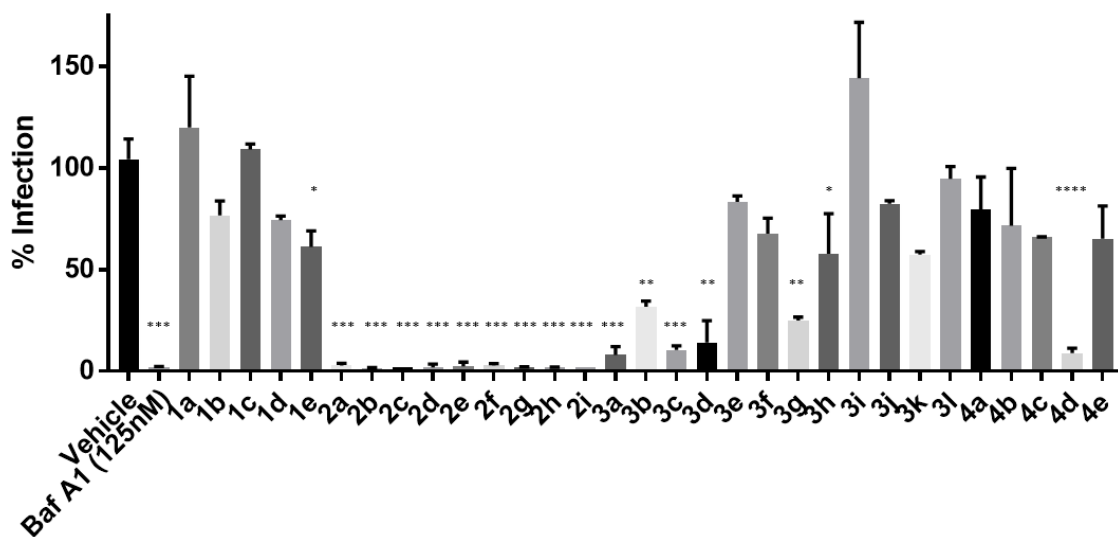


Figure 2.1. Antiviral Screening of Ebolavirus (EBOV) infection at $12.5\ \mu\text{M}$ in HeLa cells.

All four classes of compounds were screened for inhibitory activity against a GFP-expressing Ebola pseudovirus at $12.5\ \mu\text{M}$ to isolate compounds with activity against EBOV infection. Significance was determined using a one-way ANOVA test with multiple comparison to the vehicle-treated control. * $p>0.05$, ** $p>0.005$, *** $p>0.001$. ****excluded due to instability. This work was completed by Manu Anantpadma in the Davey lab at Boston University.

derivatives were synthesized by Williamson synthesis to incorporate tertiary amine and hydrophobic groups. The hydrazone derivatives were synthesized by first using the nucleophilic attack of hydrazine upon the lactone ring to create the hydrazide derivative **3a**. Then, condensation of **3a** with a set of substituted benzyl aldehydes provided a hydrazone series. Benzyl aldehydes were chosen with a broad range of physical properties, including pentafluoro, to test the toleration of modifications at the aryl position. Ring-opened amides were synthesized by nucleophilic attack of both primary and secondary amines upon the lactone ring of diphyllin to yield 1 secondary amide and 4 tertiary amides. All four classes were evaluated for potential PAINS alerts using SwissADME (**Table 2.1**).³⁸⁶ Only the hydrazone class demonstrate potential alerts, due to the imine functional group.

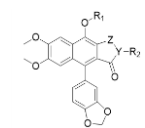
All four classes were screened for the ability to inhibit EBOV infection using a GFP-expressing EBOV GP pseudotyped vesicular stomatitis virus (VSV) in HeLa cells (**Fig. 2.1**). Diphyllin, one imide (**1e**), diphyllin hydrazide (**3a**), 5 hydrazones (**3b-d, g, h**), and all phenol ethers (**2b-i**) significantly inhibited the pseudotyped viral infection at 12.5 μ M. Compounds were then ranked by IC₅₀ to further evaluate the actives. Phenol ether derivatives demonstrated the greatest potency amongst those tested and **2e** displayed a 11.5-fold improvement in potency compared to diphyllin (**Table 2.2**). In general, phenol ether derivatives were the best class of derivatives with both hydrophobic and amino-alkyl ethers exhibiting improved potency compared to diphyllin. Hydrazones with para-substituted benzyl groups had the best activity within their class, though they were 1.4-fold less potent than diphyllin at best.

To evaluate a role for V-ATPase function as a mechanism for inhibition of EBOV cell entry, all active compounds were screened for the ability to inhibit endosomal acidification in HEK-293 cells. The dichromatic dye acridine orange (AO) freely passes through cells in its uncharged form but accumulates in acidic endosomal compartments as the dye becomes protonated and aggregates. The ratio between the neutral dye, which emits at 530 nm, and the charged dye, which shifts its emission to 650 nm, can be used to detect vesicle acidification in cells.^{381,387} Candidate V-ATPase inhibitors were identified in HEK-293 cells by a significant decrease in the 650 nm/530 nm ratio of AO fluorescence when compared to the vehicle control. The IC₅₀ values for inhibition of endosomal acidification (EA assay) were then compared with the cytotoxicity values (CC₅₀) in the same cell lines to determine if the different activities could be separated. In this assay, known V-ATPase inhibitors Baf and diphyllin (**2a**) showed a potency

Table 2.1. SwissADME LogP and PAINS Information for Compounds in Chapter 2

ID	Consensus LogP	PAINS alerts
1a	3.97	0
1b	2.34	0
1c	2.65	0
1d	2.94	0
1e	2.80	0
2a	3.23	0
2b	3.62	0
2c	3.94	0
2d	3.92	0
2e	4.56	0
2f	3.85	0
2g	3.81	0
2h	3.87	0
2i	3.35	0
3a	2.34	1 (hydrazide)
3b	4.18	1 (imine)
3c	3.45	1 (imine)
3d	4.71	1 (imine)
3e	4.79	1 (imine)
3f	4.51	1 (imine)
3g	3.96	1 (imine)
3h	5.56	1 (imine)
3i	4.77	1 (imine)
3j	4.03	1 (imine)
3k	4.25	1 (imine)
3l	5.13	1 (imine)
4a	3.46	0
4b	2.52	0
4d	2.3	0
4c	2.56	0
4e	3.52	0

Table 2.2. Activity of diphyllin and derivatives against EBOV infection, endosomal acidification and cytotoxicity.



ID	R ₁	R ₂	Y	Z	Pseudo-EBOV IC ₅₀ (nM) ^a	HEK EA IC ₅₀ (nM) ^b	HEK-293 CC ₅₀ (μM)	HEK-293 IC ₅₀ /CC ₅₀ ^c
Baf	-	-	-	-	14.9±8.93	40.5±3.31	0.32±0.042	7.90
1e			N	CO	5400±2920	>10000	ND	ND
2a	H	-	O	CH ₂	847±125	476±60.1	17.8±4.31	37.4
2b	CH ₃	-	O	CH ₂	171±40.2	265±58.6	5.73±0.841	21.6
2c	CH ₂ CH ₃	-	O	CH ₂	112±14.7	254±49.0	2.38±0.229	9.37
2d		-	O	CH ₂	175±21.7	263±46.6	2.04±0.270	7.76
2e		-	O	CH ₂	73.2±11.9	102±19.0	4.04±2.03	39.6
2f		-	O	CH ₂	93.1±26.8	98.7±29.5	3.31±0.740	31.7
2g		-	O	CH ₂	107±23.7	74.3±23.9	11.2±2.49	151
2h		-	O	CH ₂	132±32.3	172±40.6	24.7±2.68	144
2i		-	O	CH ₂	76.2±14.6	104±21.2	31.1±4.82	299
3a	H		N	CH ₂	3940±604	9060±893	48.9±3.61	5.40
3b	H		N	CH ₂	6630±437	>10000	ND	ND
3c	H		N	CH ₂	4480±467	8710±769	49.9±15.9	5.73
3d	H		N	CH ₂	1170±518	9930±140	28.4±2.71	2.86
3g	H		N	CH ₂	1690±233	>10000	ND	ND
3h	H		N	CH ₂	8740±2180	>10000	ND	ND

[a] Inhibition of GFP-expressing EBOV GP pseudotyped vesicular stomatitis virus (VSV) infection of HeLa cells; mean±SEM (n=6). [b] Inhibition of cellular endosomal acidification in HEK-293 cells; mean±SEM (n=9). [c] Selectivity Index of cytotoxicity over endosomal acidification in HEK-293 cells. The pseudo-ebolavirus work was completed by Manu Anantpadma in the Davey lab at Boston University.

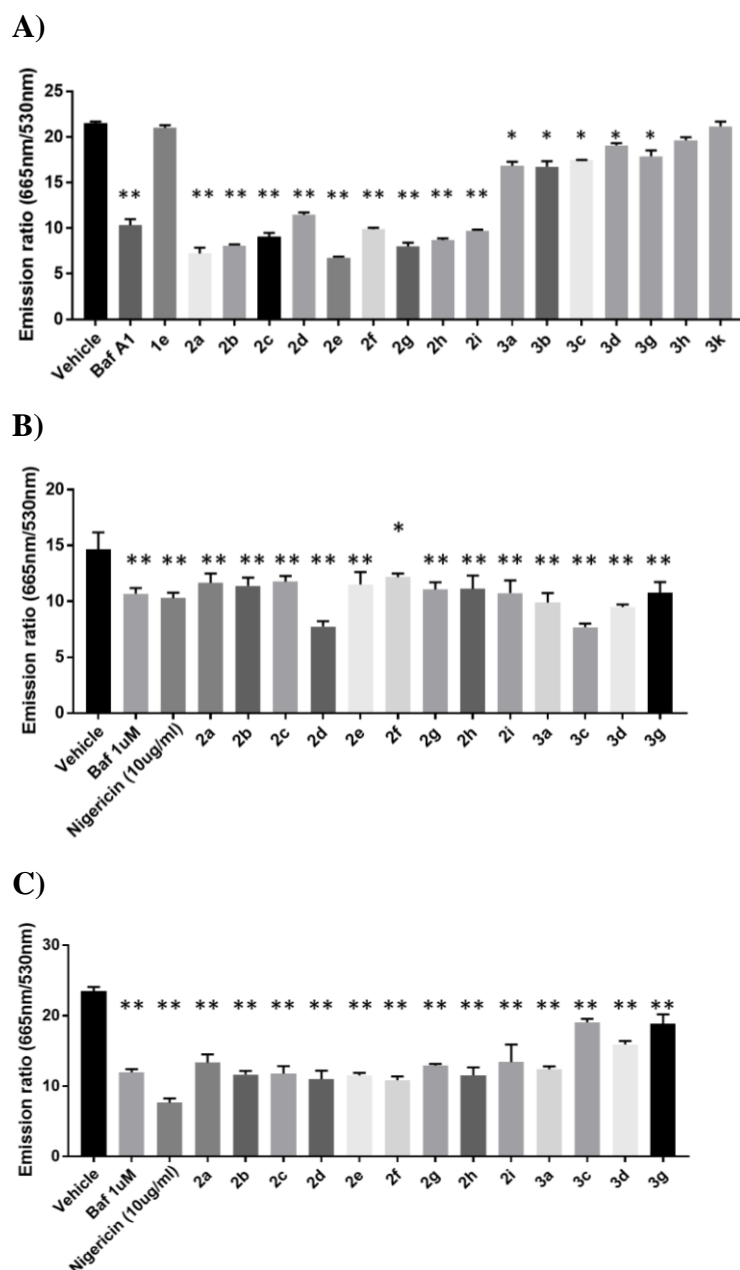


Figure 2.2. Screening of hit compounds with HEK-293 cells for activity against endosomal acidification.

A) All compounds that were active in the EBOV screen were further screened for activity against cellular endosomal acidification. To identify any compounds that may inhibit endosomal acidification through colloid formation or compound aggregation: B) Hits were further screened for inhibition in the presence of 0.01% Triton X-100 to remove any artifacts from compound aggregation using the same assay setup and C) Hits compounds were suspended in assay media and centrifuged at 14,000xg for 10min before adding to cells to remove any potential aggregates from solution before performing the endosomal acidification assay. Significance was determined using a one-way ANOVA test with multiple comparison to the vehicle-treated control (untreated). * $p > 0.01$, ** $p > 0.001$.

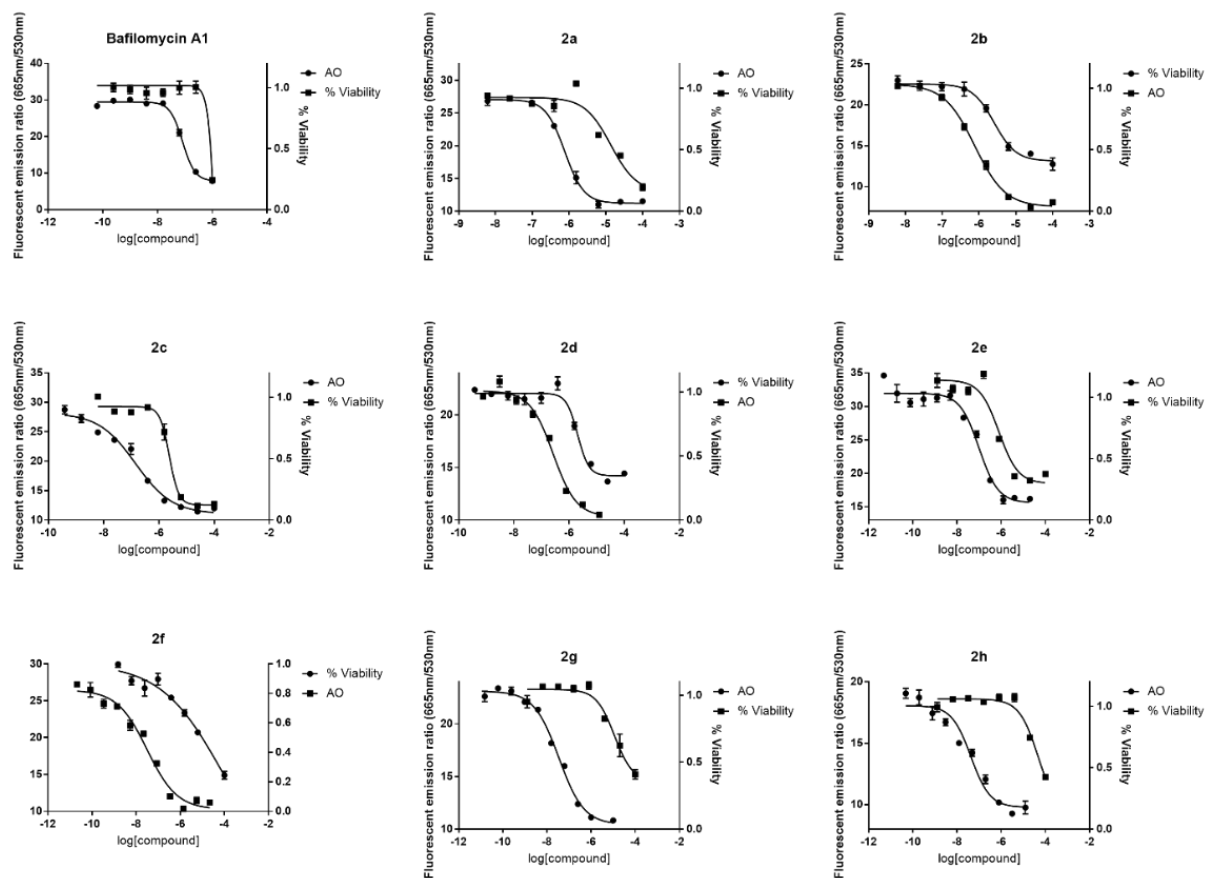
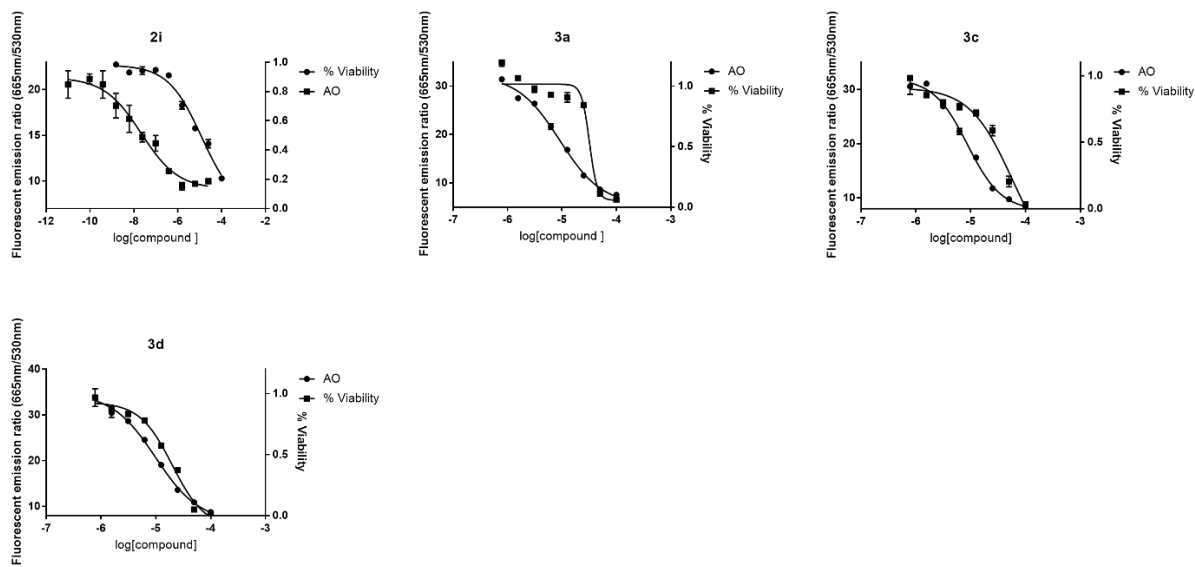


Figure 2.3. Selectivity Indices (CC₅₀/IC₅₀) graphs of compound hits in HEK-293 cells.

Graphs detail the difference between a compounds cytotoxicity (% Viability), determined by MTT assay, and its ability to inhibit endosomal acidification (AO), determined with the cellular acridine orange assay. Selectivity indices were calculated by dividing the CC₅₀ by the IC₅₀. Curves were fitted using the log[inhibitor] vs. response – Variable Slope (four parameters) function in the Analysis tool of GraphPad Prism 7.02.

Figure 2.3 (cont.)



that was consistent with those observed in the pseudo-EBOV cell entry. The well-established V-ATPase inhibitor Baf was more potent than diphyllin in the assay but its cytotoxicity was also significantly enhanced. Activity was tested in two cell lines (HEK-293 and A549) to assess the activity of derivatives in different cell environments. The A549 cell line was chosen for comparison to previous reports using diphyllin, while HEK-293 cells offer a model relevant to previous EBOV inhibitor screens.^{360,381,388,389}

The endosome acidification screen identified significant differences among the three diphyllin analog classes selected from the original screen (**Table 2.2** and **Fig. 2.2**). Overall, the relative potencies in this assay track with the EBOV cell entry effects. Imide **1e** did not cause a significant change in the fluorescence ratio, indicating a lack of any effect on endosomal acidification. Hydrazide **3a** and four of the six active hydrazones moderately inhibited acidification but none achieved the level of inhibition observed with **2a**. Only hydrazide **3a** and hydrazones **3c** and **3d** inhibited acidification to the level observed with Baf at concentrations higher than 10 μ M but these compounds were 18-fold less potent than diphyllin on average (**Fig 2.2**). Unfortunately, the cytotoxicity of this class of compounds had minimal separation from inhibition of endosomal acidification. The 10-fold difference between IC₅₀ values in the two assays for this class likely indicate activity against a separate target during EBOV entry assay.

The phenol derivatives presented a different profile from the other classes when endosomal acidification and cytotoxicity were assessed (**Table 2.2** and **Fig. 2.2**). All phenol ethers inhibited acidification at a level similar to Baf and exhibited improved IC₅₀ values compared with diphyllin. Remarkably, the basic heterocycle containing derivatives (**2g-2i**) also exhibited up to an 8-fold improvement in separation of cytotoxicity compared with diphyllin (38-fold compared to Baf) in HEK-293 cells as indicated by the IC₅₀/CC₅₀ ratios. These derivatives potently inhibited endosomal acidification and exhibited decreased cytotoxicity compared to diphyllin in both HEK-293 and A549 cell lines. The morpholino ether derivative **2g** was the more potent derivative in both cell lines and demonstrated similar cytotoxicity to diphyllin. The piperazinyl acetate ether **2h** demonstrated less activity compared to the morpholino but also had lower cytotoxicity and a similar separation as **2g** in HEK-293 cells. Derivative **2i** demonstrated the greatest separation of the ether derivatives at nearly 300. Interestingly, the lipophilic derivatives exhibited a similar, or better, potency compared to the amino ethers but also increases in cell toxicity. Derivative **2f** had a similar potency to **2g** in the endosomal acidification assay but increased cytotoxicity 5-fold

relative to diphyllin. Alkyl derivative **2c** was the most potent of all derivatives in the A549 cell line but 4-fold less potent in HEK-293 cells (**Table 2.3**) and more cytotoxic. Thus, while the lipophilic derivatives demonstrated greater potency than diphyllin, they were more cytotoxicity up to 10-fold in HEK-293 cells. Overall, far less cytotoxicity was observed in A549 cells for all tested ethers compared to HEK-293 cells but activities against endosomal acidification were similar. In general, the more basic derivatives expanded the separation of endosomal acidification and cytotoxicity in HEK-293 cells compared to diphyllin. The lack of discrimination of cytotoxicity observed with the A549 cells indicate their utility to be minimal since they lack the level of stringency needed to define therapeutically selective inhibitors.

Since acridine orange is a promiscuous dye and can integrate with nucleic acids to also give a fluorescent emission, FITC-dextran fluorescence was used to further assess the ability of our top compounds to change endosomal pH. FITC-dextran is exclusively trapped in endosomes and the FITC fluorescence is quenched by increasing acidity. Fluorescent microscopy of FITC-dextran stained cells indicated that diphyllin and amino ether **2g** demonstrated increased FITC fluorescence relative to the vehicle-treated control (**Fig. 2.4A**). FITC-dextran was also used to quantify endosomal pH in cells treated with diphyllin and derivatives. All treatments resulted in elevated endosomal pH (pH 7) at low micromolar concentrations (1-7 μ M; **Fig. 2.4B**). To ensure that the change in endosomal pH was not due to an overall change in cellular pH, cytosolic pH was measured with the BCECF-AM dye mixture. Treatment with Baf, **2a** and its derivatives showed no significant change in cytosolic pH compared to the vehicle treated control (**Fig. 2.4C**). In combination with the acridine orange assays, these results are consistent with no optical interference by the aryl naphthalene lactone chromophore.

To assess if the inhibition of endosomal acidification results from a block in V-ATPase activity, the active diphyllin derivatives were tested in the proton-pumping and ATPase functional assays. Vesicles containing V-ATPase were isolated from HEK-293 cells by adapting a published method.³⁸³ To determine the effect of compounds upon the proton-pumping function of V-ATPase, vesicles were pre-incubated with acridine orange and the test compound or vehicle for 1 h prior to the addition of ATP to initiate pump activity. Quenching of the 530 nm emission of acridine orange was measured over 1 h before addition of nigericin to relax the proton gradient within vesicles. IC₅₀ values for hit compounds from the cellular assays were calculated by measuring the change

Table 2.3. Inhibition of endosomal acidification, Cytotoxicity and SI data for A549

ID	A549 EA IC ₅₀ (nM) ^a	A549 CC ₅₀ (μM)	A549 EA IC ₅₀ /CC ₅₀ ^b
Bafilomycin A1	21.3±2.55	0.479±0.266	22.5
2a	149±20.5	50.1±15.5	336
2b	58.2±8.76	>100	>1720
2c	52.4±19.3	77.4±11.0	>1480
2e	84.8±11.9	>100	>1180
2g	56.1±15.9	>100	>1780
2h	101±13.8	>100	>990
3a	8110±670	28.7±16.6	3.40
3c	11,600±840	50.1±27.7	4.32
3d	8440±367	78.0±26.4	9.24

[a] Inhibition of cellular endosomal acidification in HEK-293 cells; mean±SEM (n=9). [b] Selectivity index of cytotoxicity over endosomal acidification.

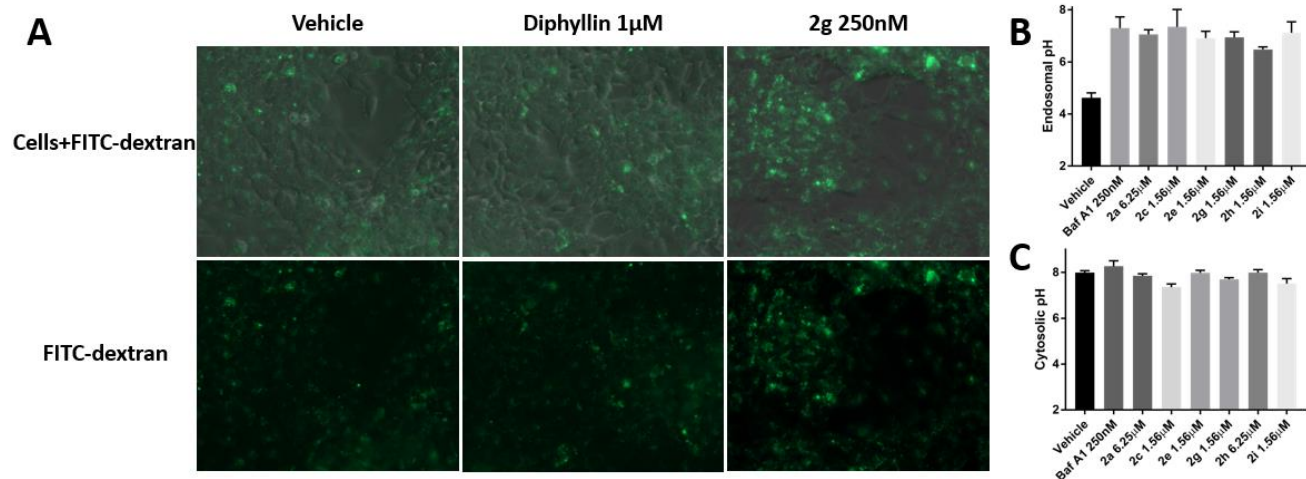


Figure 2.4. Diphyllin derivatives cause an increase in intracellular vesicle pH but no corresponding change in cytosolic pH.

A) FITC-dextran stained (0.5mg/ml) HEK-293 cells after 4h treatment with chosen inhibitor or vehicle. B) Endosomal pH measured by FITC-dextran staining of HEK-293 cells after 4h treatment with chosen inhibitor or vehicle. C) Cytosolic pH measured by BCECF-AM staining (10μg/ml) of HEK-293 cells after 4h treatment with chosen inhibitor or vehicle.

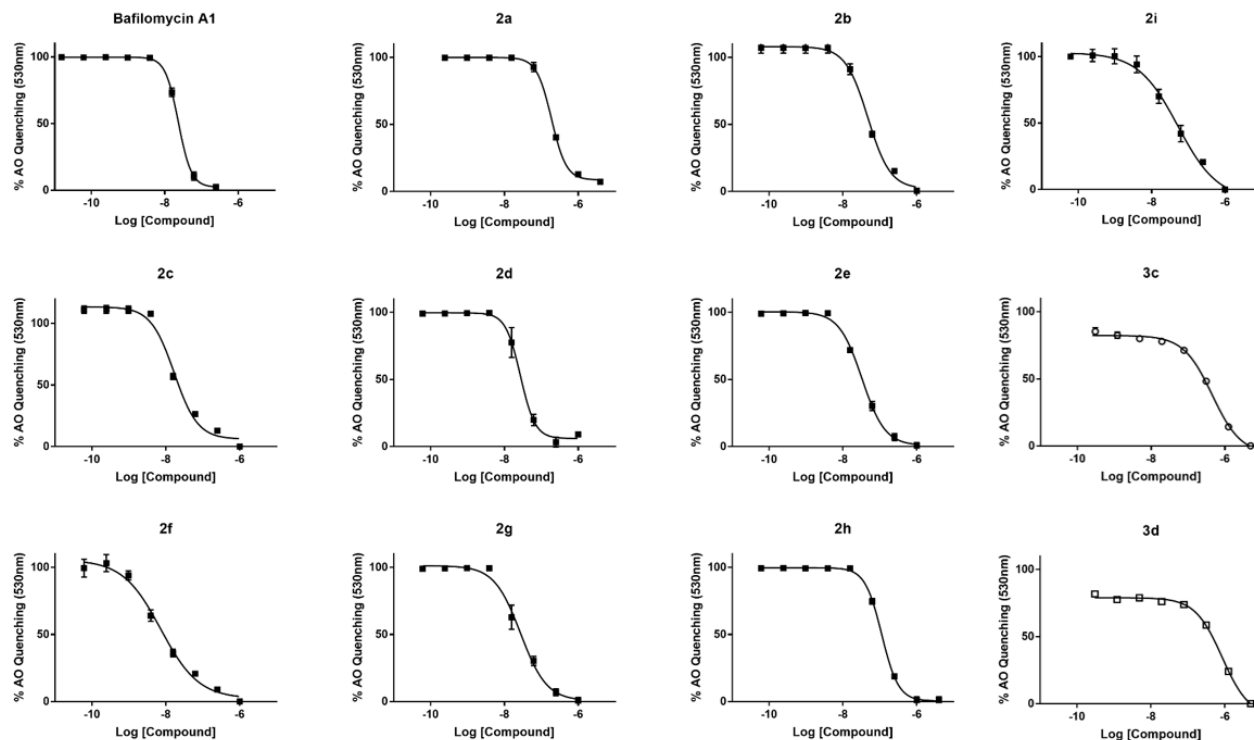


Figure 2.5. Dose-response curves of the inhibition of V-ATPase mediated proton-translocation by diphyllin and derivatives.

ATP was added to the vesicle mixture on 96-well plates and incubated for 1 h at room temperature before reading fluorescence at 530 nm when excited at 485 nm. Nigericin was then added and the fluorescence after 10 min was again measured. The difference between the two fluorescence values was used to determine the amount of acridine orange quenched. Data are shown as mean \pm standard error of the mean of the change in fluorescence at each inhibitor concentration. Curves were fitted using the log[inhibitor] vs. response – Variable Slope (four parameters) function in the Analysis tool of GraphPad Prism 7.02.

Table 2.4. Inhibitory Activity of Derivatives against Isolated Human V-ATPase

Compound	Proton Pump IC ₅₀ (nM) ^[a]	ATPase Inhibition ^[b]
Baf	24.8±2.66	(+)
2a	189±1.66	(+)
3c	423±3.96	(-)
3d	724±13.5	(-)
2b	47.5±5.28	(+)
2c	16.9±3.72	(+)
2e	11.7±2.97	(+)
2g	27.4±3.88	(+)
2h	114±1.71	(+)
2i	61.0±2.84	(+)

(+) denotes significantly less Pi released than control ($p > 0.01$). [a] Inhibition of V-ATPase induced AO quenching; mean±SEM (n=9). [b] Inhibition of V-ATPase induced ATP hydrolysis; mean±SEM (n=9).

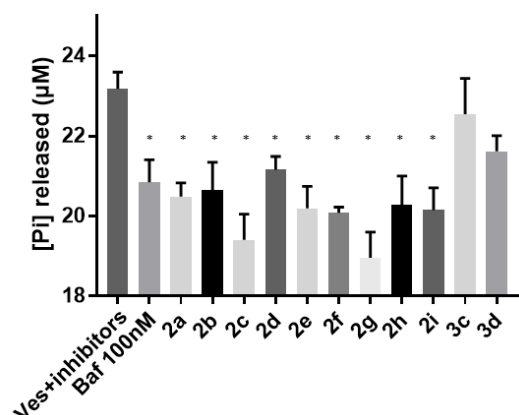


Figure 2.6. 1 μM screening of compound hits with HEK-293 vesicles for ATPase activity.

Phosphate ions (P_i) released after 1 h incubation at 37°C was quantified using the P_i detection assay with malachite green for all compounds tested for the inhibition of proton-pumping ability in the biochemical acridine orange quenching assay. Significance was determined using a one-way ANOVA test with multiple comparison to the vehicle-treated control. Compounds that were considered significantly different than the control were labeled (+) (* $p > 0.01$, Table 2).

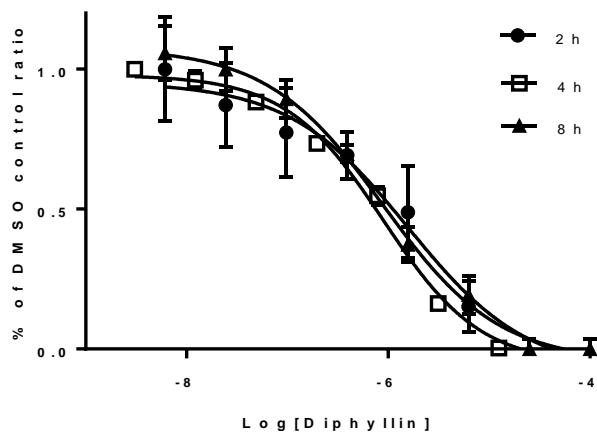


Figure 2.7. Inhibition of Cellular Endosomal Acidification is not Time-Dependent in HEK-293 cells.

HEK-293 cells were treated with doses of **2a** and endosomal acidification was assessed at 2 h, 4 h, and 8 h using the dye acridine orange. Curves were fitted using the log[inhibitor] vs. response – Variable Slope (four parameters) function in the Analysis tool of GraphPad Prism 7.02.

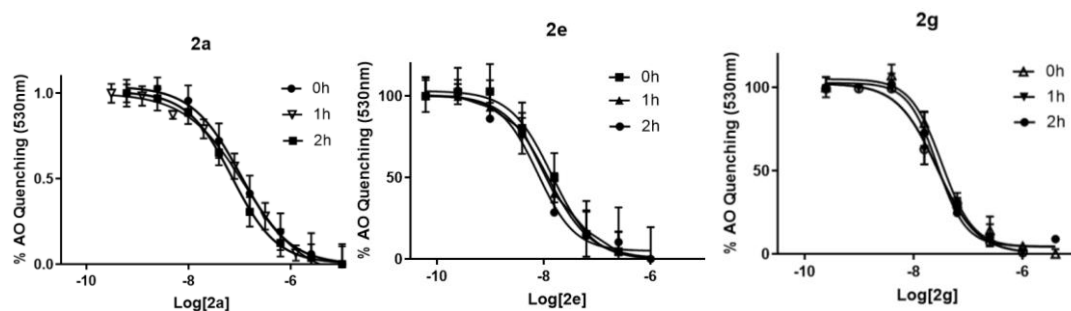


Figure 2.8. Inhibition of V-ATPase mediated acridine orange quenching is not time-dependent.

Vesicles isolated from HEK-293 cells were treated with varying concentrations of **2a**, **2e**, and **2g**. Then, the assay was either conducted immediately or incubated for 1 h or 2 h. Dose-response curves of the change in quenching of acridine orange are shown for each treatment and overlaid for each inhibitor. Curves were fitted using the log[inhibitor] vs. response – Variable Slope (four parameters) function in the Analysis tool of GraphPad Prism 7.02.

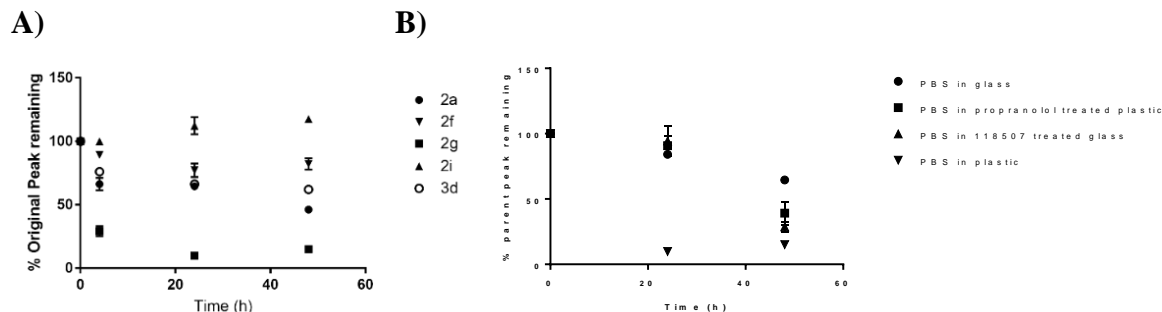


Figure 2.9. Stability of select compounds under assay conditions.

A) Compounds **2a**, **2f**, **2g**, **2i**, **3d** were tested for their time-dependent stability in DMEM+FBS over 48 h. Samples were withdrawn at 0 h, 4 h, 24 h and 48 h and diluted in 9 volumes of acetonitrile+0.1% trifluoroacetic acid to precipitate out serum proteins. Data shown are the mean \pm the standard error of the mean for each sample and time point for 5 individual experiments. B) Subsequent follow-up studies with compound **2g** showed compound loss was not due to the media but interaction with the plastic used during the assay. Conducting the assays in glass exhibited little loss of compound until 48h into the assay. Treatment of plastic or glass with 100mM propranolol for 24h also decreased loss of **2g** significantly compared with the control at the 24h mark.

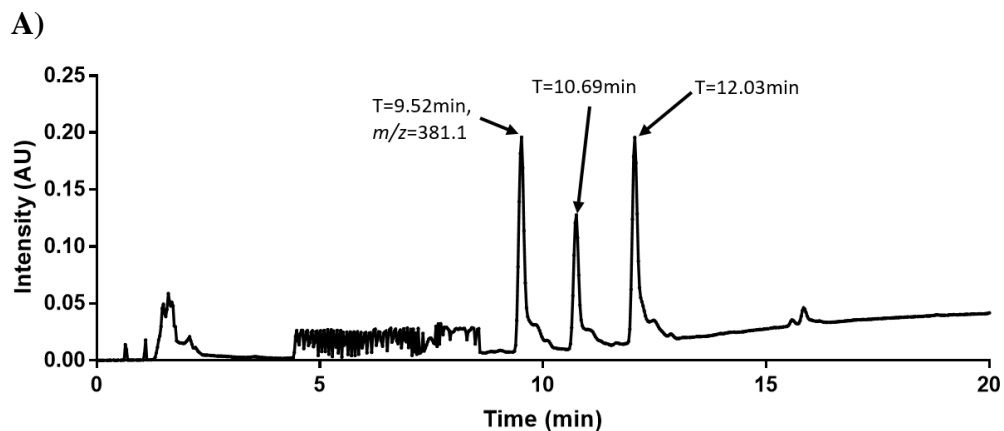
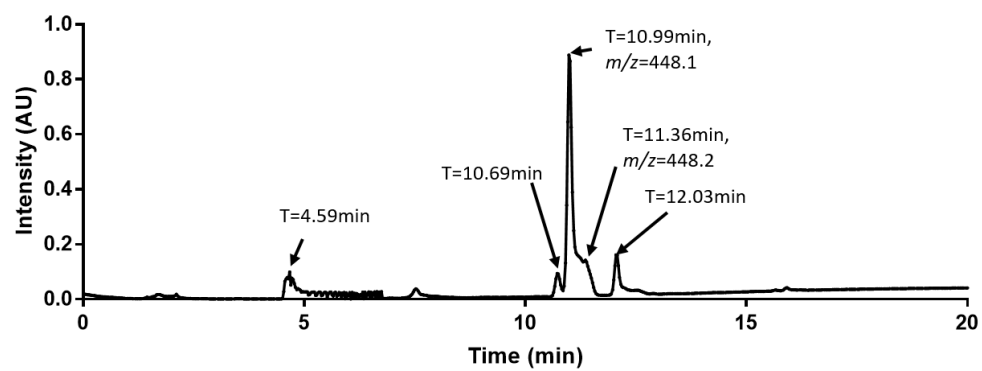


Figure 2.10. Example chromatographs from the isolation of select inhibitors from treated HEK-293 cells.

HEK-293 cells were treated with **2a** (chromatograph A), **2f** (B), and **2g** (C) for 24 h before extraction with a 1:1:0.005 methanol:acetonitrile:trifluoroacetic acid solution for 16 h. The solution was removed and centrifuged for 10 min at 14,000xg to remove remaining cellular debris and concentrated. Samples were run using a Hitachi D-7000 HPLC system to identify potential metabolic products of the select inhibitors. Peaks present in the DMSO-treated control are indicated by retention time on each chromatograph but were not further analyzed. Peaks that were not present in the DMSO-treated control sample were collected and analyzed with an Advion expression Compact Mass Spectrometer and the major m/z is indicated with the retention time of the peak.

Figure 2.10 (cont.)

B)



C)

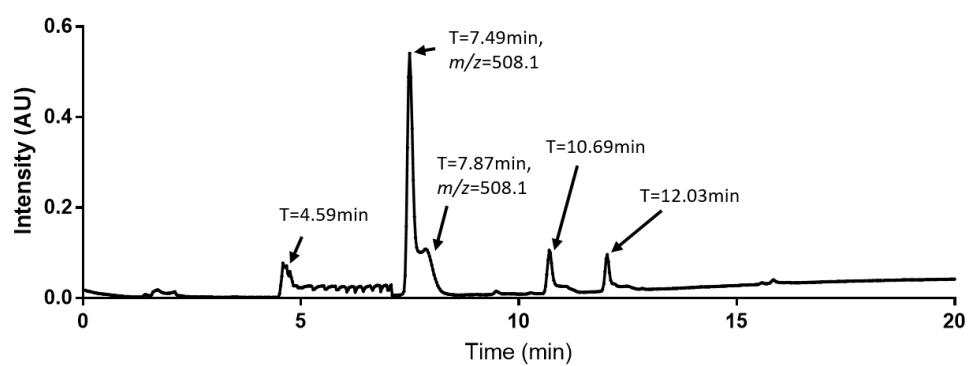


Table 2.5. Anti-Filoviral activity of Diphyllin and Top Derivatives in HeLa and Primary Human Macrophages.

Compound	HeLa CC ₅₀ (μ M) ^[a]	Pseudo- EBOV IC ₅₀ /CC ₅₀ ^[b]	Pseudo- MARV IC ₅₀ (nM) ^[c]	MARV IC ₅₀ /CC ₅₀ ^[b]	PHM EBOV IC ₅₀ (nM) ^[d]	PHM IC ₅₀ / CC ₅₀ ^[b]
2a	>100	>147	1770 \pm 80.0	>56.5	678 \pm 218	>73.7
2e	36.5 \pm 7.13	499	402 \pm 45.9	90.8	240 \pm 36.4	>416
2g	36.6 \pm 18.8	342	135 \pm 11.4	271	57.7 \pm 8.6	>1530
2h	63.0 \pm 11.2	477	81.6 \pm 28.7	772	256 \pm 21.3	>391

[a] Cellular cytotoxicity for select compounds; mean \pm SEM (n=6). [b] Selectivity index between cytotoxicity and inhibition of infection. [c] Inhibition of GFP-expressing MARV GP pseudotyped vesicular stomatitis virus (VSV) infection of HeLa cell; mean \pm SEM (n=6). [d] Inhibition of replication-competent EBOV infection; mean \pm SEM (n=6). This work was completed by Manu Anantpadma in the Davey lab at Boston University.

in AO fluorescence immediately before and after the addition of nigericin (**Fig. 2.5**). Overall, inhibition of V-ATPase activities followed a similar activity profile to the cellular assays. Diphyllin was 7.5 times less potent than Baf at inhibiting V-ATPase-mediated fluorescent quenching (**Table 2.4**). All phenol derivatives had improved inhibitory potency relative to diphyllin and several had similar activities to Baf. The lipophilic and amino phenol derivatives had 8-17 times greater potencies relative to diphyllin with 2e demonstrating a 2-fold improvement over Baf. Hydrazone derivatives **3c** and **3d** were 2 and 4 times less potent, respectively, than diphyllin which provided additional evidence that these are weak inhibitors of V-ATPase and less selective for the on-target effects.

Using the same vesicle preparations, the effect of the diphyllin derivatives on ATP hydrolysis by V-ATPase was evaluated. Isolated HEK-293 vesicles were pre-incubated with the active compounds for 1 h at a concentration of 1 μ M. ATP was then added to the vesicles and the amount of ATP hydrolyzed after 1 h was measured using malachite green to quantify free phosphate released by ATPase action. Diphyllin and the phenol ether derivatives inhibited ATP hydrolysis to a similar extent at 1 μ M compared to Baf, while hydrazones **3c** and **3d** did not (**Table**

2.4 and **Fig. 2.6**). These data are consistent with the cellular endosomal assay screen and verify that the work-flow identifies compound as significant V-ATPase inhibitors that block viral cellular entry. To further substantiate the compound effects in these assays, diphyllin and compounds **2e** and **2g** were all evaluated for time dependence of effects in both the cellular endosomal acidification assay and the biochemical assay (**Fig. 2.7, 2.8**). In both cases, there was no observed time dependent changes in the percent inhibition. The chemical stability of compounds **2a, 2f, 2g, 2i, 3d** were also evaluated in cell culture media. In the time course of the inhibition assays, no significant degradation products were observed (**Fig. 2.9**). Compounds **2a, 2f, 2g** were also tested for stability in HEK-293 cell culture for 24 h (**Fig. 2.10**) and no apparent degradation products were observed.

To determine if our derivatives are broadly active against the *Filoviridae* family, the top active derivatives were tested for the ability to inhibit MARV infection. While related to EBOV, MARV utilizes different cellular entry pathways from EBOV but it is still dependent upon endosomal acidification.⁴⁷ Therefore, the top active amino and hydrophobic phenol ether derivatives, **2e, 2g, and 2h** were further assessed for activity against MARV cellular entry in the HeLa cell model using a GFP-expressing MARV GP-pseudotyped VSV. Both derivative **2e** and diphyllin suffered significant losses in potency against MARV compared with their activities against EBOV infection. However, amino ether derivatives **2g** and **2h** did not significantly change potency against MARV compared with their activities against EBOV infection, indicating these derivatives may have a broader anti-viral activity (**Table 2.5**). These data indicate that the derivatives, especially the amino-alkyl derivatives, selectively block activities required for cell entry common to both classes of filoviruses without increasing cytotoxicity (**Table 2.5**).

The top active derivatives were used to evaluate the inhibition of replication-competent EBOV infection of primary human macrophages with impressive results. Macrophages and other monocyte-derived cells are a primary cell target of infection by EBOV and derivative activity against EBOV infection in this model may better indicate activity during host infection. The three compounds tested in macrophage had a greater than 3-fold improvement in activity over diphyllin, with **2g** having the most potent activity (11.8-fold). The derivatives also displayed greater separations (>300X) of anti-viral activity over cytotoxicity in the primary macrophages. Note that the only compound with a measurable CC₅₀ was **2g**, which had a separation of 1525 from IC₅₀ which indicates an even greater separation for the other two derivatives. For instance, compound

2h showed lower cytotoxicity than **2g**. The difference between the cytotoxicities in immortalized cell lines and primary macrophages could be due to the inhibition of the growth of the immortalized cell lines as opposed to true toxicity. The inhibitors may cause immortalized cells to stop dividing due to resource strain from the inhibition of endocytic pathways or other off-target effects while the cytostatic macrophages are not dividing and would not suffer from the same resource strain. The lack of dividing cells would cause changes in the MTT assay results while the lack of a resource strain on the macrophages would not change their ATP levels. Overall, these data indicate that these derivatives are potent inhibitors of EBOV infection of macrophages and appear safe within a wide range of active concentrations.

2.5 Discussion

In summary, we synthesized four classes of diphyllin derivatives and tested them for the ability to inhibit EBOV infection and cellular endosomal acidification. Phenol ethers proved to be among the most potent V-ATPase inhibitors reported to date and this activity directly correlated with blockade of cellular endosomal acidification and EBOV infection. The activities of the derivatives against filovirus cell entry and endosomal acidification were paralleled by the activity against isolated V-ATPase containing vesicles. Together, these data are consistent with a mechanism of blocking viral infection that involves inhibition of V-ATPase. Concordantly, the less active V-ATPase inhibition of the hydrazone and imide classes show reduced potency and dose selectivity in cell-based assays.

The best derivatives herein described have very potent V-ATPase inhibitory activities but less cytotoxicity than compared to known V-ATPase inhibitors. The increase in selectivity for the alkylamino phenol derivatives may be due to trapping within the endosome. This localization would trap the compounds in acidic organelles by protonation of the amine functional group where the virus, V-ATPase, and inhibitor must co-localize. Confining the inhibitor to the organelles where V-ATPase is active could minimize off-target effects of the inhibitors within cells and thus minimize toxicity. Further studies of the alkylamine group could lead to optimization of the compounds selectivity and *in vivo* evaluation of potential metabolic liabilities of the scaffold is also needed. Overall, these results represent the first example of structural derivatization of a natural product scaffold to enhance the selectivity of V-ATPase inhibitors for blocking viral cell entry.

CHAPTER 3. SYNTHESIS AND EVALUATION OF NOVEL, HETEROCYCLIC DIPHYLLIN ETHERS *IN VITRO* AND THEIR SAFETY PROFILES *IN VIVO*

3.1 Abstract

Despite many years of discovery research, the transition of V-ATPase inhibitors from useful probes to clinical therapies has not occurred. The multitude of potential therapeutic applications of a V-ATPase inhibitor has repeatedly spawned novel inhibitor derivatization and formulation yet none have translated into the clinic. The main objective of this study was to evaluate the class of aryl-naphthalene lactone V-ATPase inhibitors class for potential to exhibit a useful therapeutic window. Herein, several novel alkylated phenol derivatives of diphyllin were synthesized and evaluated *in vitro* for activity against V-ATPase and cytotoxicity. Evaluation of derivatives in a zebrafish developmental model indicated that inhibitors were less toxicity than known V-ATPase inhibitor bafilomycin A1. In addition, several top derivatives were well-tolerated by mice treated with high doses in formulation. These results demonstrate that alkylated diphyllin analogs exhibit therapeutic potential for the treatment of V-ATPase mediated diseases.

3.2 Introduction

Filoviruses are highly contagious, lethal viruses that cause severe hemorrhagic disease in humans and primates.¹⁻³ Viruses from two genera, Ebola virus (EBOV) and Marburg virus, are responsible for outbreaks that have up to 90% fatality, including the recent outbreak in West Africa that resulted in over 28,000 reported cases and 11,317 deaths.³⁵⁶ Efforts are underway to develop novel EBOV therapies but there are no approved therapeutic measures for the treatment of filovirus infections. While vaccine development has been prioritized, therapeutics for the treatment of individuals already infected are also needed.^{110,167} Two general targets of antiviral development are the viral proteins and the host proteins/processes that aid viral infection. Targeting the viral proteins is the more common approach but resistance to virus-targeted antivirals can quickly lead to losses in their efficacy.

Antiviral drug resistance to traditional virus-targeted antivirals is a common occurrence due to the error-prone nature of viral replication. Viruses, especially those of the RNA variety, are

prone to the production of numerous genetic mutants, deemed quasispecies, during a single cellular lifecycle due to the error-prone replication of their genomes.³⁹⁰ Most viruses have no mechanism through which to edit out genetic mutations that commonly occur during genome replication, which leads to significantly higher error rates during viral replication when compared with host cell genome replication.³⁹¹ While many of these mutants are defective in one form or another, mutations that confer resistance to a therapy are evolutionarily selected by treatment with an antiviral.³⁹² The selected mutants go on to infect new cells and carry on their mutation while the susceptible species are removed from the population. This can quickly lead to the development of resistance to common antivirals as has been shown in cases with influenza, HIV, and HCV amongst others.^{393,394}

The adamantane class of influenza virus inhibitors represent a prime example of viral evolution to resist virus-targeted antiviral therapies. The adamantane class of influenza virus inhibitors, amantadine (Symmetrel) and rimantadine (Flumadine), were the first approved therapies for influenza infection beginning in 1966.^{395,396} Both drugs blocked proton flow through the viral M2 ion channel and prevented the release of the viral ribonucleoprotein into the host cytoplasm.³⁹⁷ Resistance to adamantanes emerged during an epidemic in 1980 but resistance was limited to 1-2% of subtypes until recently.³⁹⁸ Resistance has increased markedly since 2000, with around 45% of all influenza A subtypes exhibiting resistance by 2013.³⁹⁹ Resistance to the adamantanes is caused by mutations in the M2 channel (particularly mutations of serine-31) lead to changing of the pore size that prevent the blockage of the channel by the inhibitor.⁴⁰⁰ There are further examples of resistance development in many viruses, including HIV, HCV, and HSV.^{401–}

403

To avoid the development of resistance, targeting the host proteins that are essential for viral infection presents a novel avenue for antiviral therapy development. Viruses are obligate, intracellular parasites that require the actions of host proteins and processes to replicate and form new viral particles. Numerous host factors and processes are engaged by viruses at all points of their lifecycle and many are used by multiple classes of viruses or conserved within viral families. This conservation by viruses has led to the proposal of some host-targeted therapies for use as multi-viral or pan-viral therapies. Host-targeted antivirals have a higher barrier to viral resistance because of limited mutations within host proteins which is believed to make them a more dependable option for antiviral therapy development. The downside to targeting host factors is that

many of them perform important functions within host cells and blockage of their activity may be determinantal to the cellular health, though this toxicity can also be found in virus-targeted therapies. Overall, host-targeted antivirals represent a mostly untapped potential for the development of novel therapies.

Identifying ways to selectively inhibit host factors necessary for viral infection has become a hot topic in viral research. Vacuolar-ATPase (V-ATPase) represents an important potential target for the development of broad-spectrum, host targeted antivirals. Many viruses utilize V-ATPase mediated endosomal acidification to gain access to cells.^{181,185,334,345} V-ATPase inhibitors have been investigated for the treatment of numerous diseases but attempts to utilize them in in vivo models have indicated toxicities that were not always apparent in the cell culture models.¹⁸⁸ The toxicity of the plecomacrolide class is particularly apparent due to their repeated failure in mouse models.^{277,293,404} Derivatives of bafilomycin like the indolyl class have also been proposed and used in animal models but their transition to the clinic has not occurred.^{311,314,325}

Diphyllin represents a new opportunity for the development of a V-ATPase inhibitor for clinical use. Diphyllin has shown efficacy against osteoporosis, metastatic cancer and viral infection in multiple models and demonstrated a large selectivity index between the antiviral activity against influenza and cytotoxicity.^{265,342–345} Recently, diphyllin was packaged into nanoparticles, used in the treatment of feline coronavirus infection, and evaluated for safety in mice.⁴⁰⁵ Diphyllin nanoparticles appeared well tolerated in mice and did not elicit changes in any essential factors measured during the treatment. Recent work by our lab has indicated that the potency and cytotoxicity of diphyllin could be modified through alkylation of the phenol group (Chapter 2). The addition of basic heterocycles to diphyllin was shown to improve the derivatives potency against EBOV infection and V-ATPase but also improved the selectivity index up to a factor of 9 from diphyllin.

In this work, our goal was to identify a window of selectivity for the use of the diphyllin scaffold as an inhibitor of EBOV infection based upon the previous work. We identified further modifications of the phenol group on diphyllin that could be used to improve the potency and selectivity of the molecule. New heterocycles and changes to the linker were made to further explore the pharmacophore of phenol derivatives. To further evaluate the toxicity of the diphyllin phenol ethers, studies of top derivatives in zebrafish and mice were undertaken to identify if the toxicity witnessed in cell culture was evident in the animal models.

3.3 Experimental Methodology

3.3.1 Biological Assays

Cells- HEK-293 cells (ATCC® CRL-1573™) were maintained in Dulbecco modified Eagle medium (Fisher Scientific) supplemented with 10% fetal bovine serum (FBS) (Atlanta Biologicals) (referred to here as complete medium). Caco-2 cells (ATCC® HTB-37™) were cultured in DMEM supplemented with 10% FBS, 1X Penicillin/Streptomycin, 1X Non-Essential Amino Acids, and 2mM L-Glutamine in T-75 flasks at 37°C in 5% CO₂ and 90% relative humidity. Cells were grown for at least 2 weeks after removing from cryopreservation before studies were conducted.

Inhibition of cellular vesicle acidification- HEK-293 cells were seeded into clear 96-well plates (Falcon) at 10,000 cells/well and allowed to grow for 18-20 h at 37°C and 5% CO₂ in complete medium. Cells were treated with inhibitors at varying concentrations (<2% DMSO) for 4 h before the addition of 1 µg/ml acridine orange in DMEM for 10min before media is removed and cells washed twice with 1x PBS. Fluorescent readings were taken with a Biotek Synergy 4 microplate reader using the following filter pairings: 485/20 nm-530/30 nm and 485/20 nm-665/7 nm. Data are shown the 665 nm/530 nm emission ratio for 12 individual experiments. IC₅₀ data are reported as the concentration at which 50% of the 665 nm/ 530 nm ratio was inhibited relative to the vehicle-treated control with the standard deviation. All compounds were also assayed without the acridine orange dye to determine if background fluorescence was interfering with the assay. This background fluorescence was determined by washing cells with 1x PBS twice and reading in both fluorescence wavelengths and subtracted from the total fluorescence in both channels before determining the fluorescent ratio after dye treatment.

Determination of cytotoxicity- HEK-293 cells were seeded into clear 96-well plates (Falcon) at 10,000 cells/well and allowed to grow for 18-20 h at 37°C and 5% CO₂ in complete medium until they reach ~80% confluency. Cells were then treated with inhibitors at varying concentrations (<2%DMSO) for 72 h. 0.5 mg/ml MTT was added to cells for 4 h before quenching the reaction with acidic isopropanol (10% Triton, 0.1 M HCl). After incubation for 24 h at room temperature, the absorbance at 570 nm and 650 nm was measured using a Biotek Synergy 4 microplate reader. The absorbance at 650 nm was subtracted from the 570 nm to normalize data to any residual media

fluorescence. Data are shown as mean \pm standard error of the mean of the normalized 570 nm absorbance. CC₅₀ data are reported as the concentration at which cell viability was 50% relative to the controls with the standard deviation for 12 individual experiments.

HEK-293 vesicle isolation- The following isolation and assays were performed similar to that previously described.^{383,384} In brief, cells were grown to confluency with complete medium in a 175 cm² flask (Corning) before growth media was removed and replaced with of serum-free DMEM for 2 h. To neutralize endosomes prior to lysis, FCCP was added to the cellular media to reach a final concentration of 1 μ M. Cells were incubated with FCCP for 15 min before cells were scrapped from the plate and pelleted at 1000xg for 5 min. The media was discarded and cells were re-suspended in HEK assay buffer (20 mM HEPES, 5 mM Glucose, 50 mM Sucrose, 50 mM KCl, 90 mM potassium gluconate, 1 mM EGTA, PierceTM protease inhibitor Mini tablet, pH=7.4) were then lysed by passage through a 22 g needle 10-15 times. Lysates were then centrifuged at 10,000xg for 30 s with a Beckman Coulter Microfuge 22R centrifuge. The supernatant was removed and centrifuged at 14,500xg for 20 min. The remaining supernatant was discarded and the pellet was resuspended in HEK assay buffer.

Inhibition of acridine orange quenching assay-The vesicle mixture was resuspended in HEK assay buffer+1%BSA+6 μ M acridine orange and split into fractions with the protein concentration being 100 μ g/mL and transferred to a clear 96-well plate. The isolated vesicles were pretreated with inhibitors for 60 min at 37°C. Fluorescent readings were taken with a Biotek Synergy 4 microplate reader with the 485/20 nm excitation filter and the 530/30 nm emission filter. Plates were read at 1 min intervals for 2 min to measure baseline fluorescence before 5 mM ATP and 5 mM MgCl₂ were added to initiate V-ATPase activity. Readings were taken at 1 min intervals for 60 min before the addition of 1 μ g/mL nigericin (Tocris) and further reading for 15 min at 1 min intervals. The change in fluorescence between the 60-minute timepoint after ATP addition and the reading 2 min after nigericin was added were used to quantify the activity of V-ATPase in each sample. Data are shown as mean \pm standard deviation of nine individual experiments for each compound and concentration.

Stability in cell media assessment- Compounds were suspended in DMEM+10% FBS at 100 mM concentration and aliquots were removed at 0 h, 4 h, 24 h, 48 h while incubating at 37°C with 5% CO₂. Sample media was diluted 1/10 in acetonitrile+0.1% trifluoroacetic acid and cooled to 4°C for 30 min. Samples were then centrifuged at 14,000xg and the supernatant was removed and analyzed by HPLC using a Phenomenex Kromasil C18 HPLC column. The percentage of the original sample peak was used to determine the amount of compound remaining at each time point in comparison with phenol standard. Data shown are the mean± standard error of the mean for five individual experiments.

Stability in HEK-293 cells- HEK-293 cells were seeded into Corning 6-well plates at a concentration of 5×10^5 cells/well in DMEM+10% FBS and incubated overnight at 37°C with 5% CO₂. The media was then removed and replaced with DMEM+10% FBS containing 100 mM of select inhibitors and allowed to incubate for 24 h at 37°C with 5% CO₂. Media was then collected and cells were washed three times with cold PBS before being allowed to dry for 15 min. A 1:1:0.0005 mixture of acetonitrile: methanol: trifluoroacetic acid was then added to each well and incubated at 4°C for 16 h. The supernatant was then removed and centrifuged at 14,000xg for 10 min to remove cellular debris. The new supernatant was then concentrated to 500 uL and analyzed by HPLC using Phenomenex Kromasil C18 HPLC column. Data shown are the average of 3 independent experiments.

Zebrafish toxicity assays- This study was conducted by Jason Ray Nielson in the Peterson lab at the University of Utah. Animals were maintained and embryos were obtained according to standard fish husbandry protocols. Fertilized eggs were collected from group mating of TuAB zebrafish and stored in E3 media at 28°C until 5 days post fertilization (dpf). At 5 dpf, groups of 3 larvae were distributed into the wells of flat-bottom, square 96 well plates filled with 300 µL of 20 mM HEPES pH 7.0 buffered E3 media. Compound were added to each well for a final DMSO concentration of 1% DMSO per well and the plates were then incubated at 28°C. For assessment of compound toxicity, larvae were treated for ~20 h with compounds and viability was assessed by observing heart rate and response to touch as described previously.⁴⁰⁶

Formulation of drugs and assessment of formulation stability- These studies were conducted by Monika Lavan and Mark Joseph Schopper in the Knipp lab. The compounds were dissolved in Transcutol HP and incubated at 40°C overnight. Solutions were analyzed for concentration by HPLC and appropriate dilutions were made to obtain the desired concentration in the final formulation by adding additional Transcutol HP. Solutol HS 15 was added to PBS and mixed to form a homogenous solution that was then combined with the drug solution. The final formulation composed of 25% Transcutol HP, 20% Solutol HS 15, and 55% PBS and the final concentration of the formulations were confirmed by HPLC.

To determine drug stability in formulation, samples were stored at room temperature for 72 h and analyzed by HPLC. Aliquots were removed at 0 h, 24 h, and 72 h and analyzed with an Agilent 1100 HPLC by injection and separation with a Ascentis® C18 analytical reversed phase column (15 cm x 4.6 mm, 5 µm). Time points were compared to standard curves of each drug to determine the concentration. Data shown are the mean ± standard error of the mean for five individual experiments.

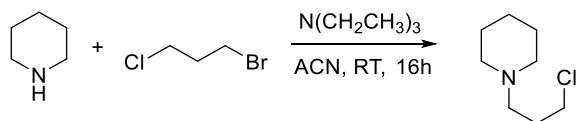
Gastrointestinal permeability estimation- This study was conducted by Kelsey Lubin in the Knipp lab. Permeability studies were conducted over 6 wells on Corning 12-well 0.4 µm polyester Transwell filter supports. Transwells were pre-treated with 65 µL of 1 mg/mL Type I rat tail collagen in 60% ethanol. Transwells were left overnight to evaporate ethanol prior to plating. Passage 46 Caco-2's was plated at a density of 70,000 cells/cm². After plating, media was changed every other day for 21 days. Drug solutions were prepared from provided 10 mM DMSO stocks of each compound. A C₀ concentration of 25 µM in Hank's Balanced Salt Solution (HBSS), containing 5% DMSO was prepared for each compound. Prior to studies, cells were washed twice with PBS and then equilibrated for 30 minutes in HBSS, pH 7.4. After equilibration, HBSS was removed and 0.5 mL of drug solutions were added to the apical chamber. Transwells were then moved into well plates with 1.5 mL of pre-warmed HBSS. 200 µL samples were removed from the basolateral compartment at 30, 60, 120, and 180-minute time points. After each sample, 200 µL of HBSS was added to replace sample volume. Apparent permeability coefficients were determined using the following equation.

$$P_{app} = \frac{V_A * (dC/dt)}{SA * C_0 * 60}$$

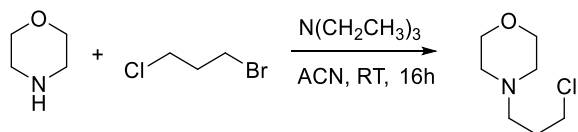
Here, P_{app} is the apparent permeability, V_A is the volume of the acceptor compartment, dC/dt is the change in basolateral compartment concentration over time, SA is the Transwell surface area, C_0 is the initial donor concentration, and 60 is a unit conversion from minutes to seconds. All HPLC analysis was performed on an Agilent 1100 HPLC with Supleco Ascentis C18 Column, 5 μ m, 4.6 mm x 150 mm. Samples were kept in the autosampler at 4°C. All sample and standard curve injections were 25 μ L.

3.3.2 Chemistry

General Procedure for synthesis of chloro-alkene precursors: of 1-bromo-3-chloropropane (1.1mL, 1.72g, 11mmol; 1.5equiv.) and amine component (1eq) were dissolved in acetonitrile (40mL) at room temperature while stirring. triethylamine (3.1 mL, 2.2g, 2eq) of was added dropwise and the reaction mixture was stirred at room temperature for 24-48 hours. When reaction was deemed complete by thin-layer chromatography, the solvent was removed under reduced pressure to yield a crude oil. The crude oil was purified by normal phase silica gel chromatography (DCM/MeOH 100/0 to 50/50) to yield the pure oil.

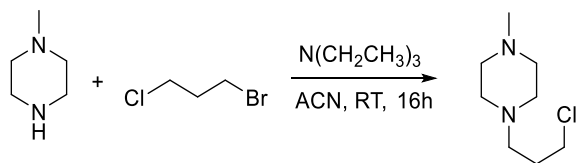


1-(3-chloropropyl)piperidine (1aa)- 1-bromo-3-chloropropane (1.1 mL, 1.72 g, 11 mmol; 1.5 equiv.) of 1-bromo-3-chloropropane and piperidine (725 μ L, 625 mg, 1 eq) were dissolved in acetonitrile (40 mL) at room temperature while stirring. Triethylamine (3.1 mL, 2.2 g, 2 eq) was then added dropwise and the reaction mixture was stirred at room temperature overnight and purified as above to yield a yellow oil (yield: 824 mg, 70%). LC-MS m/z : calculated for $C_7H_{14}ClNO+H^+$, 162.1 $[M+H]^+$, found 162.1 $[M+H]^+$.

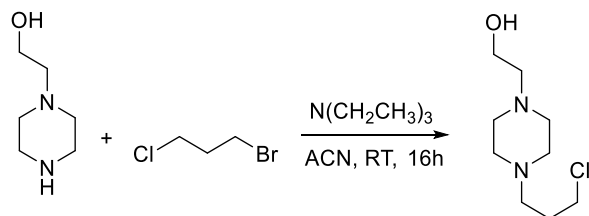


4-(3-chloropropyl)morpholine (1ba)- 1-bromo-3-chloropropane (1.1 mL, 1.72 g, 11 mmol; 1.5 equiv.) of 1-bromo-3-chloropropane and morpholine (641 μ L, 639 mg, 1 eq) were dissolved in acetonitrile (40 mL) at room temperature while stirring. triethylamine (3.1 mL, 2.2 g, 2 eq) was then added dropwise, the reaction mixture was stirred at room temperature overnight and purified

as above to yield a yellow oil (yield: 351 mg, 30%). LC-MS m/z : calculated for $C_7H_{14}ClNO+H^+$, 164.1 $[M+H]^+$, found 164.1 $[M+H]^+$.

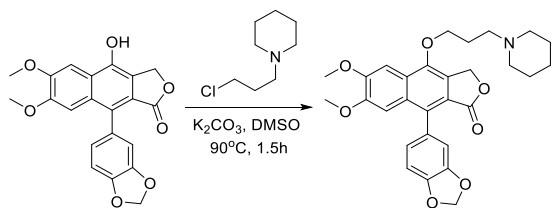


1-(3-chloropropyl)-4-methylpiperazine (1ca)- 1-bromo-3-chloropropane (1.1 mL, 1.72 g, 11 mmol; 1.5 equiv.) of 1-bromo-3-chloropropane and 1-methylpiperazine (813 μ L, 735 mg, 1 eq) were dissolved in acetonitrile (40 mL) at room temperature while stirring. triethylamine (3.1 mL, 2.2 g, 2 eq) was then added dropwise, the reaction mixture was stirred at room temperature overnight and purified as above to yield a yellow oil (yield: 452 mg, 35%). LC-MS m/z : calculated for $C_7H_{14}ClNO+H^+$, 177.1 $[M+H]^+$, found 177.2 $[M+H]^+$.

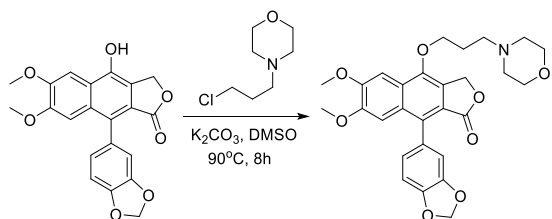


2-(4-(3-chloropropyl)piperazin-1-yl)ethan-1-ol (2ia)- 1-bromo-3-chloropropane (1.1 mL, 1.72 g, 11 mmol; 1.5 equiv.) of 1-bromo-3-chloropropane and 2-(piperazin-1-yl)ethanol (0.952 g, 1 eq) were dissolved in acetonitrile (40 mL) at room temperature while stirring. triethylamine (3.1 mL, 2.2 g, 2 eq) was then added dropwise, the reaction mixture was stirred at room temperature overnight and purified as above to yield a yellow oil (yield: 551 mg, 36%). LC-MS m/z : calculated for $C_9H_{19}ClN_2O+H^+$, 207.1 $[M+H]^+$, found 207.1 $[M+H]^+$.

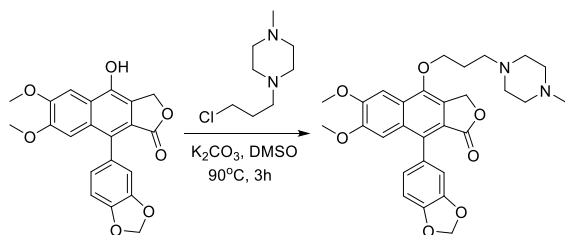
General synthetic procedure for alkylation of diphyllin phenol: **2a** (1 eq), the chloropropylamine linker (2 eq), and potassium carbonate (5 eq) were dissolved in dimethyl sulfoxide (6 mL) and heated to reflux overnight (16-20 h). The reaction was then cooled to room temperature and 20 mL of distilled water was added to the flask. The mixture was added to a separatory funnel and extracted with ethyl acetate (5x30 mL). The organic layers were combined and washed with brine (30 mL) before concentrating the organic layers under reduced pressure. The crude product was purified with normal phase silica gel chromatography (DCM/MeOH 100/0 to 80/20) to yield the pure solid.



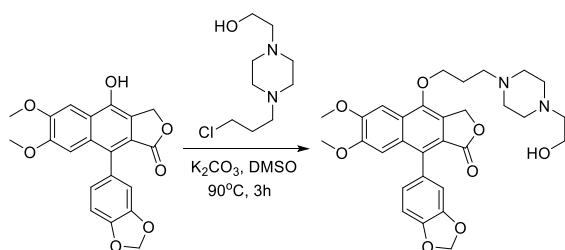
9-(benzo[d][1,3]dioxol-5-yl)-6,7-dimethoxy-4-(3-(piperidin-1-yl)propoxy)naphtho[2,3-c]furan-1(3H)-one (**1a**)- **3a** (51 mg, 0.134 mmol, 1 eq), **1aa** (42 mg, 2eq), and potassium carbonate (85 mg, 0.616 mmol, 5 eq) were dissolved in dimethyl sulfoxide (3 mL). The reaction was heated to 90°C for 1.5 h and purified as above to give a yellow solid (yield: 9.5mg, 14%, Purity: 95.7%). ¹H NMR (500 MHz, DMSO-*d*₆) δ 7.49 (s, 1H), 7.00 (d, *J* = 8.0 Hz, 1H), 6.93 (s, 1H), 6.85 (d, *J* = 1.8 Hz, 1H), 6.73 (dd, *J* = 7.9, 1.8 Hz, 1H), 6.09 (s, 2H), 5.59 (s, 2H), 4.27 (t, *J* = 6.1 Hz, 2H), 3.92 (s, 3H), 3.63 (s, 3H), 3.19 (d, *J* = 11.4 Hz, 2H), 2.59 (s, 2H), 1.99 (d, *J* = 8.4 Hz, 2H), 1.56 – 1.44 (m, 4H), 1.37 (s, 2H), 1.19 (s, 2H). ESI-MS (ESI+) *m/z*: calculated for C₂₉H₃₁NO₇+H⁺, 506.2173 [M+H]⁺, found 506.2174 [M+H]⁺.



9-(benzo[d][1,3]dioxol-5-yl)-6,7-dimethoxy-4-(3-morpholinopropoxy)naphtho[2,3-c]furan-1(3H)-one (**1b**)- **3a** (50 mg, 0.131 mmol, 1 eq), **1ba** (43 mg, 2 eq), and potassium carbonate (80 mg, 0.579 mmol, 5 eq) were dissolved in dimethyl sulfoxide (6 mL). The reaction was heated to 90°C for 8 h and purified as above to give a yellow solid (yield: 45mg, 67%, Purity: 99.3%). ¹H NMR (500 MHz, DMSO-*d*₆) δ 7.49 (s, 1H), 7.00 (d, *J* = 7.9 Hz, 1H), 6.93 (s, 1H), 6.85 (d, *J* = 1.6 Hz, 1H), 6.73 (dd, *J* = 7.9, 1.7 Hz, 1H), 6.09 (s, 2H), 5.58 (s, 2H), 4.27 (t, *J* = 6.1 Hz, 2H), 3.92 (s, 3H), 3.63 (s, 3H), 3.55 (t, *J* = 4.5 Hz, 4H), 2.53 (t, *J* = 7.3 Hz, 2H), 2.36 (s, 4H), 1.97 (p, *J* = 6.6 Hz, 2H). ¹³C NMR (201 MHz, DMSO-*d*₆) δ 169.49, 151.68, 150.40, 147.36, 147.25, 146.88, 133.33, 129.95, 128.82, 126.01, 125.84, 124.05, 119.44, 111.29, 108.38, 106.02, 101.55, 100.95, 70.42, 67.06, 66.66, 56.02, 55.66, 55.36, 53.89, 27.25. ESI-MS (ESI+) *m/z*: calculated for C₂₈H₂₉NO₈+H⁺, 508.1966 [M+H]⁺, found 508.1967 [M+H]⁺.

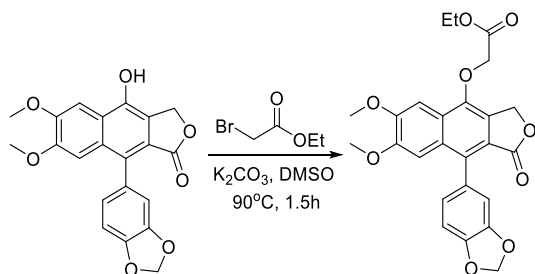


9-(benzo[d][1,3]dioxol-5-yl)-6,7-dimethoxy-4-(3-(4-methylpiperazin-1-yl)propoxy)naphtho[2,3-c]furan-1(3H)-one (**1c**)-**3a** (50 mg, 0.131 mmol, 1 eq), **1ca** (46 mg, 2 eq), and potassium carbonate (89 mg, 0.645 mmol, 5 eq) were dissolved in dimethyl sulfoxide (3 mL). The reaction was heated to 90°C for 3 h and purified as above to give a yellow solid (yield: 52mg, 73%, Purity: 97.2%). ¹H NMR (500 MHz, DMSO-*d*₆) δ 7.48 (s, 1H), 7.00 (d, *J* = 7.9 Hz, 1H), 6.93 (s, 1H), 6.85 (d, *J* = 1.7 Hz, 1H), 6.73 (dd, *J* = 7.9, 1.7 Hz, 1H), 6.09 (s, 2H), 5.57 (s, 2H), 4.25 (t, *J* = 6.1 Hz, 2H), 3.91 (s, 3H), 3.62 (s, 3H), 2.51 (d, *J* = 4.0 Hz, 6H), 2.11 (s, 3H), 1.95 (p, *J* = 6.5 Hz, 2H). ¹³C NMR (126 MHz, DMSO-*d*₆) δ 169.38, 151.52, 150.24, 147.23, 146.74, 129.80, 128.68, 125.88, 125.74, 123.92, 119.30, 111.17, 108.26, 105.83, 101.43, 100.78, 70.31, 66.95, 55.88, 55.52, 55.06, 54.76, 53.09, 46.04, 40.73, 27.45. ESI-MS (ESI+) *m/z*: calculated for C₂₉H₃₂N₂O₇+H⁺, 521.2282 [M+H]⁺, found 521.2283 [M+H]⁺.

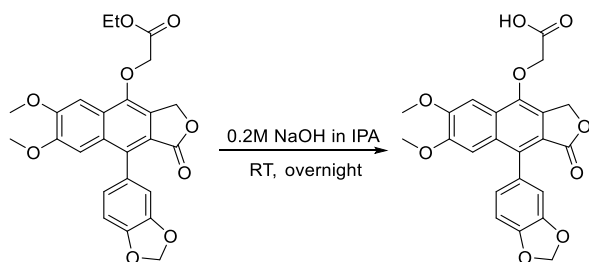


9-(benzo[d][1,3]dioxol-5-yl)-4-(3-(4-(2-hydroxyethyl)piperazin-1-yl)propoxy)-6,7-dimethoxynaphtho[2,3-c]furan-1(3H)-one (**1d**)-**3a** (51 mg, 0.134 mmol, 1 eq), **1da** (54 mg, 2 eq), and potassium carbonate (90 mg, 0.655 mmol, 5 eq) were dissolved in dimethyl sulfoxide (6 mL). The reaction was heated to 90°C for 3 h and purified as above to give a yellow, amorphous solid (Yield: 32 mg, 44%, Purity: 95.1%). ¹H NMR (500 MHz, DMSO-*d*₆) δ 7.48 (s, 1H), 7.00 (d, *J* = 7.9 Hz, 1H), 6.93 (s, 1H), 6.73 (dd, *J* = 7.9, 1.7 Hz, 1H), 6.09 (s, 2H), 5.57 (s, 2H), 4.42 (s, 1H), 4.26 (t, *J* = 6.0 Hz, 2H), 3.92 (s, 3H), 3.62 (s, 3H), 3.46 (t, *J* = 6.3 Hz, 2H), 2.57 – 2.48 (m, 4H), 2.38 (s, 8H), 1.96 (p, *J* = 6.6 Hz, 2H). ¹³C NMR (126 MHz, DMSO-*d*₆) δ 169.38, 151.52, 150.24, 147.23, 147.11, 146.73, 133.19, 129.80, 128.67, 125.87, 125.74, 123.92, 119.29, 111.17, 108.26,

105.83, 101.43, 100.78, 70.29, 66.94, 60.46, 58.62, 55.89, 55.52, 54.75, 53.41, 53.00, 27.37. ESI-MS (ESI+) m/z : calculated for $C_{30}H_{34}N_2O_7+H^+$, 551.2388 $[M+H]^+$, found 551.2383 $[M+H]^+$.



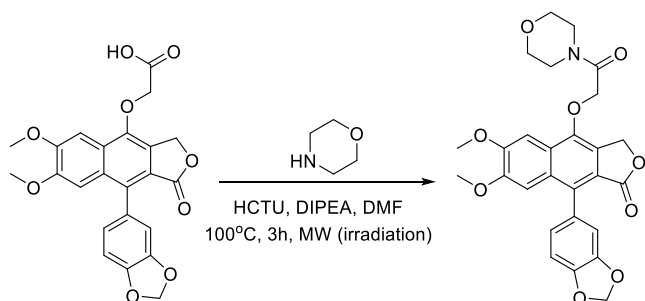
ethyl 2-((9-(benzo[d][1,3]dioxol-5-yl)-6,7-dimethoxy-1-oxo-1,3-dihydronaphtho[2,3-c]furan-4-yl)oxy) acetate (1e)- 3a (50mg, 0.131mmol, 1eq), ethyl bromoacetate (46mg, 2eq), and potassium carbonate (92mg, 0.674mmol, 5eq) were dissolved in dimethyl sulfoxide (3mL). The reaction was heated to reflux for 1h before cooling to room temperature. 20mL of distilled water was added to the flask and the mixture was transferred to a separatory funnel. The aqueous layer was extracted with dichloromethane (3x30mL). The organic layers were combined and washed with water (30mL) brine (30mL) before concentrating the organic layers under reduced pressure. The dried product was a crude, beige solid (yield 61mg, 100%) that was immediately used in the next reaction to form **1f**. LC-MS m/z : calculated for $C_{25}H_{22}O_9+H^+$, 467.1 $[M+H]^+$, found 467.0 $[M+H]^+$.



2-((9-(benzo[d][1,3]dioxol-5-yl)-6,7-dimethoxy-1-oxo-1,3-dihydronaphtho[2,3-c]furan-4-yl)oxy)acetic acid (1f)- 1e (61 mg, 0.131 mmol, 1 eq) was mixed with 5 mL of a 0.2 M NaOH in Water/Isopropanol (1:4 v/v) and mixed at room temperature overnight. After the reaction was deemed complete by TLC (all reactant had been consumed). While stirring, 1 M HCl was added to the mixture until the pH decreased to 1-2. If the product did not immediately precipitate, the solution was concentrated under reduced pressure until precipitate formed in solution. The solution was cooled to 0°C and the precipitate was collected by vacuum filtration to yield a beige solid (yield: 50mg, 88%, Purity: 97.4%). 1H NMR (500 MHz, DMSO- d_6) δ 7.75 (s, 1H), 7.00 (d, J = 7.9 Hz, 1H), 6.94 (s, 1H), 6.86 (d, J = 1.6 Hz, 1H), 6.74 (dd, J = 7.9, 1.7 Hz, 1H), 6.09 (s, 2H),

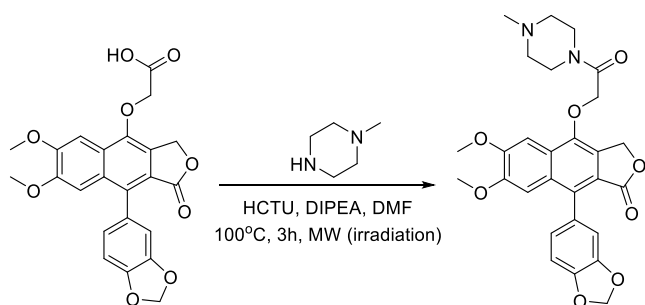
5.56 (s, 2H), 4.89 (s, 2H), 3.92 (s, 3H), 3.63 (s, 3H). ^{13}C NMR (201 MHz, DMSO) δ 170.90, 169.40, 151.76, 150.50, 147.40, 146.68, 134.09, 130.05, 128.70, 126.37, 126.12, 124.04, 119.29, 111.26, 108.42, 105.93, 101.60, 69.08, 66.81, 62.48, 56.07, 55.69, 40.46, 40.36, 40.31, 40.26, 40.21, 40.10, 40.00, 39.89, 39.79, 39.68, 25.95. ESI-MS (ESI+) m/z : calculated for $\text{C}_{23}\text{H}_{18}\text{O}_9 + \text{H}^+$, 439.1024 $[\text{M} + \text{H}]^+$, found 439.1024 $[\text{M} + \text{H}]^+$.

General synthesis of diphyllin phenol amide derivatives: **1f** (1 eq) was mixed with HCTU (2 eq), N, N-Diisopropylethylamine (5 eq), and amine component (2-5 eq) were mixed in dimethyl formamide (1 mL). The mixture was placed in a Biotage® Initiator Classic microwave synthesizer and heated to 100°C for 3 h with a 200W power limit and 600 rpm stirring. When the reaction was complete, 20 mL of water was added to the reaction and the mixture was added to a separatory funnel. The mixture was extracted with ethyl acetate (4x30 mL) and the organic layers were combined and washed with brine (30 mL). The organic layer was concentrated under reduced pressure to yield a crude product. The crude product was purified with normal phase silica gel chromatography (DCM/MeOH 100/0 to 100/0) to yield the pure product.

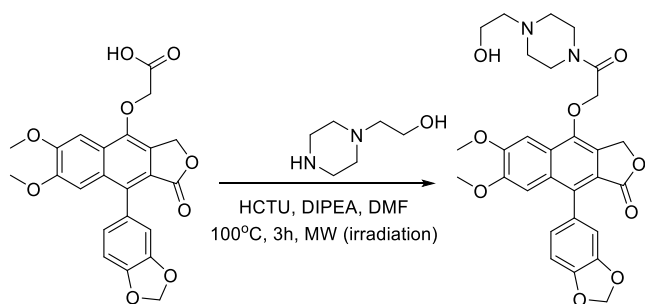


9-(benzo[d][1,3]dioxol-5-yl)-6,7-dimethoxy-4-(2-morpholino-2-oxoethoxy)naphtho[2,3-c]furan-1(3H)-one (**2a**)- **1f** (25mg, 0.0571mmol, 1eq) was mixed with HCTU (48mg, 2eq), N, N-Diisopropylethylamine (50 μ L, 37.1mg, 5eq), and morpholine (25 μ L, 25 mg, 5 eq) were mixed in dimethyl formamide (1 mL). The reaction was conducted and purified as above to yield a yellow solid (yield: 7.1mg, 25%, Purity: 97.5%). ^1H NMR (500 MHz, DMSO- d_6) δ 7.76 (s, 1H), 7.00 (d, J = 7.9 Hz, 1H), 6.92 (s, 1H), 6.84 (d, J = 1.7 Hz, 1H), 6.72 (dd, J = 7.9, 1.7 Hz, 1H), 6.09 (s, 2H), 5.59 (s, 2H), 5.09 (s, 2H), 3.91 (s, 3H), 3.63 (s, 3H), 3.56 (t, J = 4.7 Hz, 4H), 3.46 (t, J = 4.9 Hz, 2H), 3.41 (t, J = 4.8 Hz, 2H). ^{13}C NMR (201 MHz, DMSO) δ 169.60, 166.68, 151.10, 149.66, 146.75, 145.89, 134.15, 129.54, 127.69, 125.62, 122.50, 117.84, 109.49, 106.72, 104.80, 100.38, 99.94, 68.79, 65.93, 65.50, 65.49, 54.32, 53.83, 47.10, 46.99, 46.89, 46.78, 46.67, 46.57, 46.46,

44.11, 41.19, 36.66. ESI-MS (ESI+) m/z : calculated for $C_{27}H_{25}NO_9 + H^+$, 508.1602 $[M+H]^+$, found 508.1600 $[M+H]^+$.

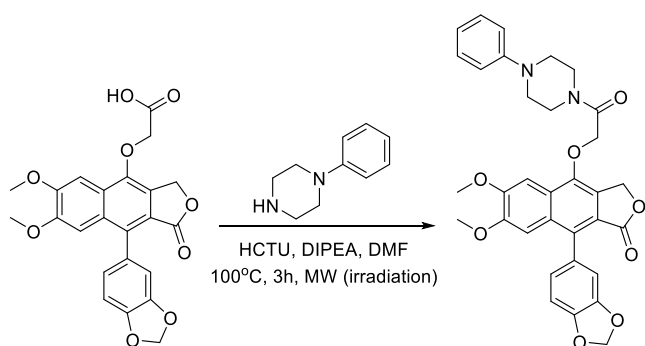


9-(benzo[d][1,3]dioxol-5-yl)-6,7-dimethoxy-4-(2-(4-methylpiperazin-1-yl)-2-oxoethoxy)naphtho[2,3-c]furan-1(3H)-one (**2b**)- **1f** (25 mg, 0.0571 mmol, 1 eq) was mixed with HCTU (48 mg, 2 eq), N, N-Diisopropylethylamine (50 μ L, 37.1 mg, 5 eq), and 1-methylpiperazine (32 μ L, 29 mg, 5 eq) were mixed in dimethyl formamide (1 mL). The reaction was conducted and purified as above to yield a yellow solid (yield: 6.4mg, 22%, Purity: 96.6%). 1H NMR (500 MHz, DMSO- d_6) δ 7.74 (s, 1H), 7.00 (d, J = 8.0 Hz, 1H), 6.92 (s, 1H), 6.84 (d, J = 1.6 Hz, 1H), 6.72 (dd, J = 7.9, 1.7 Hz, 1H), 6.09 (s, 2H), 5.58 (s, 2H), 5.08 (s, 2H), 4.43 (s, 1H), 3.91 (s, 3H), 3.63 (s, 3H), 3.47 (q, J = 5.6, 4.7 Hz, 4H), 3.39 (t, J = 5.0 Hz, 2H), 2.40 (t, J = 5.0 Hz, 2H), 2.37 (t, J = 6.0 Hz, 4H). ^{13}C NMR (126 MHz, DMSO- d_6) δ 169.29, 166.24, 151.47, 150.29, 147.23, 147.13, 146.80, 133.48, 129.83, 128.62, 125.74, 125.29, 123.89, 119.13, 111.13, 108.28, 105.68, 101.54, 101.43, 69.62, 66.88, 60.40, 58.79, 55.96, 55.52, 53.57, 53.13, 44.40, 41.67. ESI-MS (ESI+) m/z : calculated for $C_{29}H_{30}N_2O_9 + H^+$, 551.2023 $[M+H]^+$, found 551.2023 $[M+H]^+$.

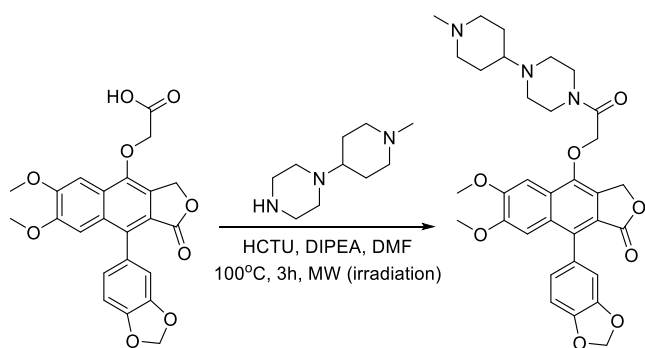


9-(benzo[d][1,3]dioxol-5-yl)-4-(2-(4-(2-hydroxyethyl)piperazin-1-yl)-2-oxoethoxy)-6,7-dimethoxynaphtho[2,3-c]furan-1(3H)-one (**2c**)- **1f** (25 mg, 0.0571 mmol, 1 eq) was mixed with HCTU (48 mg, 2 eq), N, N-Diisopropylethylamine (50 μ L, 37.1 mg, 5 eq), and 2-(piperazin-1-yl)ethanol (15 mg, 2 eq) were mixed in dimethyl formamide (1 mL). The reaction was conducted

and purified as above to yield an amorphous, yellow solid (yield: 7.6mg, 24%, Purity: 97.5%). ^1H NMR (500 MHz, $\text{DMSO}-d_6$) δ 7.74 (s, 1H), 7.00 (d, $J = 8.0$ Hz, 1H), 6.92 (s, 1H), 6.84 (d, $J = 1.6$ Hz, 1H), 6.72 (dd, $J = 7.9, 1.7$ Hz, 1H), 6.09 (s, 2H), 5.58 (s, 2H), 5.08 (s, 2H), 4.43 (s, 1H), 3.91 (s, 3H), 3.63 (s, 3H), 3.47 (q, $J = 5.6, 4.7$ Hz, 4H), 3.39 (t, $J = 5.0$ Hz, 2H), 2.40 (t, $J = 5.0$ Hz, 2H), 2.37 (t, $J = 6.0$ Hz, 4H). ^{13}C NMR (126 MHz, $\text{DMSO}-d_6$) δ 169.29, 166.24, 151.47, 150.29, 147.23, 147.13, 146.80, 133.48, 129.83, 128.62, 125.74, 125.29, 123.89, 119.13, 111.13, 108.28, 105.68, 101.54, 101.43, 69.62, 66.88, 60.40, 58.79, 55.96, 55.52, 53.57, 53.13, 44.40, 41.67. ESI-MS (ESI+) m/z : calculated for $\text{C}_{29}\text{H}_{30}\text{N}_2\text{O}_9 + \text{H}^+$, 551.2023 $[\text{M} + \text{H}]^+$, found 551.2023 $[\text{M} + \text{H}]^+$.

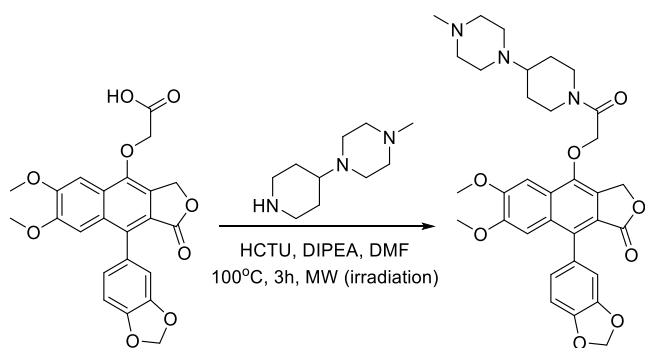


9-(benzo[d][1,3]dioxol-5-yl)-6,7-dimethoxy-4-(2-oxo-2-(4-phenylpiperazin-1-yl)ethoxy)naphtho[2,3-c]furan-1(3H)-one (**2d**)-**1f** (27 mg, 0.0616 mmol, 1 eq) was mixed with HCTU (46 mg, 2 eq), N, N-Diisopropylethylamine (50 μL , 37.1 mg, 5 eq), and 1-phenylpiperazine (28 mg, 3 eq) were mixed in dimethyl formamide (1 mL). The reaction was conducted and purified as above to yield a yellow solid (yield: 8.6mg, 24%, Purity: 95.1%). ^1H NMR (800 MHz, $\text{DMSO}-d_6$) δ 7.81 (d, $J = 2.1$ Hz, 1H), 7.24 (t, $J = 7.9$ Hz, 2H), 7.04 (dd, $J = 7.9, 2.1$ Hz, 1H), 6.97 (q, $J = 3.7, 2.5$ Hz, 3H), 6.89 (d, $J = 2.2$ Hz, 1H), 6.82 (t, $J = 7.3$ Hz, 1H), 6.77 (d, $J = 7.7$ Hz, 1H), 6.13 (s, 2H), 5.65 (s, 2H), 5.19 (s, 2H), 3.95 (d, $J = 2.1$ Hz, 3H), 3.67 (s, 5H), 3.61 (d, $J = 5.0$ Hz, 2H), 3.31 (s, 2H), 3.17 (dt, $J = 28.1, 5.0$ Hz, 4H). ^{13}C NMR (201 MHz, DMSO) δ 169.42, 166.58, 162.76, 151.67, 151.20, 150.47, 147.38, 147.28, 146.97, 133.71, 129.48, 125.97, 125.62, 124.03, 119.87, 119.31, 116.37, 111.28, 108.43, 105.92, 101.76, 101.59, 69.83, 67.02, 56.11, 55.69, 49.06, 48.74, 44.37, 41.64, 40.46, 40.36, 40.31, 40.25, 40.20, 40.15, 40.10, 39.99, 39.89, 39.78, 39.68, 38.71, 36.25, 31.24. ESI-MS (ESI+) m/z : calculated for $\text{C}_{33}\text{H}_{30}\text{N}_2\text{O}_8 + \text{H}^+$, 583.2075 $[\text{M} + \text{H}]^+$, found 583.2076 $[\text{M} + \text{H}]^+$.



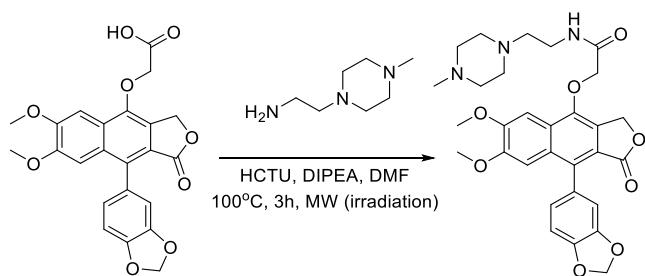
9-(benzo[d][1,3]dioxol-5-yl)-6,7-dimethoxy-4-(2-(4-methylpiperazin-1-yl)-2-

oxoethoxy)naphtho[2,3-c]furan-1(3H)-one (**2e**)- **1f** (27 mg, 0.0616 mmol, 1 eq) was mixed with HCTU (46 mg, 2 eq), N, N-Diisopropylethylamine (50 μ L, 37.1 mg, 5 eq), and 1-(1-methylpiperidin-4-yl)piperazine (31 mg, 3 eq) were mixed in dimethyl formamide (1 mL). The reaction was conducted and purified as above to yield a beige solid (yield: 3.6mg, 10%, Purity: 96.9%). ^1H NMR (500 MHz, DMSO- d_6) δ 7.74 (s, 1H), 7.00 (d, J = 7.9 Hz, 1H), 6.92 (s, 1H), 6.84 (d, J = 1.6 Hz, 1H), 6.72 (dd, J = 7.8, 1.7 Hz, 1H), 6.09 (d, J = 2.6 Hz, 2H), 5.59 (s, 2H), 5.09 (s, 2H), 3.91 (s, 3H), 3.62 (s, 3H), 3.45 (s, 2H), 3.19 (s, 2H), 2.92 (s, 2H), 2.43 (s, 2H), 2.27 (m, 3H), 1.87 (s, 2H), 1.71 (d, J = 12.1 Hz, 2H), 1.51 (s, 2H), 1.19 (s, 2H). ^{13}C NMR (201 MHz, DMSO- d_6) δ 169.41, 166.74, 162.76, 151.68, 150.50, 147.40, 147.32, 146.99, 142.05, 133.86, 132.75, 130.02, 128.85, 128.72, 126.06, 125.76, 124.03, 121.39, 119.26, 111.24, 109.75, 108.43, 105.89, 101.59, 69.73, 66.97, 56.10, 55.70, 45.90, 36.24, 31.23. ESI-MS (ESI+) m/z : calculated for $\text{C}_{33}\text{H}_{37}\text{N}_3\text{O}_8 + \text{H}^+$, 604.2654 $[\text{M} + \text{H}]^+$, found 604.2654 $[\text{M} + \text{H}]^+$.

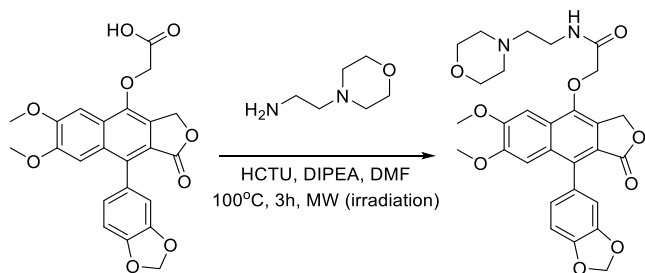


9-(benzo[d][1,3]dioxol-5-yl)-6,7-dimethoxy-4-(2-(4-(4-methylpiperazin-1-yl)piperidin-1-yl)-2-oxoethoxy)naphtho[2,3-c]furan-1(3H)-one (**2f**)- **1f** (27 mg, 0.0616 mmol, 1 eq) was mixed with HCTU (46 mg, 2 eq), N, N-Diisopropylethylamine (50 μ L, 37.1 mg, 5 eq), and 1-methyl-4-(piperidin-4-yl)piperazine (31 mg, 3 eq) were mixed in dimethyl formamide (1 mL). The reaction

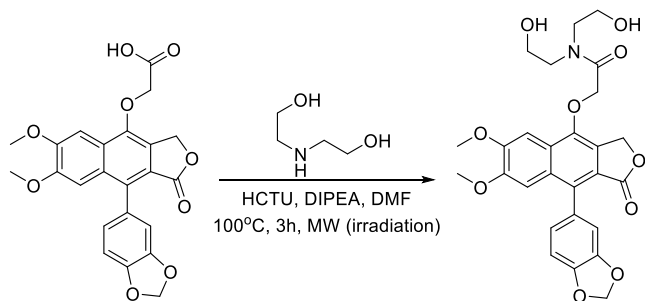
was conducted and purified as above to yield a beige solid (yield: 13mg, 35%, Purity: 95.4%). ^1H NMR (500 MHz, $\text{DMSO-}d_6$) δ 7.74 (s, 1H), 7.00 (d, $J = 7.9$ Hz, 1H), 6.92 (s, 1H), 6.84 (d, $J = 1.6$ Hz, 1H), 6.72 (dd, $J = 7.8, 1.7$ Hz, 1H), 6.09 (d, $J = 2.6$ Hz, 2H), 5.59 (s, 2H), 5.09 (s, 2H), 3.91 (s, 3H), 3.62 (s, 3H), 3.45 (s, 2H), 3.19 (s, 2H), 2.92 (s, 2H), 2.43 (s, 2H), 2.27 (m, 3H), 1.87 (s, 2H), 1.71 (d, $J = 12.1$ Hz, 2H), 1.51 (s, 2H), 1.19 (s, 2H). ^{13}C NMR (201 MHz, $\text{DMSO-}d_6$) δ 169.41, 166.74, 162.76, 151.68, 150.50, 147.40, 147.32, 146.99, 142.05, 133.86, 132.75, 130.02, 128.85, 128.72, 126.06, 125.76, 124.03, 121.39, 119.26, 111.24, 109.75, 108.43, 105.89, 101.59, 69.73, 66.97, 56.10, 55.70, 45.90, 36.24, 31.23. ESI-MS (ESI+) m/z : calculated for $\text{C}_{33}\text{H}_{37}\text{N}_3\text{O}_8 + \text{H}^+$, 604.2653 $[\text{M} + \text{H}]^+$, found 604.2654 $[\text{M} + \text{H}]^+$.



2-((9-(benzo[d][1,3]dioxol-5-yl)-6,7-dimethoxy-1-oxo-1,3-dihydronaphtho[2,3-c]furan-4-yl)oxy)-N-(2-(4-methylpiperazin-1-yl)ethyl)acetamide (**2g**)- **1f** (27 mg, 0.0616 mmol, 1 eq) was mixed with HCTU (46 mg, 2 eq), N, N-Diisopropylethylamine (50 μL , 37.1 mg, 5 eq), and 2-(4-methylpiperazin-1-yl)ethylamine (25 mg, 3 eq) were mixed in dimethyl formamide (1 mL). The reaction was conducted and purified as above to yield an amorphous, yellow solid (yield: 8.5 mg, 25%, Purity: 98.7%). ^1H NMR (800 MHz, $\text{DMSO-}d_6$) δ 9.01 (s, 1H), 8.44 (s, 1H), 8.35 (d, $J = 7.8$ Hz, 1H), 8.15 – 8.11 (m, 2H), 7.46 (d, $J = 7.0$ Hz, 2H), 6.97 (s, 2H), 6.18 (s, 2H), 5.43 (s, 3H), 5.13 (s, 3H), 5.04 – 5.00 (m, 2H), 4.81 (s, 2H), 4.73 (s, 4H), 4.33 (d, $J = 8.3$ Hz, 5H). ^{13}C NMR (201 MHz, $\text{DMSO-}d_6$) δ 169.49, 169.38, 169.38, 151.21, 151.21, 149.69, 149.69, 146.79, 145.42, 140.48, 134.52, 132.64, 129.61, 129.61, 127.82, 127.57, 125.79, 125.23, 122.53, 118.84, 117.86, 109.52, 108.22, 106.79, 104.94, 100.43, 99.53, 70.05, 65.75, 55.27, 54.32, 53.86, 51.69, 48.65, 41.32, 34.24. ESI-MS (ESI+) m/z : calculated for $\text{C}_{30}\text{H}_{33}\text{N}_3\text{O}_8 + \text{H}^+$, 564.2340 $[\text{M} + \text{H}]^+$, found 564.2338 $[\text{M} + \text{H}]^+$.

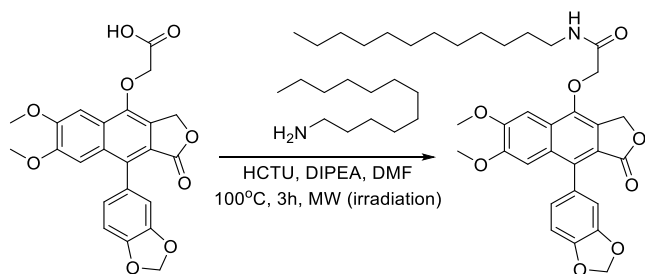


2-((9-(benzo[d][1,3]dioxol-5-yl)-6,7-dimethoxy-1-oxo-1,3-dihydronaphtho[2,3-c]furan-4-yl)oxy)-*N*-(2-morpholinoethyl)acetamide (**2h**)- **1f** (26 mg, 0.0594 mmol, 1 eq) was mixed with HCTU (48 mg, 2 eq), *N,N*-Diisopropylethylamine (50 μ L, 37.1 mg, 5 eq), and 2-morpholinoethylamine (22 mg, 3 eq) were mixed in dimethyl formamide (1 mL). The reaction was conducted and purified as above to yield an amorphous, brown solid (yield: 2.3mg, 7.0%, Purity: 97.8%). ^1H NMR (800 MHz, DMSO- d_6) δ 7.70 (s, 1H), 7.18 (s, 1H), 7.12 (s, 1H), 7.06 (d, J = 1.7 Hz, 1H), 7.00 (s, 1H), 6.90 (d, J = 1.7 Hz, 1H), 6.78 (dd, J = 7.9, 1.7 Hz, 1H), 6.14 (s, 2H), 5.60 (s, 2H), 4.80 (s, 2H), 4.00 (s, 3H), 3.68 (s, 3H), 3.59 (m, 2H), 3.43 (dd, J = 5.6 Hz, 2H), 3.37 (dd, J = 10.9, 5.3 Hz, 4H), 3.29 (dd, J = 10.9, 5.8 Hz, 2H), 3.15 (m, 2H). ^{13}C NMR (201 MHz, DMSO- d_6) δ 169.36, 151.87, 150.53, 147.43, 146.36, 134.41, 130.09, 128.59, 126.09, 124.04, 119.32, 111.23, 108.46, 106.03, 101.62, 101.54, 72.96, 71.23, 66.76, 63.55, 56.20, 55.71. ESI-MS (ESI+) m/z : calculated for $\text{C}_{29}\text{H}_{30}\text{N}_2\text{O}_9 + \text{H}^+$, 551.2023 $[\text{M} + \text{H}]^+$, found 551.2023 $[\text{M} + \text{H}]^+$.

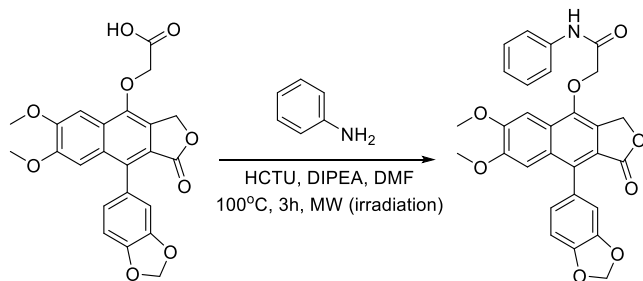


2-((9-(benzo[d][1,3]dioxol-5-yl)-6,7-dimethoxy-1-oxo-1,3-dihydronaphtho[2,3-c]furan-4-yl)oxy)-*N,N*-bis(2-hydroxyethyl)acetamide (**2i**)- **1f** (26 mg, 0.0594 mmol, 1 eq) was mixed with HCTU (49 mg, 2 eq), *N,N*-Diisopropylethylamine (50 μ L, 37.1 mg, 5 eq), and diethanolamine (30 mg, 5 eq) were mixed in dimethyl formamide (1 mL). The reaction was conducted and purified as above to yield an amorphous, off-white solid (yield: 12mg, 40%, Purity: 95.3%). ^1H NMR (800 MHz, DMSO- d_6) δ 7.19 (s, 1H), 6.95 (s, 1H), 6.20 (s, 1H), 6.12 (d, J = 7.7 Hz, 1H), 5.88 (s, 1H), 5.24 (d, J = 6.8 Hz, 3H), 4.77 (s, 2H), 4.38 (s, 2H), 3.22 (s, 3H), 2.99 (t, J = 5.9 Hz, 2H), 2.94 (t, J = 5.3 Hz, 2H), 2.91 (d, J = 2.1 Hz, 4H), 2.82 (t, J = 6.0 Hz, 2H), 2.72 (d, J = 5.3 Hz, 2H), 2.26

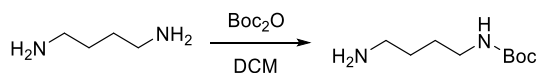
(d, $J = 12.8$ Hz, 1H), 2.20 (d, $J = 2.0$ Hz, 3H), 2.07 (s, 3H), 0.48 (d, $J = 27.6$ Hz, 1H). ^{13}C NMR (201 MHz, DMSO- d_6) δ 169.72, 169.12, 162.64, 151.00, 149.59, 146.73, 146.01, 133.96, 129.51, 127.76, 125.64, 122.53, 117.83, 109.54, 106.72, 104.77, 100.38, 100.02, 58.33, 57.98, 54.30, 53.81, 48.99, 47.11, 47.00, 46.89, 46.79, 46.68, 46.57, 46.47, 34.73. ESI-MS (ESI+) m/z : calculated for $\text{C}_{27}\text{H}_{27}\text{NO}_{10} + \text{H}^+$, 526.1708 $[\text{M} + \text{H}]^+$, found 526.1706 $[\text{M} + \text{H}]^+$.



2-((9-(benzo[d][1,3]dioxol-5-yl)-6,7-dimethoxy-1-oxo-1,3-dihydronaphtho[2,3-c]furan-4-yl)oxy)-N-dodecylacetamide (**2j**)- **1f** (26 mg, 0.0594 mmol, 1 eq) was mixed with HCTU (49 mg, 2 eq), N, N-Diisopropylethylamine (50 μL , 37.1 mg, 5 eq), and dodecylamine (32 mg, 3 eq) were mixed in dimethyl formamide (1 mL). The reaction was conducted and purified as above to yield a beige solid (yield: 23 mg, 66%, Purity: 99.1%). ^1H NMR (500 MHz, DMSO- d_6) δ 8.28 (t, $J = 5.8$ Hz, 1H), 7.98 (d, $J = 8.9$ Hz, 1H), 7.79 (d, $J = 1.9$ Hz, 1H), 7.66 (s, 1H), 7.37 (dd, $J = 8.8, 1.9$ Hz, 1H), 7.00 (d, $J = 7.9$ Hz, 1H), 6.94 (s, 1H), 6.84 (d, $J = 1.7$ Hz, 1H), 6.73 (dd, $J = 7.9, 1.8$ Hz, 1H), 6.09 (s, 2H), 5.55 (s, 2H), 4.69 (s, 2H), 3.94 (s, 3H), 3.63 (s, 4H), 3.14 (h, $J = 6.6$ Hz, 3H), 2.05 (s, 2H), 1.41 (t, $J = 6.9$ Hz, 2H), 1.18 (d, $J = 5.7$ Hz, 22H), 0.80 (t, $J = 6.7$ Hz, 3H). ^{13}C NMR (126 MHz, DMSO- d_6) δ 167.75, 167.75, 151.60, 150.32, 147.25, 147.18, 146.31, 141.88, 134.00, 132.49, 129.88, 128.62, 126.43, 125.96, 125.57, 123.89, 121.22, 119.10, 111.10, 109.57, 108.28, 101.45, 71.12, 66.69, 55.94, 55.50, 38.67, 31.62, 31.01, 29.39, 29.34, 29.09, 29.05, 26.67, 22.42, 14.27. ESI-MS (ESI+) m/z : calculated for $\text{C}_{35}\text{H}_{43}\text{NO}_8 + \text{H}^+$, 606.3061 $[\text{M} + \text{H}]^+$, found 606.3061 $[\text{M} + \text{H}]^+$.

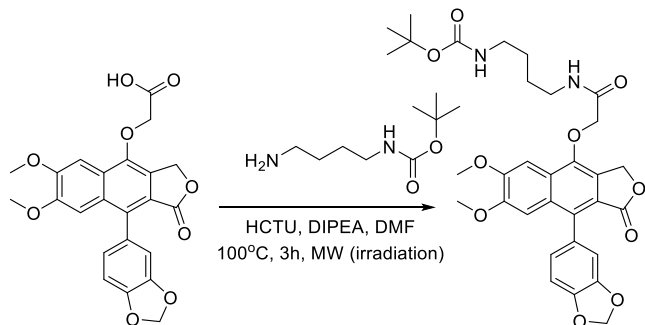


2-((9-(benzo[d][1,3]dioxol-5-yl)-6,7-dimethoxy-1-oxo-1,3-dihydronaphtho[2,3-c]furan-4-yl)oxy)-N-phenylacetamide (**2k**)- **1f** (25 mg, 0.0571 mmol, 1 eq) was mixed with HCTU (48 mg, 2 eq), N, N-Diisopropylethylamine (50 μ L, 37.1 mg, 5 eq), and aniline (27 μ L, 27 mg, 5 eq) were mixed in dimethyl formamide (1 mL). The reaction was conducted and purified as above to yield a light yellow solid (yield: 15mg, 51%, Purity: 98.2%). ^1H NMR (500 MHz, $\text{DMSO-}d_6$) δ 10.23 (s, 1H), 7.77 (s, 1H), 7.67 – 7.61 (m, 2H), 7.31 (dd, J = 8.5, 7.4 Hz, 2H), 7.10 – 6.98 (m, 2H), 6.95 (s, 1H), 6.87 (d, J = 1.7 Hz, 1H), 6.75 (dd, J = 7.9, 1.7 Hz, 1H), 6.09 (s, 2H), 5.60 (s, 1H), 4.93 (s, 2H), 3.93 (s, 3H), 3.64 (s, 3H). ^{13}C NMR (126 MHz, $\text{DMSO-}d_6$) δ 169.28, 166.87, 151.63, 150.34, 147.26, 147.19, 138.67, 129.93, 129.16, 128.51, 126.58, 126.06, 124.13, 123.92, 120.00, 111.14, 108.30, 105.78, 101.46, 71.32, 66.73, 55.99, 55.53. ESI-MS (ESI+) m/z : calculated for $\text{C}_{29}\text{H}_{23}\text{NO}_8 + \text{H}^+$, 514.1496 $[\text{M} + \text{H}]^+$, found 514.1495 $[\text{M} + \text{H}]^+$.

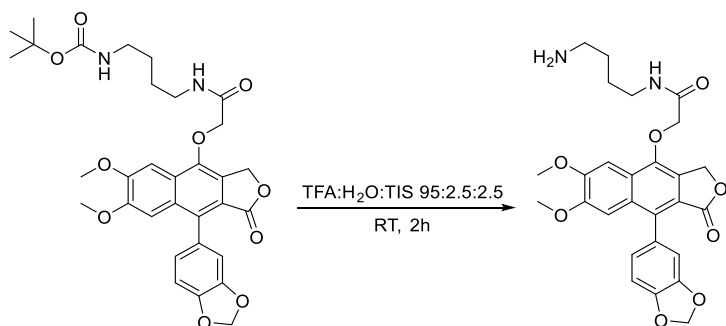


3

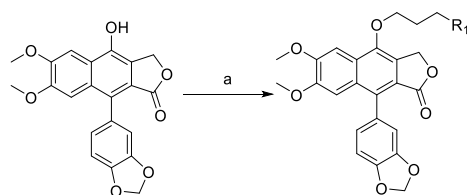
tert-butyl (4-aminobutyl)carbamate (**2la**, from the thesis of Matthew D. Bartolowits). 1,4-diaminobutane (50.02 g, 95eq) was dissolved in chloroform (600 mL) and was cooled to 0°C. di-*tert*-butyl dicarbonate (13.17 g, 1eq) dissolved in chloroform (300 mL) was added drop-wise over the course of two hours and the reaction was stirred overnight, allowing it to reach room temperature. After 21 hours of reaction time, the entire reaction mixture was transferred to a separatory funnel and was washed with water (8 x 200 mL), dried over sodium sulfate and evaporated in vacuo to give 10.71 g (94.3% yield) of **3** as a clear oil. ^1H NMR (300 MHz, CDCl_3) δ 4.84 (s, 1H), 3.04 (t, 2H), 2.64 (t, J = 6.7 Hz, 2H), 1.46 – 1.38 (m, 4H), 1.37 (s, 9H). ^{13}C NMR (75 MHz, CDCl_3) δ 155.93, 78.82, 41.70, 40.30, 30.77, 28.32, 27.37. ESI-MS (ESI+) m/z : calculated mass ($\text{C}_9\text{H}_{21}\text{N}_2\text{O}_2$) $[\text{M} + \text{H}]^{1+}$: 189.1603, mass found m/z : 189.1601 $[\text{M} + \text{H}]^{1+}$.



tert-butyl (4-(2-((9-(benzo[d][1,3]dioxol-5-yl)-6,7-dimethoxy-1-oxo-1,3-dihydronaphtho[2,3-*c*]furan-4-yl)oxy)acetamido)butyl)carbamate (**2f**) (26 mg, 0.0594 mmol, 1 eq) was mixed with HCTU (49 mg, 2 eq), N, N-Diisopropylethylamine (50 μ L, 37.1 mg, 5 eq), and NLys (32 μ L, 29 mg, 5 eq) were mixed in dimethyl formamide (1 mL). The reaction was conducted and purified as above to yield an amorphous, yellow solid (yield: 24 mg, 68%, Purity: 98.2%). ^1H NMR (500 MHz, DMSO- d_6) δ 8.31 (s, 1H), 7.66 (s, 1H), 7.00 (d, J = 7.8 Hz, 1H), 6.94 (s, 1H), 6.86 (s, 1H), 6.78 (s, 1H), 6.73 (d, J = 7.9 Hz, 1H), 6.09 (s, 2H), 5.55 (s, 2H), 4.69 (s, 2H), 3.94 (s, 3H), 3.63 (s, 3H), 3.15 (d, J = 7.8 Hz, 3H), 2.87 (d, J = 6.6 Hz, 2H), 1.41 (s, 4H), 1.33 (s, 9H). ^{13}C NMR (201 MHz, DMSO) δ 169.39, 167.89, 162.78, 156.04, 150.51, 147.43, 146.49, 134.22, 130.07, 128.69, 126.72, 126.13, 124.06, 119.30, 111.27, 108.44, 105.99, 101.60, 77.82, 71.31, 66.81, 56.15, 55.69, 40.46, 40.36, 40.31, 40.25, 40.20, 40.15, 40.10, 39.99, 39.89, 39.79, 39.68, 38.71, 38.64, 36.24, 31.23, 28.74, 27.43, 26.98. ESI-MS (ESI+) m/z : calculated for $\text{C}_{32}\text{H}_{36}\text{N}_2\text{O}_{10}+\text{Na}^+$, 631.2262 $[\text{M}+\text{Na}]^+$, found 631.2264 $[\text{M}+\text{Na}]^+$.



N-(4-aminobutyl)-2-((9-(benzo[d][1,3]dioxol-5-yl)-6,7-dimethoxy-1-oxo-1,3-dihydronaphtho[2,3-*c*]furan-4-yl)oxy)acetamide (**2m**)- 2l (50 mg, 0.082 mmol) was dissolved in 5mL of a solution of Trifluoroacetic acid: water: triisopropylsilane (95:2.5:2.5%) and stirred at room temperature for 2h. After the reaction was deemed complete by TLC, the solution was



Scheme 3.1. Synthesis of diphyllin phenol derivatives with alkyl linkers.

Reagents and conditions. (a) $\text{ClCH}_2\text{CH}_2\text{CH}_2\text{R}_1$, K_2CO_3 , DMSO, 3-16 h, 100°C (14-67%).

Table 3.1. Activity of basic alkyl phenol ethers against V-ATPase in biochemical and cell-based assays, in addition to inhibitor cytotoxicity.

ID	R_1	HEK-293	HEK-293	HEK-293	HEK-293
		EA IC_{50} (nM) ^a	CC ₅₀ (nM) ^b	CC ₅₀ / IC_{50} ^c	Vesicle Proton Flux Assay IC_{50} (nM) ^d
3a ^e	-	476±60.1	17,800±1,180	37.4	189±1.66
1a		338±81.8	64,200±5,300	190	35.4±2.91
1b ^e		74.3±23.9	11,200±580	151	27.4±3.88
1c		0.356±0.030	74.0±9.65	208	2.78±0.53
1d ^e		76.2±14.6	31,100±4,820	299	61.0±2.84

[a] Inhibition of cellular endosomal acidification in HEK-293 cells; mean±SEM (n=9). [b] Cytotoxicity assessed with MTT assay. [c] Selectivity Index of cytotoxicity over endosomal acidification in HEK-293 cells. [d] Inhibition of V-ATPase induced AO quenching using vesicles isolated from HEK-293 cells; mean±SEM (n=9). [e] Activities determined in Chapter 2.

condensed under reduced pressure. The solution was then dissolved in 10mL of distilled water and the pH was raised to ~12 by the dropwise addition of 1M NaOH. The mixture was then added to a separatory funnel and extracted with ethyl acetate (3x20 mL). The organic layers were combined, washed with brine (20 mL), and removed under reduced pressure to yield a dark, yellow oil. (yield: 27mg, 65%, Purity: 99.4%). ^1H NMR (500 MHz, DMSO- d_6) δ 8.37 (t, J = 6.0 Hz, 1H), 7.67 (s, 1H), 7.00 (d, J = 7.9 Hz, 1H), 6.95 (s, 1H), 6.86 (s, 1H), 6.73 (d, J = 8.1 Hz, 1H), 6.09 (s, 2H), 5.56 (s, 2H), 4.70 (s, 2H), 3.94 (s, 3H), 3.63 (s, 3H), 3.18 – 3.13 (m, 2H), 2.59 (s, 2H), 1.78 (s, 2H), 1.47 (q, J = 7.2 Hz, 2H), 1.44 – 1.37 (m, 2H). ^{13}C NMR (201 MHz, DMSO- d_6) δ 169.39, 167.85, 165.96, 162.75, 151.82, 150.53, 147.42, 146.51, 134.19, 130.07, 128.70, 126.65, 126.13, 124.06, 119.29, 111.27, 108.43, 105.97, 101.60, 71.31, 66.83, 56.15, 55.68, 50.70, 38.75, 38.71, 36.24, 31.23, 31.15, 29.23, 28.31, 27.68, 18.48. ESI-MS (ESI+) m/z : calculated for $\text{C}_{27}\text{H}_{28}\text{N}_2\text{O}_8 + \text{H}^+$, 509.1918 $[\text{M} + \text{H}]^+$, found 509.1919 $[\text{M} + \text{H}]^+$.

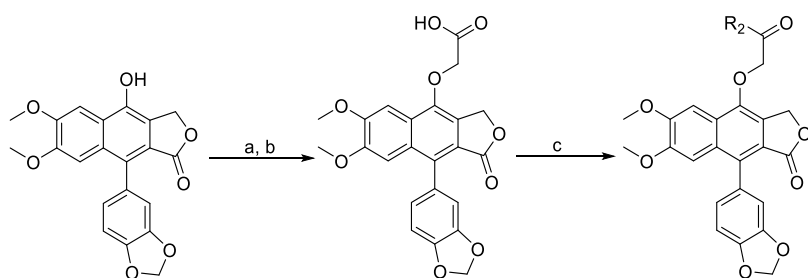
3.4 Results

To further explore the structure-activity relationship of the basic heterocycle functionality, two new basic propyl ethers of diphyllin were synthesized utilizing similar methods to the previous diphyllin propyl ethers. Diphyllin (**3a**) was completed using modified procedures from Charlton et al.³⁸⁵ Chloropropyl amino ethers with piperidine (**1aa**) and 1-methylpiperazine (**1ca**) groups were synthesized through nucleophilic attack upon 1-bromo-3-chloropropane. The propylamino linkers were then added to **3a** by nucleophilic attack of the phenol to yield derivatives **1a** and **1c** (**Scheme 3.1**). Intermediate **1e** was also synthesized through nucleophilic attack of diphyllin upon ethyl bromoacetate before the ester was hydrolyzed to form derivative **1f** (**Scheme 3.2**).

Derivatives **1a** and **1c** were assayed for the ability to inhibit cellular endosomal acidification in HEK-293 cells and yielded startling results (**Table 3.1**, **Fig. 3.1**). The removal of a heteroatom from the 4-position of the cyclohexane ring reduced activity of **1c** by a factor of 4.5 compared with previously tested derivative **1b**. However, the modification of the oxygen to a methylated amine improved activity nearly 200-fold. The cytotoxicity of both derivatives appeared to scale with the cellular activity against endosomal acidification as **1a** decreased cytotoxicity relative to **1b** and **1c** increased cytotoxicity relative to **1b**. The biochemical activity of the derivatives against proton flux induced by V-ATPase also shifted relative to their cellular activity but not to the same degree. Interestingly, the addition of an acidic functional group appears to significantly reduce the potency

Table 3.2. Physicochemical properties of alkyl and acetamide derivatives in Chapter 3

ID	Consensus Log P	pKa value(s)
1a	4.66	9.52
1b	3.81	7.48
1c	3.79	3.79, 8.92
1d	3.35	3.44, 8.39
1f	3.05	2.68
2a	3.06	-
2b	3.01	7.89
2c	2.58	7.07
2d	4.11	-
2e	3.26	5.21, 9.71
2f	3.31	3.30, 8.87
2h	2.92	6.72
2g	2.87	3.02, 8.76
2k	4.2	-
2i	2.32	-
2j	6.82	-
2l	4.24	-
2m	3.14	10
2n	5.93	-

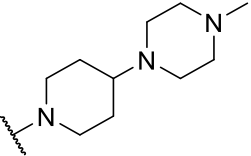
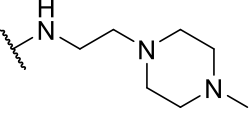
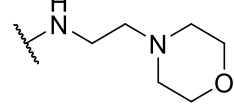
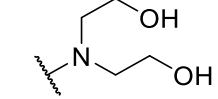
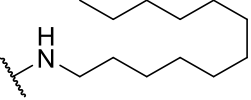
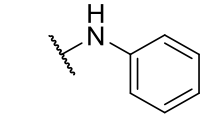
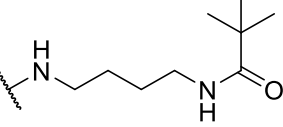
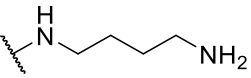
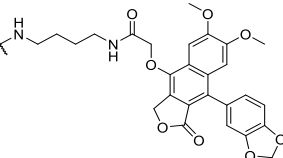


Scheme 3.2. Synthesis of diphyllin acetamide series of derivatives.

Reagents and Conditions. (a) $\text{BrCH}_2\text{COOEt}$, K_2CO_3 , DMSO, 100°C , 2 h (~100%); (b) 0.2M NaOH H_2O :IPA (1:4), rt, 16 h (88%); (c) R_2NH , TEA, HCTU, DMF, 3 h, MW (irradiation), 100°C .

Table 3.3. Activity of acetamide phenol ethers against V-ATPase in biochemical and cell-based assays, in addition to inhibitor cytotoxicity.

ID	R_2	HEK-293	HEK-293	HEK-293	HEK-293
		EA IC_{50} (nM) ^a	CC_{50} (nM) ^b	$\text{CC}_{50}/\text{IC}_{50}$ ^c	Vesicle Proton Flux Assay IC_{50} (nM) ^d
1f	-OH	3,710±845	>100,000	>27.0	460±33.6
2a		245±32.7	>100,000	>230	17.9±3.30
2b		166±18.9	>100,000	>524	4.02±0.698
2c		411±63.1	>100,000	>243	8.91±3.29
2d		440±59.3	>100,000	>227	150±31.3
2e		271±60.3	>100,000	>369	33.3±5.02

2f		140±23.4	>100,000	>714	14.8±3.19
2g		448±73.3	>100,000	>223	7.19±1.06
2h		2,410±705	76,600±9,510	31.8	14.2±2.5
2i		1,190±400	>100,000	>84.0	15.0±3.69
2j		487±60.5	71,000±9,500	146	14.7±1.64
2k		391±33.0	22,500±9,950	57.5	68.2±12.0
2l		591±123	71,800±3,770	121	43.6±7.49
2m		4,300±1,110	>100,000	>23.3	11.5±1.23
2n		502±105	>100,000	>199	

[a] Inhibition of cellular endosomal acidification in HEK-293 cells; mean±SEM (n=9). [b] Cytotoxicity assessed with MTT assay. [c] Selectivity Index of cytotoxicity over endosomal acidification in HEK-293 cells. [d] Inhibition of V-ATPase induced AO quenching using vesicles isolated from HEK-293 cells; mean±SEM (n=9).

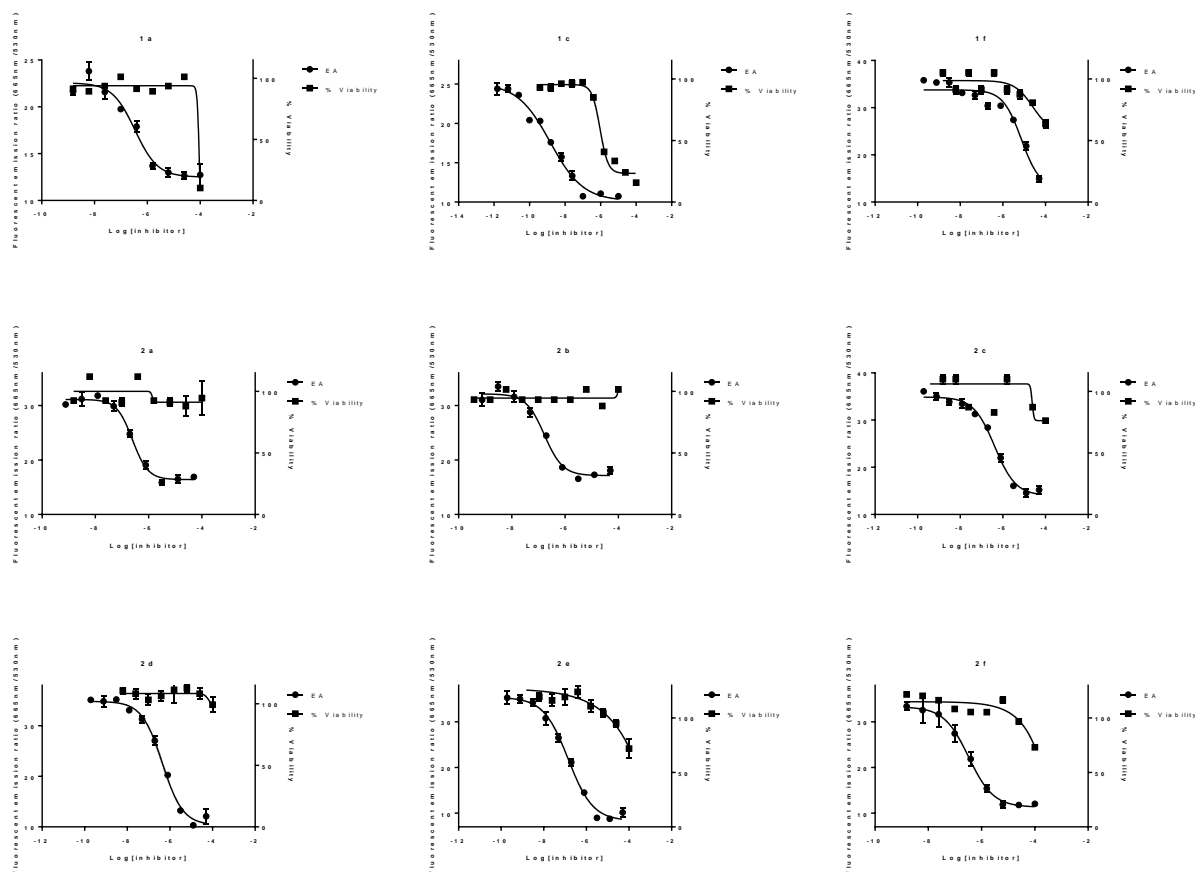
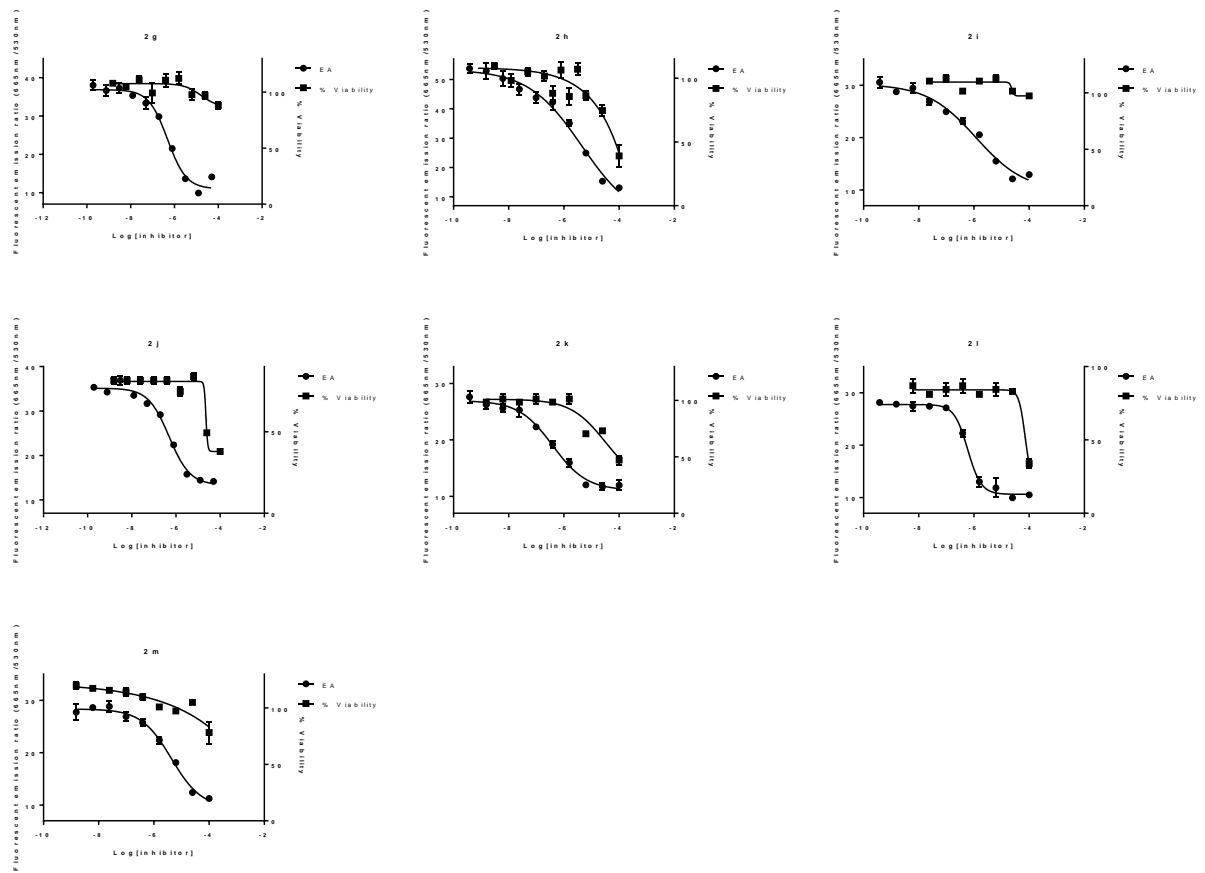


Figure 3.1. Selectivity Indices (CC₅₀/IC₅₀) graphs of compound hits in HEK-293 cells.

Graphs detail the difference between a compounds cytotoxicity (% Viability), determined by MTT assay, and its ability to inhibit endosomal acidification (EA), determined with the cellular acridine orange assay. Selectivity indices were calculated by dividing the CC₅₀ by the IC₅₀. Curves were fitted using the log[inhibitor] vs. response – Variable Slope (four parameters) function in the Analysis tool of GraphPad Prism 7.02.

Figure 3.1 (cont.)



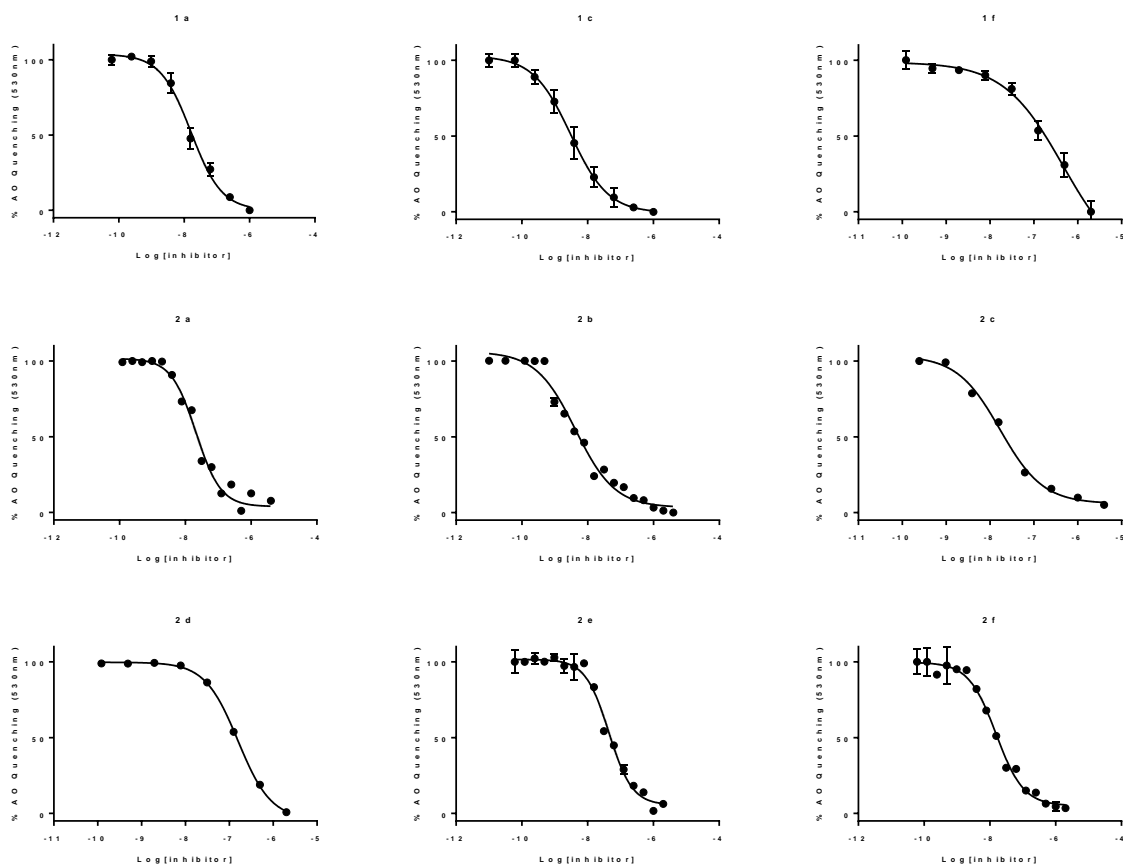
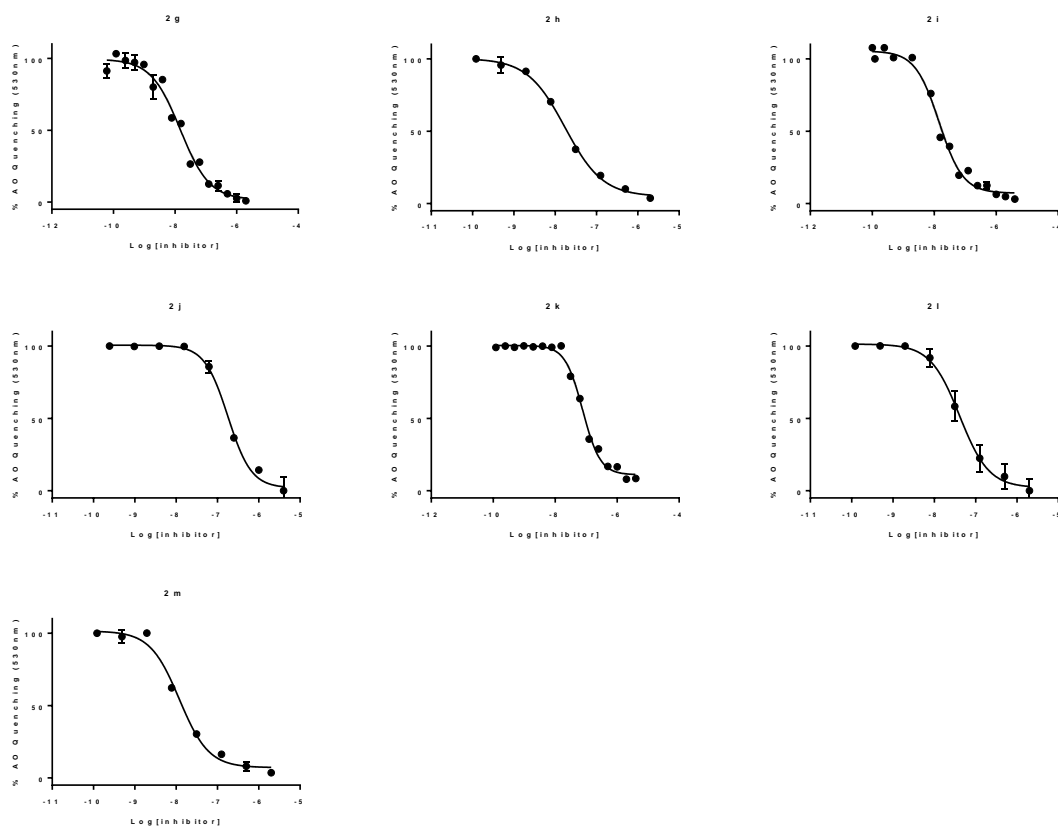


Figure 3.2. Dose-response curves of the inhibition of V-ATPase mediated inhibition of proton translocation by diphyllin alkyl and acetamide derivatives.

Vesicles were mixed with inhibitors and incubated for 1 h at 37°C in the presence of acridine orange. ATP was added to the vesicle mixture on 96-well plates and incubated for 1 h at room temperature before reading fluorescence at 530 nm when excited at 485 nm. Nigericin was then added and the fluorescence after 10 min was again measured. The difference between the two fluorescence values was used to determine the amount of acridine orange quenched. Data are shown as mean \pm standard error of the mean of the change in fluorescence at each inhibitor concentration. Curves were fitted using the log[inhibitor] vs. response – Variable Slope (four parameters) function in the Analysis tool of GraphPad Prism 7.02.

Figure 3.2 (cont.)



of derivative **1f** in both biochemical and cellular assays. Thus, basic heterocycle derivatives appear to have the preferred activity against V-ATPase while decreasing the cytotoxicity of the molecule. The exact mechanism of this change is not understood but could be due to the increased localization of the basic derivatives to acidic compartments created by V-ATPase activity in addition to enhanced activity against the enzyme. This change in subcellular localization could prevent diphyllin from exhibiting off-target effects on other processes.

The differences in activity amongst the alkyl derivatives could be due to several characteristics of the amine functional groups (**Table 3.2**). The basicity of the amine is not the sole determinant of cellular activity for these derivatives as the piperidine moiety of **1a** has the highest ammonium ion pK_a (9.5) of all derivatives created and had the lowest activity, while **1c** has the second highest pK_a and is the most active. The number of basic sites could also be implicated in the improved activity of **1c** (two; pK_a=3.8, 8.9) but **1d** also has two basic sites (pK_a=3.4, 8.4) and while the pK_a values are relatively similar, the cellular activities of the derivatives are significantly different. The consensus LogP of **1c** (3.79) is nearly identical to the LogP of **1b** (3.81) and these values are in between those of **1a** and **1d** as well. Overall, the enhanced activity of **1c** compared to the other derivatives may be due to a unique confluence of these factors or another occurrence of the “magic methyl” effect. The difference in the potency increases between the biochemical and cellular activities of **1c** could be due to the improved cellular targeting of the inhibitor to acidic apartments caused by the doubling of the basic sites in the methylpiperazine side chain.

To further explore the structure-activity relationship of diphyllin phenol derivatives, a series of acetamide derivatives were synthesized with a variety of different functional groups (**Scheme 3.2**). The acetamide series was chosen because of the high yield of **1f** produced and the ability to rapidly and efficiently couple a variety of groups through amide coupling. Groups with similar basic heterocycles to those used in the alkyl derivative series were used for comparison and their previously identified favorability for activity. Derivatives with modified physical characteristics were also chosen to determine the tolerance of coupling and the tolerance of side chain modification. To investigate the relationship of basic side chains to the molecules V-ATPase activity, derivatives with an increased number of basic groups were also created.

As a whole, the acetamide class retained activity against V-ATPase containing vesicles and demonstrated potencies greater than nearly all formerly described alkyl derivatives (**Table 3.3, Fig. 3.2**). Shortening the linker by a carbon or the addition of a new hydrogen bond acceptor may

contribute to enhanced binding with V-ATPase or improved access to the binding site. Derivatives with short basic groups (**2b**, **2c**) were the most active and appear to indicate a preference for shorter side chains. However, derivatives **2g** and **2m** had similar potencies, which may be due to the flexibility of the side chain in addition to the having a basic group. Longer basic derivatives with basic sites **2e** and **2f** were also potent inhibitors, while replacement of the cyclohexane with a phenyl ring (**2d**) dramatically reduced activity. Intriguingly, flexible hydrophobic and hydrophilic groups (**2i**, **2j**) were favored over a phenyl ring (**2k**) in other derivatives.

Unfortunately, the activity of the derivatives against cellular endosomal acidification did not exhibit the same increase in activity shown in the biochemical assay. Derivatives with basic side chains were able to exhibit activity greater than diphyllin, but activity did not match activities observed in the alkyl derivatives (**Tables 3.1, 3.3**). Derivatives **2b** and **2f** exhibited activities like those observed for the alkyl derivatives but the activities of other derivatives were not significantly different than that observed for diphyllin (**3a**) or much worse. More interestingly, derivatives exhibited little cytotoxicity in all cases and even the most toxic of the acetamide inhibitors only exhibited cytopathic effects at the highest concentrations.

To determine if the activity of derivatives was being diminished through degradation of the inhibitor in cells, the stability of several derivatives was tested in media for 48 h and in cell culture for 24 h (**Fig. 3.3 and 3.4**). Only derivative **2c** exhibited more than 10% loss after 4 h in media, which could explain the loss in the activity of this derivative. Derivatives **2b**, **2f**, and **2g** exhibited little loss after 4 h and their loss appeared to plateau after the 24 h similar to what was observed with the alkyl derivative **1c**. This loss could be due to interactions with plastic that have been identified previously with derivative **1b**. Correspondingly, derivative **2d** had no loss over 48 h which indicates that the derivatives without amines are stable and that the amines undergo plastic binding. After exposure of the same derivatives to cells for 24 h, chromatographs of extracts from the cells indicated no peak besides the parent compound and those present in the DMSO control (**Fig. 3.4**). Thus, the activity of some derivatives in cells may be caused by degradation of the parent molecule, but the most potent inhibitors are stable in solution and upon exposure to cells. Further investigation needs to be made into these derivatives to explore the increase in observed selectivity window and the structure-activity relationship of the stable derivatives.

To further assess the toxicity of the alkyl derivatives in relation to the acetamide series, we decided that animal models may be more indicative of the activity of these derivatives in a patient

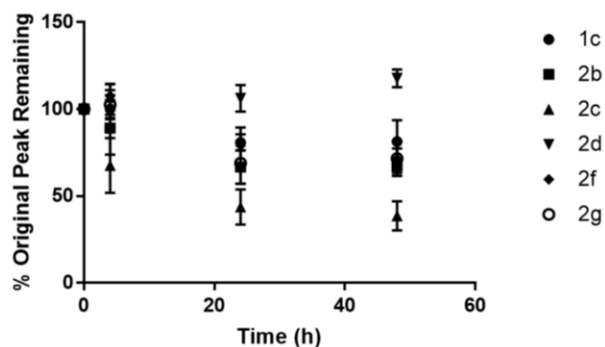


Figure 3.3. Stability of **1c** and top acetamide derivatives in cell culture media over 48h.

Compounds **1c**, **2b**, **2c**, **2d**, **2f**, and **2g** were tested for their time-dependent stability in DMEM+FBS over 48 h. Samples were withdrawn at 0 h, 4 h, 24 h and 48 h and diluted in 9 volumes of acetonitrile+0.1% trifluoroacetic acid to precipitate out serum proteins. Data shown are the mean \pm the standard error of the mean for each sample and time point for 3 individual experiments.

A)

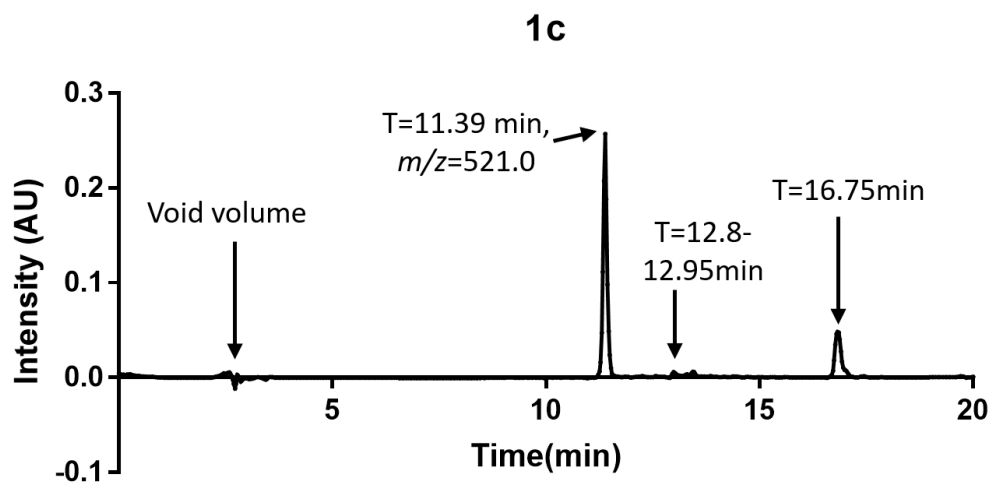
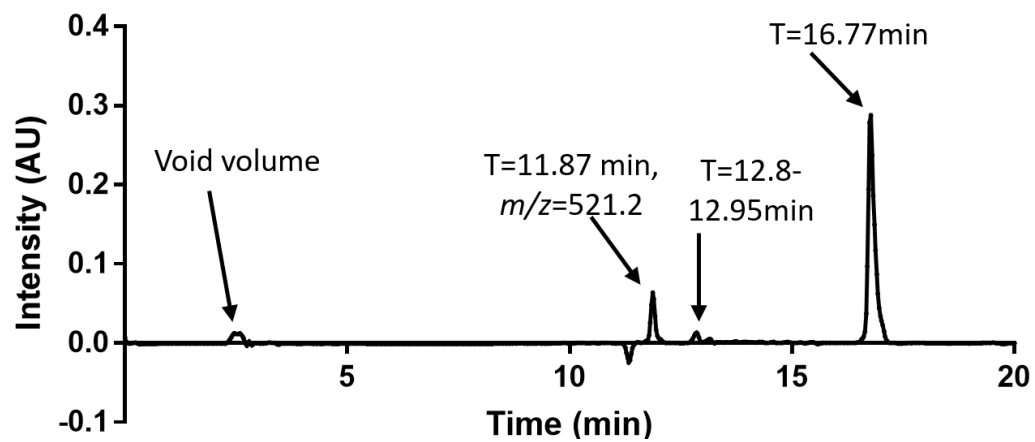


Figure 3.4. Example chromatographs from the isolation of select inhibitors from treated HEK-293 cells.

HEK-293 cells were treated with **1c** (A), **2b** (B), **2c** (C), **2d** (D), **2f** (E), and **2g** (F) for 24 h before extraction with a 1:1:0.005 methanol:acetonitrile:trifluoroacetic acid solution for 16 h. The solution was removed and centrifuged for 10 min at 14,000xg to remove remaining cellular debris and concentrated. Samples were run using a Hitachi D-7000 HPLC system to identify potential metabolic products of the select inhibitors. Peaks present in the DMSO-treated control are indicated by retention time on each chromatograph but were not further analyzed. Peaks that were not present in the DMSO-treated control sample were collected and analyzed with an Advion expression Compact Mass Spectrometer and the major m/z is indicated with the retention time of the peak.

Figure 3.4 (cont.)

B)

2b

C)

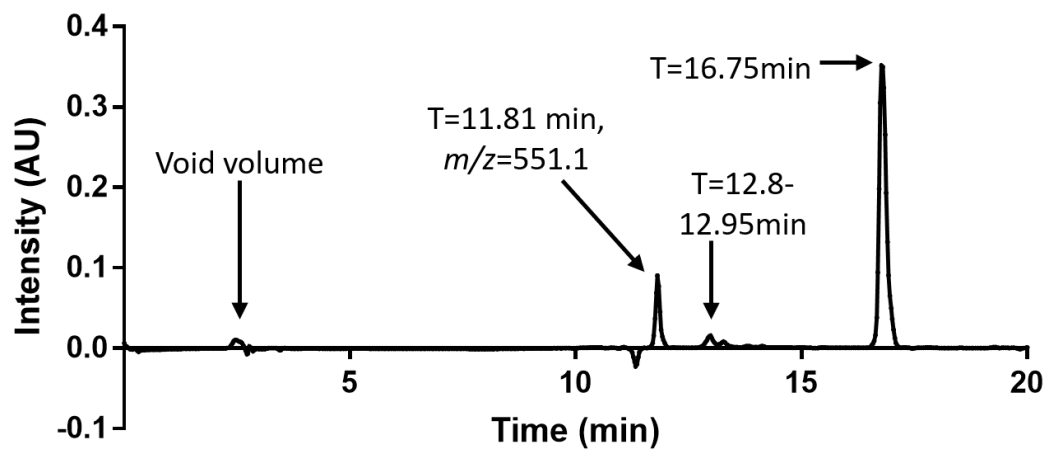
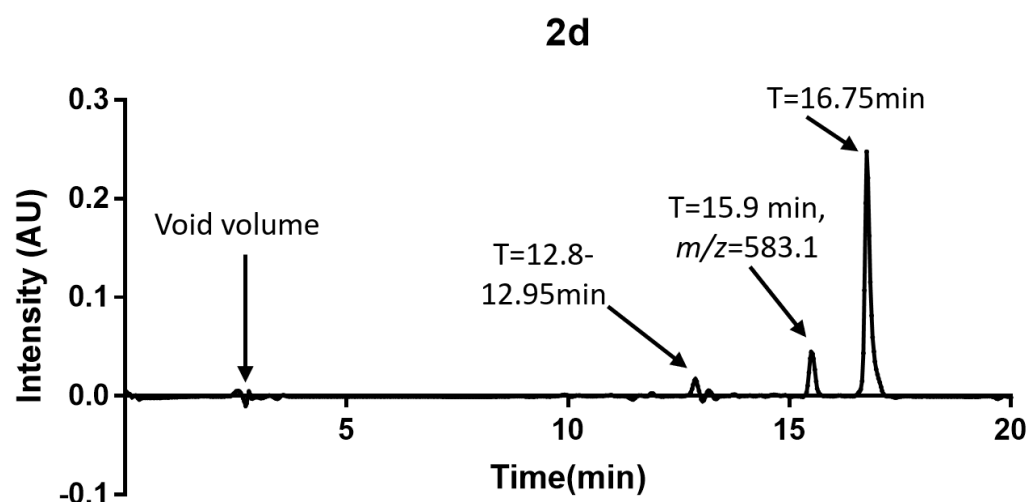
2c

Figure 3.4 (cont.)

D)



E)

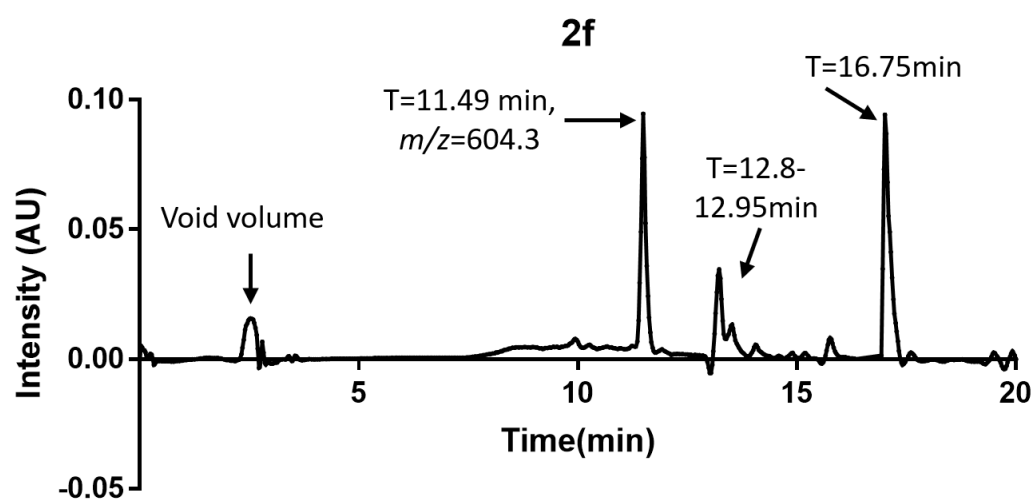


Figure 3.4 (cont.)

F)

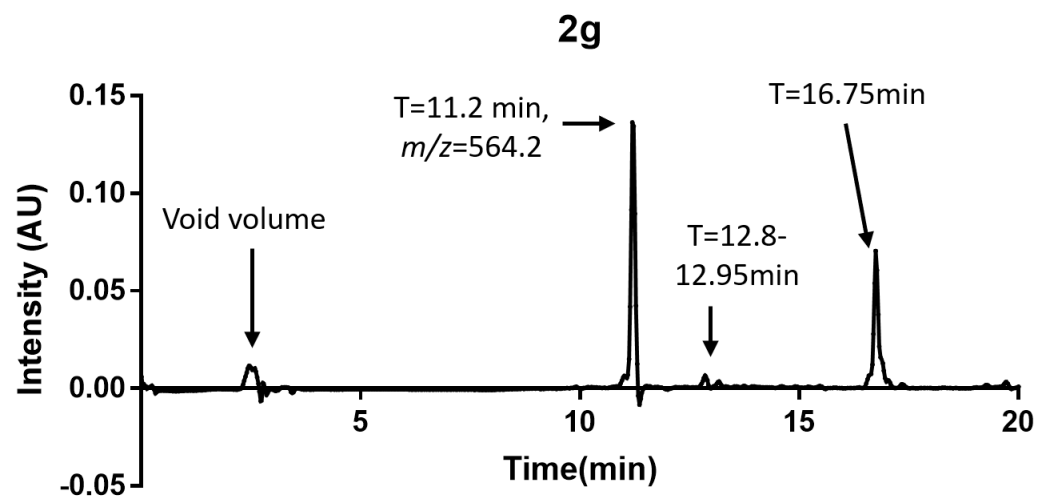


Table 3.4. LD50 values 5dpf zebrafish embryos treated with inhibitors.^a

ID	Zebrafish Embryo LD ₅₀ (μM)
Bafilomycin A1	0.1262
3a	>100
1a	6.484
1b	1.318
1c	1.205
1d	3.857
1f	>100
2a	19.41
2b	30.86
2c	>100
2d	35.79
2e	14.06
2f	14.05
2g	34.18
2h	19.38
2i	10.52
2j	>100
2k	28.43
2l	19.41
2m	>100

[a] This work was completed by Jason Ray Nielson in the Peterson lab at the University of Utah.

Table 3.5. Formulation Stability and gastrointestinal permeability of derivatives.^a

ID	24 h Formulation Stability	72 h Formulation Stability	Apparent Caco-2 Permeability (nm/sec)
3a	1.0 ± 3.5%	-9.0 ± 2.6%	9.20±0.40
1b	-1.0 ± 3.6%	-9.3 ± 2.1%	1.17±0.57
1c	-20.0 ± 2.0%	-28.3 ± 1.2%	1.37±0.79
1d	-6.0 ± 3.0%	-12.0 ± 4.0%	7.22±0.37

[a] This work was completed by Kelsey Lubin, Monika Lavan, and Mark Joseph Schopper in the Knipp lab at Purdue University.

than cell culture. Also, different types of cells in culture responded differently to compound treatment as HEK-293 cells proved by the most susceptible to cytotoxicity of the inhibitors compared resistance to inhibitor cytotoxicity in the A549 and HeLa cell lines and primary human macrophages assess previously. To gain a better estimate of host toxicity, we decided to use a zebrafish and mouse model to test the toxicity of the inhibitors compared with the parent diphyllin and standard V-ATPase inhibitor bafilomycin A1. Derivatives **1b**, **1c**, and **1d** were compared with known V-ATPase inhibitors bafilomycin A1 and **3a** in a zebrafish embryo model to determine if whole organism toxicity corresponds to cell culture observations. Accordingly, 5dpf zebrafish embryos exposed to the compounds for 20 h were evaluated and scored for toxicity. The variations in toxicity of the derivatives and known V-ATPase inhibitors in zebrafish indicated promising results when comparing the different inhibitors (**Table 3.4**). Bafilomycin A1 was 10-fold more toxic to zebrafish embryos than any of the diphyllin derivatives tested. Diphyllin exhibited no toxicity up to 100 μ M though it was potentially ionized in solution and unavailable for uptake into the fish. Interestingly, both **1b** and **1c** exhibited similar toxicity to one another though **1c** was significantly more toxic than **1b** in the cell culture studies. Derivative **1d** was 3-fold less toxic than **1b/1c** though this fits the profile previously observed in cell culture relative to **1b**. Overall, these data suggest that diphyllin derivatives may not elicit the same toxic phenotype evidenced by bafilomycin A1. The acetamide class of derivatives displayed 100-fold less toxicity compared with bafilomycin A1 and they were 10-fold less toxic than the alkylamine derivatives. The acetamide derivatives with more basic groups like **2b** and **2g** appeared to be less toxic than other acetamide derivatives but the basic derivatives **2e** and **2f** did not parallel the decrease in toxicity. Overall, the equivalence between the lack of cytotoxicity and lower toxicity in zebrafish indicate that our previous cell-based results are potentially good indicators of the derivatives overall toxicity.

Before assessing the toxicity of derivatives in mice, we developed a formulation strategy for the derivatives and determined the stability of the formulations. Derivative **1b**, **1d**, and diphyllin had previously been shown to be stable for up to 24 h in cell culture media and during exposure to cells (Chapter 2). Further studies with **1c** also showed it was stable in cell culture media for up to 48 h with little loss of material and **1c** appear stable when exposed to cells for 24 h. All four compounds (**1b**, **1c**, **1d**, diphyllin) were formulated in a solution composed of 25% Transcutol HP, 20% Solutol HS 15, and 55% PBS and their stabilities were assessed over 72 h at room temperature. After 72 h, three compounds (diphyllin, **1b**, and **1d**) exhibited less than 10%

loss in solution that indicated that they may be stable long-term (**Table 3.5**). However, **1c** lost on average 28% over 72 h but two-thirds of that was lost within 24 h which indicates it may have been due to potential interactions with plastic. To prevent any loss of the active compounds, all solutions were made daily for animal administration. In the interest of developing orally bioavailable therapies in the future, the gastrointestinal permeability of the derivatives was estimated using Caco-2 cells (**Table 3.5**). Compounds **1b** and **1c** were the most permeable of the compounds, and the permeability would likely predict good oral bioavailability in terms of permeation, while **3a** and **1d** were approximately 1.5-fold slower at $\sim 8 \times 10^{-6}$ cm/s. Many drugs dosed orally have Papp values in this range, however, it isn't necessarily expected that 100% bioavailability would be reached.

CD-1 mice were used to determine the toxicity of **3a**, **1b**, **1c**, and **1d** at doses determined to be active in cell culture. The doses of **3a** and **1b** were selected so that blood concentrations would reach 5x the IC₉₀ for the inhibition of EBOV infection of primary human macrophages (12.5 μ M and 3.3 μ M respectively), while the doses of **1c** and **1d** were extrapolated from the activity of **1b**. The maximum blood concentration of **1d** was chosen to be 3.3 μ M due to the similar activities to **1b**, while the maximum concentration of **1c** was 0.33 μ M because of its increased potency. The formulations were administered once a day for 5 days and allowed a three-day recovery period before blood collection and analysis. Analysis of blood protein parameters indicated that the doses were safe and well tolerated in the case of **3a**, **1b**, and **1d** (**Fig. 3.5**). Nevertheless, **1c** produced marked hemolysis in a sample from female mice and those were unable to be analyzed. Data for the male mice are included with the sample data for both sexes treated with the other three compounds. Normal levels of blood urea nitrogen (BUN) were reported for all compound and all compounds except **1c** reported normal levels of creatinine (CREA). These indicate that no kidney damage was apparent for diphyllin, **1b**, and **1d** at the doses used which could be expected for V-ATPase inhibitors that may block critical V-ATPase function in the kidneys. Alanine aminotransferase (ALT), alkaline phosphatase (ALKP), and total bilirubin (TBil) levels were also reported as normal, indicating that liver function was not impaired by treatment with the formulations. **1c** was also the only derivative that was used at a concentration higher than its CC₅₀ in HEK-293 cells, which may indicate toxicity is associated with the increased dose of the derivative. Thus, three of the inhibitors could be deemed safe for use while **1c** potentially had differential effects based on the sex of the mice, though it appeared non-toxic to the male mice.

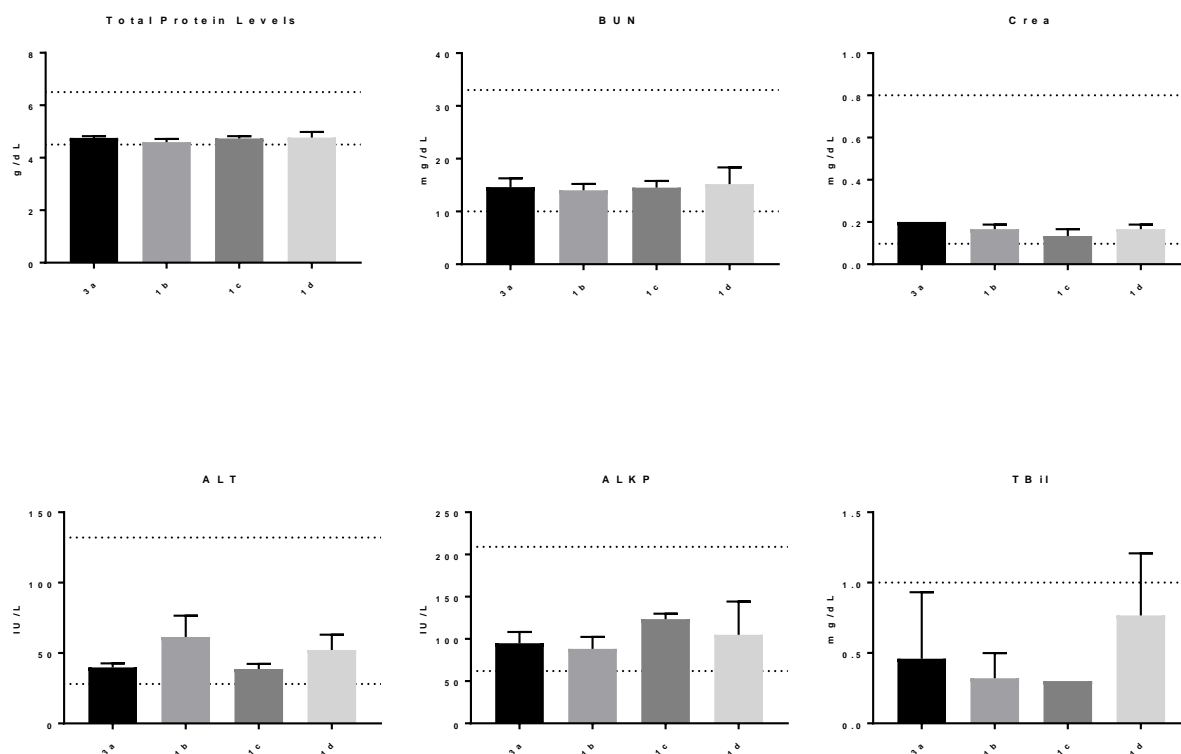


Figure 3.5. Blood chemistry mice treated with diphyllin and derivatives.

Mice treated with intraperitoneal injections of formulated **3a**, **1b**, **1c**, and **1d** were evaluated for changes in blood chemistry parameters, including total protein, blood urea nitrogen (BUN), creatinine (Crea), alanine transaminase (ALT), alkaline phosphatase (ALKP), and total bilirubin (TBil). Dotted lines represent the normal ranges in CD-1 mice. Data in the plot represent the mean \pm SEM of 3-6 mice. This work was completed by Kelsey Lubin, Monika Lavan, and Mark Joseph Schopper in the Knipp lab at Purdue University.

3.5 Discussion

V-ATPase inhibitors represent a novel way to treat viral infections by targeting a pathway that is conserved in many viruses. Numerous viruses require the acidification of endosomes to release themselves from the endosome and initiate cellular infection. Inhibition of the proton pump responsible for endosomal acidification, V-ATPase, has been shown to block infection of many viruses. This has led to the investigation of V-ATPase inhibitors for the clinical treatment of viral infection. However, the toxicity associated with V-ATPase inhibitors treatment has prevented their progress from cellular probes to clinical therapies and increased bias against the development of new inhibitors. The natural product diphyllin represents a new opportunity as the chemotype has shown an unprecedented lack of toxicity while retaining potent activity against V-ATPase.

To improve diphyllin's physicochemical properties, potency and selectivity, we previously created several series of diphyllin derivatives and determined that the alkylation of the diphyllin phenol with propyl amine groups improved all three categories. Herein, we further investigated if the properties could be further optimized and if derivatives exhibited cytotoxicity in animal models. The modification of the alkyl derivatives to include a 1-methylpiperazine group improved cellular activity 200-fold over previous inhibitors, while the modification of the alkyl linker into an acetamide abolished toxicity in cell culture. The mechanism through which these cases occurred is not known but could be due to the increased targeting of the basic side chains to sites of V-ATPase activity. V-ATPase containing endosomes and lysosomes form the most acidic areas within a cell and have previously been shown to trap amine-containing compounds. When these compounds enter an acidic compartment, the amine becomes protonated and the increased charge on the molecule prevents its escape from the compartment. This mechanism has been associated with drug resistance mechanisms in cancer and other diseases for amine-containing drugs. However, the trapping of V-ATPase inhibitors within endosomes localizes them to sites of V-ATPase and likely enhances their activity against the complex. Also, trapping may prevent the inhibitors from reaching other targets within the cells that may cause off-target effects of the drug. Thus, the increased selectivity of the amine-containing diphyllin derivatives may be due to their increased localization at sites of V-ATPase activity.

To assess if our derivatives would face the same problems, we measured the response of zebrafish and mice to treatment with these inhibitors. The decrease toxicity in the zebrafish development model and lack of toxicity in mice indicates that these derivatives could be used in

animal disease models at therapeutically-efficacious doses. Previously, other V-ATPase inhibitors have been used in animal models, but further studies have not been released. This has led to the belief that V-ATPase inhibitors cannot be developed into clinical therapies. Hopefully, further investigation with these derivatives in animal infection models will show that bias to be mistaken.

3.6 Conclusions

In this work, novel derivatives of diphyllin were created that both exhibited activity against V-ATPase as potent as any known inhibitor and an improved the selectivity index greater than any previous V-ATPase inhibitor. The addition of basic side chains as modifications of the diphyllin phenol group appear to be a unique way to modulate the activity of diphyllin. Comparison of toxicity between the derivatives and bafilomycin indicates that they are at least 10-times less toxic in a zebrafish model. Mice appeared to tolerate doses of several inhibitors that block EBOV entry *in vitro*. Thus, the addition of basic heterocycles to diphyllin appears to be a promising treatment for EBOV infection and potentially other diseases.

CHAPTER 4. FUTURE DIRECTIONS

4.1 Introduction

The search for novel therapies is continuous due to the never-ending identification of new diseases and disease targets. EBOV is a significant example in recent work as many new targets for treating the EBOV infection have been identified in the large body of work that has occurred since the 2014-2016 outbreak in west Africa. Further structural modifications of diphyllin can be employed to further optimize derivative activity through modification of all facets of the structure to enhance the potency and selectivity while decreasing metabolic instabilities present in the diphyllin core. Identification of the binding site of diphyllin with the V-ATPase complex could also aid in further structure-based studies the diphyllin-V-ATPase interaction and could be used to identify novel inhibitors through computational screening. Selective diphyllin-based V-ATPase can also be used to treat a host of diseases that have not been accessible for previous V-ATPase inhibitors.

4.2 Structural Optimization of the Diphyllin Chemotype

The scaffold of diphyllin has been relatively unexplored for modifications and further modification of all parts of the structure could be used to optimize the activity of the compounds (**Fig 4.1**). The replacement of the lactone functional group with a lactam is easily accessible and has the possibility of quickly revolutionizing the activity of the structure. Further modification of the phenol ethers could be used to synergize the selectivity and potency observed in previous derivatives. Finally, the incorporation of novel structures on the A- and D-rings can decrease the metabolic liabilities of the structure and modulated the activity of the derivative.

The replacement of the lactone with a lactam can be used to increase the physicochemical properties and activity of the diphyllin scaffold. A prime example of this activity in medicinal chemistry is the semi-synthetic, breast cancer therapy 15-aza-epothilone B (Ixabepilone). 15-aza-epothilone B substituted a lactam for the lactone found in the natural product epothilone B with impressive results.⁴⁰⁷ The activity of 15-aza-epothilone B was 10-fold better against the CCRF-CEM leukemia cell line and 50-fold less cytotoxic.⁴⁰⁸ Thus, substitution of the diphyllin lactone with a lactam may yield similar effects. The lactam derivative is also synthetically accessible through the synthesis of an imide precursor (**Scheme 4.1**). A benzyl imide can be

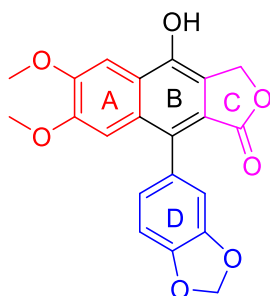
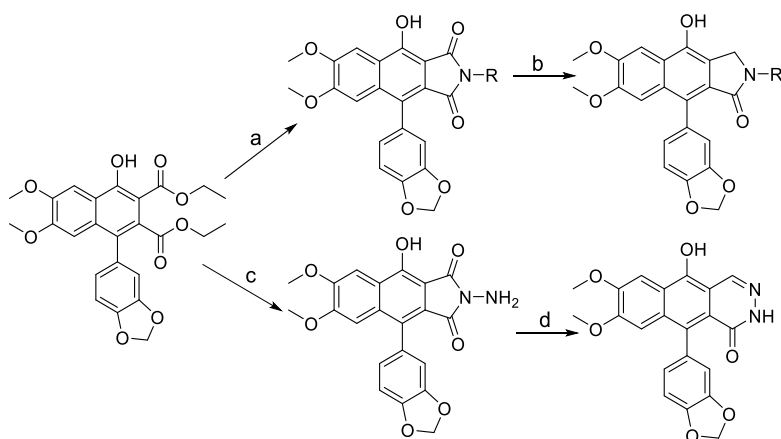


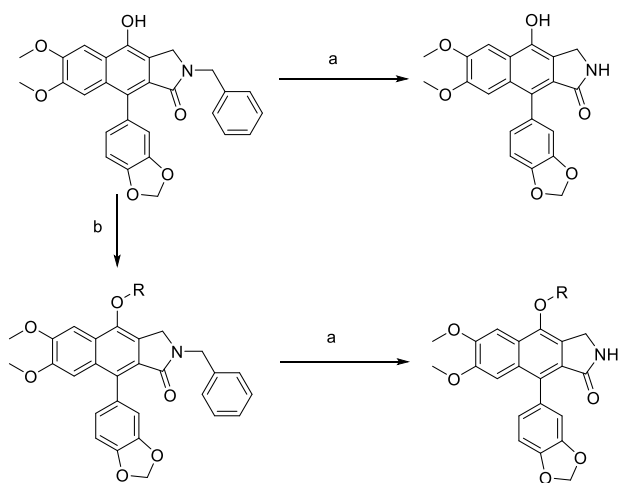
Figure 4.1. Structure of diphyllin with labeled rings.

Each of the rings in diphyllin offers an opportunity for the synthesis of novel derivatives and potential optimization of activity and selectivity.



Scheme 4.1. Synthesis of novel C-ring analogs.

Reagents and Conditions. (a) RNH_2 , MeOH, reflux; (b) LiAlH_4 , THF, 0°C ; (c) H_2NNH_2 , MeOH, reflux; (d) Zn, AcOH, reflux.



Scheme 4.2. Synthesis of diphyllin lactam and potential alkylated derivatives.

Reagents and Conditions. (a) H_2 , Pd/C, EtOH, RT; (b) R-X, K_2CO_3 , DMSO, 90°C .

synthesized by the condensation reaction between benzylamine and the diester precursor to diphyllin. The benzyl imide can be reduced with lithium aluminum hydride to yield a benzyl lactam, which can be deprotected with hydrogen gas and palladium on carbon. This phenol group of the lactam can be alkylated prior to the debenzylation reaction to yield multiple combinatorial derivatives (**Scheme 4.2**). The lactam derivative would have improved aqueous solubility and would not suffer from steric hindrance at the position that were deemed unfavorable in the work with imide and hydrazone derivatives.

Another potential substitution of the lactone is a pyridazinone ring that has already been synthesized. The phthalazinone derivative produced through reduction of the hydrazine imide has proved to be an inhibitor of similar potency to diphyllin against V-ATPase activity but was 2-fold weaker against EBOV infection (**Scheme 4.1**). Alkylation of this derivative was found to change the subcellular localization of the drug within cells and abolished its activity against cellular endosomal acidification within cells. The biochemical activity of this derivatives needs to be further evaluated but appears to be weaker than the parent derivative. Alkylation of this derivative with hydrophobic groups may prevent the change in subcellular localization and improve the activity of the derivatives against V-ATPase. In addition, the change in subcellular localization between active and inactive compounds could signal that the derivatives are active against a separate target within cells. Identification of this target could provide a novel method for targeting EBOV infection or in the treatment of other diseases. Given the similarity of the phthalazinone structure to kinase inhibitors, the derivative may act as a ATP analog against a kinase or other target.

Novel phenol derivatives of diphyllin could also be created to further probe the SAR of this highly variable region. Optimization of the amine sidechain for both selectivity and potency needs to be completed as both properties have been optimized individually but have not been combined. Modification of either the amine terminus, the linker between diphyllin and the terminus, or both may provide methods to unite selectivity and potency. Since the acetamide series lacked stability compared with alkyl series, the incorporation of a stable bioisostere to the amide functionality may lead to the improvement in activity in conjunction with decreased cytotoxicity (**Fig. 4.2**). Utilizing click chemistry, the propargyl or pentynyl diphyllin ethers could be used to create triazole linkages with amines at the terminus. Since azide-containing amines are expensive or unavailable, it may be simpler to form an azide-diphyllin ether and add alkynyl-containing

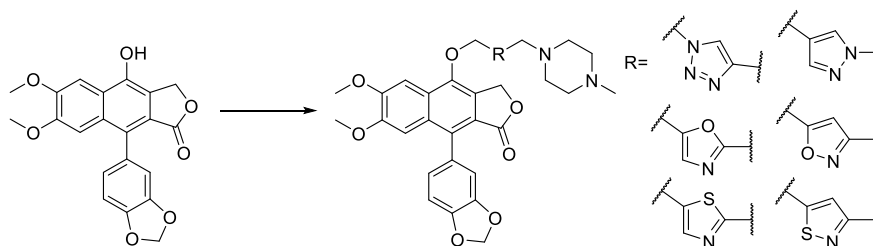
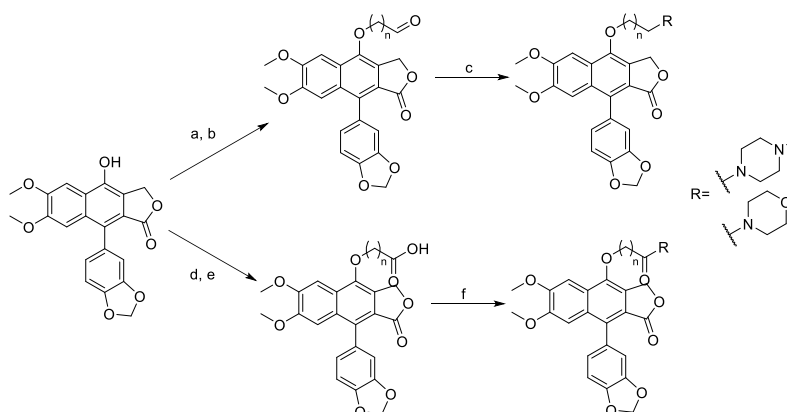


Figure 4.2. Incorporation of amide bioisosteres into the linker of diphyllin ethers.

These are more stable groups that exhibit similar physicochemical properties to the amide chain that decreases the cytotoxicity of derivatives. Variations in the carbon chains on either side of the heterocycle could also be optimized as these are likely the shortest derivatives that could be synthesized through this method. The 1-methylpiperazine terminus could be used initially given its already favorable activity profile. Further rigidification and heteroatom additions could also be explored.



Scheme 4.3. Synthesis of novel alkylated phenol derivatives.

Reagents and conditions: (a) $\text{BrCH}_2(\text{OCH}_2\text{CH}_3)_2$, K_2CO_3 , DMSO, reflux; (b) 0.5M HCl, Acetone:Water (5:1), RT; (c) R_2NH , $\text{NaBH}(\text{OAc})_3$, dichloroethane, RT. (d) $\text{BrCH}_2\text{COOEt}$, K_2CO_3 , DMSO, 100°C , 2 h (~100%); (e) 0.2M NaOH H_2O :IPA (1:4), rt, 16 h (88%); (f) R_2NH , TEA, HCTU, DMF, 3 h, MW (irradiation), 100°C

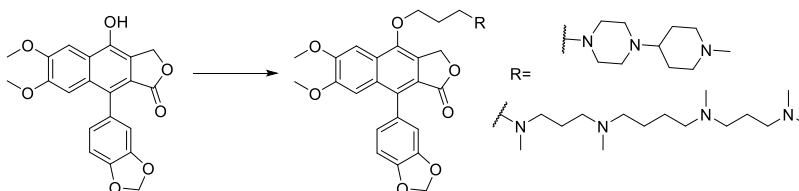


Figure 4.3. Amino-termini with an increased number of basic groups.

These derivatives would have 3-4 basic groups and are all tertiary amines due to the preference of these for activity. These would likely function as probes of activity but could provide interesting activity profiles. The spermine derivative could have applications in diseases like metastatic cancer in addition to antiviral uses.

amine groups that are easily accessible. Other linkers like oxazoles, thiazoles, and imidazoles are also synthetically compatible with the diphyllin core and would provide variants to be used to replace the triazole linker or provide access to specific products not accessible through click chemistry.

Optimization of the linker length can be done to maximize interactions with V-ATPase and may also provide novel insights to the diphyllin binding site. The acetamide series contained derivatives with longer and more rigid sidechains that appeared well tolerated by the enzyme but did not fully explore potential interactors in the binding site. It is possible that the binding mode of diphyllin forces the sidechain to be solvent exposed and able to interact with any number of partners, but further evidence is needed. Utilizing reductive amination or further amide couplings could be used to explore the toleration of shorter or longer linkers. Protected halo-aldehyde and halo-ester derivatives are commercially available, and the nucleophilic addition would be similar to reactions already completed reactions with high yields (**Scheme 4.3**). Activity of derivatives that incorporate a morpholine or 1-methylpiperazine terminus would be a useful indicator of whether the linker was functional for retaining or improving activity. Additionally, identification of length tolerance may allow for the incorporation of groups like biotin that can be used during pulldowns of V-ATPase during biochemical studies (discussed later).

Modification of the amino terminus could also be used to explore the relationship the number of basic sites to the activity of derivatives and their endosomal targeting. Alkyl derivatives with 1-(1-methylpiperidin-4-yl)piperazine or alkylated spermine side chains would have multiple basic groups and could enhance derivative targeting to the endosome, if that is a determinant of activity (**Fig 4.3**). Alkylated spermine derivatives or arginine would also improve the uptake of derivatives into monocyte-derived cells and may enhance their activity against EBOV infection.^{409,410} These derivatives also may be useful against cancers that increase the uptake of polyamines that are used during increased cell growth.⁴¹¹ However, the addition of polyamine groups to lignans has been demonstrated to increase their topoisomerase activity so care would need to be taken when interrogating there activities.⁴¹²

Modification of the aromatic rings of the core structure may also provide novel derivatives that can be combined with the derivations above to yield significantly different chemotypes from diphyllin. The 3,4-dimethoxybenzyl and 3,4-methylenedioxy functional groups pose metabolic risks and can be substituted with known bioisosteres that retain similar electrostatic distributions

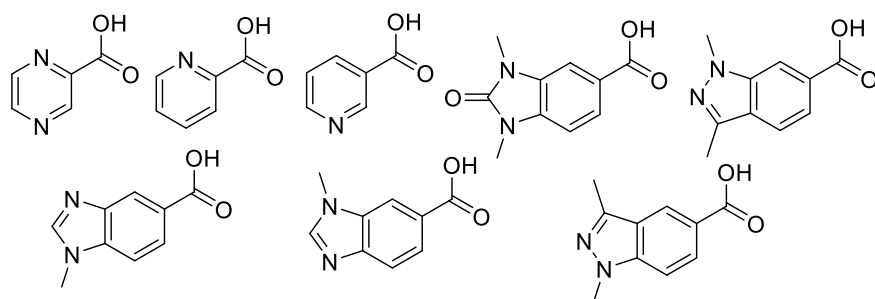
but remove the liability. Previous modifications of these areas have focused on changing the number and position of methoxy or methylenedioxy groups or the addition of halogens or glycosyl moieties.^{413,414} Modification of these areas with novel heterocycles would create new chemotypes and could exploit novel interactions that have not been explored. Novel synthetic methods may also be necessary for the incorporation of these derivatives into the diphyllin core.

A-ring derivatives can be used to modify the physicochemical properties of diphyllin, improve metabolic stability, and explore the conformational states of the ring. The potential demethylation of the 3,4-dimethoxybenzyl group by cytochrome P450 can form a catechol structure with numerous off-target effects. To avoid this activity, the 3,4-dimethoxybenzyl group can be replaced with bioisosteres like indazole and benzimidazole that lack metabolic liabilities. Indazole and benzimidazole groups retain similar steric and electrostatic configurations to the 3,4-dimethoxybenzyl group while offering innovative chemotypes. Changing the ring to a pyridine or pyrazine would significantly change the ring system but allow for the incorporation of different electrostatics to the ring and additional basic groups, with regards to the pyridine, to aid in endosomal targeting.

Derivatization of the D-ring of diphyllin also represents an unexplored area for the addition of novel heterocycles. Natural products related to diphyllin have incorporated glycosyl groups at the 6 position of the phenyl ring exist (justicidinoids) but have not shown strong biological activities.³³⁹ Limited derivatives of the methylenedioxy portion of the substructure have also been created but none have ever been evaluated for activity against V-ATPase or viral infection.⁴¹⁵ Limited derivation of the 3,4-methylenedioxy to incorporate a deuterated or fluorinated methylene group would provide metabolic stability without changing the steric bulk of the group but the fluorinated derivative would have modified electrostatic properties. Further modification by the addition of similar functional groups to those proposed for the A ring may bring more novelty but have an increased risk of failure given the previous lack of tolerance for modification of this group.

To incorporate these novel derivatives, a new synthetic route would likely be required to tolerate the new functional groups (**Scheme 4.4**). Several recent synthetic schemes have been proposed to optimize the synthesis of lignans that could be used for the creation of the novel derivatives proposed above.^{416,417} The synthesis hinges upon a regioselective addition catalyzed by silver acetate (d) before proceeding through the reduction of a diester precursor to yield the a regiospecific lactone. However, this reduction may be hampered by modifications to the D-ring or

A)



B)

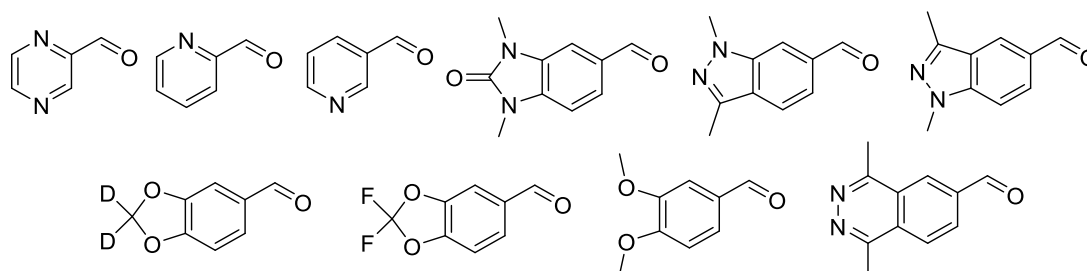
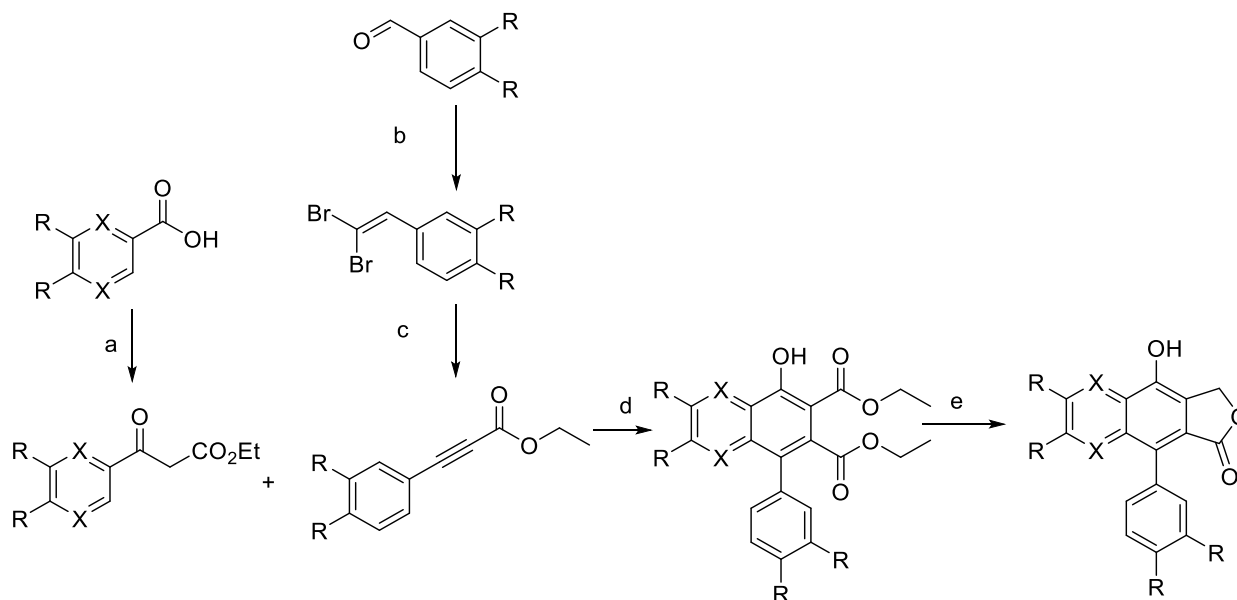


Figure 4.4. Ring derivatives for the synthesis diphyllin derivatives.

A) A-ring derivative precursors; B) D-ring derivatives precursors.



Scheme 4.4. Synthesis of A- and D-ring derivatives of the diphyllin core structure.

Reagents and Conditions. (a) CDI, THF, $K^+O_2CCH_2CO_2Et/MgCl_2$; (b) CBr_4 , PPH_3 , DCM; (c) $nBuLi$, $ClCO_2Et$; (d) $AgOAc$, $Na_2S_2O_8$, SDS, H_2O ; (e) $LiAlH_4$, THF.

changes to the phenol that drive the selectivity of the reaction. The old synthetic methods could also be used as a replacement in case of the lack of compatibility in reactions.

4.3 Identification of the Diphyllin Binding Site

In addition to novel structural derivatives of diphyllin, identification of the binding site of diphyllin could lead to improved effort for structure-based improvements to the diphyllin scaffold instead of the probing of ligand-based design. Competition studies with labeling dyes have traditionally been used to determine the binding sites of derivatives but new techniques with spin-labeling have pinpointed the binding sites of several derivatives (**Fig 4.5**). Competition with new V_1 targeted probes could also be used if diphyllin interacts with binding sites identified in this domain (**Fig. 4.5**). The first step in determining the binding site would be to isolate which V-ATPase domain diphyllin interacts with.

To ascertain whether diphyllin binds to the V_0 or the V_1 domain, V-ATPase can be purified from yeast or bovine sources through density centrifugation and separated into separate domains.²⁹⁵ The isolated V_1 domain's ability to hydrolyze ATP in the presence of the inhibitor can be compared to the activity of the inhibitor against the full complex to determine if the inhibitor has the same effect upon the V_1 domain as the complete complex. The activity of inhibitors against proton flux through the isolated V_0 domain can also be measured to determine if they bind to the membrane-bound domain. Through these methods, the domain to which the inhibitor binds should be elucidated.

To further determine the binding site of diphyllin in whichever domain it binds to, several approaches are available depending on which domain with which it interacts. If diphyllin is an inhibitor of proton conductance through the V_0 domain, several assays can be used that have previously worked with other V-ATPase inhibitors. Traditional studies to identify V_0 inhibitors have relied upon the inhibition of labeling by fluorescent derivatives of DCCD, photolabeling studies, and site-directed mutagenesis. NCD-4, a fluorescent derivative of known V-ATPase inhibitor dicyclohexylcarbodiimide (DCCD) irreversibly binds to a glutamate on the c subunit that is responsible for proton translocation. The plecomacrolide and archazolid classes are known to inhibit the binding of NCD-4 and inhibition of its binding by diphyllin would signal that it has a

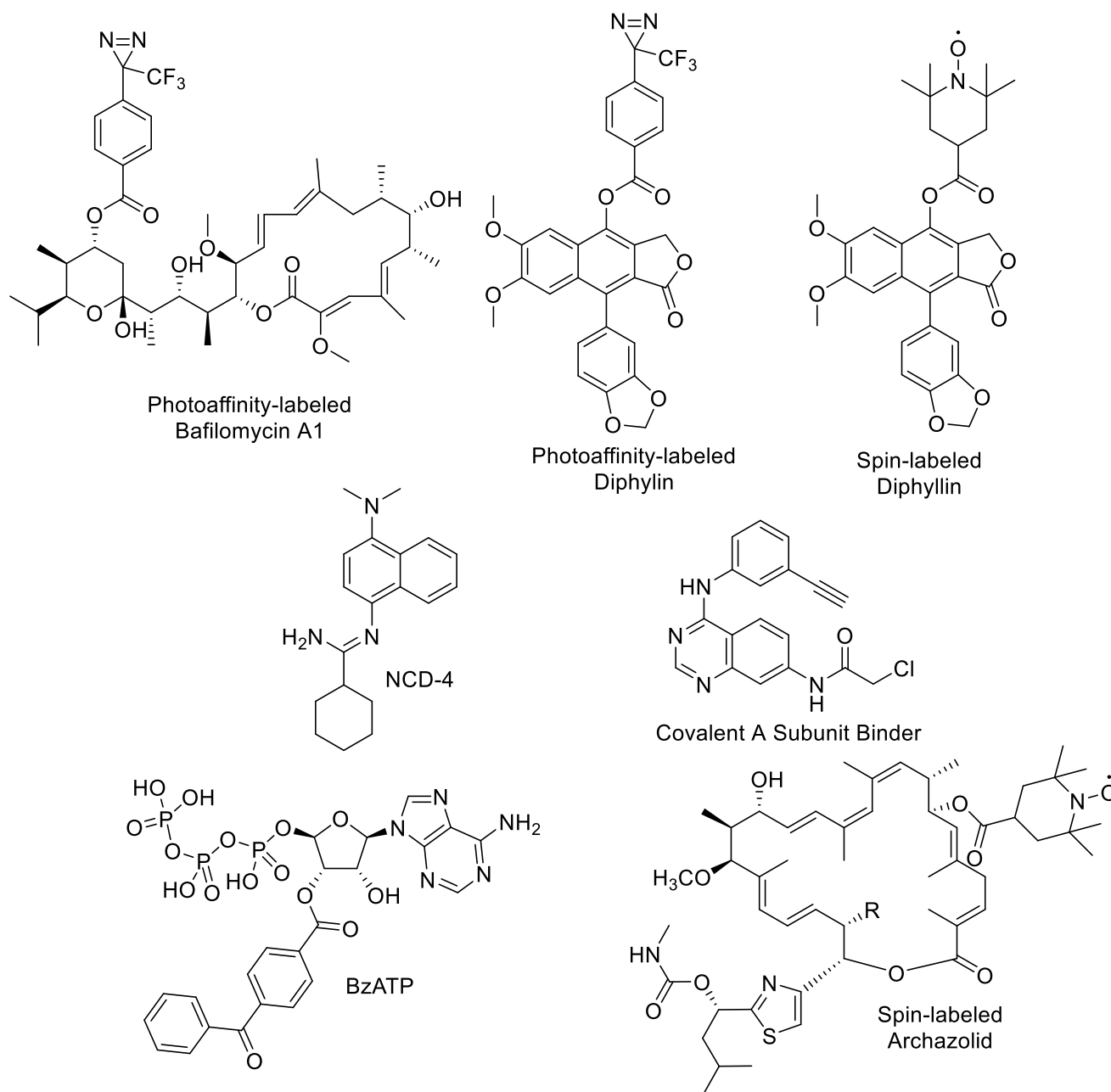


Figure 4.5. Molecules to be used in the determination of diphyllin's binding site.

The spin- and photoaffinity-labeled diphyllin derivatives can be used to identify the subunits they interact with. If these direct methods fail, competition of diphyllin with the photoaffinity-labeled bafilomycin A1 and spin-labeled archazolid could be used to explore diphyllin's interactions with the V_0 domain. The covalent binder to subunit A and BzATP can be used to identify the binding region on the V_1 domain if diphyllin inhibits the ATPase activity of the isolated domain.

similar interactions to the known inhibitors.²⁸¹ A diazirinyl photoaffinity group could also be added to diphyllin to determine its ability to label specific subunits or diphyllin could be used in competition assays with other photoaffinity labeled inhibitors like bafilomycin A1 or concanamycin A. The ability of diphyllin to inhibit the activity of bafilomycin, archazolid or salicylhalamide resistant V-ATPase mutants could also be used to assess its binding site.^{281,295,296} If diphyllin proves to be a potent inhibitor of these resistant mutants, diphyllin likely has a unique binding site within the complex. More recent studies that have utilized spin-labeling techniques to confirm the binding sites of archazolid, concanamycin A, and SB242784 can be used with diphyllin.^{280,313} Electron paramagnetic resonance spectroscopy and double electron-electron resonance measurements of spin-labeled diphyllin derivatives could further reveal the binding site of diphyllin.²⁸⁰ The number of techniques to identify V_0 inhibitors has been well-studied to the localization of most V-ATPase inhibitors to this domain but several techniques can also be used to identify a V_1 inhibitor.

If diphyllin inhibits ATP hydrolysis in the V_1 domain, the binding site can be potentially identified by competition studies for the labeling of several sites within the AB heterohexamer. The alternate nucleotide site on the B subunit can be labeled using irradiation of the nucleotide analog 2'(3')-O-(4-Benzoylbenzoyl)adenosine 5'-triphosphate (BzATP). BzATP was previously used to identify a novel ATP binding site within the B subunit that is important for the proper function of the V_1 domain.^{200,418} Alternatively, diphyllin could interfere with the binding of covalent inhibitors at a recently identified site within the non-homologous region of V-ATPase. If diphyllin can compete for the labeling of cysteine-138 by the covalent probe, it may also interact with the non-homologous region of the A subunit.²⁰¹ The interaction of diphyllin with either binding site would be a novel mechanism of inhibition by a non-covalent modifier.

Another method for identifying the binding pocket of the diphyllin scaffold would be to screen yeast V-ATPase mutants with diphyllin and derivatives to identify those that are resistant to V-ATPase inhibition. Due to the toxic phenotype observed in yeast when they are treated with other V-ATPase inhibitors in the neutral media, it has previously been possible to identify resistant mutants by cytotoxicity screening. This would be the most broad-spectrum way to identify the binding site by screening all known mutant for cytotoxicity. A more targeted screen for direct V-ATPase activity would be to isolate mutated V-ATPase from the yeast that contain modifications that are known to be important for bafilomycin A1, archazolid, and other V-ATPase inhibitors.

Diphyllin likely wouldn't engage all of the amino acids that the larger macrocycles do but it may require several of the known amino acids if diphyllin binds in the same relative area of the proteolipid ring observed for other V-ATPase inhibitors.

A main problem in V-ATPase inhibitor development has been the lack of a complete structure of V-ATPase with bound inhibitors because the complex is too large for normal crystallography. Cryo-electron microscopy (cryo-em) structures of the yeast enzyme are now available but not have been created with a bound inhibitor.¹⁹² Affinity-based purification of V-ATPase complexes through capture with a covalently-bound inhibitor could be used to lock V-ATPase with a ligand for new cryo-em structures.⁴¹⁹ The addition of a chloroacetate functional group to the diphyllin phenol may be the easiest method for creation of a covalently-active diphyllin derivative but a host of other types of electrophilic derivatives could be added to the phenol given its propensity for modification. The problem with this approach is that the phenol may not take a position that would allow it to react with a nucleophilic side chain like cysteine or serine. This may be the most direct way to determine the binding site of diphyllin on the structure but the optimization of the linker and the binding affinity of diphyllin may not meet the necessary requirements for the study to work.

4.4 Novel therapeutic Targets for the use of selective V-ATPase inhibitors

The treatment of many cancers could be revolutionized with a selective V-ATPase inhibitor. Increased invasiveness of cancer is correlated with the increased expression of V-ATPase at the plasma membrane of cancerous cells.²⁶³ The increased removal of protons from the cytosol of cancer cells dependent upon glycolysis has been determined to aid in cancer cell survival, while the proton extrusion can degrade the extracellular matrix and activate excrete proteases.⁴²⁰ V-ATPase is also involved in the resistance mechanisms of cancer cells to treatment with other inhibitors. The trapping of amine-containing drugs within endosomes could be prevented with V-ATPase inhibitors, which would revitalize many therapies that have lost efficacy.⁴²¹ Acidic extracellular pH can also prevent inhibitors from reaching or passing through the plasma membrane of cancer cells.

Further study of the mechanism of toxicity of diphyllin and its derivatives may provide avenues for improving its therapeutic selectivity. The exact mechanism through which V-ATPase

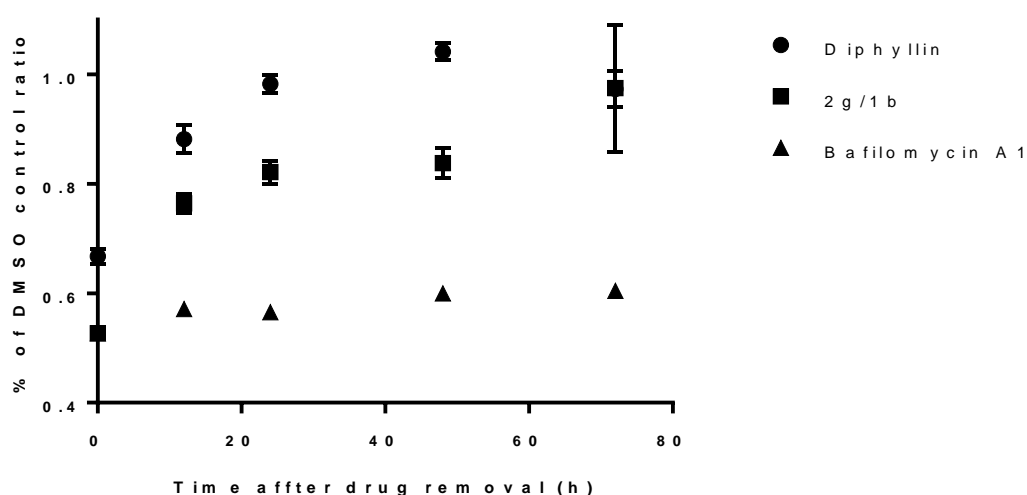


Figure 4.6. Recovery of HEK-293 cells that were treated with diphyllin, **2g/1b**, and bafilomycin A1.

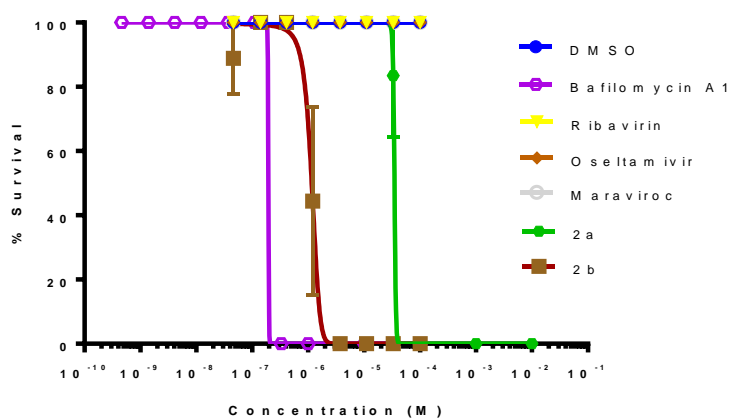
HEK-293 cells were treated with diphyllin (1 μ M), **2g/1b** (200 nM), and bafilomycin A1 (200 nM) for 4 hours before the removal of the drug media and replacement with complete media. Cells at the 0 h time point replaced the drug media with complete media and acridine orange was added and the plate was read with a Biotek Synergy 4 microplate reader. Cells were then incubated for 12 h, 24 h, 48 h, and 72 h before the addition of acridine orange and reading with the plate reader. Each reading was over six individual wells treated with drug and two wells treated with vehicle media. Data are shown as mean \pm standard error of the mean of the fluorescent ratio of the drug-treated cells divided by the fluorescent ratio of vehicle-treated cells at each time point.

inhibitors induce toxicity is not currently well-understood. The plecomacrolides are known to act as K^+ ionophores and appear to target the mitochondria and either of those activities may be responsible for their observed toxicity.²⁷⁶ Blockade of endosomal acidification and lysosomal function may also be responsible for toxicity as both derivatives appear to cause long-term damage to the acidification of the endosome and lysosome. Initial studies over 72 h indicate that bafilomycin-induced endosomal alkalization does not reverse while alkalization caused by diphyllin and the morpholino propyl ether cause reversible inhibition and cells recover endosomal acidification over 72h (**Fig 4.6**). This data appears to indicate that diphyllin and its derivatives interact differently from bafilomycin A1 in the cellular environment. Further study of the effects of diphyllin derivatives upon the mitochondrial function needs to be studied as the glycoside derivatives of diphyllin appear to induce apoptosis through mitochondrial pathways.³⁵³

The development of a non-cytotoxic V-ATPase inhibitor opens many therapeutic windows that have not been fully explored due to previous undesired effects.^{188,422} The host of viruses that rely on V-ATPase driven activity has been mentioned previously but can be mentioned again for emphasis. Dangerous pathogens like influenza viruses, flaviviruses (Zika, Dengue, West Nile, etc.), alphaviruses (Semliki Forest, Venezuelan equine encephalitis, etc.), and even the common cold (rhinoviruses) are potential targets of therapeutic V-ATPase inhibitors.^{181,345,423} The development of V-ATPase inhibitors as therapies for the treatment of osteoporosis could be used to address the anticipated explosion in cases due to the expanding elderly population.³⁴² V-ATPase inhibitors have also been proposed as treatments for neurodegenerative diseases.⁴²⁴ Conclusively, there are nearly unlimited applications of a selective V-ATPase inhibitor in the treatment of disease.

APPENDIX A- ADDITIONAL DATA

A)



B)

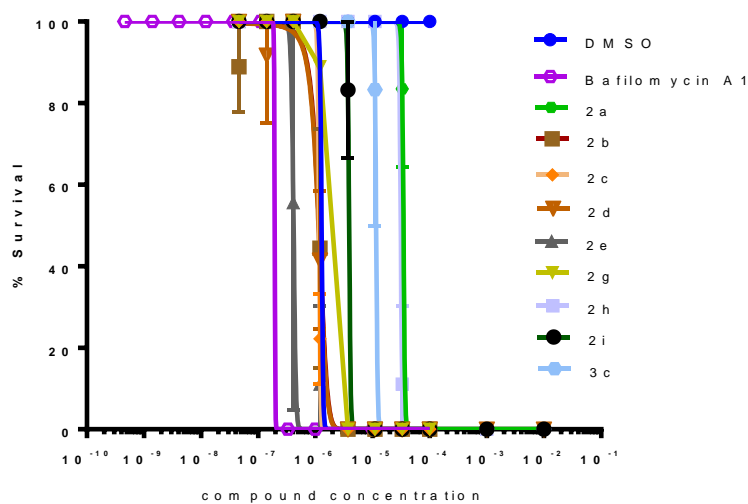
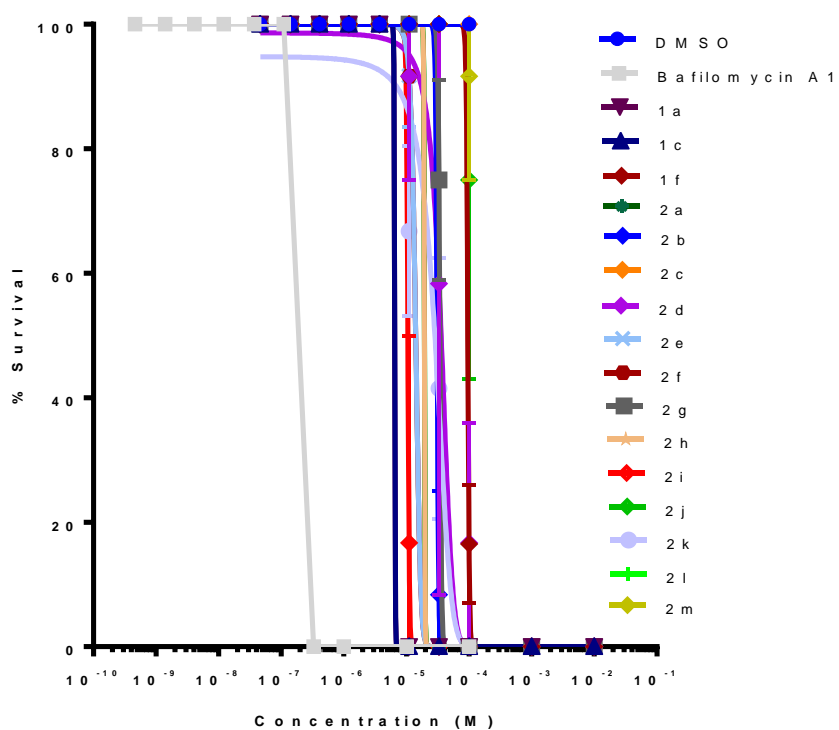
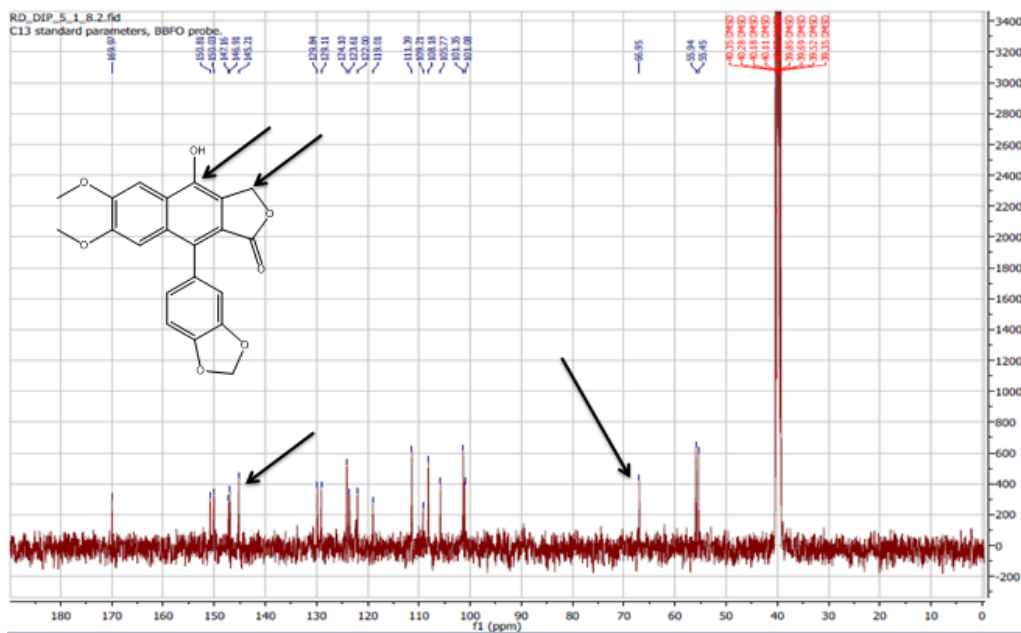


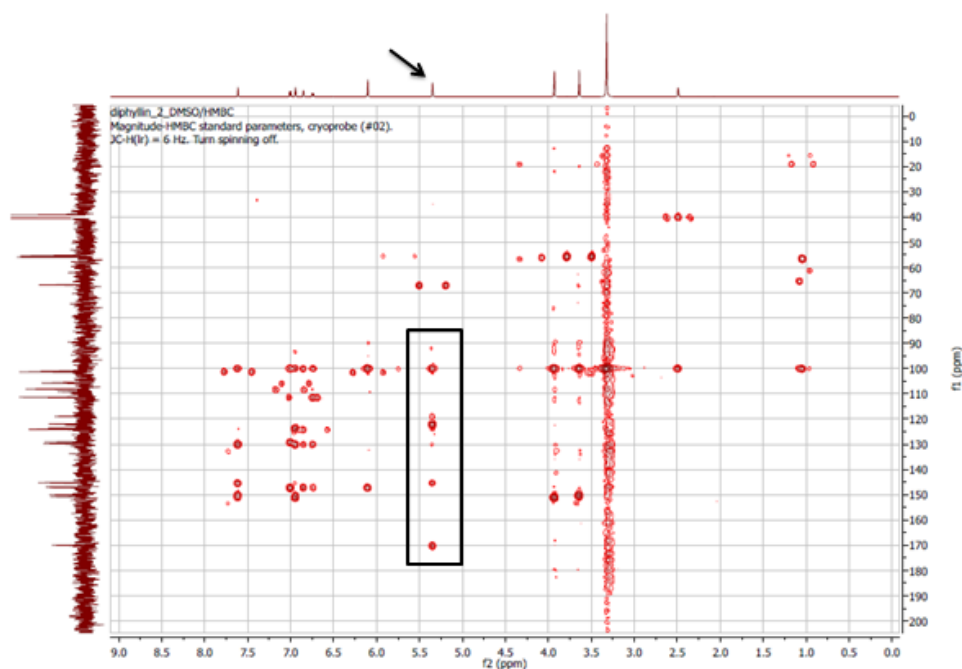
Figure A.1. LD50 curves of zebrafish treated with known and novel compounds. Known antiviral compounds ribavirin, oseltamivir phosphate, and maraviroc were tested for toxicity alongside known V-ATPase inhibitors (A). Inhibitors from chapter 2 (B) and chapter 3 (C) were all assessed for toxicity in the zebrafish model.



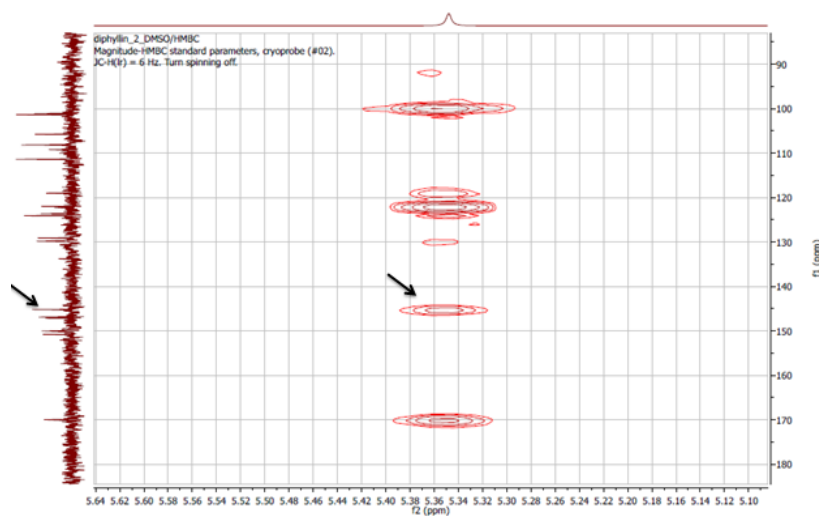
RD_DIP 5_1_8-1.fid
H1 standard parameters, BBFO probe.

10.5 (s, 0.4H)
7.5 (d, 1.0H)
7.0 (m, 1.0H)
6.8 (m, 1.0H)
6.6 (m, 1.0H)
6.0 (s, 2.0H)
5.1 (s, 1.5H)
3.9 (d, 3.0H)
3.6 (d, 3.0H)
3.3 (s, 3.0H)
2.5 (s, 2.0H)



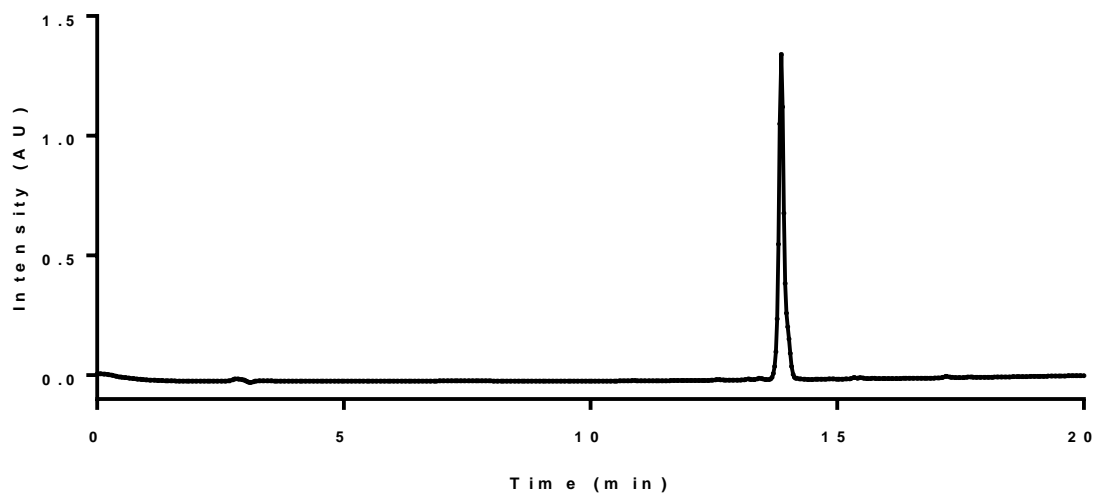


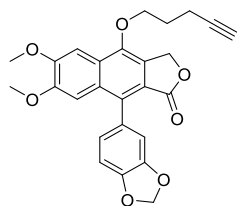
Full diphyllin HMBC spectrum, HMBC indicates that protons affiliated with the phenolic carbon used to justify lactone regiochemistry.



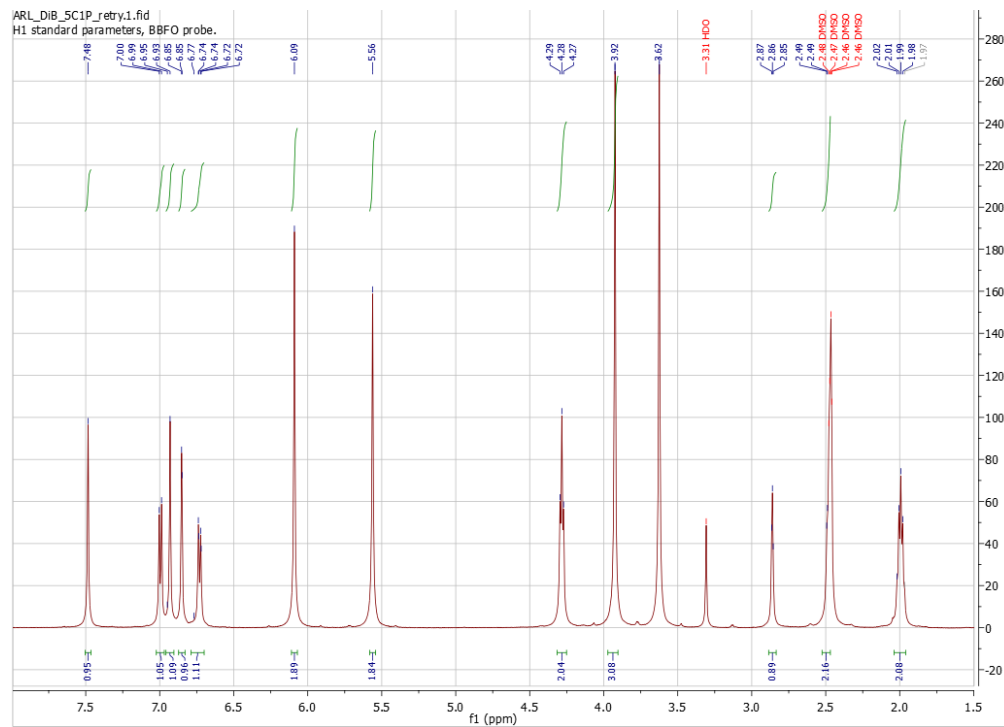
Expanded version of HMBC spectrum of H protons and corresponding carbon peaks. Arrows indicate the presence of a peak showing the coupling of H protons and phenolic carbon.

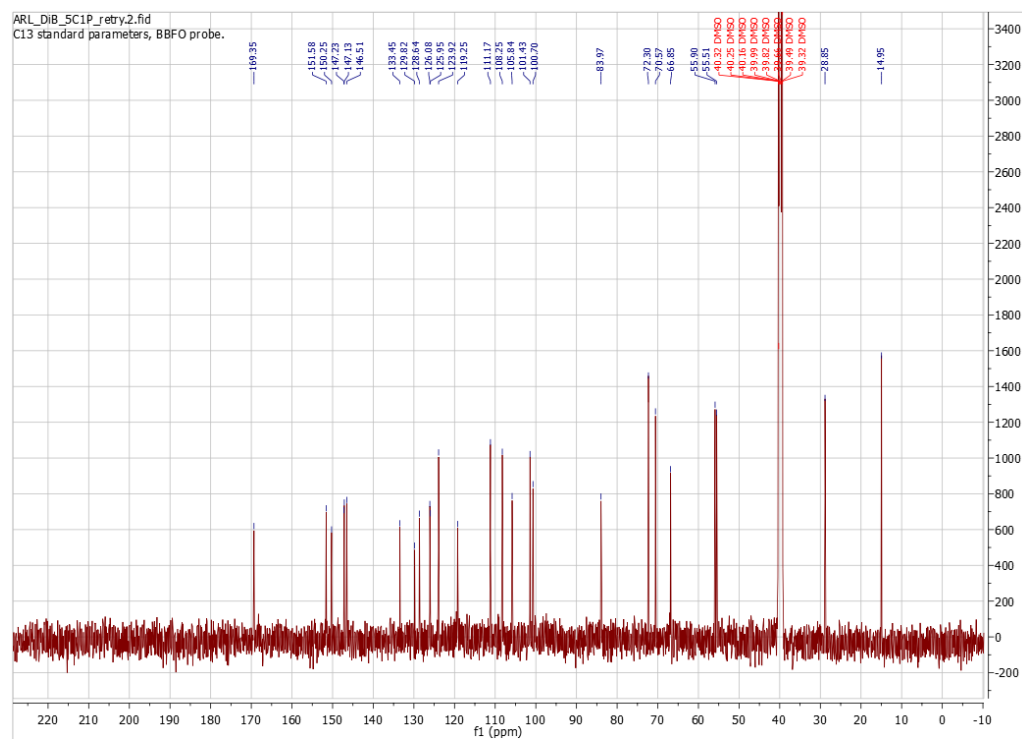
D i p h y l l i n P u r i t y (9 9 . 2 %)



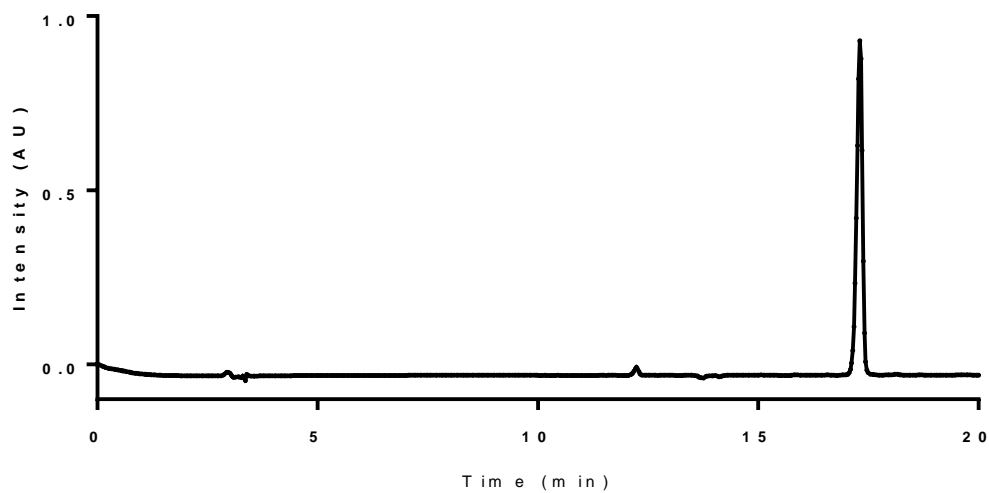


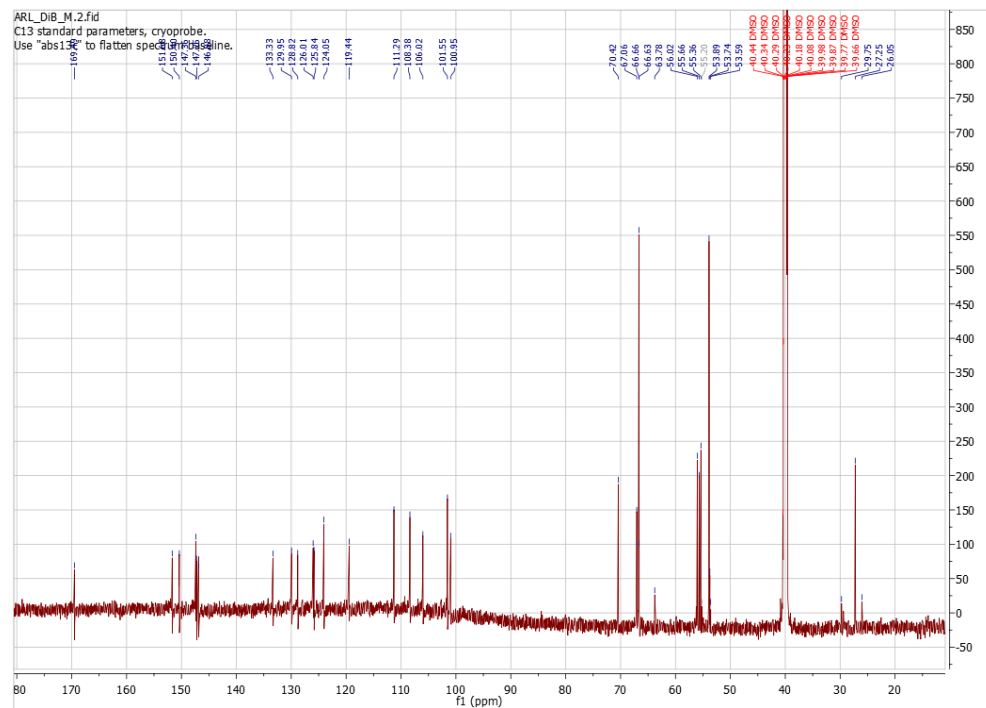
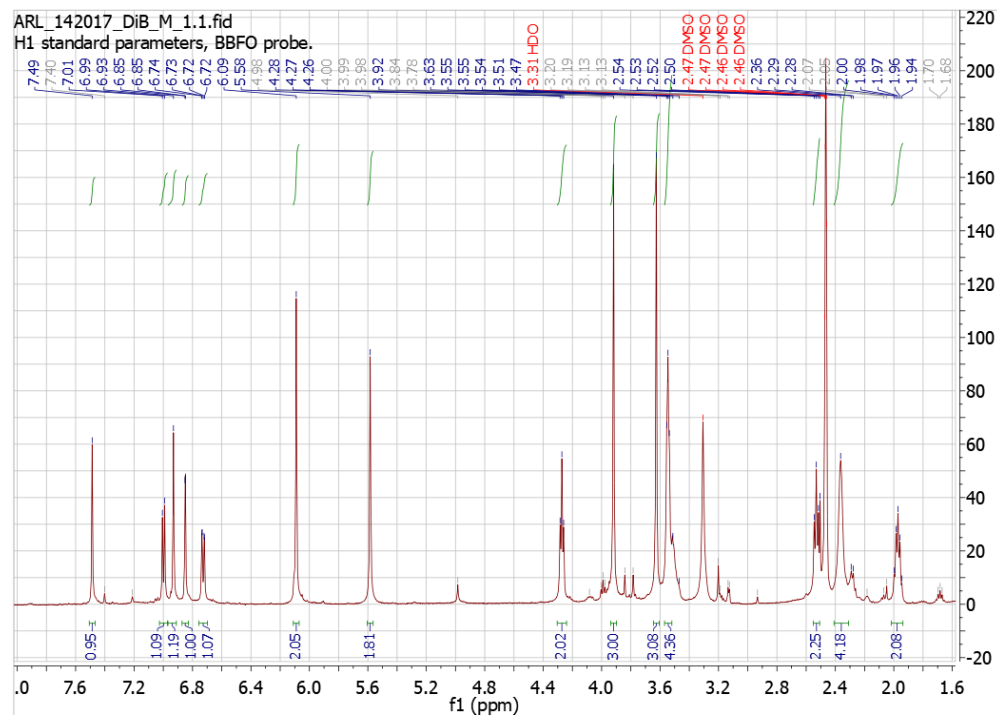
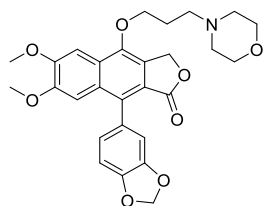
ARL_DiB_5C1P_retry.1.fid
H1 standard parameters, BBFO probe.



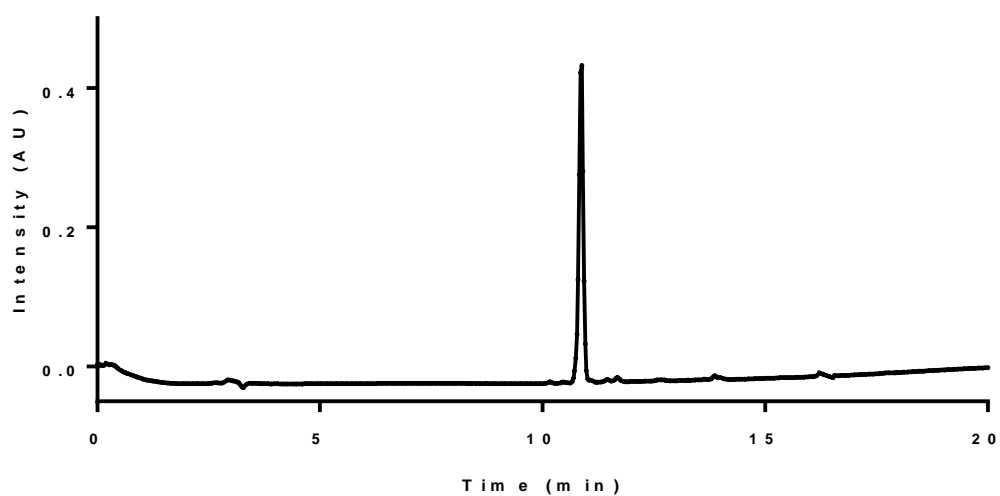


2 e P u r i t y (9 8 %)

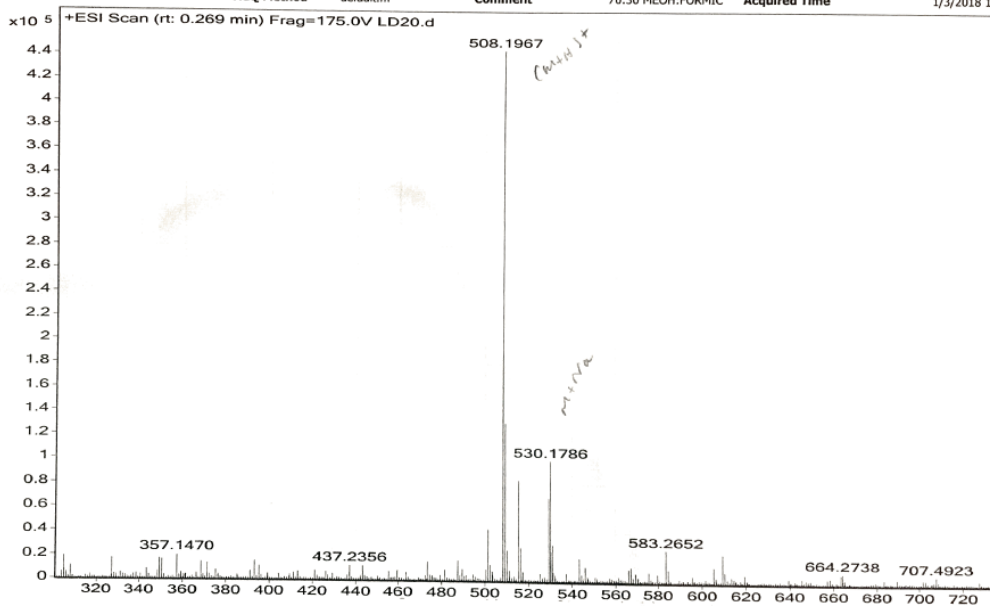


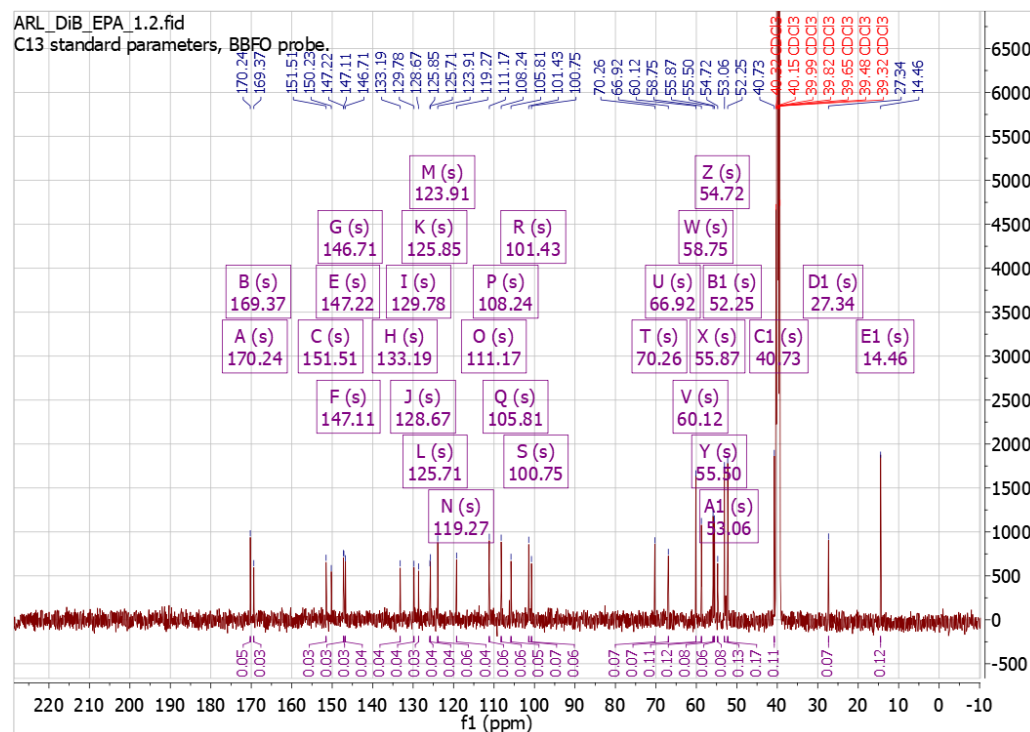
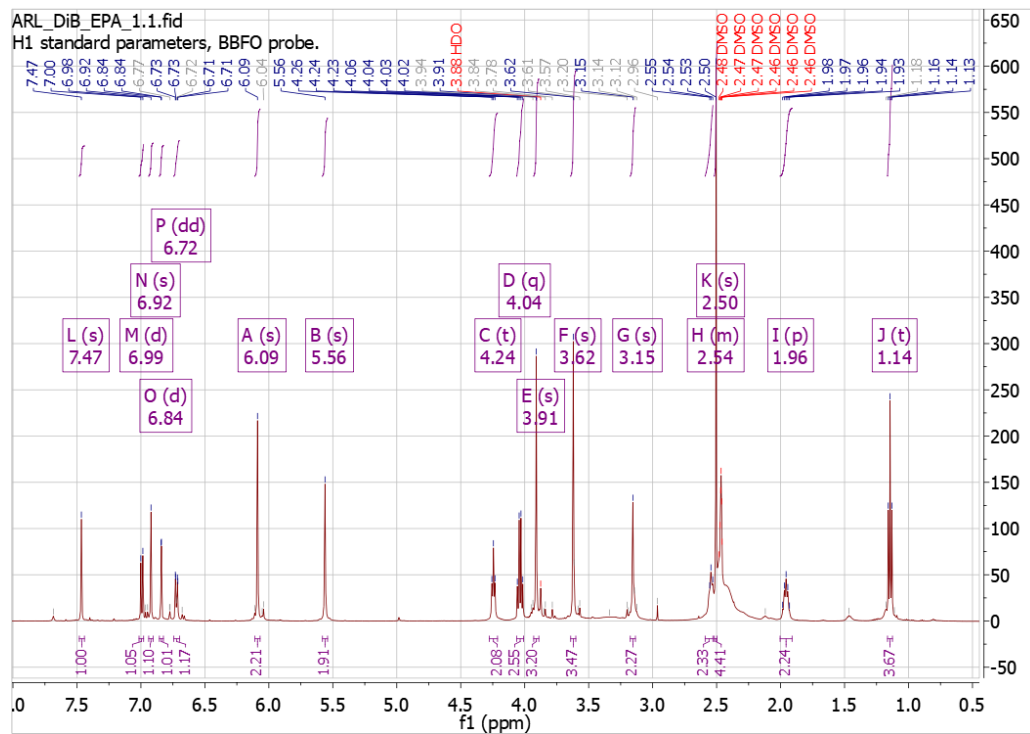
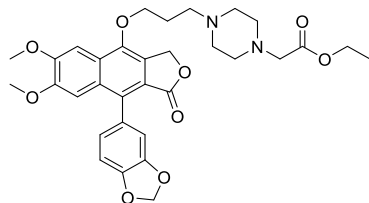


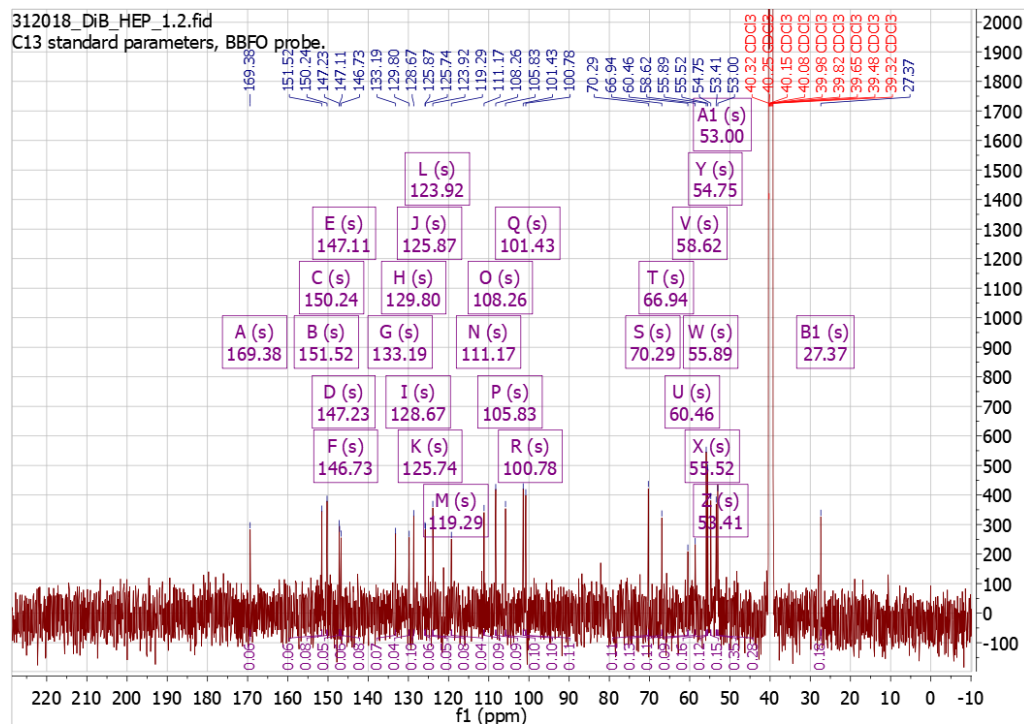
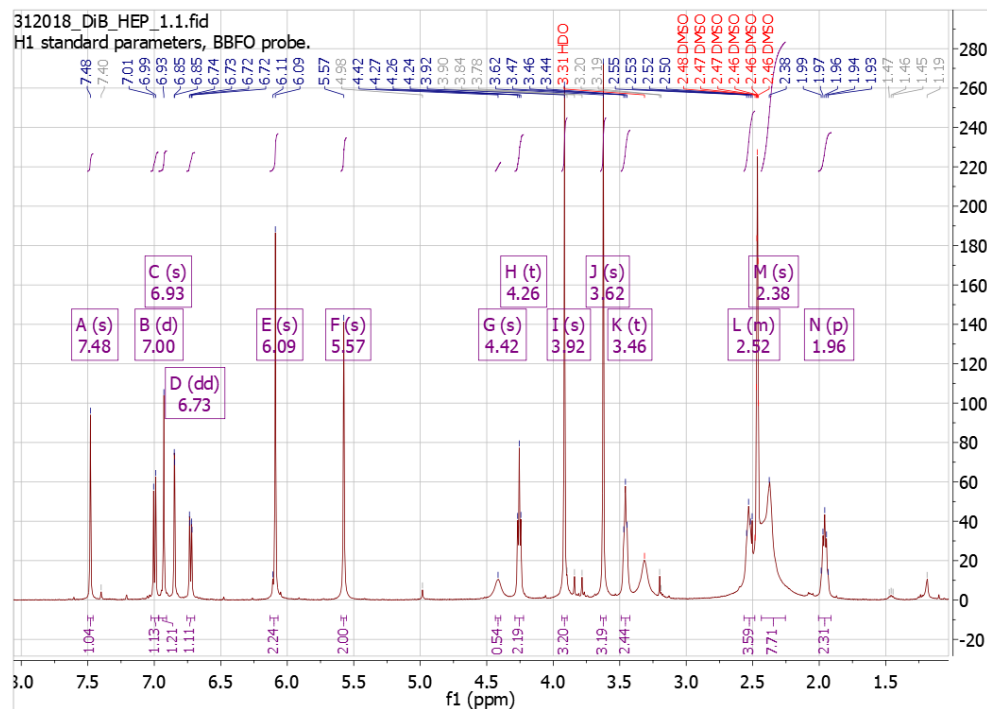
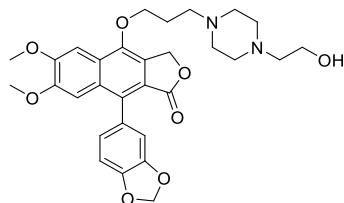
2 g Purity (99.3 %)

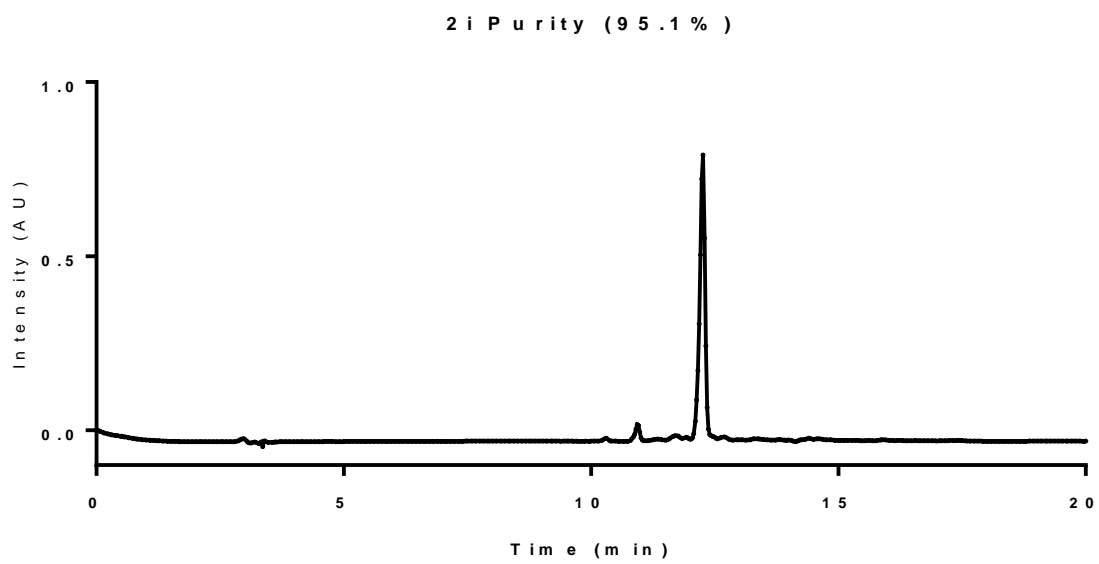


Sample Name	525507-1	Position	VIAL2	Instrument Name	6550 Drug Discovery	User Name	6550-QTOF-HP\6550-QT
Inj Vol	2	InjPosition		SampleType	Sample	IRM Calibration Status	Success
Data Filename	LD20.d	ACQ Method	default.m	Comment	70:30 MEOH:FORMIC	Acquired Time	1/3/2018 1:20:37 PM

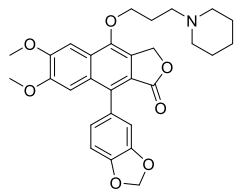






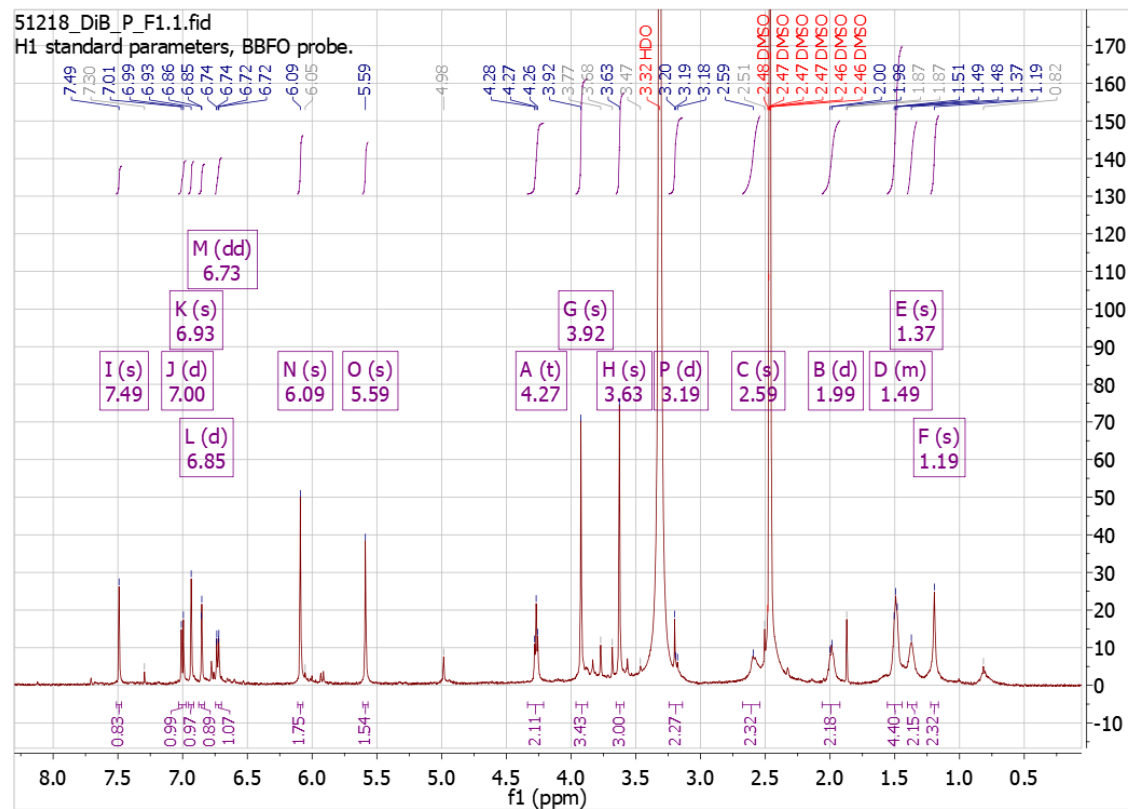
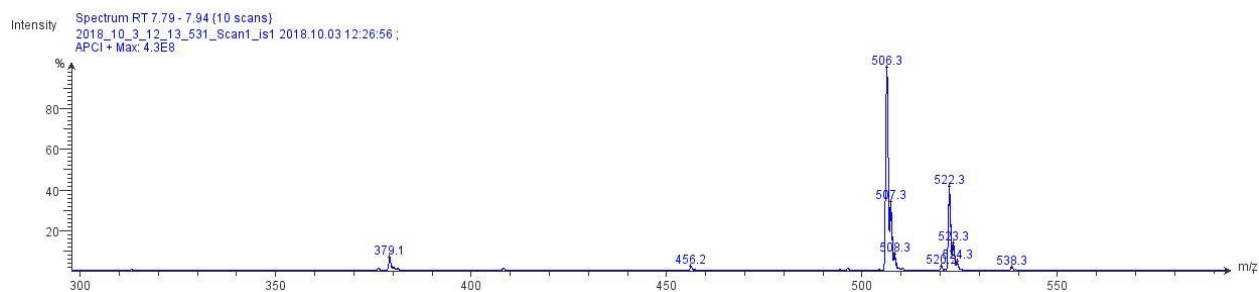


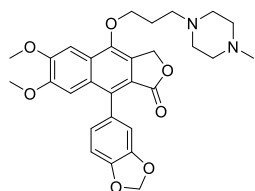
APPENDIX C- SPECTRAL CHARACTERIZATION OF SELECT CHAPTER 3 DERIVATIVES



1a=C₂₉H₃₁NO₇+H⁺, 506.2179 [M+H]⁺

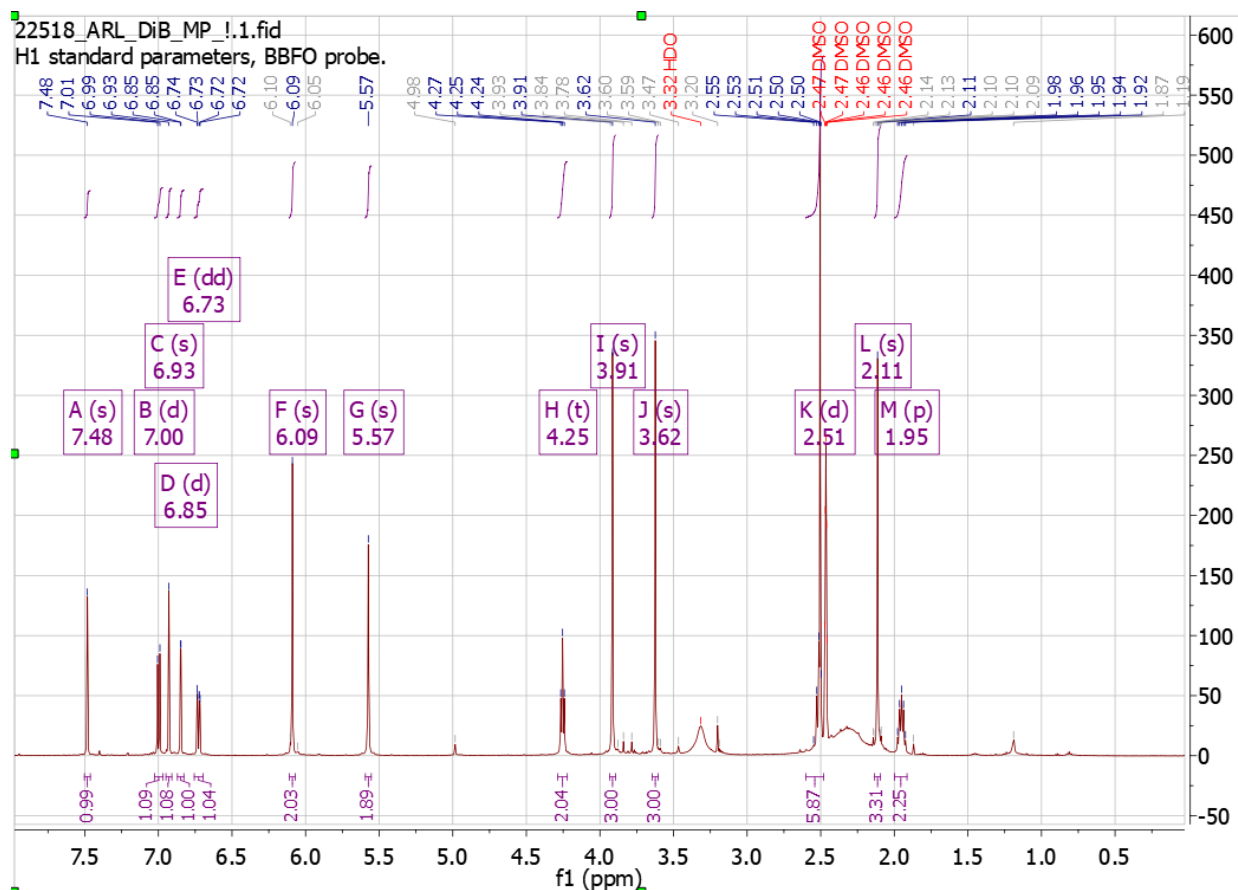
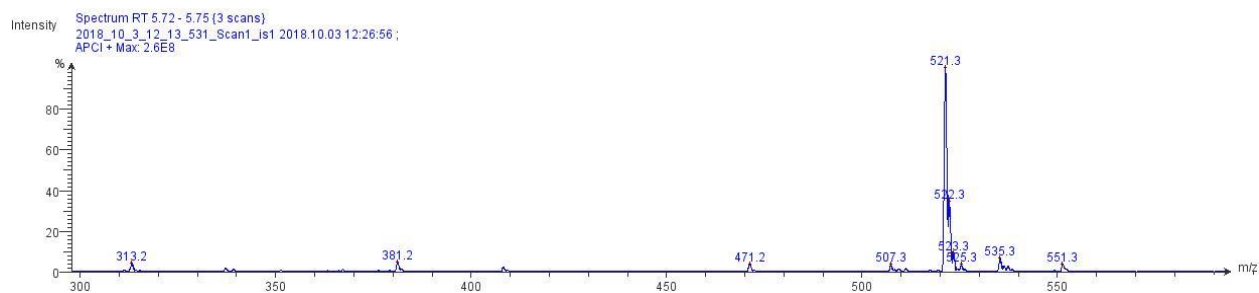
LRMS

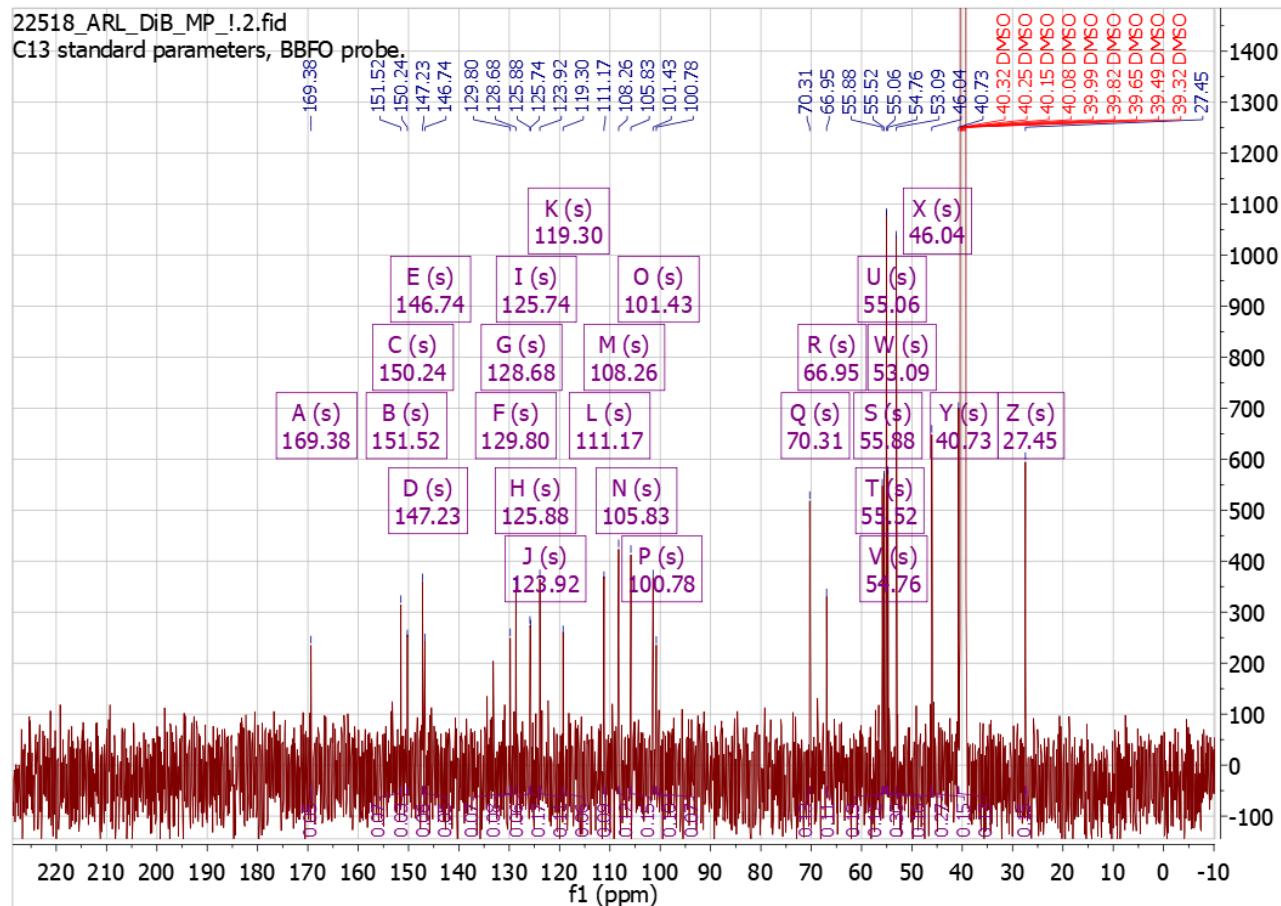




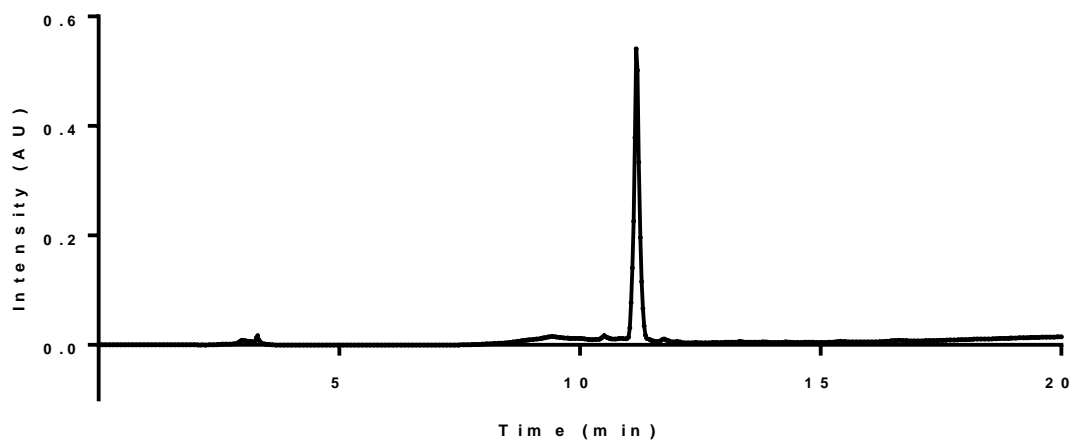
1c=C₂₉H₃₂N₂O₇+H⁺, 521.2288 [M+H]⁺

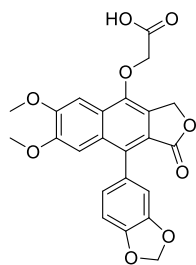
LRMS





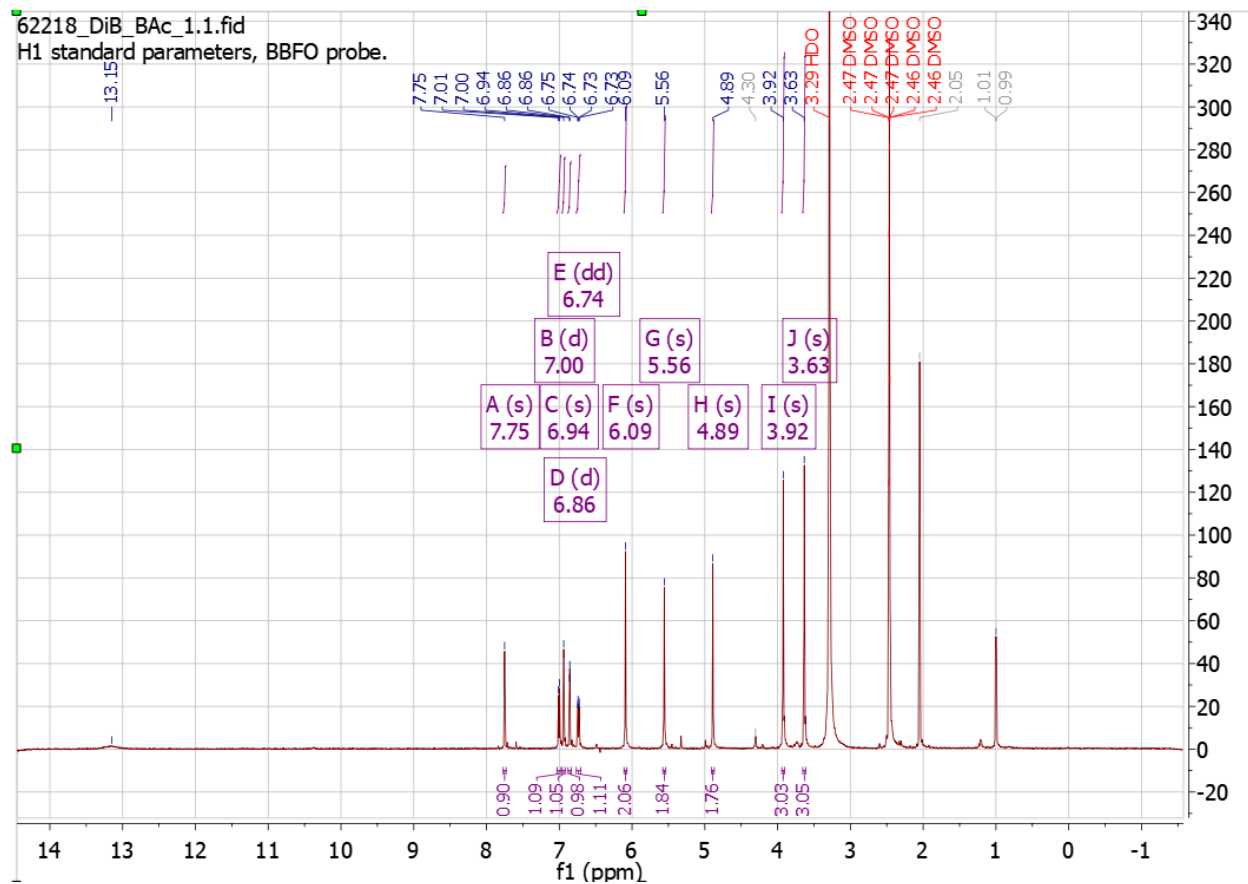
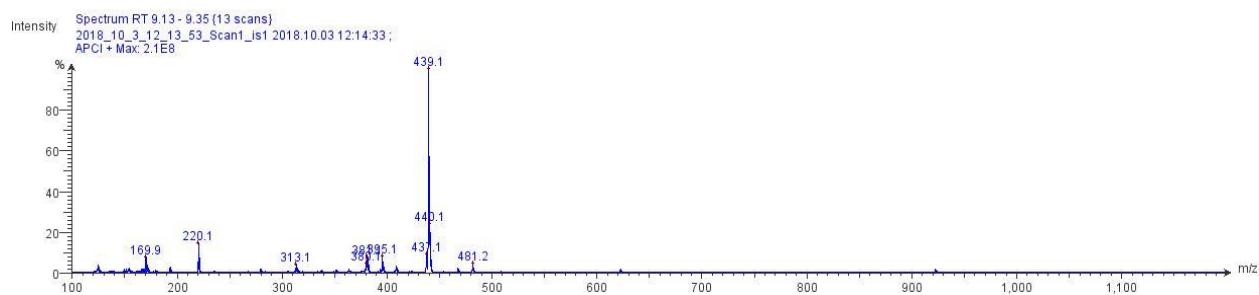
1 c Purity (97.2 %)

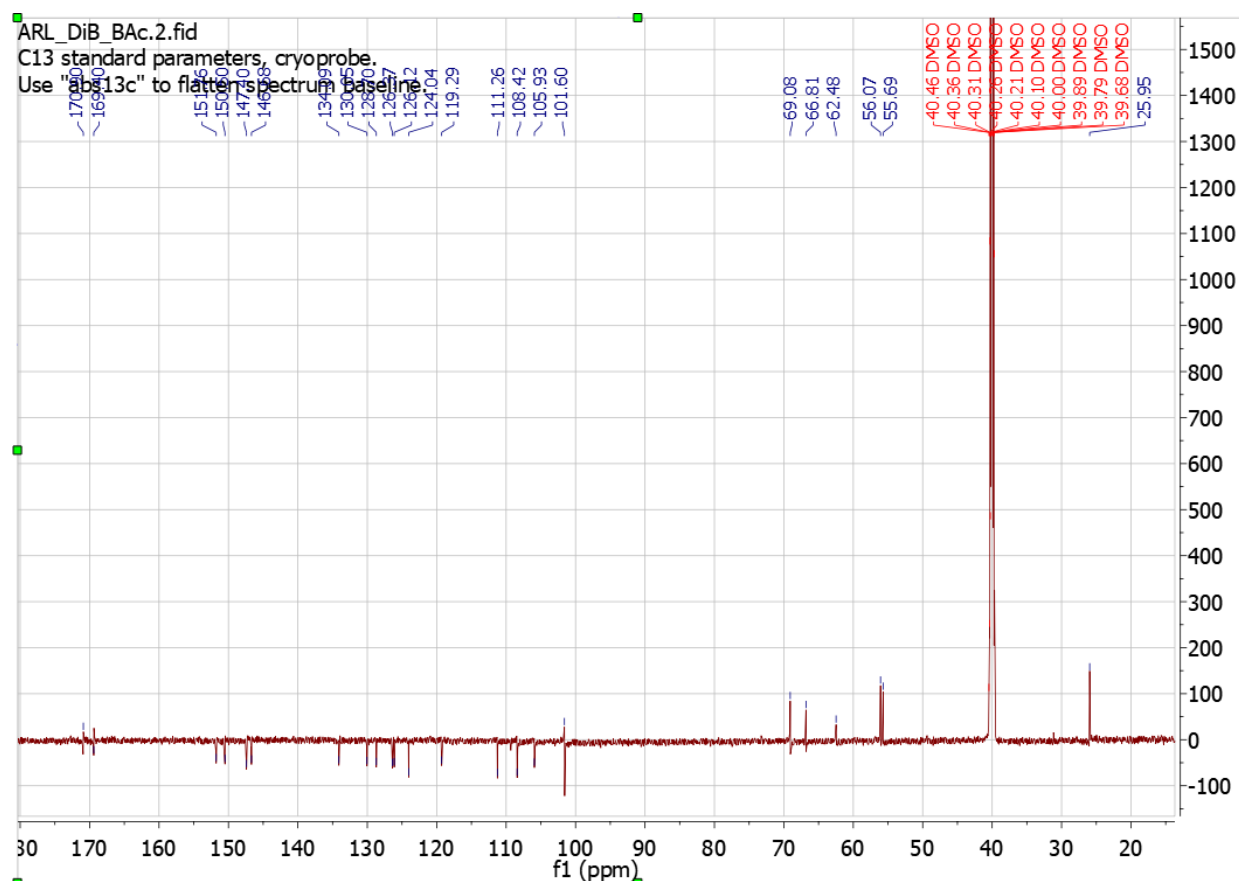




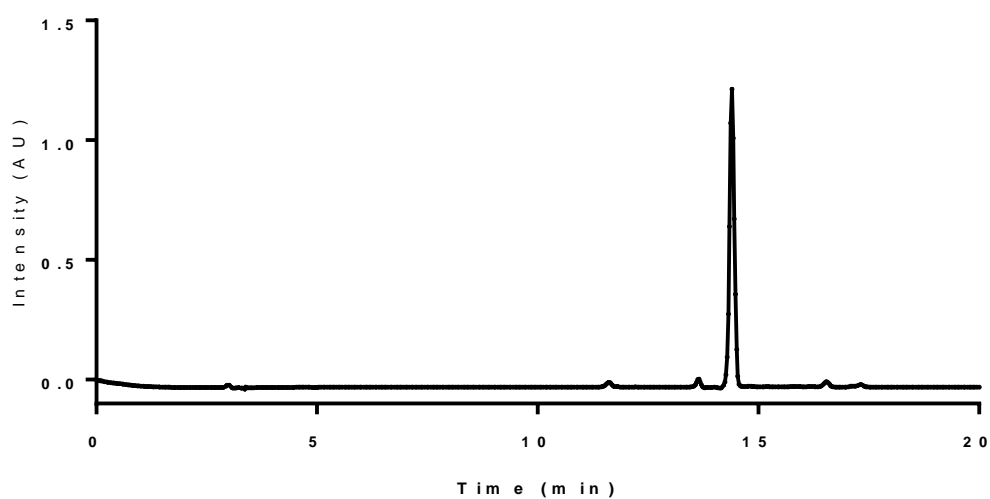
1f=C₂₃H₁₈O₉+H⁺, 439.1029 [M+H]⁺

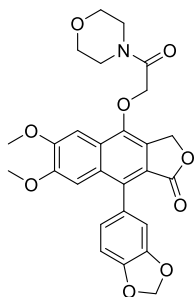
LRMS





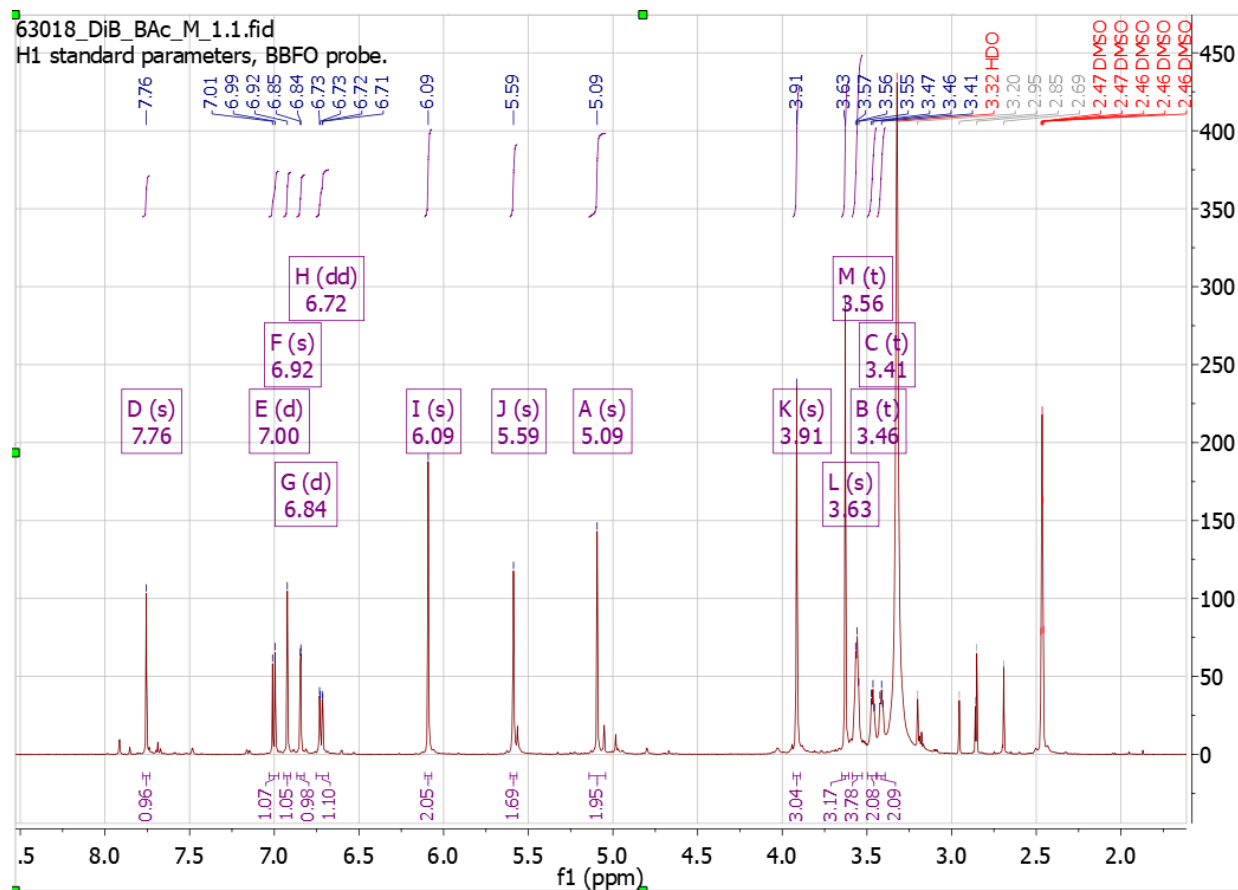
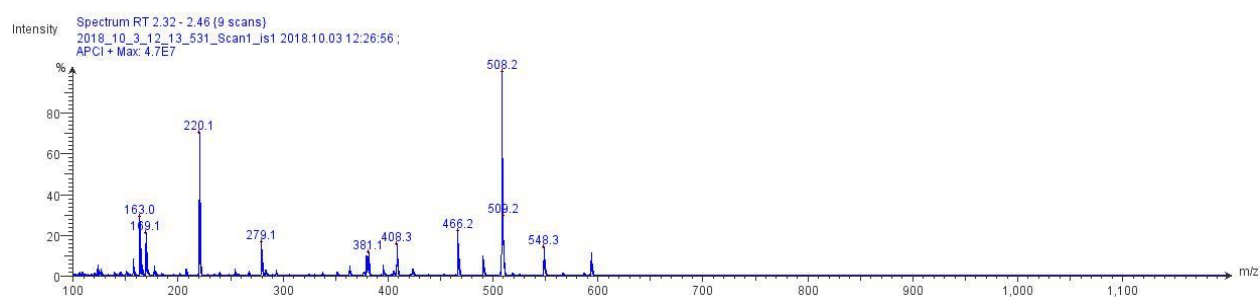
1 f P u r i t y (9 7 . 4 %)

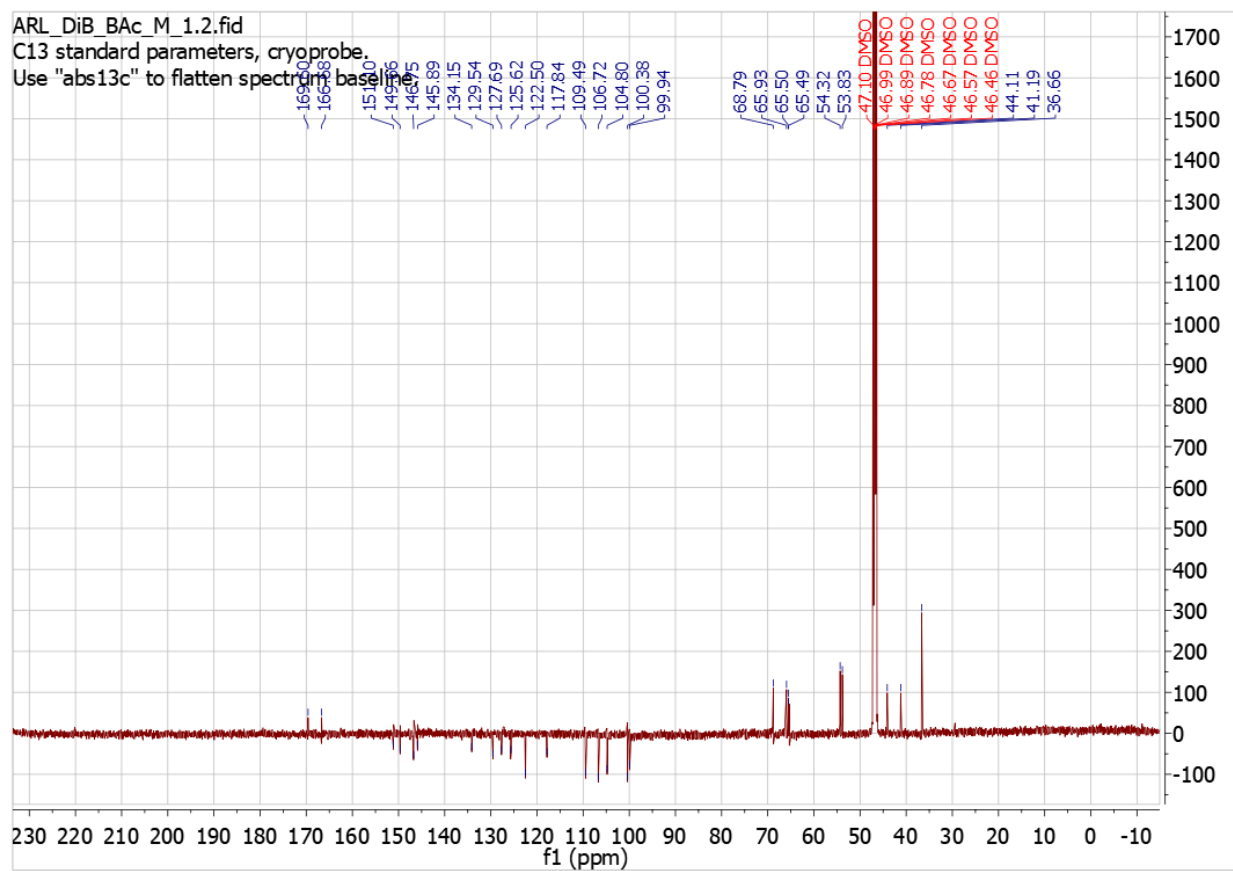




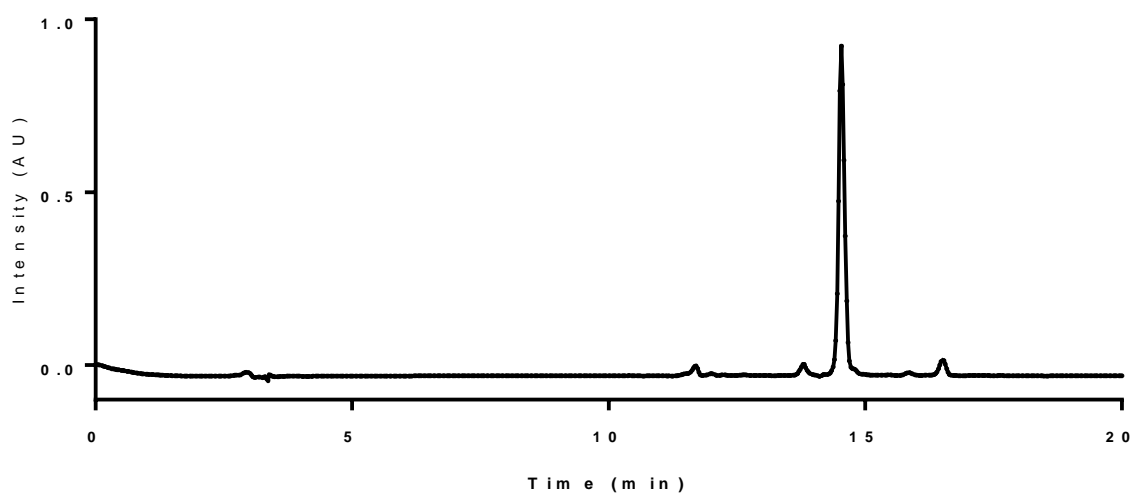
2a=C₂₇H₂₅NO₉+H⁺, 508.1608 [M+H]⁺

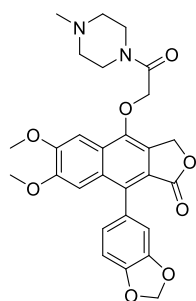
LRMS





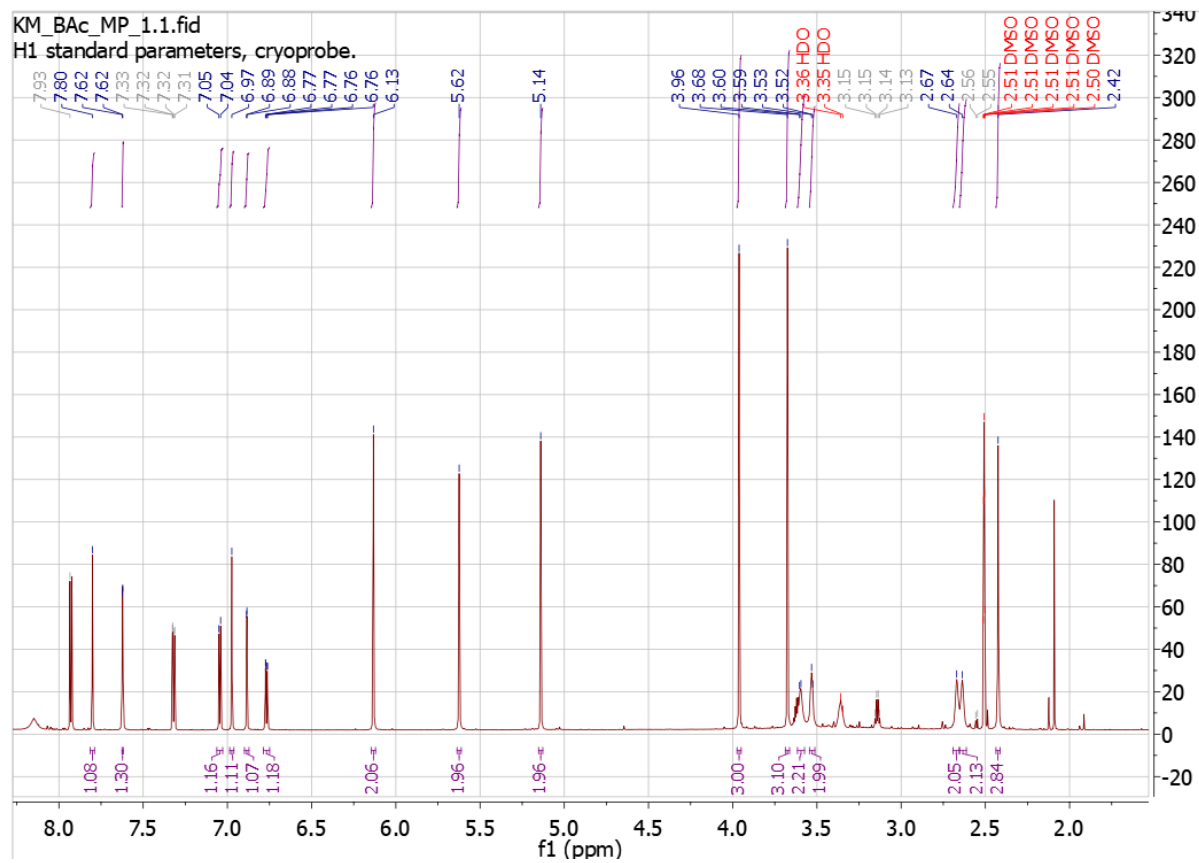
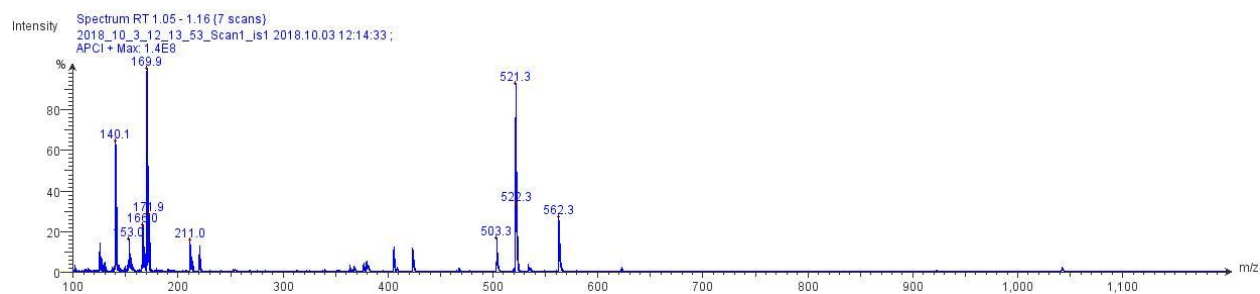
2 a P u r i t y (9 7 . 5 %)

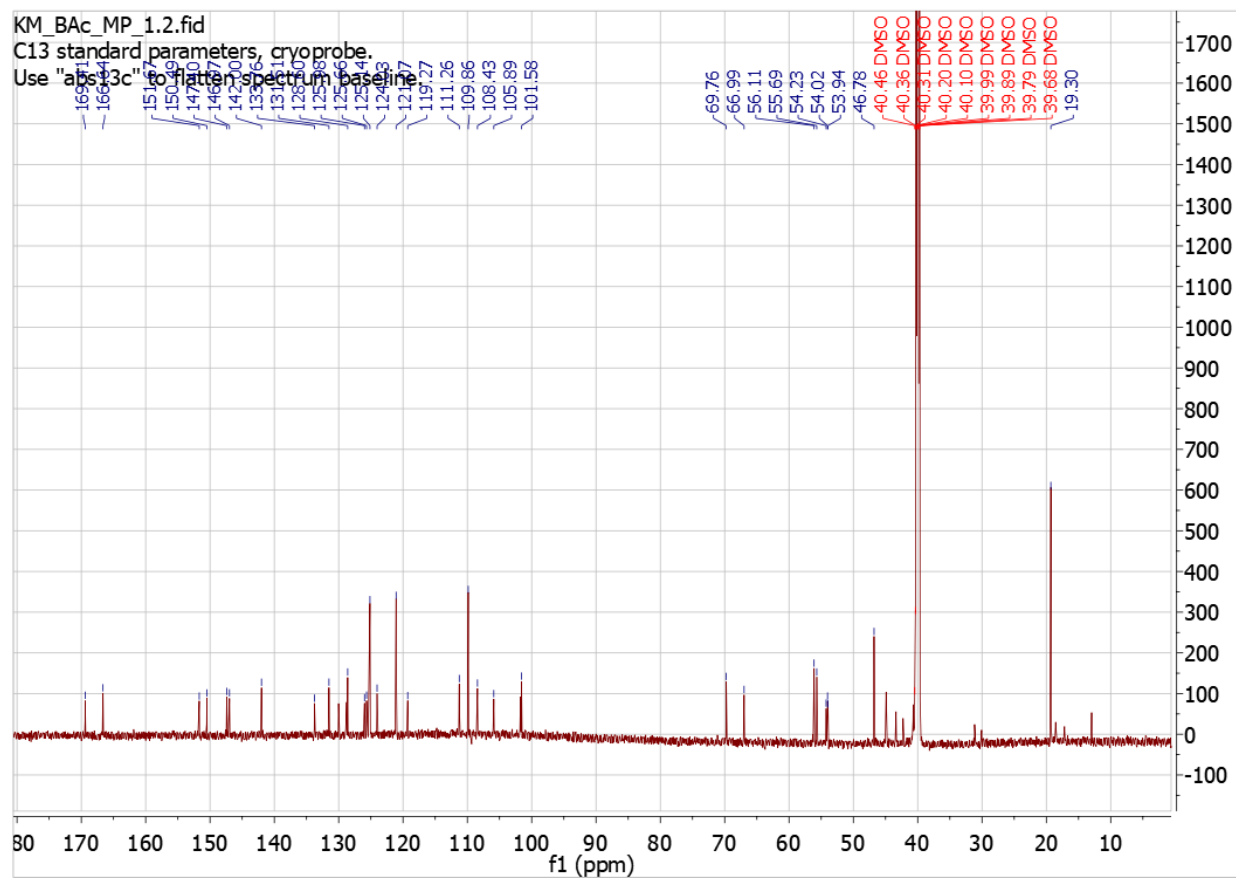




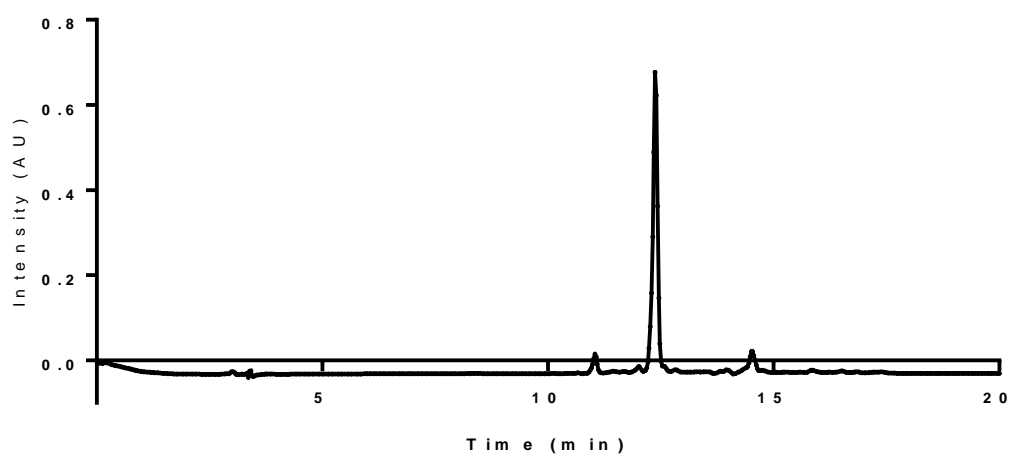
2b=C₂₈H₂₈N₂O₈+H⁺, 521.1924 [M+H]⁺

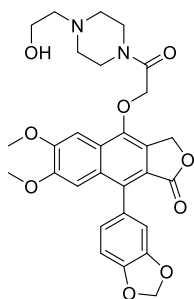
LRMS





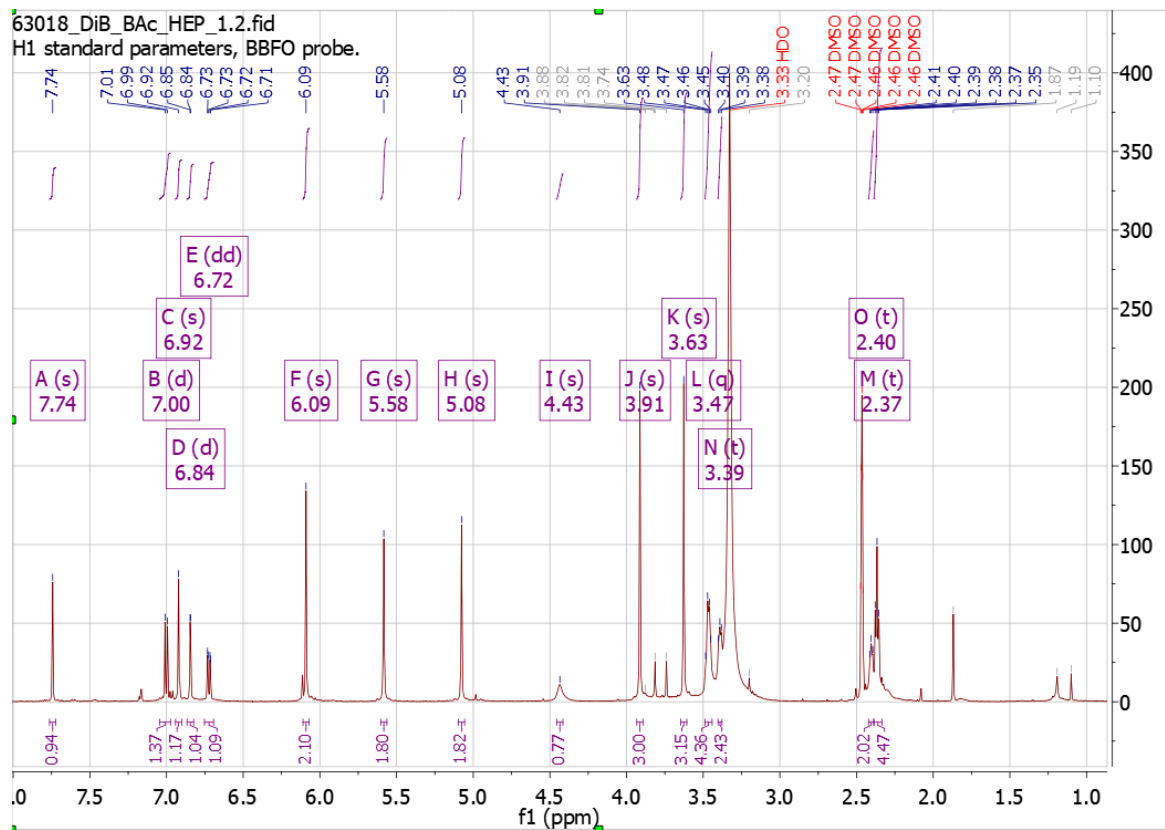
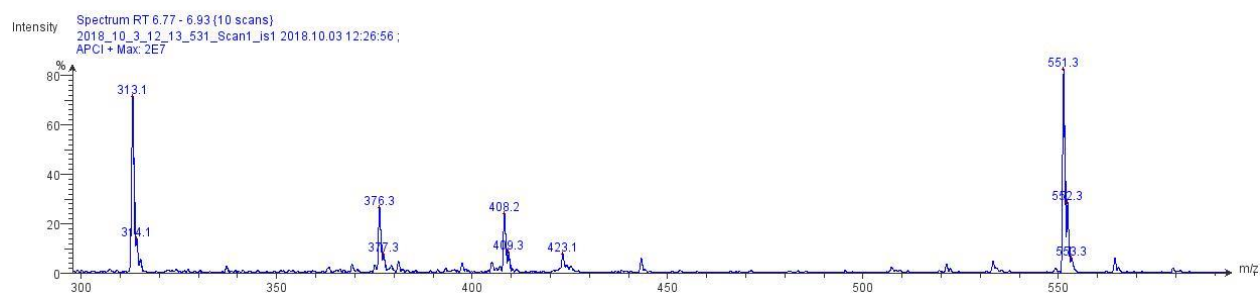
2 b Purity (9 6 . 6 %)

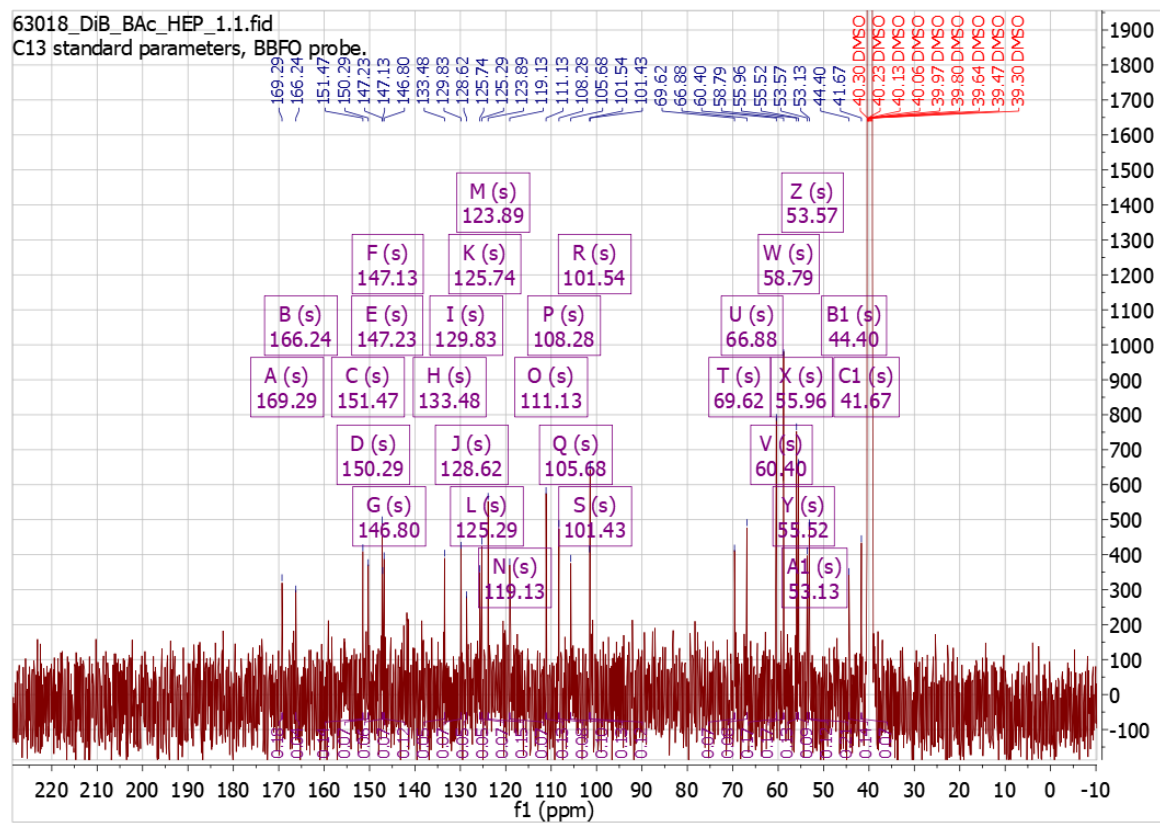


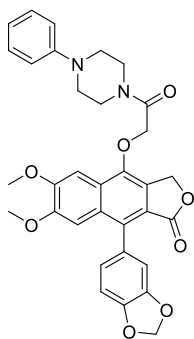


2c=C₂₉H₃₀N₂O₉+H⁺, 551.2030 [M+H]⁺

LRMS

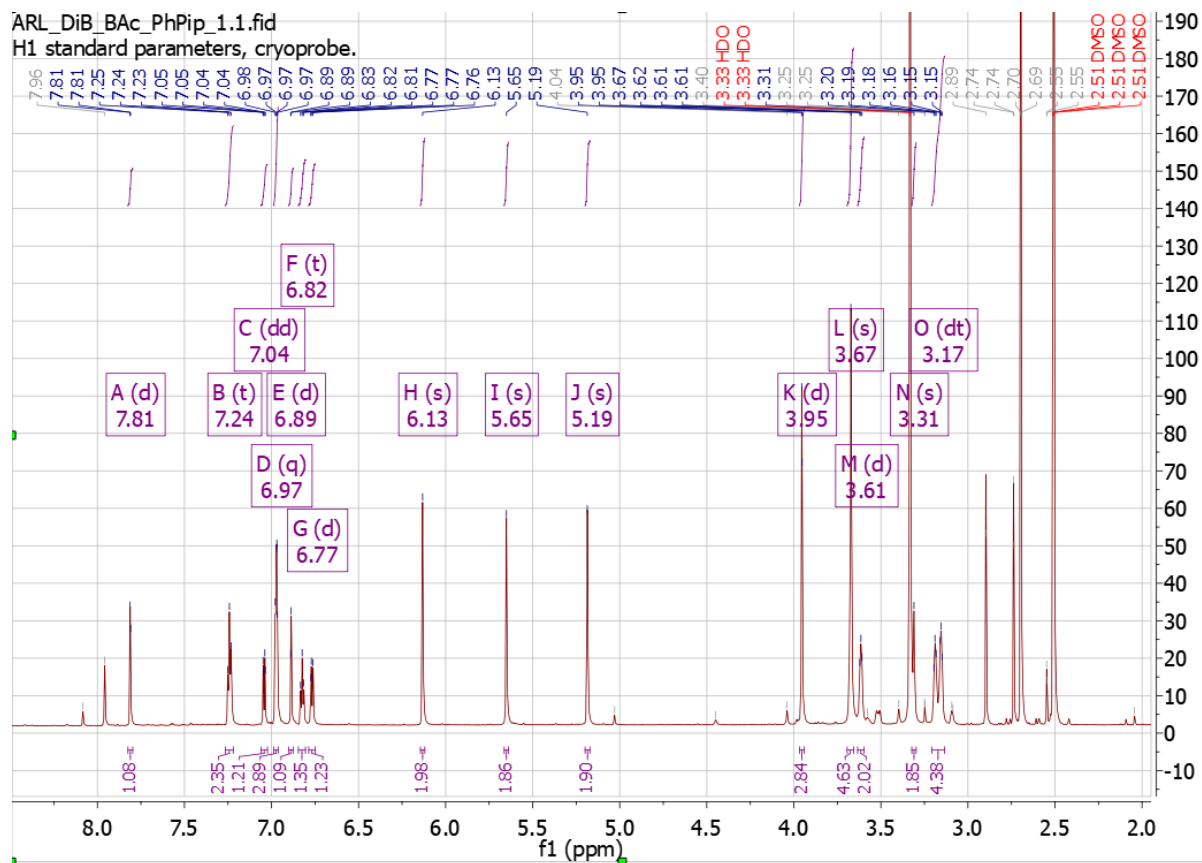
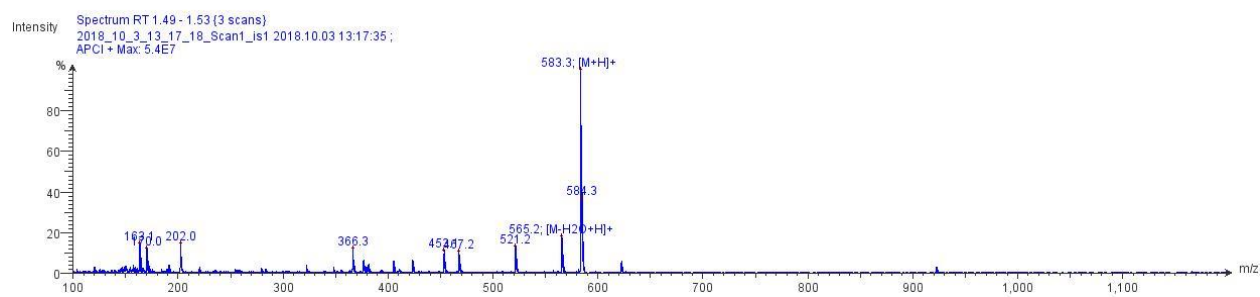


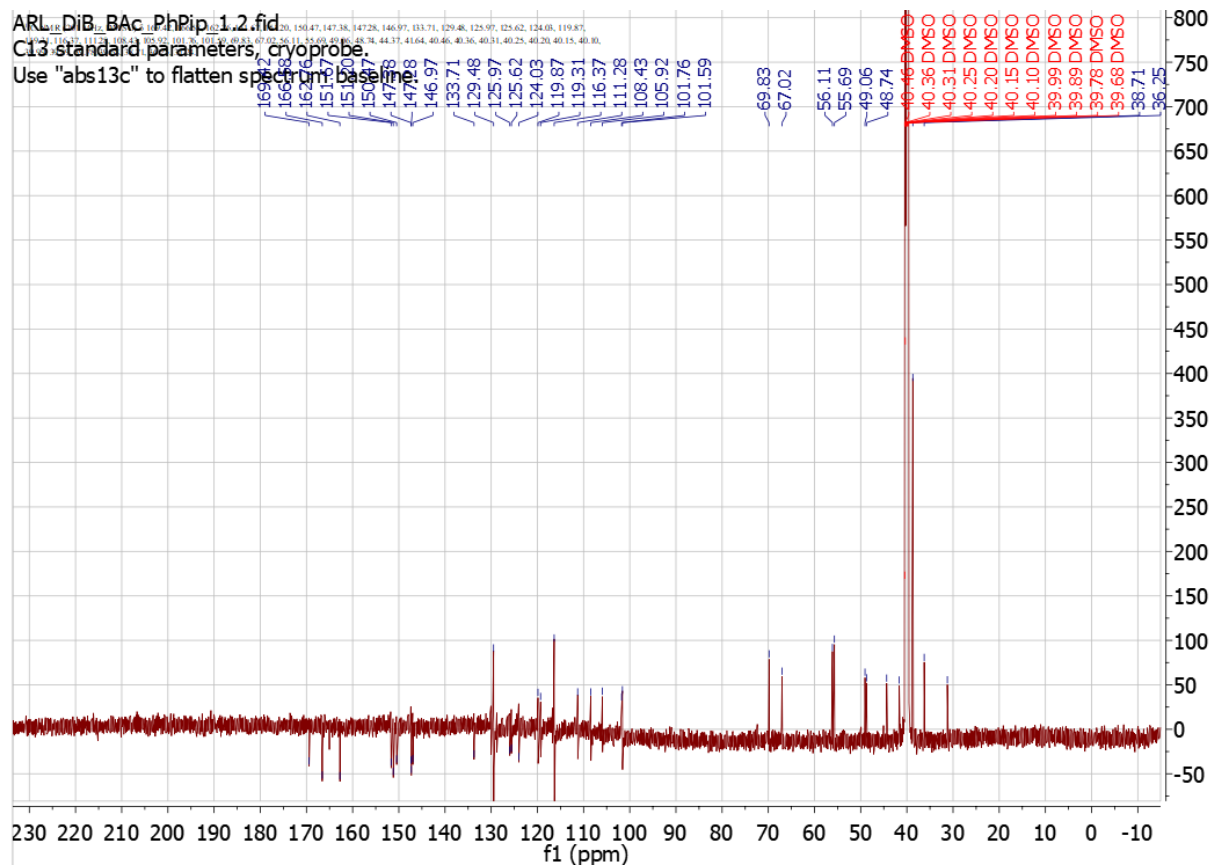




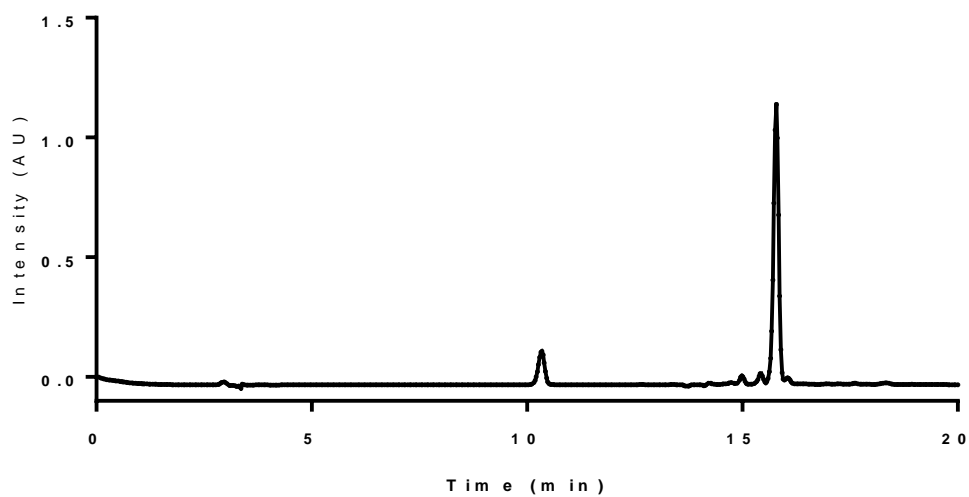
2d=C₃₃H₃₀N₂O₈+H⁺, 583.2080 [M+H]⁺

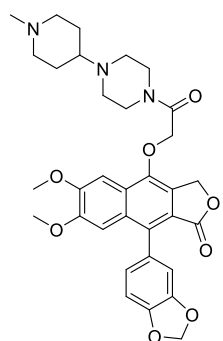
LRMS





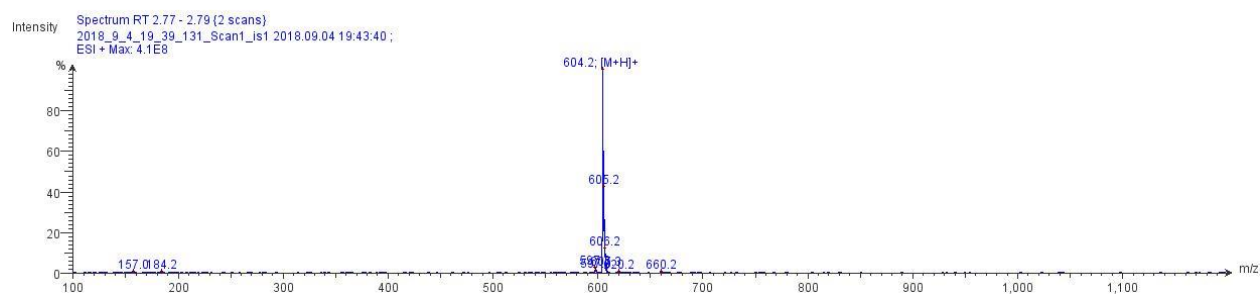
2 d Purity (95.1 %)

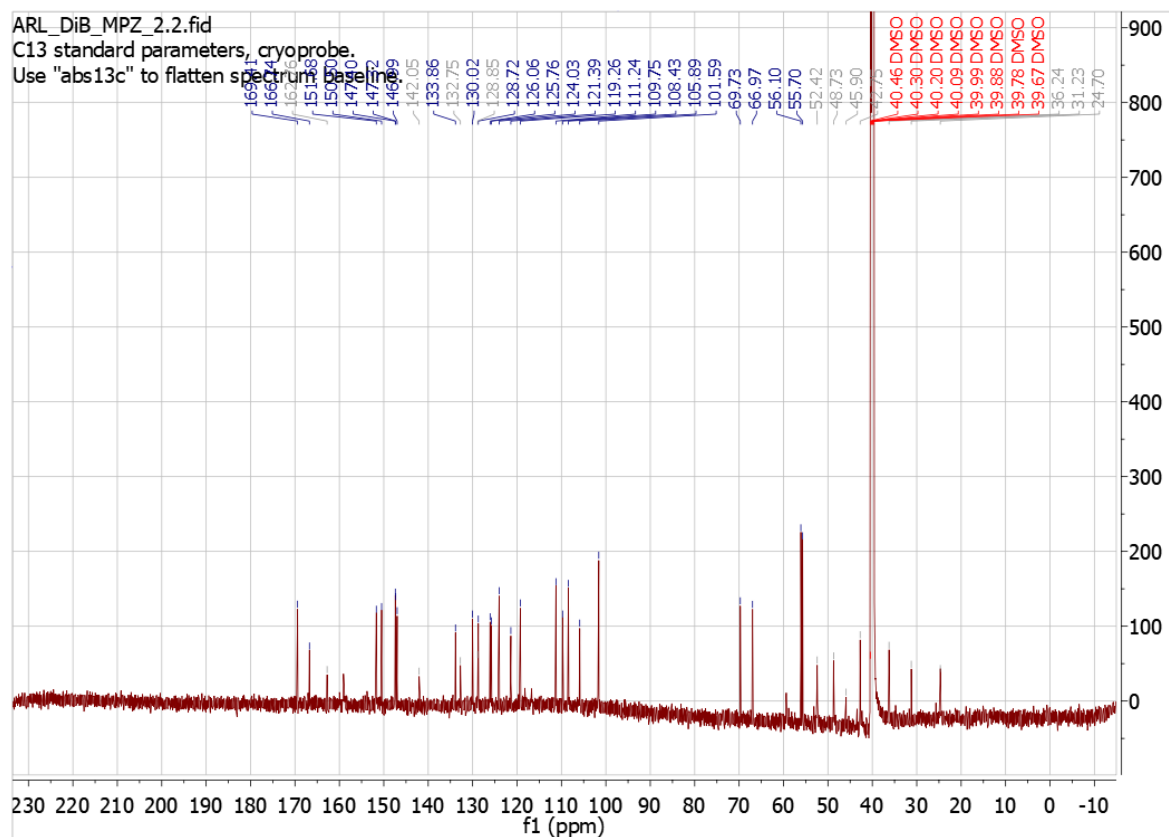




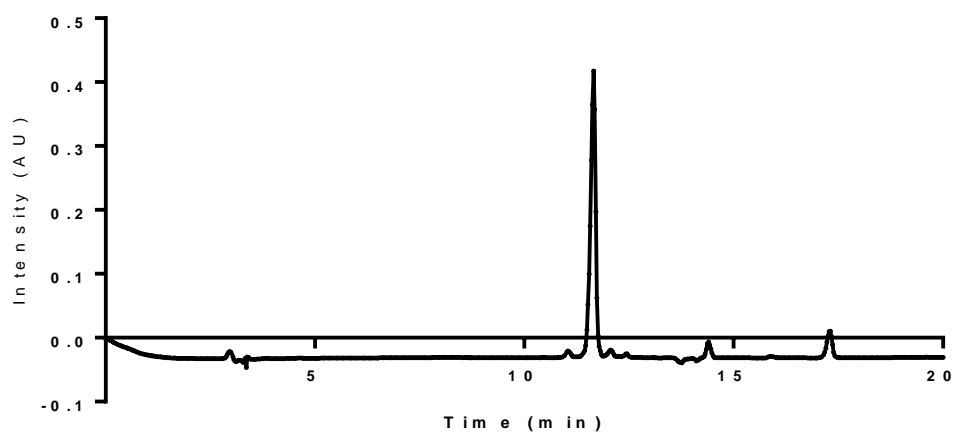
$2e=C_{33}H_{37}N_3O_8+H^+$, 604.2659 [M+H]⁺

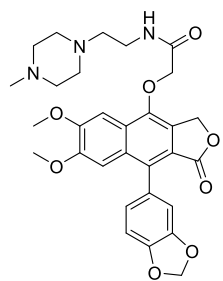
LRMS





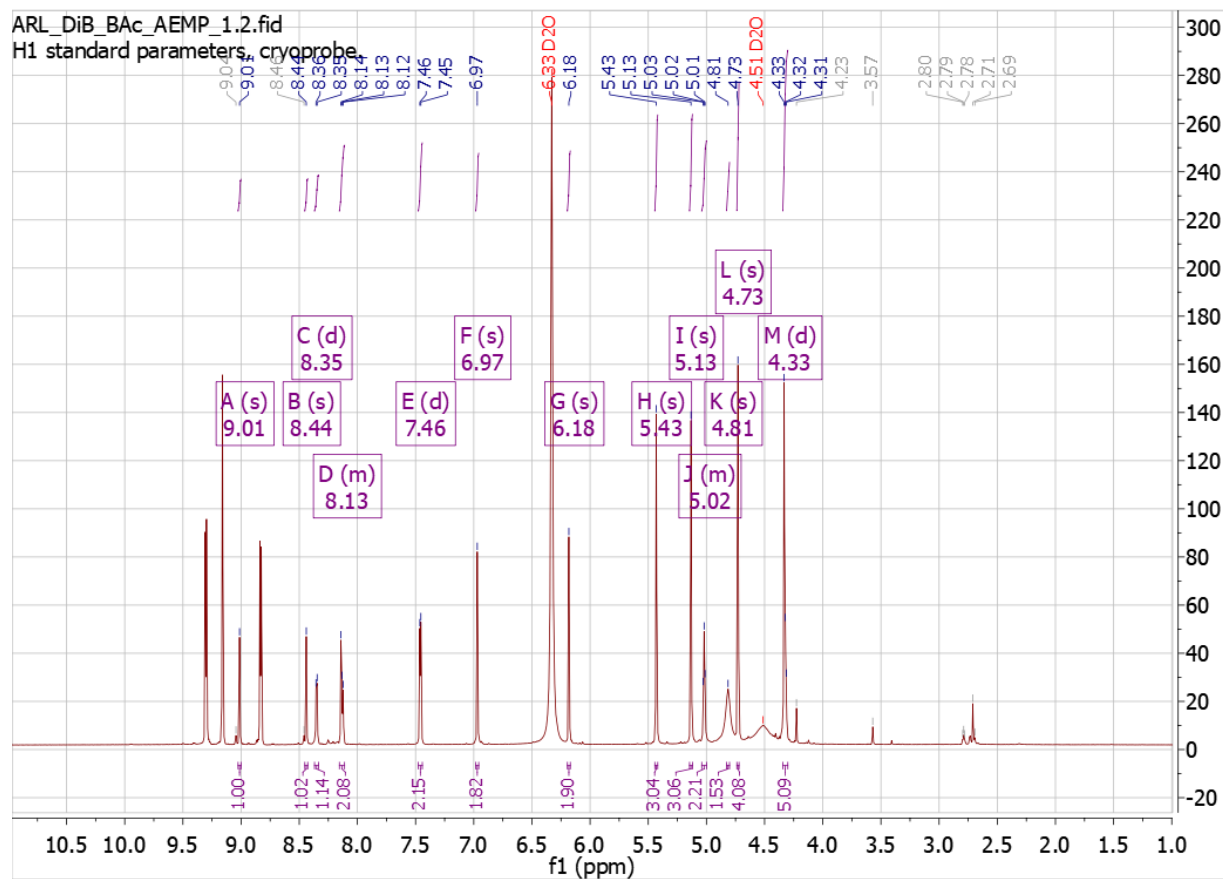
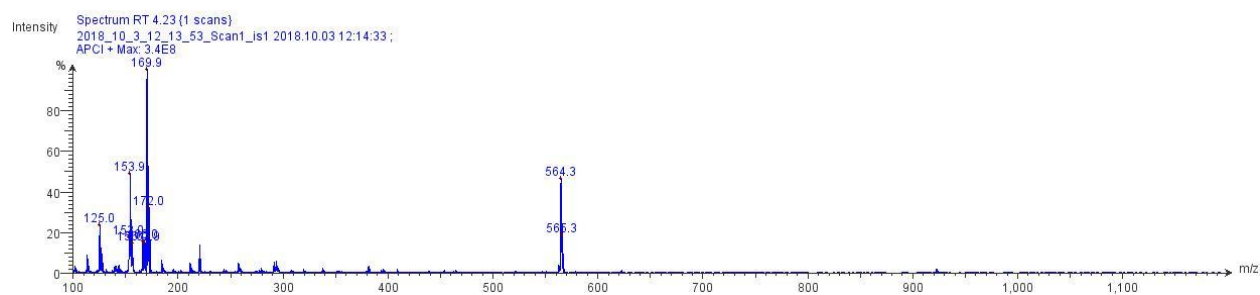
2 e Purity (96.9 %)

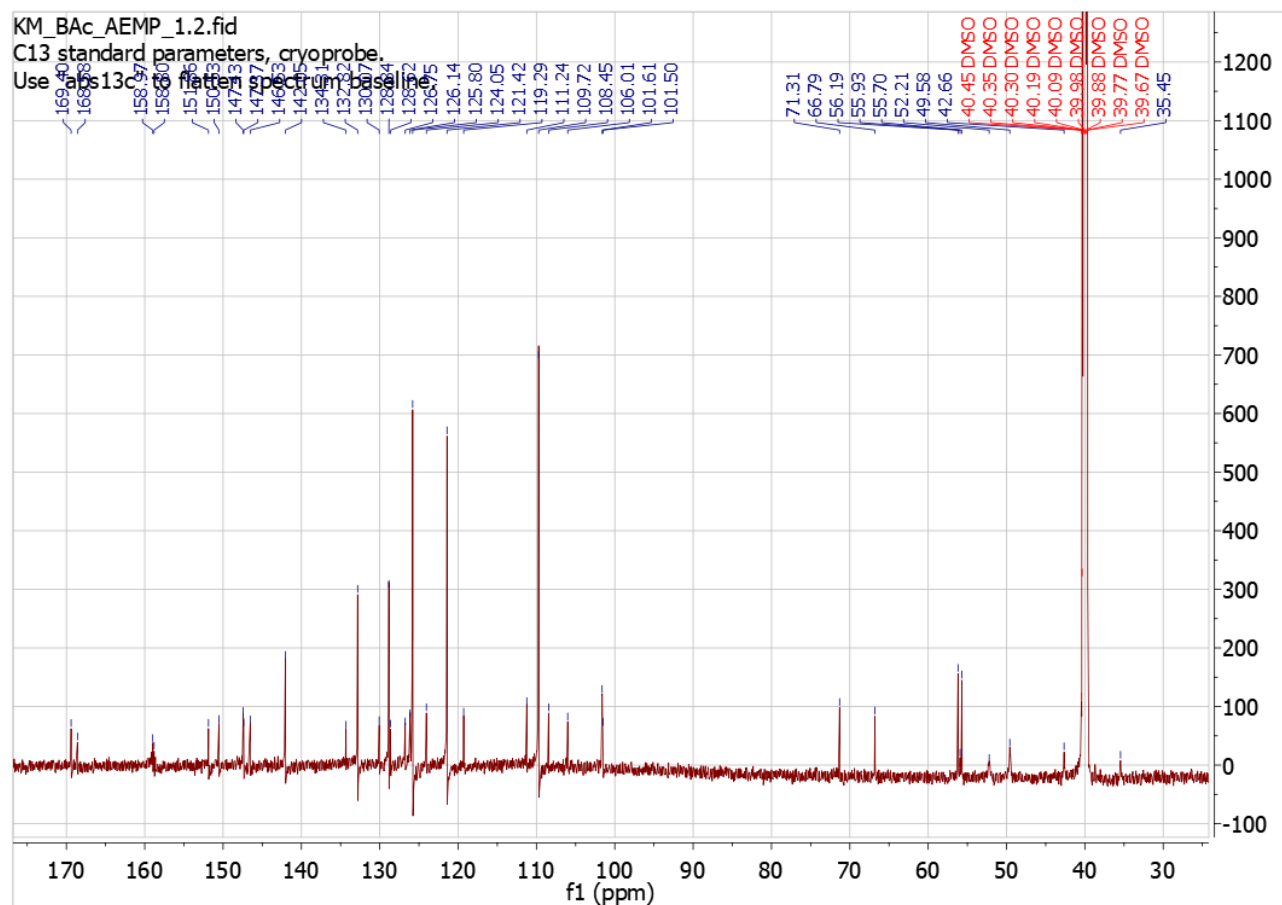




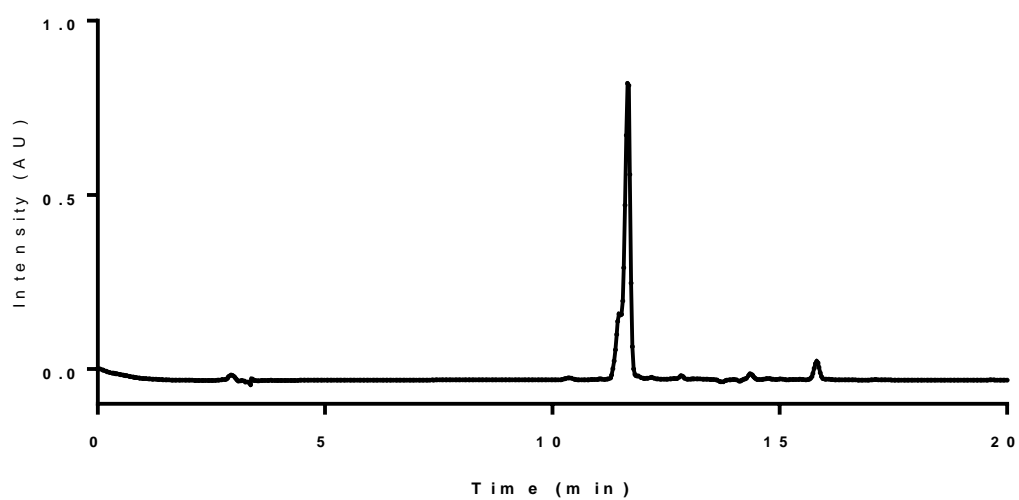
2g=C₃₀H₃₃N₃O₈+H⁺, 564.2346 [M+H]⁺

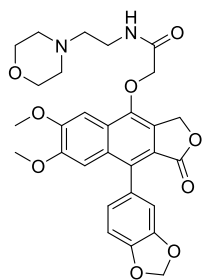
LRMS





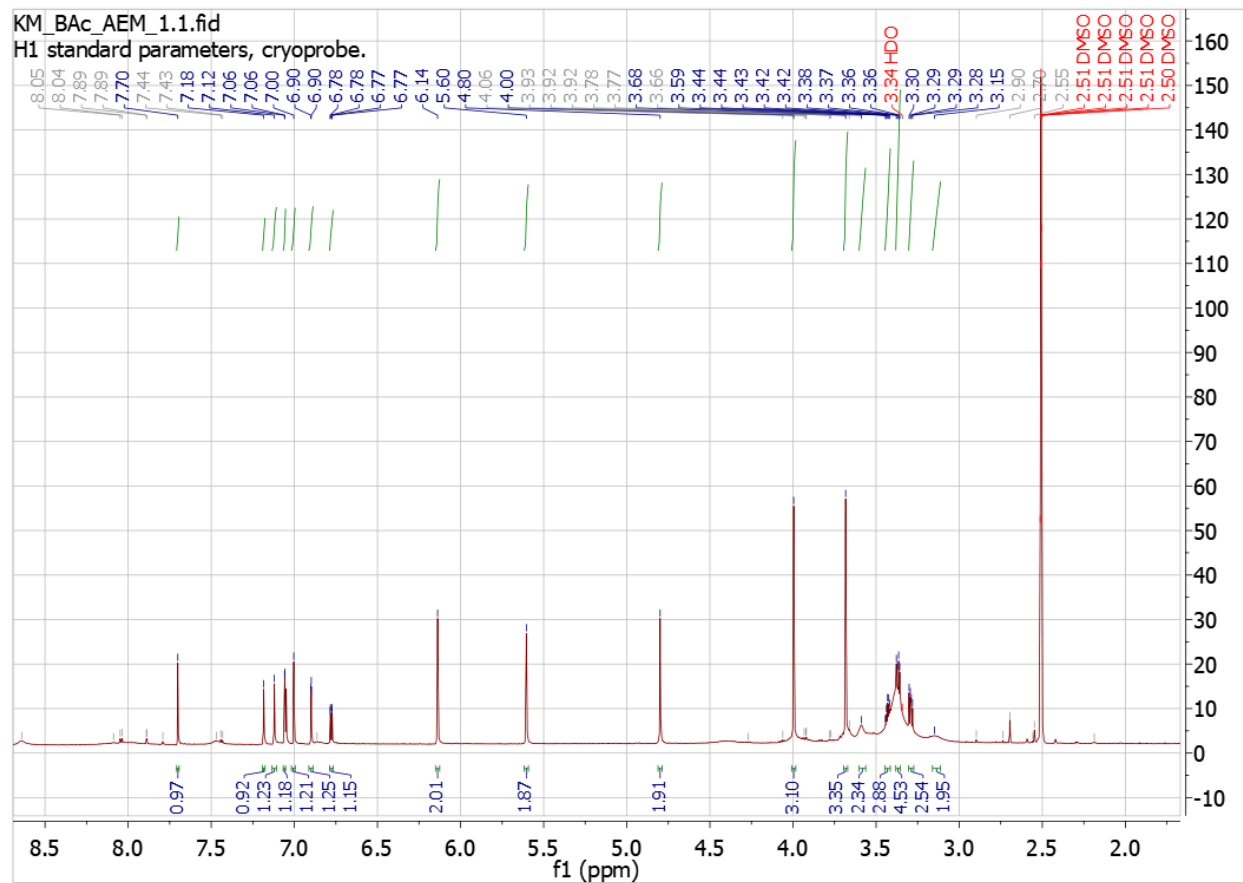
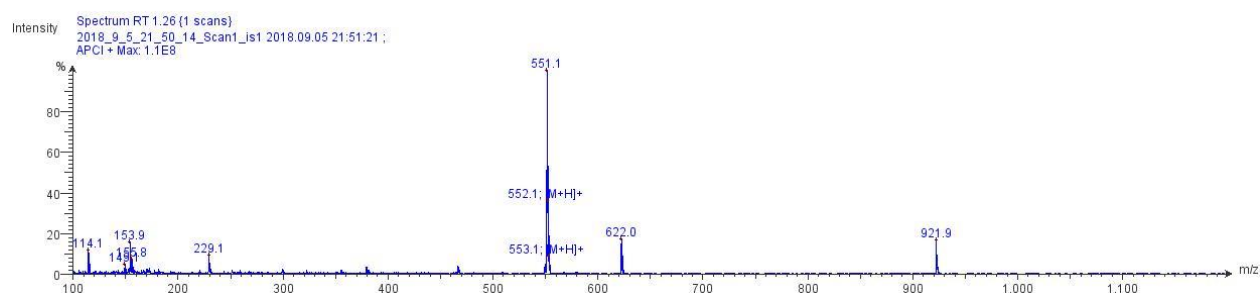
2 g Purity (98.7 %)

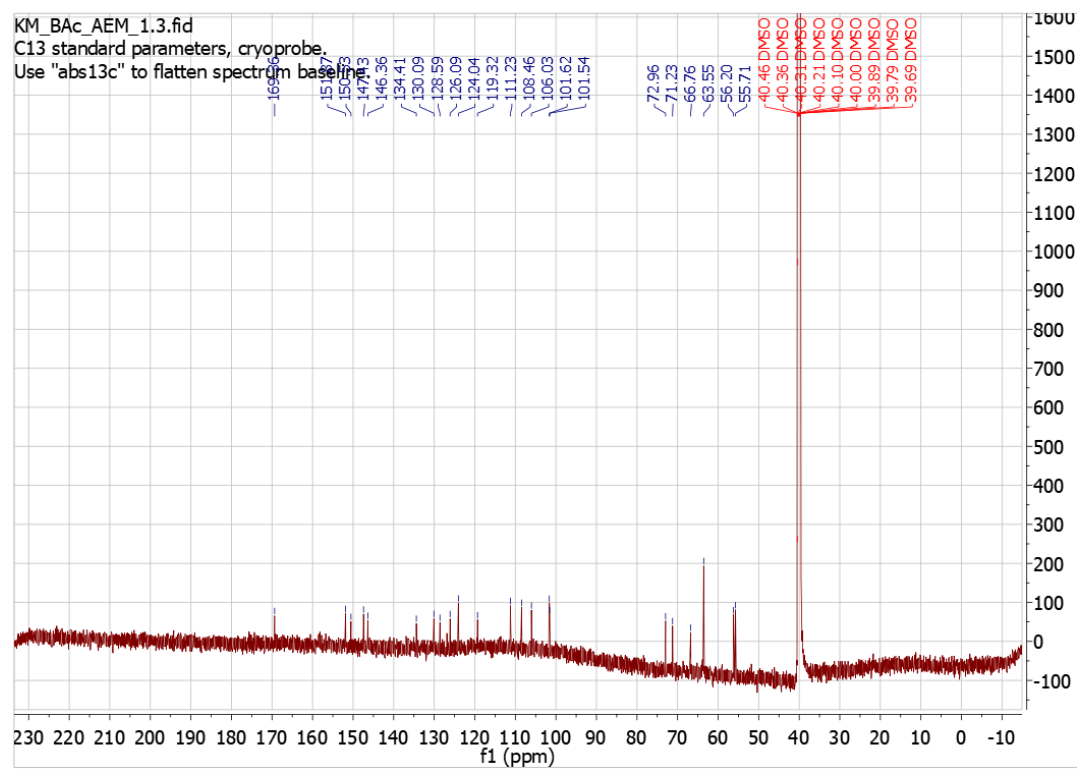


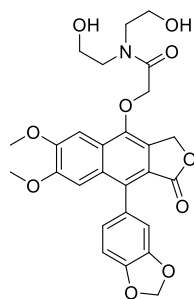


2h=C₂₉H₃₀N₂O₉+H⁺, 551.2030 [M+H]⁺

LRMS

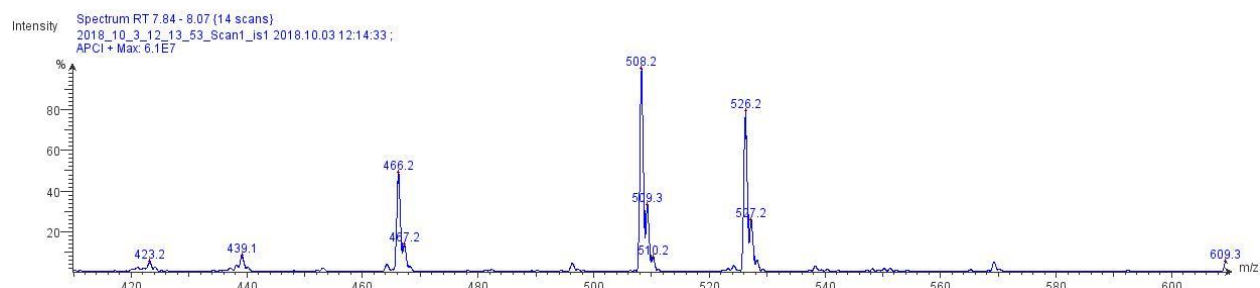


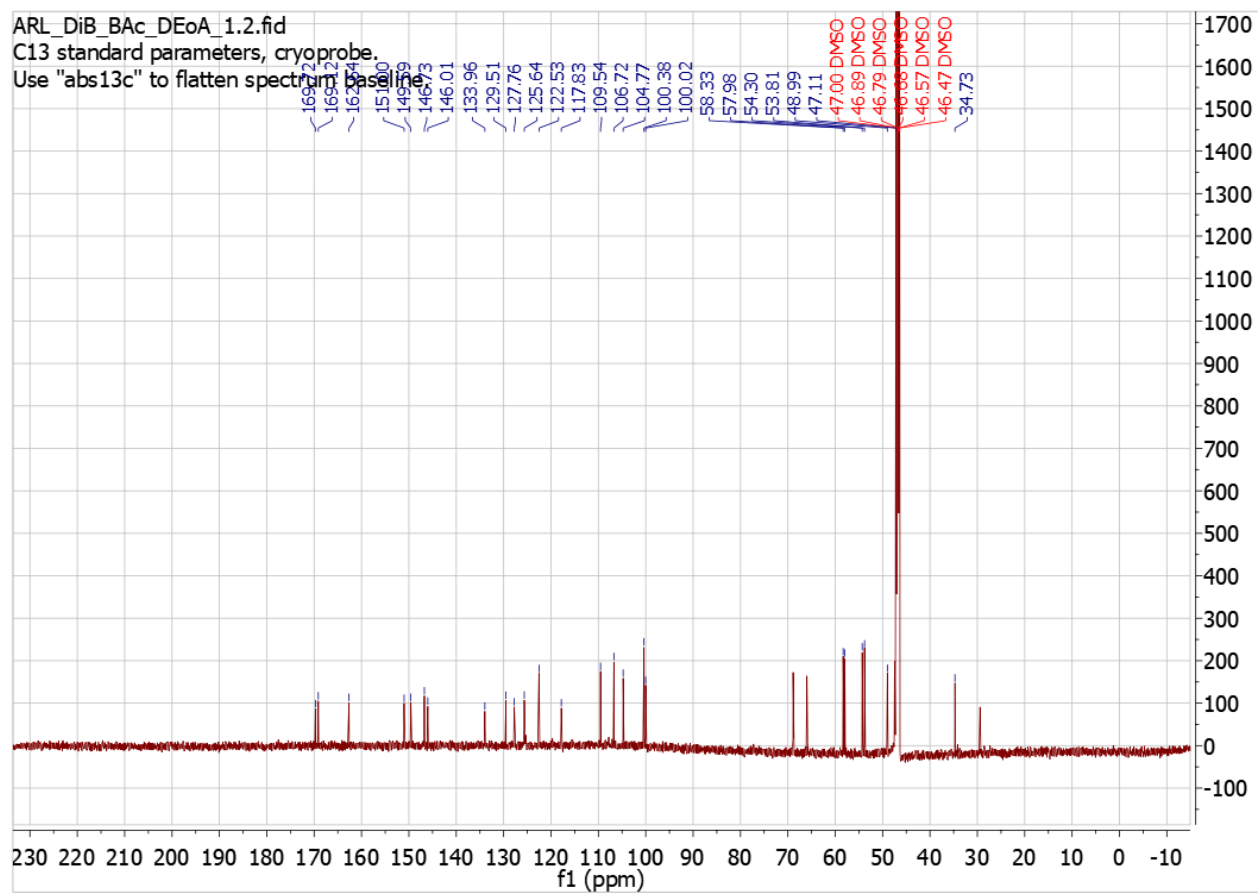


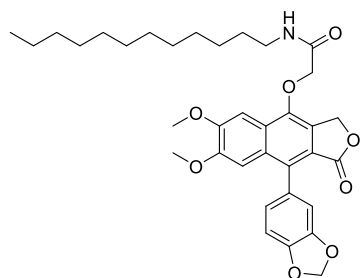


2i=C₂₇H₂₇NO₁₀+H⁺, 526.1713 [M+H]⁺

LRMS

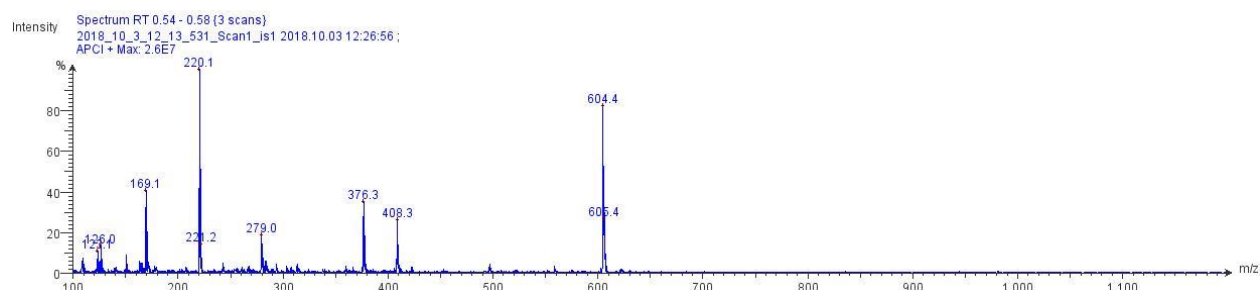


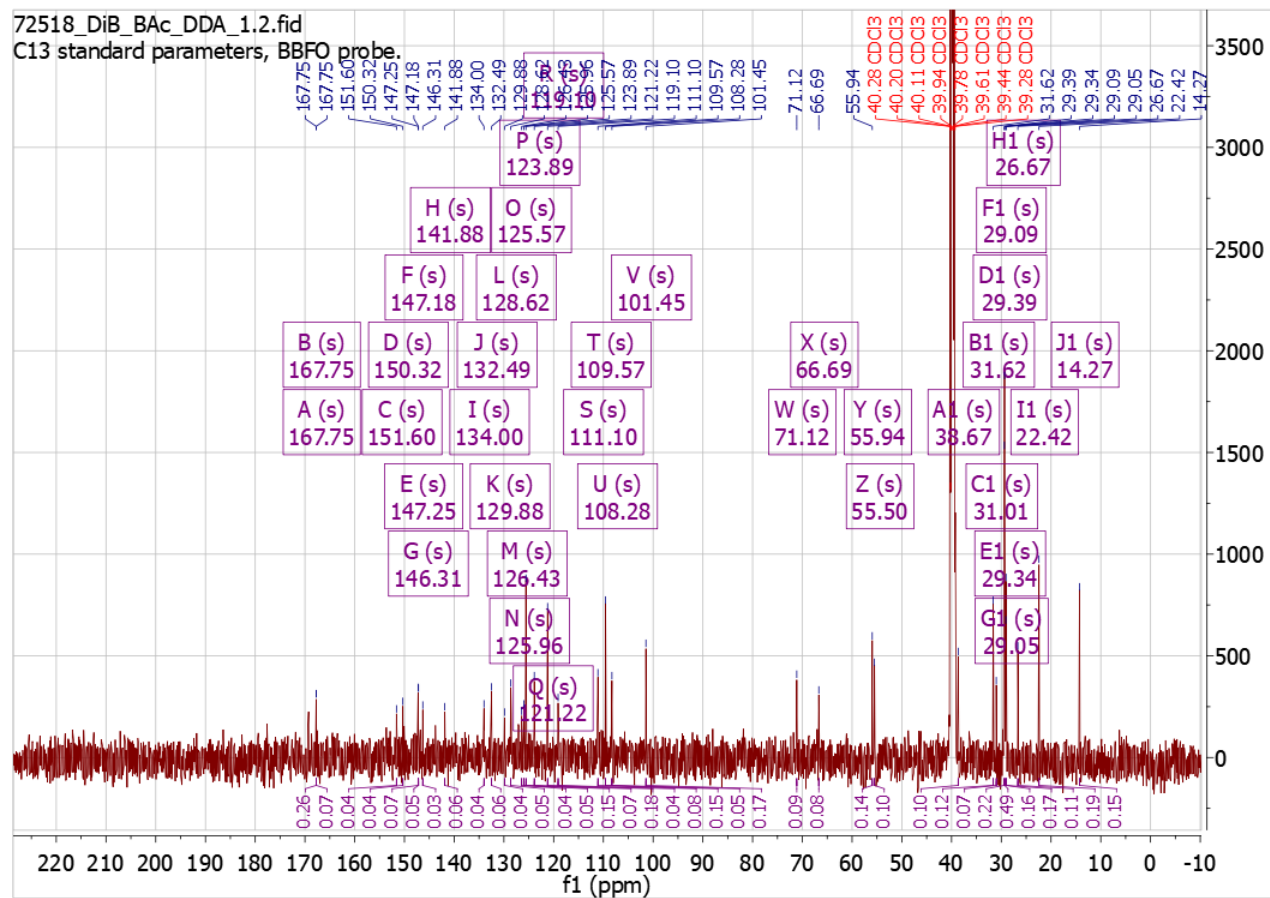


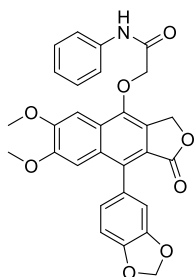


2j=C₃₅H₄₃NO₈+H⁺, 606.3067 [M+H]⁺

LRMS

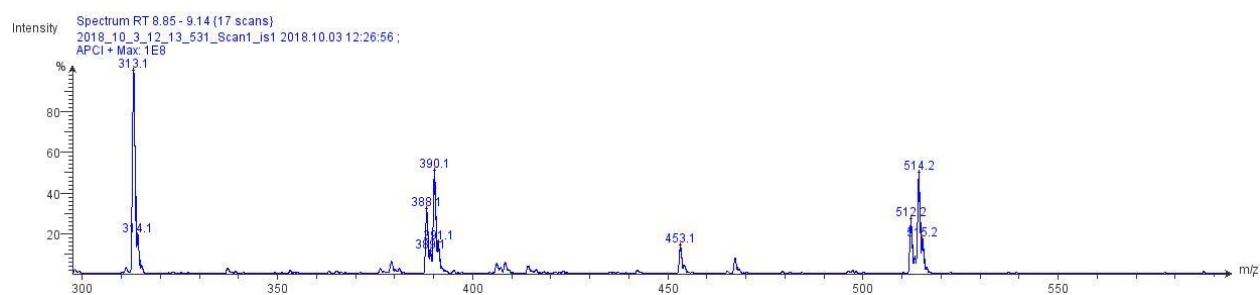


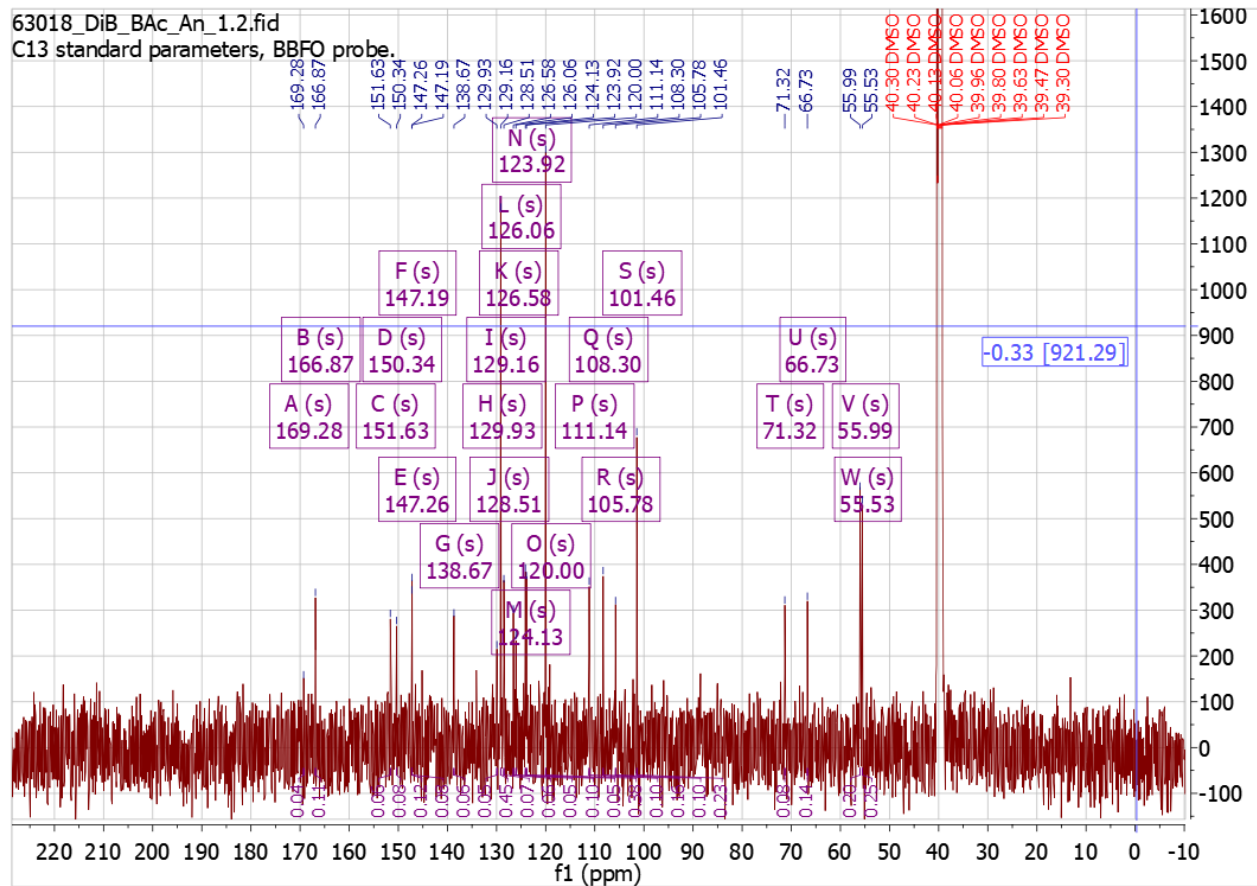




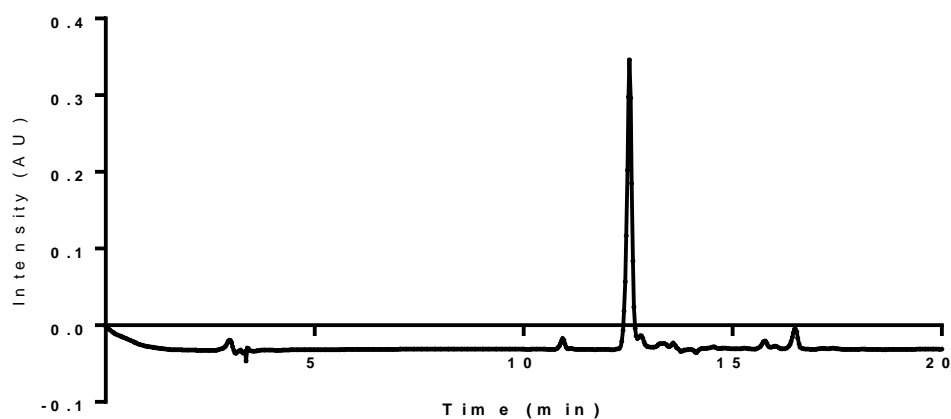
2k=C₂₉H₂₃NO₈+H⁺, 521.1924 [M+H]⁺

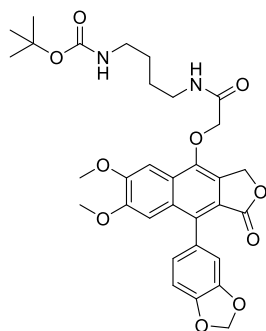
LRMS





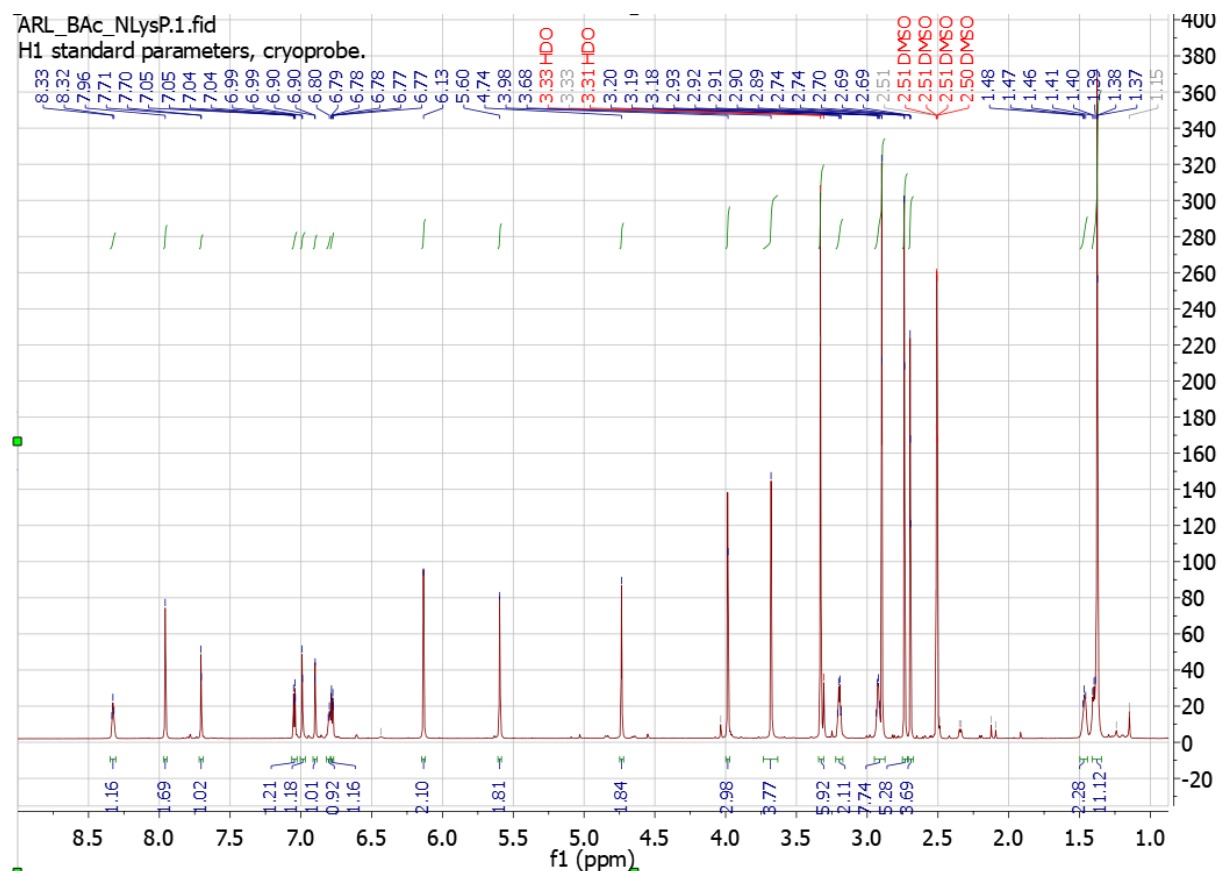
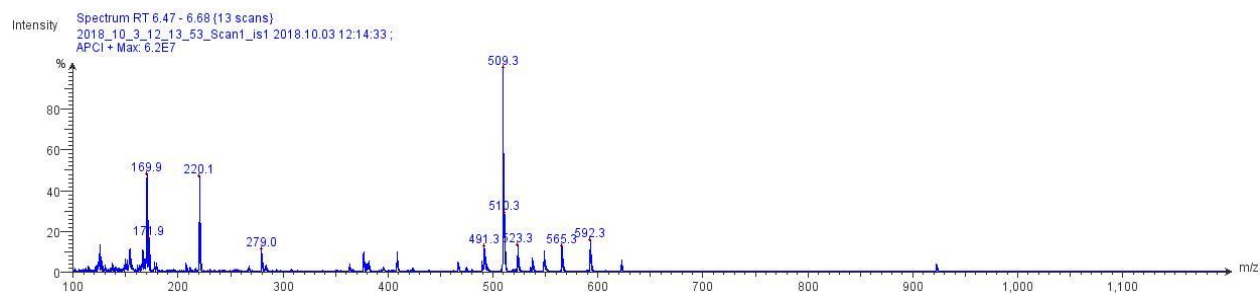
2 k Purity (98.2 %)

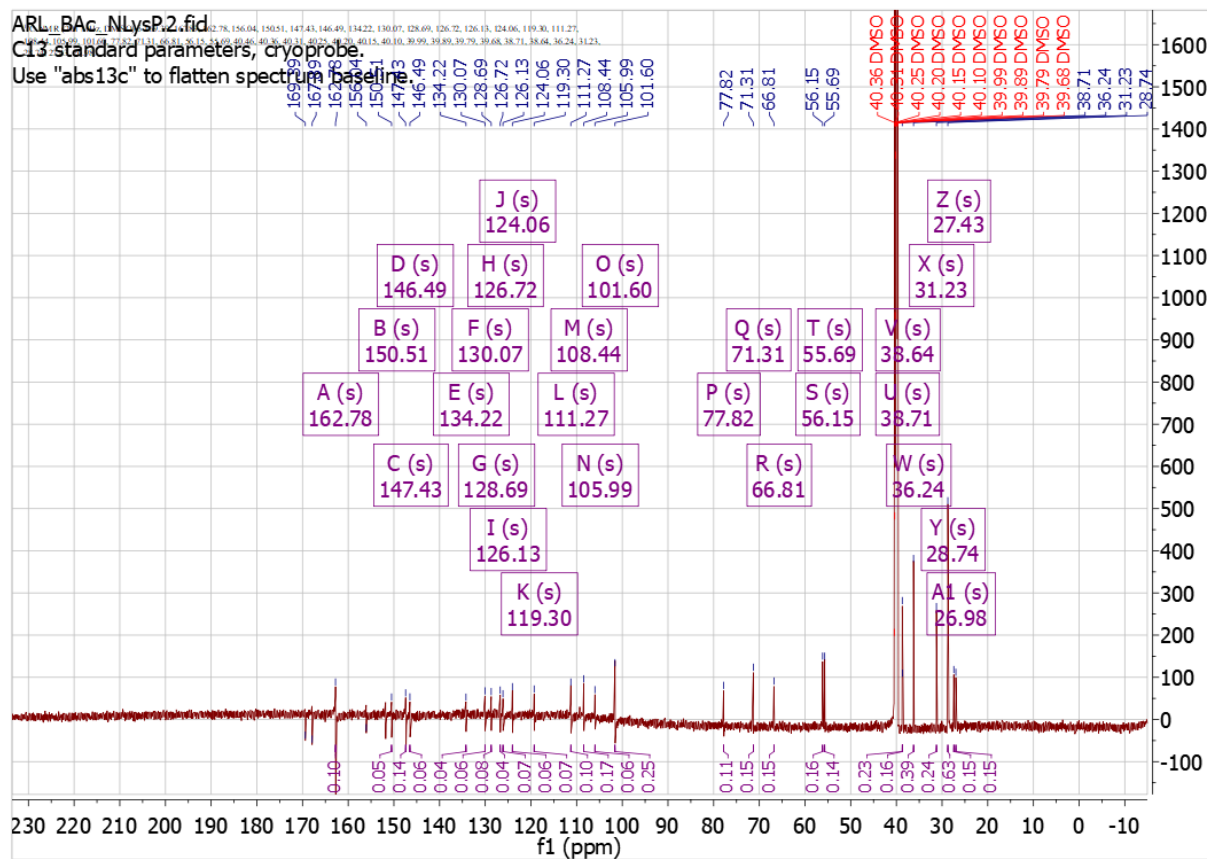


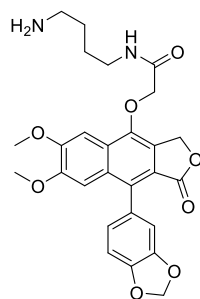


$2l=C_{32}H_{36}N_2O_{10}+H^+$, 609.2448 $[M+H]^+$

LRMS

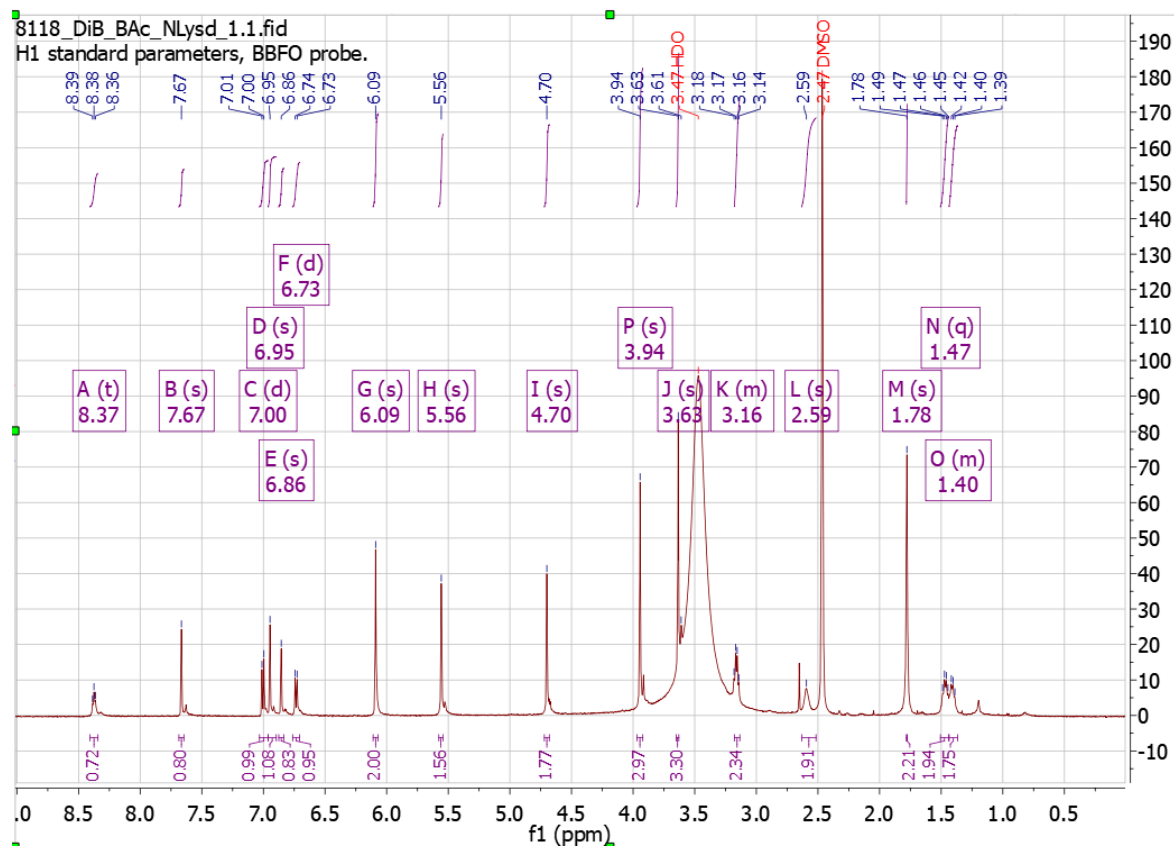
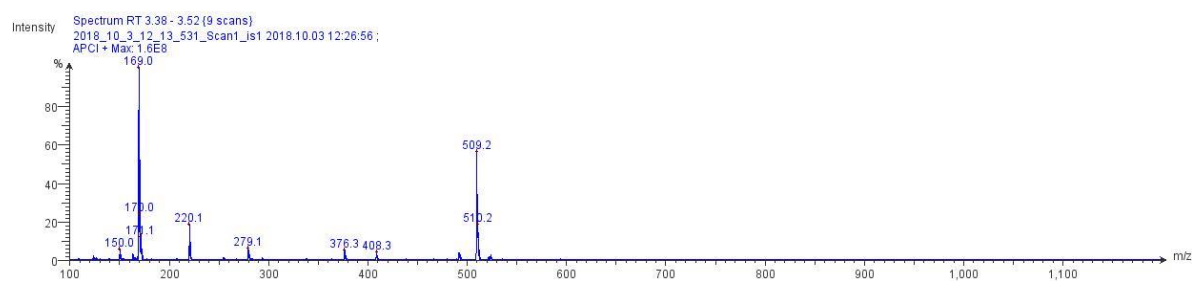


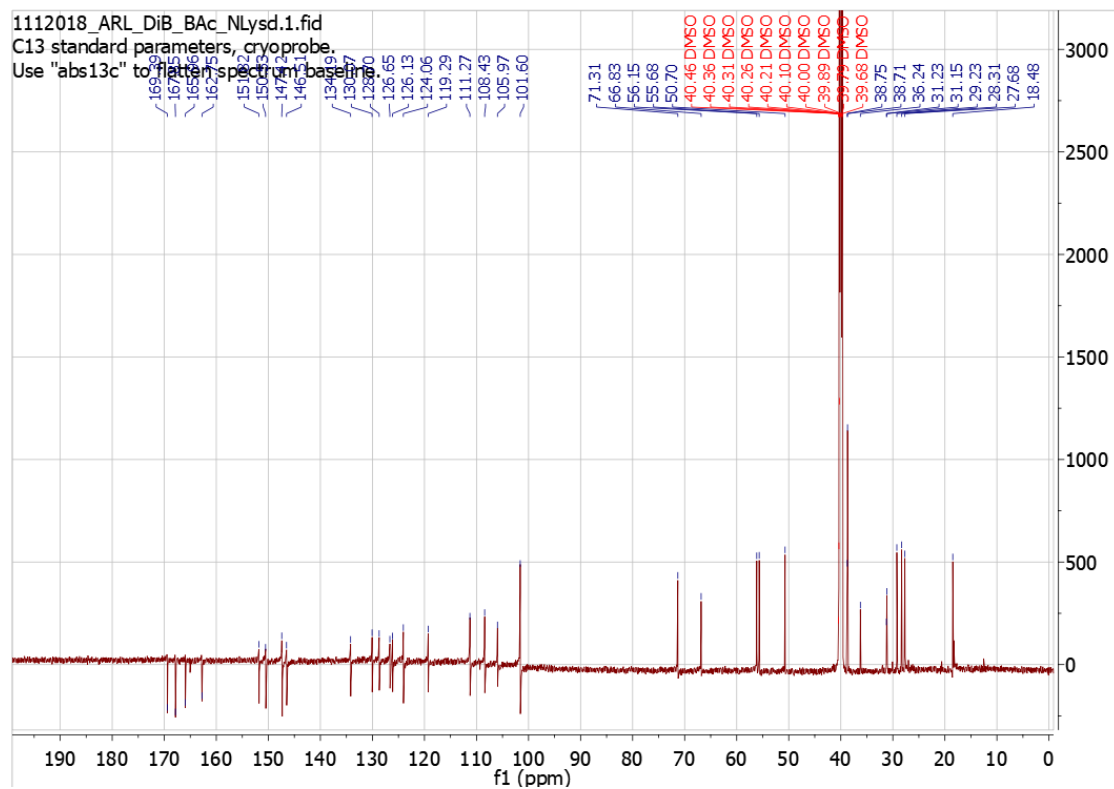




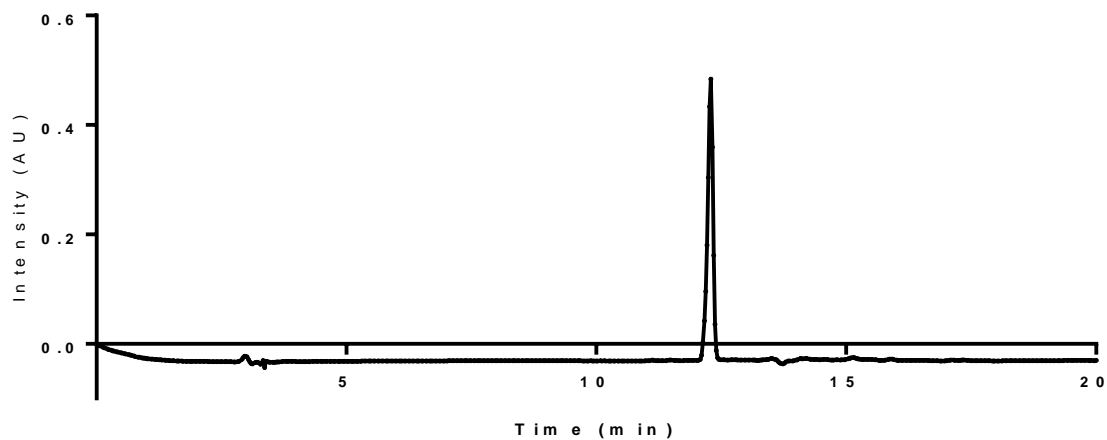
2m=C₂₇H₂₈N₂O₈+H⁺, 509.1924 [M+H]⁺

LRMS





2 m P u r i t y (9 9 . 4 %)



LIST OF REFERENCES

- (1) Messaoudi, I.; Amarasinghe, G. K.; Basler, C. F. Filovirus Pathogenesis and Immune Evasion: Insights from Ebola Virus and Marburg Virus. *Nat Rev Micro* **2015**, *13* (11), 663–676. <https://doi.org/10.1038/nrmicro3524>.
- (2) White, J. M.; Schornberg, K. L. A New Player in the Puzzle of Filovirus Entry. *Nat Rev Micro* **2012**, *10* (5), 317–322. <https://doi.org/10.1038/nrmicro2764>.
- (3) Ansari, A. A. Clinical Features and Pathobiology of Ebolavirus Infection. *Journal of Autoimmunity* **2014**, *55*, 1–9. <https://doi.org/10.1016/j.jaut.2014.09.001>.
- (4) Chen, H.-W.; Cheng, J. X.; Liu, M.-T.; King, K.; Peng, J.-Y.; Zhang, X.-Q.; Wang, C.-H.; Shrestha, S.; Schooley, R. T.; Liu, Y.-T. Inhibitory and Combinatorial Effect of Diphyllin, a v-ATPase Blocker, on Influenza Viruses. *Antiviral research* **2013**, *99* (3), 371–382. <https://doi.org/10.1016/j.antiviral.2013.06.014>.
- (5) Shen, W.; Zou, X.; Chen, M.; Liu, P.; Shen, Y.; Huang, S.; Guo, H.; Zhang, L. Effects of Diphyllin as a Novel V-ATPase Inhibitor on Gastric Adenocarcinoma. *European journal of pharmacology* **2011**, *667* (1–3), 330–338. <https://doi.org/10.1016/j.ejphar.2011.05.042>.
- (6) Sørensen, M. G.; Henriksen, K.; Neutzsky-Wulff, A. V.; Dziegiel, M. H.; Karsdal, M. A. Diphyllin, a Novel and Naturally Potent V-ATPase Inhibitor, Abrogates Acidification of the Osteoclastic Resorption Lacunae and Bone Resorption. *Journal of bone and mineral research : the official journal of the American Society for Bone and Mineral Research* **2007**, *22* (10), 1640–1648. <https://doi.org/10.1359/jbmr.070613>.
- (7) Kuhn, J. H.; Becker, S.; Ebihara, H.; Geisbert, T. W.; Johnson, K. M.; Kawaoka, Y.; Lipkin, W. I.; Negredo, A. I.; Netesov, S. V.; Nichol, S. T.; et al. Proposal for a Revised Taxonomy of the Family Filoviridae: Classification, Names of Taxa and Viruses, and Virus Abbreviations. *Arch. Virol.* **2010**, *155* (12), 2083–2103. <https://doi.org/10.1007/s00705-010-0814-x>.
- (8) Bukreyev, A. A.; Chandran, K.; Dolnik, O.; Dye, J. M.; Ebihara, H.; Leroy, E. M.; Mühlberger, E.; Netesov, S. V.; Patterson, J. L.; Paweska, J. T.; et al. Discussions and Decisions of the 2012–2014 International Committee on Taxonomy of Viruses (ICTV) Filoviridae Study Group, January 2012–June 2013. *Arch Virol* **2014**, *159* (4), 821–830. <https://doi.org/10.1007/s00705-013-1846-9>.
- (9) Burk, R.; Bollinger, L.; Johnson, J. C.; Wada, J.; Radoshitzky, S. R.; Palacios, G.; Bavari, S.; Jahrling, P. B.; Kuhn, J. H. Neglected Filoviruses. *FEMS Microbiol Rev* **2016**, *40* (4), 494–519. <https://doi.org/10.1093/femsre/fuw010>.
- (10) Negredo, A.; Palacios, G.; Vázquez-Morón, S.; González, F.; Dopazo, H.; Molero, F.; Juste, J.; Quetglas, J.; Savji, N.; Martínez, M. de la C.; et al. Discovery of an Ebolavirus-Like Filovirus in Europe. *PLOS Pathogens* **2011**, *7* (10), e1002304. <https://doi.org/10.1371/journal.ppat.1002304>.
- (11) Martin, B.; Canard, B.; Decroly, E. Filovirus Proteins for Antiviral Drug Discovery: Structure/Function Bases of the Replication Cycle. *Antiviral Research* **2017**, *141*, 48–61. <https://doi.org/10.1016/j.antiviral.2017.02.004>.
- (12) Martin, B.; Canard, B.; Decroly, E. Filovirus Proteins for Antiviral Drug Discovery: Structure/Function Bases of the Replication Cycle. *Antiviral Research* **2017**, *141*, 48–61. <https://doi.org/10.1016/j.antiviral.2017.02.004>.

- (13) Mehedi, M.; Falzarano, D.; Seebach, J.; Hu, X.; Carpenter, M. S.; Schnittler, H.-J.; Feldmann, H. A New Ebola Virus Nonstructural Glycoprotein Expressed through RNA Editing. *Journal of Virology* **2011**, *85* (11), 5406–5414. <https://doi.org/10.1128/JVI.02190-10>.
- (14) Licata, J. M.; Johnson, R. F.; Han, Z.; Harty, R. N. Contribution of Ebola Virus Glycoprotein, Nucleoprotein, and VP24 to Budding of VP40 Virus-like Particles. *J. Virol.* **2004**, *78* (14), 7344–7351. <https://doi.org/10.1128/JVI.78.14.7344-7351.2004>.
- (15) DiCarlo, A.; Biedenkopf, N.; Hartlieb, B.; Klußmeier, A.; Becker, S. Phosphorylation of Marburg Virus NP Region II Modulates Viral RNA Synthesis. *J Infect Dis* **2011**, *204* (suppl_3), S927–S933. <https://doi.org/10.1093/infdis/jir319>.
- (16) Huang, Y.; Xu, L.; Sun, Y.; Nabel, G. J. The Assembly of Ebola Virus Nucleocapsid Requires Virion-Associated Proteins 35 and 24 and Posttranslational Modification of Nucleoprotein. *Molecular Cell* **2002**, *10* (2), 307–316. [https://doi.org/10.1016/S1097-2765\(02\)00588-9](https://doi.org/10.1016/S1097-2765(02)00588-9).
- (17) Basler, C. F.; Mikulasova, A.; Martinez-Sobrido, L.; Paragas, J.; Mühlberger, E.; Bray, M.; Klenk, H.-D.; Palese, P.; García-Sastre, A. The Ebola Virus VP35 Protein Inhibits Activation of Interferon Regulatory Factor 3. *J. Virol.* **2003**, *77* (14), 7945–7956.
- (18) Trunschke, M.; Conrad, D.; Enterlein, S.; Olejnik, J.; Brauburger, K.; Mühlberger, E. The L–VP35 and L–L Interaction Domains Reside in the Amino Terminus of the Ebola Virus L Protein and Are Potential Targets for Antivirals. *Virology* **2013**, *441* (2), 135–145. <https://doi.org/10.1016/j.virol.2013.03.013>.
- (19) Kirchdoerfer, R. N.; Abelson, D. M.; Li, S.; Wood, M. R.; Saphire, E. O. Assembly of the Ebola Virus Nucleoprotein from a Chaperoned VP35 Complex. *Cell Reports* **2015**, *12* (1), 140–149. <https://doi.org/10.1016/j.celrep.2015.06.003>.
- (20) Leung, D. W.; Prins, K. C.; Basler, C. F.; Amarasinghe, G. K. Ebolavirus VP35 Is a Multifunctional Virulence Factor. *Virulence* **2010**, *1* (6), 526–531.
- (21) Yen, B.; Mulder, L. C. F.; Martinez, O.; Basler, C. F. Molecular Basis for Ebolavirus VP35 Suppression of Human Dendritic Cell Maturation. *J. Virol.* **2014**, *88* (21), 12500–12510. <https://doi.org/10.1128/JVI.02163-14>.
- (22) Jasenosky, L. D.; Neumann, G.; Lukashevich, I.; Kawaoka, Y. Ebola Virus VP40-Induced Particle Formation and Association with the Lipid Bilayer. *J Virol* **2001**, *75* (11), 5205–5214. <https://doi.org/10.1128/JVI.75.11.5205-5214.2001>.
- (23) Adu-Gyamfi, E.; Soni, S. P.; Xue, Y.; Digman, M. A.; Gratton, E.; Stahelin, R. V. The Ebola Virus Matrix Protein Penetrates into the Plasma Membrane A KEY STEP IN VIRAL PROTEIN 40 (VP40) OLIGOMERIZATION AND VIRAL EGRESS. *J. Biol. Chem.* **2013**, *288* (8), 5779–5789. <https://doi.org/10.1074/jbc.M112.443960>.
- (24) Nanbo, A.; Imai, M.; Watanabe, S.; Noda, T.; Takahashi, K.; Neumann, G.; Halfmann, P.; Kawaoka, Y. Ebolavirus Is Internalized into Host Cells via Macropinocytosis in a Viral Glycoprotein-Dependent Manner. *PLOS Pathogens* **2010**, *6* (9), e1001121. <https://doi.org/10.1371/journal.ppat.1001121>.
- (25) Volchkov, V. E.; Feldmann, H.; Volchkova, V. A.; Klenk, H. D. Processing of the Ebola Virus Glycoprotein by the Proprotein Convertase Furin. *Proc. Natl. Acad. Sci. U.S.A.* **1998**, *95* (10), 5762–5767.

- (26) Bavari, S.; Bosio, C. M.; Wiegand, E.; Ruthel, G.; Will, A. B.; Geisbert, T. W.; Hevey, M.; Schmaljohn, C.; Schmaljohn, A.; Aman, M. J. Lipid Raft Microdomains: A Gateway for Compartmentalized Trafficking of Ebola and Marburg Viruses. *Journal of Experimental Medicine* **2002**, *195* (5), 593–602. <https://doi.org/10.1084/jem.20011500>.
- (27) Rhein, B. A.; Brouillette, R. B.; Schaack, G. A.; Chiorini, J. A.; Maury, W. Characterization of Human and Murine T-Cell Immunoglobulin Mucin Domain 4 (TIM-4) IgV Domain Residues Critical for Ebola Virus Entry. *Journal of Virology* **2016**, *90* (13), 6097–6111. <https://doi.org/10.1128/JVI.00100-16>.
- (28) Lee, J. E.; Saphire, E. O. Ebolavirus Glycoprotein Structure and Mechanism of Entry. *Future Virology* **2009**, *4* (6), 621–635. <https://doi.org/10.2217/fvl.09.56>.
- (29) Sanchez, A.; Trappier, S. G.; Mahy, B. W.; Peters, C. J.; Nichol, S. T. The Virion Glycoproteins of Ebola Viruses Are Encoded in Two Reading Frames and Are Expressed through Transcriptional Editing. *PNAS* **1996**, *93* (8), 3602–3607. <https://doi.org/10.1073/pnas.93.8.3602>.
- (30) He, J.; Melnik, L. I.; Komin, A.; Wiedman, G.; Fuselier, T.; Morris, C. F.; Starr, C. G.; Searson, P. C.; Gallaher, W. R.; Hristova, K.; et al. Ebola Virus Delta Peptide Is a Viroporin. *Journal of Virology* **2017**, JVI.00438-17. <https://doi.org/10.1128/JVI.00438-17>.
- (31) Biedenkopf, N.; Hartlieb, B.; Hoenen, T.; Becker, S. Phosphorylation of Ebola Virus VP30 Influences the Composition of the Viral Nucleocapsid Complex IMPACT ON VIRAL TRANSCRIPTION AND REPLICATION. *J. Biol. Chem.* **2013**, *288* (16), 11165–11174. <https://doi.org/10.1074/jbc.M113.461285>.
- (32) Ilinykh, P. A.; Tigabu, B.; Ivanov, A.; Ammosova, T.; Obukhov, Y.; Garron, T.; Kumari, N.; Kovalsky, D.; Platonov, M. O.; Naumchik, V. S.; et al. Role of Protein Phosphatase 1 in Dephosphorylation of Ebola Virus VP30 Protein and Its Targeting for the Inhibition of Viral Transcription. *J Biol Chem* **2014**, *289* (33), 22723–22738. <https://doi.org/10.1074/jbc.M114.575050>.
- (33) Zhang, A. P. P.; Abelson, D. M.; Bornholdt, Z. A.; Liu, T.; Woods, Jr, V. L.; Saphire, E. O. The Ebolavirus VP24 Interferon Antagonist. *Virulence* **2012**, *3* (5), 440–445. <https://doi.org/10.4161/viru.21302>.
- (34) Zhang, A. P. P.; Bornholdt, Z. A.; Liu, T.; Abelson, D. M.; Lee, D. E.; Li, S.; Woods, V. L.; Saphire, E. O. The Ebola Virus Interferon Antagonist VP24 Directly Binds STAT1 and Has a Novel, Pyramidal Fold. *PLoS Pathog.* **2012**, *8* (2), e1002550. <https://doi.org/10.1371/journal.ppat.1002550>.
- (35) Mateo, M.; Carbonnelle, C.; Martinez, M. J.; Reynard, O.; Page, A.; Volchkova, V. A.; Volchkov, V. E. Knockdown of Ebola Virus VP24 Impairs Viral Nucleocapsid Assembly and Prevents Virus Replication. *J Infect Dis* **2011**, *204* (suppl_3), S892–S896. <https://doi.org/10.1093/infdis/jir311>.
- (36) Volchkov, V. E.; Volchkova, V. A.; Chepurnov, A. A.; Blinov, V. M.; Dolnik, O.; Netesov, S. V.; Feldmann, H. Characterization of the L Gene and 5' Trailer Region of Ebola Virus. *Journal of General Virology* **1999**, *80* (2), 355–362. <https://doi.org/10.1099/0022-1317-80-2-355>.
- (37) Ferron, F.; Longhi, S.; Henrissat, B.; Canard, B. Viral RNA-Polymerases – a Predicted 2'-O-Ribose Methyltransferase Domain Shared by All Mononegavirales. *Trends in Biochemical Sciences* **2002**, *27* (5), 222–224. [https://doi.org/10.1016/S0968-0004\(02\)02091-1](https://doi.org/10.1016/S0968-0004(02)02091-1).

- (38) Mehedi, M.; Hoenen, T.; Robertson, S.; Ricklefs, S.; Dolan, M. A.; Taylor, T.; Falzarano, D.; Ebihara, H.; Porcella, S. F.; Feldmann, H. Ebola Virus RNA Editing Depends on the Primary Editing Site Sequence and an Upstream Secondary Structure. *PLOS Pathogens* **2013**, *9* (10), e1003677. <https://doi.org/10.1371/journal.ppat.1003677>.
- (39) Pavadai, E.; Gerstman, B. S.; Chapagain, P. P. A Cylindrical Assembly Model and Dynamics of the Ebola Virus VP40 Structural Matrix. *Sci Rep* **2018**, *8* (1), 9776. <https://doi.org/10.1038/s41598-018-28077-7>.
- (40) Bharat, T. A. M.; Noda, T.; Riches, J. D.; Kraehling, V.; Kolesnikova, L.; Becker, S.; Kawaoka, Y.; Briggs, J. A. G. Structural Dissection of Ebola Virus and Its Assembly Determinants Using Cryo-Electron Tomography. *PNAS* **2012**, *109* (11), 4275–4280. <https://doi.org/10.1073/pnas.1120453109>.
- (41) Hunt, C. L.; Kolokoltsov, A. A.; Davey, R. A.; Maury, W. The Tyro3 Receptor Kinase Axl Enhances Macropinocytosis of Zaire Ebolavirus. *Journal of Virology* **2011**, *85* (1), 334–347. <https://doi.org/10.1128/JVI.01278-09>.
- (42) Takada, A.; Fujioka, K.; Tsuiji, M.; Morikawa, A.; Higashi, N.; Ebihara, H.; Kobasa, D.; Feldmann, H.; Irimura, T.; Kawaoka, Y. Human Macrophage C-Type Lectin Specific for Galactose and N-Acetylgalactosamine Promotes Filovirus Entry. *Journal of Virology* **2004**, *78* (6), 2943–2947. <https://doi.org/10.1128/JVI.78.6.2943-2947.2004>.
- (43) Moller-Tank, S.; Kondratowicz, A. S.; Davey, R. A.; Rennert, P. D.; Maury, W. Role of the Phosphatidylserine Receptor TIM-1 in Enveloped-Virus Entry. *J. Virol.* **2013**, *87* (15), 8327–8341. <https://doi.org/10.1128/JVI.01025-13>.
- (44) Saeed, M. F.; Kolokoltsov, A. A.; Albrecht, T.; Davey, R. A. Cellular Entry of Ebola Virus Involves Uptake by a Macropinocytosis-Like Mechanism and Subsequent Trafficking through Early and Late Endosomes. *PLoS Pathog* **2010**, *6* (9), e1001110. <https://doi.org/10.1371/journal.ppat.1001110>.
- (45) Brecher, M.; Schornberg, K. L.; Delos, S. E.; Fusco, M. L.; Saphire, E. O.; White, J. M. Cathepsin Cleavage Potentiates the Ebola Virus Glycoprotein To Undergo a Subsequent Fusion-Relevant Conformational Change. *Journal of Virology* **2012**, *86* (1), 364–372. <https://doi.org/10.1128/JVI.05708-11>.
- (46) Marzi, A.; Reinheckel, T.; Feldmann, H. Cathepsin B & L Are Not Required for Ebola Virus Replication. *PLoS Negl Trop Dis* **2012**, *6* (12), e1923. <https://doi.org/10.1371/journal.pntd.0001923>.
- (47) Gnirß, K.; Kühl, A.; Karsten, C.; Glowacka, I.; Bertram, S.; Kaup, F.; Hofmann, H.; Pöhlmann, S. Cathepsins B and L Activate Ebola but Not Marburg Virus Glycoproteins for Efficient Entry into Cell Lines and Macrophages Independent of TMPRSS2 Expression. *Virology* **2012**, *424* (1), 3–10. <https://doi.org/10.1016/j.virol.2011.11.031>.
- (48) Bornholdt, Z. A.; Ndungo, E.; Fusco, M. L.; Bale, S.; Flyak, A. I.; Crowe, J. E.; Chandran, K.; Saphire, E. O. Host-Primed Ebola Virus GP Exposes a Hydrophobic NPC1 Receptor-Binding Pocket, Revealing a Target for Broadly Neutralizing Antibodies. *mBio* **2016**, *7* (1), e02154-15. <https://doi.org/10.1128/mBio.02154-15>.
- (49) Wang, H.; Shi, Y.; Song, J.; Qi, J.; Lu, G.; Yan, J.; Gao, G. F. Ebola Viral Glycoprotein Bound to Its Endosomal Receptor Niemann-Pick C1. *Cell* **2016**, *164* (1), 258–268. <https://doi.org/10.1016/j.cell.2015.12.044>.

- (50) Côté, M.; Misasi, J.; Ren, T.; Bruchez, A.; Lee, K.; Filone, C. M.; Hensley, L.; Li, Q.; Ory, D.; Chandran, K.; et al. Small Molecule Inhibitors Reveal Niemann-Pick C1 Is Essential for Ebolavirus Infection. *Nature* **2011**, 477 (7364), 344–348. <https://doi.org/10.1038/nature10380>.
- (51) Hoffmann, M.; Hernández, M. G.; Berger, E.; Marzi, A.; Pöhlmann, S. The Glycoproteins of All Filovirus Species Use the Same Host Factors for Entry into Bat and Human Cells but Entry Efficiency Is Species Dependent. *PLOS ONE* **2016**, 11 (2), e0149651. <https://doi.org/10.1371/journal.pone.0149651>.
- (52) Lee, J.; Gregory, S. M.; Nelson, E. A.; White, J. M.; Tamm, L. K. The Roles of Histidines and Charged Residues as Potential Triggers of a Conformational Change in the Fusion Loop of Ebola Virus Glycoprotein. *PLOS ONE* **2016**, 11 (3), e0152527. <https://doi.org/10.1371/journal.pone.0152527>.
- (53) Markosyan, R. M.; Miao, C.; Zheng, Y.-M.; Melikyan, G. B.; Liu, S.-L.; Cohen, F. S. Induction of Cell-Cell Fusion by Ebola Virus Glycoprotein: Low PH Is Not a Trigger. *PLoS Pathog.* **2016**, 12 (1), e1005373. <https://doi.org/10.1371/journal.ppat.1005373>.
- (54) Sakurai, Y.; Kolokoltsov, A. A.; Chen, C.-C.; Tidwell, M. W.; Bauta, W. E.; Klugbauer, N.; Grimm, C.; Wahl-Schott, C.; Biel, M.; Davey, R. A. Two Pore Channels Control Ebolavirus Host Cell Entry and Are Drug Targets for Disease Treatment. *Science* **2015**, 347 (6225), 995–998. <https://doi.org/10.1126/science.1258758>.
- (55) Weik, M.; Modrof, J.; Klenk, H.-D.; Becker, S.; Mühlberger, E. Ebola Virus VP30-Mediated Transcription Is Regulated by RNA Secondary Structure Formation. *Journal of Virology* **2002**, 76 (17), 8532–8539. <https://doi.org/10.1128/JVI.76.17.8532-8539.2002>.
- (56) Mühlberger, E.; Trommer, S.; Funke, C.; Volchkov, V.; Klenk, H.-D.; Becker, S. Termini of All MRNA Species of Marburg Virus: Sequence and Secondary Structure. *Virology* **1996**, 223 (2), 376–380. <https://doi.org/10.1006/viro.1996.0490>.
- (57) Whelan, S. P. J.; Barr, J. N.; Wertz, G. W. Transcription and Replication of Nonsegmented Negative-Strand RNA Viruses. In *Biology of Negative Strand RNA Viruses: The Power of Reverse Genetics*; Kawaoka, Y., Ed.; Current Topics in Microbiology and Immunology; Springer Berlin Heidelberg: Berlin, Heidelberg, 2004; pp 61–119. https://doi.org/10.1007/978-3-662-06099-5_3.
- (58) Sanchez, A.; Kiley, M. P.; Holloway, B. P.; Auperin, D. D. Sequence Analysis of the Ebola Virus Genome: Organization, Genetic Elements, and Comparison with the Genome of Marburg Virus. *Virus Research* **1993**, 29 (3), 215–240. [https://doi.org/10.1016/0168-1702\(93\)90063-S](https://doi.org/10.1016/0168-1702(93)90063-S).
- (59) Ogino, T.; Banerjee, A. K. Unconventional Mechanism of MRNA Capping by the RNA-Dependent RNA Polymerase of Vesicular Stomatitis Virus. *Molecular Cell* **2007**, 25 (1), 85–97. <https://doi.org/10.1016/j.molcel.2006.11.013>.
- (60) Calain, P.; Monroe, M. C.; Nichol, S. T. Ebola Virus Defective Interfering Particles and Persistent Infection. *Virology* **1999**, 262 (1), 114–128. <https://doi.org/10.1006/viro.1999.9915>.
- (61) Leung, D. W.; Borek, D.; Luthra, P.; Binning, J. M.; Anantpadma, M.; Liu, G.; Harvey, I. B.; Su, Z.; Endlich-Frazier, A.; Pan, J.; et al. An Intrinsically Disordered Peptide from Ebola Virus VP35 Controls Viral RNA Synthesis by Modulating Nucleoprotein-RNA Interactions. *Cell Reports* **2015**, 11 (3), 376–389. <https://doi.org/10.1016/j.celrep.2015.03.034>.

- (62) Watt, A.; Moukambi, F.; Banadyga, L.; Groseth, A.; Callison, J.; Herwig, A.; Ebihara, H.; Feldmann, H.; Hoenen, T. A Novel Life Cycle Modeling System for Ebola Virus Shows a Genome Length-Dependent Role of VP24 in Virus Infectivity. *Journal of Virology* **2014**, *88* (18), 10511–10524. <https://doi.org/10.1128/JVI.01272-14>.
- (63) Kolesnikova, L.; Mittler, E.; Schudt, G.; Shams-Eldin, H.; Becker, S. Phosphorylation of Marburg Virus Matrix Protein VP40 Triggers Assembly of Nucleocapsids with the Viral Envelope at the Plasma Membrane. *Cellular Microbiology* **2012**, *14* (2), 182–197. <https://doi.org/10.1111/j.1462-5822.2011.01709.x>.
- (64) Yasuda, J.; Nakao, M.; Kawaoka, Y.; Shida, H. Nedd4 Regulates Egress of Ebola Virus-Like Particles from Host Cells. *Journal of Virology* **2003**, *77* (18), 9987–9992. <https://doi.org/10.1128/JVI.77.18.9987-9992.2003>.
- (65) Bornholdt, Z. A.; Noda, T.; Abelson, D. M.; Halfmann, P.; Wood, M. R.; Kawaoka, Y.; Saphire, E. O. Structural Rearrangement of Ebola Virus VP40 Begets Multiple Functions in the Virus Life Cycle. *Cell* **2013**, *154* (4), 763–774. <https://doi.org/10.1016/j.cell.2013.07.015>.
- (66) Johnson, K. A.; Taghon, G. J. F.; Scott, J. L.; Stahelin, R. V. The Ebola Virus Matrix Protein, VP40, Requires Phosphatidylinositol 4,5-Bisphosphate (PI(4,5)P₂) for Extensive Oligomerization at the Plasma Membrane and Viral Egress. *Scientific Reports* **2016**, *6*, 19125. <https://doi.org/10.1038/srep19125>.
- (67) Beniac, D. R.; Melito, P. L.; deVarenes, S. L.; Hiebert, S. L.; Rabb, M. J.; Lamboo, L. L.; Jones, S. M.; Booth, T. F. The Organisation of Ebola Virus Reveals a Capacity for Extensive, Modular Polyploidy. *PLOS ONE* **2012**, *7* (1), e29608. <https://doi.org/10.1371/journal.pone.0029608>.
- (68) Reid, S. P.; Leung, L. W.; Hartman, A. L.; Martinez, O.; Shaw, M. L.; Carbonnelle, C.; Volchkov, V. E.; Nichol, S. T.; Basler, C. F. Ebola Virus VP24 Binds Karyopherin Alpha1 and Blocks STAT1 Nuclear Accumulation. *J. Virol.* **2006**, *80* (11), 5156–5167. <https://doi.org/10.1128/JVI.02349-05>.
- (69) Halfmann, P.; Neumann, G.; Kawaoka, Y. The Ebolavirus VP24 Protein Blocks Phosphorylation of P38 Mitogen-Activated Protein Kinase. *J Infect Dis* **2011**, *204* (Suppl 3), S953–S956. <https://doi.org/10.1093/infdis/jir325>.
- (70) Volchkova, V. A.; Klenk, H.-D.; Volchkov, V. E. Delta-Peptide Is the Carboxy-Terminal Cleavage Fragment of the Nonstructural Small Glycoprotein SGP of Ebola Virus. *Virology* **1999**, *265* (1), 164–171. <https://doi.org/10.1006/viro.1999.0034>.
- (71) Ito, H.; Watanabe, S.; Takada, A.; Kawaoka, Y. Ebola Virus Glycoprotein: Proteolytic Processing, Acylation, Cell Tropism, and Detection of Neutralizing Antibodies. *J. Virol.* **2001**, *75* (3), 1576–1580. <https://doi.org/10.1128/JVI.75.3.1576-1580.2001>.
- (72) Sanchez, A.; Lukwiya, M.; Bausch, D.; Mahanty, S.; Sanchez, A. J.; Wagoner, K. D.; Rollin, P. E. Analysis of Human Peripheral Blood Samples from Fatal and Nonfatal Cases of Ebola (Sudan) Hemorrhagic Fever: Cellular Responses, Virus Load, and Nitric Oxide Levels. *J. Virol.* **2004**, *78* (19), 10370–10377. <https://doi.org/10.1128/JVI.78.19.10370-10377.2004>.
- (73) Zampieri, C. A.; Sullivan, N. J.; Nabel, G. J. Immunopathology of Highly Virulent Pathogens: Insights from Ebola Virus. *Nat. Immunol.* **2007**, *8* (11), 1159–1164. <https://doi.org/10.1038/ni1519>.

- (74) Villinger, F.; Rollin, P. E.; Brar, S. S.; Chikkala, N. F.; Winter, J.; Sundstrom, J. B.; Zaki, S. R.; Swanepoel, R.; Ansari, A. A.; Peters, C. J. Markedly Elevated Levels of Interferon (IFN)-Gamma, IFN-Alpha, Interleukin (IL)-2, IL-10, and Tumor Necrosis Factor-Alpha Associated with Fatal Ebola Virus Infection. *J. Infect. Dis.* **1999**, *179 Suppl 1*, S188-191. <https://doi.org/10.1086/514283>.
- (75) Feldmann, H.; Bugany, H.; Mahner, F.; Klenk, H. D.; Drenckhahn, D.; Schnittler, H. J. Filovirus-Induced Endothelial Leakage Triggered by Infected Monocytes/Macrophages. *J. Virol.* **1996**, *70* (4), 2208–2214.
- (76) Geisbert, T. W.; Young, H. A.; Jahrling, P. B.; Davis, K. J.; Larsen, T.; Kagan, E.; Hensley, L. E. Pathogenesis of Ebola Hemorrhagic Fever in Primate Models: Evidence That Hemorrhage Is Not a Direct Effect of Virus-Induced Cytolysis of Endothelial Cells. *Am. J. Pathol.* **2003**, *163* (6), 2371–2382. [https://doi.org/10.1016/S0002-9440\(10\)63592-4](https://doi.org/10.1016/S0002-9440(10)63592-4).
- (77) Zaki, S. R.; Goldsmith, C. S. Pathologic Features of Filovirus Infections in Humans. *Curr. Top. Microbiol. Immunol.* **1999**, *235*, 97–116.
- (78) Conway, E. M.; Rosenberg, R. D. Tumor Necrosis Factor Suppresses Transcription of the Thrombomodulin Gene in Endothelial Cells. *Mol. Cell. Biol.* **1988**, *8* (12), 5588–5592.
- (79) Neumann, F. J.; Ott, I.; Marx, N.; Luther, T.; Kenngott, S.; Gawaz, M.; Kotzsch, M.; Schömig, A. Effect of Human Recombinant Interleukin-6 and Interleukin-8 on Monocyte Procoagulant Activity. *Arterioscler. Thromb. Vasc. Biol.* **1997**, *17* (12), 3399–3405.
- (80) Baseler, L.; Chertow, D. S.; Johnson, K. M.; Feldmann, H.; Morens, D. M. The Pathogenesis of Ebola Virus Disease. *Annual Review of Pathology: Mechanisms of Disease* **2017**, *12* (1), 387–418. <https://doi.org/10.1146/annurev-pathol-052016-100506>.
- (81) Viana, M.; Mancy, R.; Biek, R.; Cleaveland, S.; Cross, P. C.; Lloyd-Smith, J. O.; Haydon, D. T. Assembling Evidence for Identifying Reservoirs of Infection. *Trends Ecol. Evol. (Amst.)* **2014**, *29* (5), 270–279. <https://doi.org/10.1016/j.tree.2014.03.002>.
- (82) Plowright, R. K.; Eby, P.; Hudson, P. J.; Smith, I. L.; Westcott, D.; Bryden, W. L.; Middleton, D.; Reid, P. A.; McFarlane, R. A.; Martin, G.; et al. Ecological Dynamics of Emerging Bat Virus Spillover. *Proc. Biol. Sci.* **2015**, *282* (1798), 20142124. <https://doi.org/10.1098/rspb.2014.2124>.
- (83) Glynn, J. R. Age-Specific Incidence of Ebola Virus Disease. *Lancet* **2015**, *386* (9992), 432. [https://doi.org/10.1016/S0140-6736\(15\)61446-5](https://doi.org/10.1016/S0140-6736(15)61446-5).
- (84) Dowell, S. F.; Mukunu, R.; Ksiazek, T. G.; Khan, A. S.; Rollin, P. E.; Peters, C. J. Transmission of Ebola Hemorrhagic Fever: A Study of Risk Factors in Family Members, Kikwit, Democratic Republic of the Congo, 1995. Commission de Lutte Contre Les Epidémies à Kikwit. *J. Infect. Dis.* **1999**, *179 Suppl 1*, S87-91. <https://doi.org/10.1086/514284>.
- (85) Dean, N. E.; Halloran, M. E.; Yang, Y.; Longini, I. M. Transmissibility and Pathogenicity of Ebola Virus: A Systematic Review and Meta-Analysis of Household Secondary Attack Rate and Asymptomatic Infection. *Clin. Infect. Dis.* **2016**, *62* (10), 1277–1286. <https://doi.org/10.1093/cid/ciw114>.
- (86) Martinez, R. B.; Ng, D. L.; Greer, P. W.; Rollin, P. E.; Zaki, S. R. Tissue and Cellular Tropism, Pathology and Pathogenesis of Ebola and Marburg Viruses. *The Journal of Pathology* **2015**, *235* (2), 153–174. <https://doi.org/10.1002/path.4456>.

- (87) Ajelli, M.; Parlamento, S.; Bome, D.; Kebbi, A.; Atzori, A.; Frasson, C.; Putoto, G.; Carraro, D.; Merler, S. The 2014 Ebola Virus Disease Outbreak in Pujehun, Sierra Leone: Epidemiology and Impact of Interventions. *BMC Med* **2015**, *13*, 281. <https://doi.org/10.1186/s12916-015-0524-z>.
- (88) Lokuge, K.; Caleo, G.; Greig, J.; Duncombe, J.; McWilliam, N.; Squire, J.; Lamin, M.; Veltus, E.; Wolz, A.; Kobinger, G.; et al. Successful Control of Ebola Virus Disease: Analysis of Service Based Data from Rural Sierra Leone. *PLoS Negl Trop Dis* **2016**, *10* (3), e0004498. <https://doi.org/10.1371/journal.pntd.0004498>.
- (89) Fischer, R.; Judson, S.; Miazgowicz, K.; Bushmaker, T.; Prescott, J.; Munster, V. J. Ebola Virus Stability on Surfaces and in Fluids in Simulated Outbreak Environments. *Emerging Infect. Dis.* **2015**, *21* (7), 1243–1246. <https://doi.org/10.3201/eid2107.150253>.
- (90) Johnson, E.; Jaax, N.; White, J.; Jahrling, P. Lethal Experimental Infections of Rhesus Monkeys by Aerosolized Ebola Virus. *Int J Exp Pathol* **1995**, *76* (4), 227–236.
- (91) Reed, D. S.; Lackemeyer, M. G.; Garza, N. L.; Sullivan, L. J.; Nichols, D. K. Aerosol Exposure to Zaire Ebolavirus in Three Nonhuman Primate Species: Differences in Disease Course and Clinical Pathology. *Microbes Infect.* **2011**, *13* (11), 930–936. <https://doi.org/10.1016/j.micinf.2011.05.002>.
- (92) Geisbert, T. W.; Hensley, L. E.; Larsen, T.; Young, H. A.; Reed, D. S.; Geisbert, J. B.; Scott, D. P.; Kagan, E.; Jahrling, P. B.; Davis, K. J. Pathogenesis of Ebola Hemorrhagic Fever in Cynomolgus Macaques. *Am J Pathol* **2003**, *163* (6), 2347–2370.
- (93) Twenhafel, N. A.; Mattix, M. E.; Johnson, J. C.; Robinson, C. G.; Pratt, W. D.; Cashman, K. A.; Wahl-Jensen, V.; Terry, C.; Olinger, G. G.; Hensley, L. E.; et al. Pathology of Experimental Aerosol Zaire Ebolavirus Infection in Rhesus Macaques. *Vet. Pathol.* **2013**, *50* (3), 514–529. <https://doi.org/10.1177/0300985812469636>.
- (94) Gatherer, D. The 2014 Ebola Virus Disease Outbreak in West Africa. *J. Gen. Virol.* **2014**, *95* (Pt 8), 1619–1624. <https://doi.org/10.1099/vir.0.067199-0>.
- (95) Kortepeter, M. G.; Bausch, D. G.; Bray, M. Basic Clinical and Laboratory Features of Filoviral Hemorrhagic Fever. *J. Infect. Dis.* **2011**, *204 Suppl 3*, S810–816. <https://doi.org/10.1093/infdis/jir299>.
- (96) Tiffany, A.; Vetter, P.; Mattia, J.; Dayer, J.-A.; Bartsch, M.; Kasztura, M.; Sterk, E.; Tijerino, A. M.; Kaiser, L.; Ciglenecki, I. Ebola Virus Disease Complications as Experienced by Survivors in Sierra Leone. *Clin. Infect. Dis.* **2016**, *62* (11), 1360–1366. <https://doi.org/10.1093/cid/ciw158>.
- (97) Jacobs, M.; Rodger, A.; Bell, D. J.; Bhagani, S.; Cropley, I.; Filipe, A.; Gifford, R. J.; Hopkins, S.; Hughes, J.; Jabeen, F.; et al. Late Ebola Virus Relapse Causing Meningoencephalitis: A Case Report. *Lancet* **2016**, *388* (10043), 498–503. [https://doi.org/10.1016/S0140-6736\(16\)30386-5](https://doi.org/10.1016/S0140-6736(16)30386-5).
- (98) Faye, O.; Andronico, A.; Faye, O.; Salje, H.; Boëlle, P.-Y.; Magassouba, N.; Bah, E. I.; Koivogui, L.; Diallo, B.; Diallo, A. A.; et al. Use of Viremia to Evaluate the Baseline Case Fatality Ratio of Ebola Virus Disease and Inform Treatment Studies: A Retrospective Cohort Study. *PLoS Med* **2015**, *12* (12). <https://doi.org/10.1371/journal.pmed.1001908>.

- (99) Rowe, A. K.; Bertolli, J.; Khan, A. S.; Mukunu, R.; Muyembe-Tamfum, J. J.; Bressler, D.; Williams, A. J.; Peters, C. J.; Rodriguez, L.; Feldmann, H.; et al. Clinical, Virologic, and Immunologic Follow-Up of Convalescent Ebola Hemorrhagic Fever Patients and Their Household Contacts, Kikwit, Democratic Republic of the Congo. *J Infect Dis* **1999**, *179* (Supplement_1), S28–S35. <https://doi.org/10.1086/514318>.
- (100) Hunt, L.; Gupta-Wright, A.; Simms, V.; Tamba, F.; Knott, V.; Tamba, K.; Heisenberg-Mansaray, S.; Tamba, E.; Sheriff, A.; Conteh, S.; et al. Clinical Presentation, Biochemical, and Haematological Parameters and Their Association with Outcome in Patients with Ebola Virus Disease: An Observational Cohort Study. *Lancet Infect Dis* **2015**, *15* (11), 1292–1299. [https://doi.org/10.1016/S1473-3099\(15\)00144-9](https://doi.org/10.1016/S1473-3099(15)00144-9).
- (101) Outbreaks Chronology: Marburg Hemorrhagic Fever | Marburg Hemorrhagic Fever (Marburg HF) | CDC <https://www.cdc.gov/vhf/marburg/outbreaks/chronology.html> (accessed Sep 13, 2018).
- (102) Years of Ebola Virus Disease Outbreaks | 2014-2016 Outbreak West Africa | History | Ebola (Ebola Virus Disease) | CDC <https://www.cdc.gov/vhf/ebola/history/chronology.html> (accessed Sep 13, 2018).
- (103) Martini, G. A. Marburg Virus Disease. Clinical Syndrome. In *Marburg Virus Disease*; Martini, G. A., Siegert, R., Eds.; Springer Berlin Heidelberg: Berlin, Heidelberg, 1971; pp 1–9. https://doi.org/10.1007/978-3-662-01593-3_1.
- (104) Smith, D. H.; Isaacson, M.; Johnson, K. M.; Bagshawe, A.; Johnson, B. K.; Swanapoel, R.; Killey, M.; Siongok, T.; Koinange Keruga, W. MARBURG-VIRUS DISEASE IN KENYA. *The Lancet* **1982**, *319* (8276), 816–820. [https://doi.org/10.1016/S0140-6736\(82\)91871-2](https://doi.org/10.1016/S0140-6736(82)91871-2).
- (105) Ebola Haemorrhagic Fever in Sudan, 1976. *Bull World Health Organ* **1978**, *56* (2), 247–270.
- (106) Ebola Haemorrhagic Fever in Zaire, 1976. *Bull World Health Organ* **1978**, *56* (2), 271–293.
- (107) Bell, B. P. Overview, Control Strategies, and Lessons Learned in the CDC Response to the 2014–2016 Ebola Epidemic. *MMWR Suppl* **2016**, *65*. <https://doi.org/10.15585/mmwr.su6503a2>.
- (108) Coltart, C. E. M.; Lindsey, B.; Ghinai, I.; Johnson, A. M.; Heymann, D. L. The Ebola Outbreak, 2013–2016: Old Lessons for New Epidemics. *Phil. Trans. R. Soc. B* **2017**, *372* (1721), 20160297. <https://doi.org/10.1098/rstb.2016.0297>.
- (109) Lupton, H.; Lambert, R.; Bumgardner, D.; Moe, J.; Eddy, G. INACTIVATED VACCINE FOR EBOLA VIRUS EFFICACIOUS IN GUINEAPIG MODEL. *The Lancet* **1980**, *316* (8207), 1294–1295. [https://doi.org/10.1016/S0140-6736\(80\)92352-1](https://doi.org/10.1016/S0140-6736(80)92352-1).
- (110) Gross, L.; Lhomme, E.; Pasin, C.; Richert, L.; Thiebaut, R. Ebola Vaccine Development: Systematic Review of Pre-Clinical and Clinical Studies, and Meta-Analysis of Determinants of Antibody Response Variability after Vaccination. *International Journal of Infectious Diseases* **2018**, *74*, 83–96. <https://doi.org/10.1016/j.ijid.2018.06.022>.
- (111) Grant-Klein, R. J.; Van Deusen, N. M.; Badger, C. V.; Hannaman, D.; Dupuy, L. C.; Schmaljohn, C. S. A Multiagent Filovirus DNA Vaccine Delivered by Intramuscular Electroporation Completely Protects Mice from Ebola and Marburg Virus Challenge. *Hum Vaccin Immunother* **2012**, *8* (11), 1703–1706. <https://doi.org/10.4161/hv.21873>.

- (112) Vanderzanden, L.; Bray, M.; Fuller, D.; Roberts, T.; Custer, D.; Spik, K.; Jahrling, P.; Huggins, J.; Schmaljohn, A.; Schmaljohn, C. DNA Vaccines Expressing Either the GP or NP Genes of Ebola Virus Protect Mice from Lethal Challenge. *Virology* **1998**, *246* (1), 134–144. <https://doi.org/10.1006/viro.1998.9176>.
- (113) Patel, A.; Scott, V.; Wong, G.; Reuschel, E.; Villarreal, D.; Muthumani, K.; Shedlock, D.; Yan, J.; Tierney, K.; Sardesai, N.; et al. A Single Immunization with Optimized DNA Vaccines Protects against Lethal Ebola Virus Challenge in Mice (VAC8P.1057). *The Journal of Immunology* **2015**, *194* (1 Supplement), 144.13-144.13.
- (114) Martin, J. E.; Sullivan, N. J.; Enama, M. E.; Gordon, I. J.; Roederer, M.; Koup, R. A.; Bailer, R. T.; Chakrabarti, B. K.; Bailey, M. A.; Gomez, P. L.; et al. A DNA Vaccine for Ebola Virus Is Safe and Immunogenic in a Phase I Clinical Trial. *Clin Vaccine Immunol* **2006**, *13* (11), 1267–1277. <https://doi.org/10.1128/CVI.00162-06>.
- (115) Kibuuka, H.; Berkowitz, N. M.; Millard, M.; Enama, M. E.; Tindikahwa, A.; Sekiziyivu, A. B.; Costner, P.; Sitar, S.; Glover, D.; Hu, Z.; et al. Safety and Immunogenicity of Ebola Virus and Marburg Virus Glycoprotein DNA Vaccines Assessed Separately and Concomitantly in Healthy Ugandan Adults: A Phase 1b, Randomised, Double-Blind, Placebo-Controlled Clinical Trial. *Lancet* **2015**, *385* (9977), 1545–1554. [https://doi.org/10.1016/S0140-6736\(14\)62385-0](https://doi.org/10.1016/S0140-6736(14)62385-0).
- (116) Sarwar, U. N.; Costner, P.; Enama, M. E.; Berkowitz, N.; Hu, Z.; Hendel, C. S.; Sitar, S.; Plummer, S.; Mulangu, S.; Bailer, R. T.; et al. Safety and Immunogenicity of DNA Vaccines Encoding Ebolavirus and Marburgvirus Wild-Type Glycoproteins in a Phase I Clinical Trial. *J. Infect. Dis.* **2015**, *211* (4), 549–557. <https://doi.org/10.1093/infdis/jiu511>.
- (117) Cooper, C. L.; Martins, K. A.; Stronsky, S. M.; Langan, D. P.; Steffens, J.; Van Tongeren, S.; Bavari, S. T-Cell-Dependent Mechanisms Promote Ebola VLP-Induced Antibody Responses, but Are Dispensable for Vaccine-Mediated Protection. *Emerg Microbes Infect* **2017**, *6* (6), e46. <https://doi.org/10.1038/emi.2017.31>.
- (118) Warfield, K. L.; Bosio, C. M.; Welcher, B. C.; Deal, E. M.; Mohamadzadeh, M.; Schmaljohn, A.; Aman, M. J.; Bavari, S. Ebola Virus-like Particles Protect from Lethal Ebola Virus Infection. *Proc Natl Acad Sci U S A* **2003**, *100* (26), 15889–15894. <https://doi.org/10.1073/pnas.2237038100>.
- (119) Warfield, K. L.; Posten, N. A.; Swenson, D. L.; Olinger, G. G.; Esposito, D.; Gillette, W. K.; Hopkins, R. F.; Costantino, J.; Panchal, R. G.; Hartley, J. L.; et al. Filovirus-Like Particles Produced in Insect Cells: Immunogenicity and Protection in Rodents. *J Infect Dis* **2007**, *196* (Supplement_2), S421–S429. <https://doi.org/10.1086/520612>.
- (120) Sun, Y.; Carrion, R.; Ye, L.; Wen, Z.; Ro, Y.-T.; Brasky, K.; Ticer, A. E.; Schwegler, E. E.; Patterson, J. L.; Compans, R. W.; et al. Protection against Lethal Challenge by Ebola Virus-like Particles Produced in Insect Cells. *Virology* **2009**, *383* (1), 12–21. <https://doi.org/10.1016/j.virol.2008.09.020>.
- (121) Melito, P. L.; Qiu, X.; Fernando, L. M.; deVarenes, S. L.; Beniac, D. R.; Booth, T. F.; Jones, S. M. The Creation of Stable Cell Lines Expressing Ebola Virus Glycoproteins and the Matrix Protein VP40 and Generating Ebola Virus-like Particles Utilizing an Ecdysone Inducible Mammalian Expression System. *Journal of Virological Methods* **2008**, *148* (1), 237–243. <https://doi.org/10.1016/j.jviromet.2007.12.004>.

- (122) Chepurinov, A. A.; Ternovoï, V. A.; Dadaeva, A. A.; Dmitriev, I. P.; Sizikova, L. P.; Volchkov, V. E.; Kudoiarova, N. M.; Rudzevich, T. N.; Netesov, S. V.
[Immunobiological properties of vp24 protein of Ebola virus expressed by recombinant vaccinia virus]. *Vopr. Virusol.* **1997**, 42 (3), 115–120.
- (123) Herbert, A. S.; Kuehne, A. I.; Barth, J. F.; Ortiz, R. A.; Nichols, D. K.; Zak, S. E.; Stonier, S. W.; Muhammad, M. A.; Bakken, R. R.; Prugar, L. I.; et al. Venezuelan Equine Encephalitis Virus Replicon Particle Vaccine Protects Nonhuman Primates from Intramuscular and Aerosol Challenge with Ebolavirus. *J Virol* **2013**, 87 (9), 4952–4964. <https://doi.org/10.1128/JVI.03361-12>.
- (124) Reynard, O.; Mokhonov, V.; Mokhonova, E.; Leung, J.; Page, A.; Mateo, M.; Pyankova, O.; Georges-Courbot, M. C.; Raoul, H.; Khromykh, A. A.; et al. Kunjin Virus Replicon-Based Vaccines Expressing Ebola Virus Glycoprotein GP Protect the Guinea Pig Against Lethal Ebola Virus Infection. *J Infect Dis* **2011**, 204 (suppl_3), S1060–S1065. <https://doi.org/10.1093/infdis/jir347>.
- (125) Zhu, F.-C.; Hou, L.-H.; Li, J.-X.; Wu, S.-P.; Liu, P.; Zhang, G.-R.; Hu, Y.-M.; Meng, F.-Y.; Xu, J.-J.; Tang, R.; et al. Safety and Immunogenicity of a Novel Recombinant Adenovirus Type-5 Vector-Based Ebola Vaccine in Healthy Adults in China: Preliminary Report of a Randomised, Double-Blind, Placebo-Controlled, Phase 1 Trial. *The Lancet* **2015**, 385 (9984), 2272–2279. [https://doi.org/10.1016/S0140-6736\(15\)60553-0](https://doi.org/10.1016/S0140-6736(15)60553-0).
- (126) Sullivan, N. J.; Geisbert, T. W.; Geisbert, J. B.; Xu, L.; Yang, Z.; Roederer, M.; Koup, R. A.; Jahrling, P. B.; Nabel, G. J. Accelerated Vaccination for Ebola Virus Haemorrhagic Fever in Non-Human Primates. *Nature* **2003**, 424 (6949), 681–684. <https://doi.org/10.1038/nature01876>.
- (127) Sullivan, N. J.; Hensley, L.; Asiedu, C.; Geisbert, T. W.; Stanley, D.; Johnson, J.; Honko, A.; Olinger, G.; Bailey, M.; Geisbert, J. B.; et al. CD8⁺ Cellular Immunity Mediates RAd5 Vaccine Protection against Ebola Virus Infection of Nonhuman Primates. *Nature Medicine* **2011**, 17 (9), 1128–1131. <https://doi.org/10.1038/nm.2447>.
- (128) Ledgerwood, J. E.; Costner, P.; Desai, N.; Holman, L.; Enama, M. E.; Yamshchikov, G.; Mulangu, S.; Hu, Z.; Andrews, C. A.; Sheets, R. A.; et al. A Replication Defective Recombinant Ad5 Vaccine Expressing Ebola Virus GP Is Safe and Immunogenic in Healthy Adults. *Vaccine* **2010**, 29 (2), 304–313. <https://doi.org/10.1016/j.vaccine.2010.10.037>.
- (129) Stanley, D. A.; Honko, A. N.; Asiedu, C.; Trefry, J. C.; Lau-Kilby, A. W.; Johnson, J. C.; Hensley, L.; Ammendola, V.; Abbate, A.; Grazioli, F.; et al. Chimpanzee Adenovirus Vaccine Generates Acute and Durable Protective Immunity against Ebolavirus Challenge. *Nature Medicine* **2014**, 20 (10), 1126–1129. <https://doi.org/10.1038/nm.3702>.
- (130) De Santis, O.; Audran, R.; Pothin, E.; Warpelin-Decrausaz, L.; Vallotton, L.; Wuerzner, G.; Cochet, C.; Estoppey, D.; Steiner-Monard, V.; Lonchamp, S.; et al. Safety and Immunogenicity of a Chimpanzee Adenovirus-Vectored Ebola Vaccine in Healthy Adults: A Randomised, Double-Blind, Placebo-Controlled, Dose-Finding, Phase 1/2a Study. *The Lancet Infectious Diseases* **2016**, 16 (3), 311–320. [https://doi.org/10.1016/S1473-3099\(15\)00486-7](https://doi.org/10.1016/S1473-3099(15)00486-7).

- (131) Tapia, M. D.; Sow, S. O.; Lyke, K. E.; Haidara, F. C.; Diallo, F.; Doumbia, M.; Traore, A.; Coulibaly, F.; Kodio, M.; Onwuchekwa, U.; et al. Use of ChAd3-EBO-Z Ebola Virus Vaccine in Malian and US Adults, and Boosting of Malian Adults with MVA-BN-Filo: A Phase 1, Single-Blind, Randomised Trial, a Phase 1b, Open-Label and Double-Blind, Dose-Escalation Trial, and a Nested, Randomised, Double-Blind, Placebo-Controlled Trial. *The Lancet Infectious Diseases* **2016**, *16* (1), 31–42. [https://doi.org/10.1016/S1473-3099\(15\)00362-X](https://doi.org/10.1016/S1473-3099(15)00362-X).
- (132) Geisbert, T. W.; Daddario-Dicaprio, K. M.; Lewis, M. G.; Geisbert, J. B.; Grolla, A.; Leung, A.; Paragas, J.; Matthias, L.; Smith, M. A.; Jones, S. M.; et al. Vesicular Stomatitis Virus-Based Ebola Vaccine Is Well-Tolerated and Protects Immunocompromised Nonhuman Primates. *PLoS Pathog.* **2008**, *4* (11), e1000225. <https://doi.org/10.1371/journal.ppat.1000225>.
- (133) Mire, C. E.; Miller, A. D.; Carville, A.; Westmoreland, S. V.; Geisbert, J. B.; Mansfield, K. G.; Feldmann, H.; Hensley, L. E.; Geisbert, T. W. Recombinant Vesicular Stomatitis Virus Vaccine Vectors Expressing Filovirus Glycoproteins Lack Neurovirulence in Nonhuman Primates. *PLoS Negl Trop Dis* **2012**, *6* (3), e1567. <https://doi.org/10.1371/journal.pntd.0001567>.
- (134) Jones, S. M.; Feldmann, H.; Ströher, U.; Geisbert, J. B.; Fernando, L.; Grolla, A.; Klenk, H.-D.; Sullivan, N. J.; Volchkov, V. E.; Fritz, E. A.; et al. Live Attenuated Recombinant Vaccine Protects Nonhuman Primates against Ebola and Marburg Viruses. *Nature Medicine* **2005**, *11* (7), 786–790. <https://doi.org/10.1038/nm1258>.
- (135) Agnandji, S. T.; Huttner, A.; Zinser, M. E.; Njuguna, P.; Dahlke, C.; Fernandes, J. F.; Yerly, S.; Dayer, J.-A.; Kraehling, V.; Kasonta, R.; et al. Phase 1 Trials of RVSF Ebola Vaccine in Africa and Europe. *N Engl J Med* **2016**, *374* (17), 1647–1660. <https://doi.org/10.1056/NEJMoa1502924>.
- (136) Halperin, S. A.; Arribas, J. R.; Rupp, R.; Andrews, C. P.; Chu, L.; Das, R.; Simon, J. K.; Onorato, M. T.; Liu, K.; Martin, J.; et al. Six-Month Safety Data of Recombinant Vesicular Stomatitis Virus–Zaire Ebola Virus Envelope Glycoprotein Vaccine in a Phase 3 Double-Blind, Placebo-Controlled Randomized Study in Healthy Adults. *J Infect Dis* **2017**, *215* (12), 1789–1798. <https://doi.org/10.1093/infdis/jix189>.
- (137) Regules, J. A.; Beigel, J. H.; Paolino, K. M.; Voell, J.; Castellano, A. R.; Hu, Z.; Muñoz, P.; Moon, J. E.; Ruck, R. C.; Bennett, J. W.; et al. A Recombinant Vesicular Stomatitis Virus Ebola Vaccine. *N Engl J Med* **2017**, *376* (4), 330–341. <https://doi.org/10.1056/NEJMoa1414216>.
- (138) Feldmann, H.; Jones, S. M.; Daddario-DiCaprio, K. M.; Geisbert, J. B.; Ströher, U.; Grolla, A.; Bray, M.; Fritz, E. A.; Fernando, L.; Feldmann, F.; et al. Effective Post-Exposure Treatment of Ebola Infection. *PLoS Pathog.* **2007**, *3* (1), e2. <https://doi.org/10.1371/journal.ppat.0030002>.
- (139) Jones, S. M.; Stroher, U.; Fernando, L.; Qiu, X.; Alimonti, J.; Melito, P.; Bray, M.; Klenk, H.-D.; Feldmann, H. Assessment of a Vesicular Stomatitis Virus-Based Vaccine by Use of the Mouse Model of Ebola Virus Hemorrhagic Fever. *J. Infect. Dis.* **2007**, *196 Suppl 2*, S404–412. <https://doi.org/10.1086/520591>.

- (140) Henao-Restrepo, A. M.; Camacho, A.; Longini, I. M.; Watson, C. H.; Edmunds, W. J.; Egger, M.; Carroll, M. W.; Dean, N. E.; Diatta, I.; Doumbia, M.; et al. Efficacy and Effectiveness of an RVS-V-Vectored Vaccine in Preventing Ebola Virus Disease: Final Results from the Guinea Ring Vaccination, Open-Label, Cluster-Randomised Trial (Ebola Ça Suffit!). *Lancet* **2017**, 389 (10068), 505–518. [https://doi.org/10.1016/S0140-6736\(16\)32621-6](https://doi.org/10.1016/S0140-6736(16)32621-6).
- (141) Dolzhikova, I. V.; Zubkova, O. V.; Tukhvatulin, A. I.; Dzharullaeva, A. S.; Tukhvatulina, N. M.; Shcheblyakov, D. V.; Shmarov, M. M.; Tokarskaya, E. A.; Simakova, Y. V.; Egorova, D. A.; et al. Safety and Immunogenicity of GamEvac-Combi, a Heterologous VSV- and Ad5-Vectored Ebola Vaccine: An Open Phase I/II Trial in Healthy Adults in Russia. *Hum Vaccin Immunother* **2017**, 13 (3), 613–620. <https://doi.org/10.1080/21645515.2016.1238535>.
- (142) Furuta, Y.; Gowen, B. B.; Takahashi, K.; Shiraki, K.; Smee, D. F.; Barnard, D. L. Favipiravir (T-705), a Novel Viral RNA Polymerase Inhibitor. *Antiviral Res.* **2013**, 100 (2), 446–454. <https://doi.org/10.1016/j.antiviral.2013.09.015>.
- (143) Oestereich, L.; Lüdtke, A.; Wurr, S.; Rieger, T.; Muñoz-Fontela, C.; Günther, S. Successful Treatment of Advanced Ebola Virus Infection with T-705 (Favipiravir) in a Small Animal Model. *Antiviral Res.* **2014**, 105, 17–21. <https://doi.org/10.1016/j.antiviral.2014.02.014>.
- (144) Smither, S. J.; Eastaugh, L. S.; Steward, J. A.; Nelson, M.; Lenk, R. P.; Lever, M. S. Post-Exposure Efficacy of Oral T-705 (Favipiravir) against Inhalational Ebola Virus Infection in a Mouse Model. *Antiviral Res.* **2014**, 104, 153–155. <https://doi.org/10.1016/j.antiviral.2014.01.012>.
- (145) Sissoko, D.; Laouenan, C.; Folkesson, E.; M'Lebing, A.-B.; Beavogui, A.-H.; Baize, S.; Camara, A.-M.; Maes, P.; Shepherd, S.; Danel, C.; et al. Experimental Treatment with Favipiravir for Ebola Virus Disease (the JIKI Trial): A Historically Controlled, Single-Arm Proof-of-Concept Trial in Guinea. *PLoS Med.* **2016**, 13 (3), e1001967. <https://doi.org/10.1371/journal.pmed.1001967>.
- (146) Cho, A.; Saunders, O. L.; Butler, T.; Zhang, L.; Xu, J.; Vela, J. E.; Feng, J. Y.; Ray, A. S.; Kim, C. U. Synthesis and Antiviral Activity of a Series of 1'-Substituted 4-Aza-7,9-Dideazaadenosine C-Nucleosides. *Bioorg. Med. Chem. Lett.* **2012**, 22 (8), 2705–2707. <https://doi.org/10.1016/j.bmcl.2012.02.105>.
- (147) Siegel, D.; Hui, H. C.; Doerffler, E.; Clarke, M. O.; Chun, K.; Zhang, L.; Neville, S.; Carra, E.; Lew, W.; Ross, B.; et al. Discovery and Synthesis of a Phosphoramidate Prodrug of a Pyrrolo[2,1-f][Triazin-4-Amino] Adenine C-Nucleoside (GS-5734) for the Treatment of Ebola and Emerging Viruses. *J. Med. Chem.* **2017**, 60 (5), 1648–1661. <https://doi.org/10.1021/acs.jmedchem.6b01594>.
- (148) Warren, T. K.; Jordan, R.; Lo, M. K.; Ray, A. S.; Mackman, R. L.; Soloveva, V.; Siegel, D.; Perron, M.; Bannister, R.; Hui, H. C.; et al. Therapeutic Efficacy of the Small Molecule GS-5734 against Ebola Virus in Rhesus Monkeys. *Nature* **2016**, 531 (7594), 381–385. <https://doi.org/10.1038/nature17180>.
- (149) Dörnemann, J.; Burzio, C.; Ronsse, A.; Sprecher, A.; De Clerck, H.; Van Herp, M.; Kolić, M.-C.; Yosifiva, V.; Caluwaerts, S.; McElroy, A. K.; et al. First Newborn Baby to Receive Experimental Therapies Survives Ebola Virus Disease. *J. Infect. Dis.* **2017**, 215 (2), 171–174. <https://doi.org/10.1093/infdis/jiw493>.

- (150) Warren, T. K.; Wells, J.; Panchal, R. G.; Stuthman, K. S.; Garza, N. L.; Van Tongeren, S. A.; Dong, L.; Retterer, C. J.; Eaton, B. P.; Pegoraro, G.; et al. Protection against Filovirus Diseases by a Novel Broad-Spectrum Nucleoside Analogue BCX4430. *Nature* **2014**, *508* (7496), 402–405. <https://doi.org/10.1038/nature13027>.
- (151) Julander, J. G.; Bantia, S.; Taubenheim, B. R.; Minning, D. M.; Kotian, P.; Morrey, J. D.; Smee, D. F.; Sheridan, W. P.; Babu, Y. S. BCX4430, a Novel Nucleoside Analog, Effectively Treats Yellow Fever in a Hamster Model. *Antimicrob. Agents Chemother.* **2014**, *58* (11), 6607–6614. <https://doi.org/10.1128/AAC.03368-14>.
- (152) Taylor, R.; Kotian, P.; Warren, T.; Panchal, R.; Bavari, S.; Julander, J.; Dobo, S.; Rose, A.; El-Kattan, Y.; Taubenheim, B.; et al. BCX4430 - A Broad-Spectrum Antiviral Adenosine Nucleoside Analog under Development for the Treatment of Ebola Virus Disease. *J Infect Public Health* **2016**, *9* (3), 220–226. <https://doi.org/10.1016/j.jiph.2016.04.002>.
- (153) Hostetler, K. Y. Synthesis and Early Development of Hexadecyloxypropylcidofovir: An Oral Antipoxvirus Nucleoside Phosphonate. *Viruses* **2010**, *2* (10), 2213–2225. <https://doi.org/10.3390/v2102213>.
- (154) McMullan, L. K.; Flint, M.; Dyall, J.; Albariño, C.; Olinger, G. G.; Foster, S.; Sethna, P.; Hensley, L. E.; Nichol, S. T.; Lanier, E. R.; et al. The Lipid Moiety of Brincidofovir Is Required for in Vitro Antiviral Activity against Ebola Virus. *Antiviral Res.* **2016**, *125*, 71–78. <https://doi.org/10.1016/j.antiviral.2015.10.010>.
- (155) Dunning, J.; Kennedy, S. B.; Antierens, A.; Whitehead, J.; Ciglenecki, I.; Carson, G.; Kanapathipillai, R.; Castle, L.; Howell-Jones, R.; Pardinaz-Solis, R.; et al. Experimental Treatment of Ebola Virus Disease with Brincidofovir. *PLoS ONE* **2016**, *11* (9), e0162199. <https://doi.org/10.1371/journal.pone.0162199>.
- (156) Shurtleff, A. C.; Whitehouse, C. A.; Ward, M. D.; Cazares, L. H.; Bavari, S. Pre-Symptomatic Diagnosis and Treatment of Filovirus Diseases. *Front Microbiol* **2015**, *6*, 108. <https://doi.org/10.3389/fmicb.2015.00108>.
- (157) Thi, E. P.; Mire, C. E.; Lee, A. C. H.; Geisbert, J. B.; Zhou, J. Z.; Agans, K. N.; Snead, N. M.; Deer, D. J.; Barnard, T. R.; Fenton, K. A.; et al. Lipid Nanoparticle SiRNA Treatment of Ebola-Virus-Makona-Infected Nonhuman Primates. *Nature* **2015**, *521* (7552), 362–365. <https://doi.org/10.1038/nature14442>.
- (158) Kugelman, J. R.; Sanchez-Lockhart, M.; Andersen, K. G.; Gire, S.; Park, D. J.; Sealfon, R.; Lin, A. E.; Wohl, S.; Sabeti, P. C.; Kuhn, J. H.; et al. Evaluation of the Potential Impact of Ebola Virus Genomic Drift on the Efficacy of Sequence-Based Candidate Therapeutics. *mBio* **2015**, *6* (1), e02227-14. <https://doi.org/10.1128/mBio.02227-14>.
- (159) Dunning, J.; Sahr, F.; Rojek, A.; Gannon, F.; Carson, G.; Idriss, B.; Massaquoi, T.; Gandi, R.; Joseph, S.; Osman, H. K.; et al. Experimental Treatment of Ebola Virus Disease with TKM-130803: A Single-Arm Phase 2 Clinical Trial. *PLoS Med.* **2016**, *13* (4), e1001997. <https://doi.org/10.1371/journal.pmed.1001997>.
- (160) Iversen, P. L.; Warren, T. K.; Wells, J. B.; Garza, N. L.; Mourich, D. V.; Welch, L. S.; Panchal, R. G.; Bavari, S. Discovery and Early Development of AVI-7537 and AVI-7288 for the Treatment of Ebola Virus and Marburg Virus Infections. *Viruses* **2012**, *4* (11), 2806–2830. <https://doi.org/10.3390/v4112806>.

- (161) Warren, T. K.; Whitehouse, C. A.; Wells, J.; Welch, L.; Heald, A. E.; Charleston, J. S.; Sazani, P.; Reid, S. P.; Iversen, P. L.; Bavari, S. A Single Phosphorodiamidate Morpholino Oligomer Targeting VP24 Protects Rhesus Monkeys against Lethal Ebola Virus Infection. *mBio* **2015**, *6* (1), e02344-14. <https://doi.org/10.1128/mBio.02344-14>.
- (162) Heald, A. E.; Iversen, P. L.; Saoud, J. B.; Sazani, P.; Charleston, J. S.; Axtelle, T.; Wong, M.; Smith, W. B.; Vutikullird, A.; Kaye, E. Safety and Pharmacokinetic Profiles of Phosphorodiamidate Morpholino Oligomers with Activity against Ebola Virus and Marburg Virus: Results of Two Single-Ascending-Dose Studies. *Antimicrob. Agents Chemother.* **2014**, *58* (11), 6639–6647. <https://doi.org/10.1128/AAC.03442-14>.
- (163) Gutfraind, A.; Meyers, L. A. Evaluating Large-Scale Blood Transfusion Therapy for the Current Ebola Epidemic in Liberia. *J Infect Dis* **2015**, *211* (8), 1262–1267. <https://doi.org/10.1093/infdis/jiv042>.
- (164) van Griensven, J.; Edwards, T.; de Lamballerie, X.; Semple, M. G.; Gallian, P.; Baize, S.; Horby, P. W.; Raoul, H.; Magassouba, N.; Antierens, A.; et al. Evaluation of Convalescent Plasma for Ebola Virus Disease in Guinea. *N. Engl. J. Med.* **2016**, *374* (1), 33–42. <https://doi.org/10.1056/NEJMoa1511812>.
- (165) Dye, J. M.; Herbert, A. S.; Kuehne, A. I.; Barth, J. F.; Muhammad, M. A.; Zak, S. E.; Ortiz, R. A.; Prugar, L. I.; Pratt, W. D. Postexposure Antibody Prophylaxis Protects Nonhuman Primates from Filovirus Disease. *Proc. Natl. Acad. Sci. U.S.A.* **2012**, *109* (13), 5034–5039. <https://doi.org/10.1073/pnas.1200409109>.
- (166) Lyon, G. M.; Mehta, A. K.; Varkey, J. B.; Brantly, K.; Plyler, L.; McElroy, A. K.; Kraft, C. S.; Towner, J. S.; Spiropoulou, C.; Ströher, U.; et al. Clinical Care of Two Patients with Ebola Virus Disease in the United States http://www.nejm.org/doi/10.1056/NEJMoa1409838?url_ver=Z39.88-2003&rfr_id=ori%3Arid%3Acrossref.org&rfr_dat=cr_pub%3Dwww.ncbi.nlm.nih.gov (accessed Sep 14, 2018). <https://doi.org/10.1056/NEJMoa1409838>.
- (167) Mendoza, E. J.; Qiu, X.; Kobinger, G. P. Progression of Ebola Therapeutics During the 2014-2015 Outbreak. *Trends Mol Med* **2016**, *22* (2), 164–173. <https://doi.org/10.1016/j.molmed.2015.12.005>.
- (168) Zhao, Y.; Ren, J.; Harlos, K.; Jones, D. M.; Zeltina, A.; Bowden, T. A.; Padilla-Parra, S.; Fry, E. E.; Stuart, D. I. Toremifene Interacts with and Destabilizes the Ebola Virus Glycoprotein. *Nature* **2016**, *535* (7610), 169–172. <https://doi.org/10.1038/nature18615>.
- (169) Ren, J.; Zhao, Y.; Fry, E. E.; Stuart, D. I. Target Identification and Mode of Action of Four Chemically Divergent Drugs against Ebolavirus Infection. *J Med Chem* **2018**, *61* (3), 724–733. <https://doi.org/10.1021/acs.jmedchem.7b01249>.
- (170) Zhao, Y.; Ren, J.; Fry, E. E.; Xiao, J.; Townsend, A. R.; Stuart, D. I. Structures of Ebola Virus Glycoprotein Complexes with Tricyclic Antidepressant and Antipsychotic Drugs. *J. Med. Chem.* **2018**, *61* (11), 4938–4945. <https://doi.org/10.1021/acs.jmedchem.8b00350>.
- (171) Qiu, S.; Leung, A.; Bo, Y.; Kozak, R. A.; Anand, S. P.; Warkentin, C.; Salambanga, F. D. R.; Cui, J.; Kobinger, G.; Kobasa, D.; et al. Ebola Virus Requires Phosphatidylinositol (3,5) Bisphosphate Production for Efficient Viral Entry. *Virology* **2018**, *513*, 17–28. <https://doi.org/10.1016/j.virol.2017.09.028>.

- (172) Nelson, E. A.; Dyall, J.; Hoenen, T.; Barnes, A. B.; Zhou, H.; Liang, J. Y.; Michelotti, J.; Dewey, W. H.; DeWald, L. E.; Bennett, R. S.; et al. The Phosphatidylinositol-3-Phosphate 5-Kinase Inhibitor Apilimod Blocks Filoviral Entry and Infection. *PLoS Negl Trop Dis* **2017**, *11* (4), e0005540. <https://doi.org/10.1371/journal.pntd.0005540>.
- (173) Liu, H.; Tian, Y.; Lee, K.; Krishnan, P.; Wang, M. K.-M.; Whelan, S.; Mevers, E.; Soloveva, V.; Dedic, B.; Liu, X.; et al. Identification of Potent Ebola Virus Entry Inhibitors with Suitable Properties for in Vivo Studies. *J. Med. Chem.* **2018**, *61* (14), 6293–6307. <https://doi.org/10.1021/acs.jmedchem.8b00704>.
- (174) Lu, F.; Liang, Q.; Abi-Mosleh, L.; Das, A.; De Brabander, J. K.; Goldstein, J. L.; Brown, M. S. Identification of NPC1 as the Target of U18666A, an Inhibitor of Lysosomal Cholesterol Export and Ebola Infection. *eLife* **4**. <https://doi.org/10.7554/eLife.12177>.
- (175) Sun, W.; He, S.; Martínez-Romero, C.; Kouznetsova, J.; Tawa, G.; Xu, M.; Shinn, P.; Fisher, E.; Long, Y.; Motabar, O.; et al. Synergistic Drug Combination Effectively Blocks Ebola Virus Infection. *Antiviral Res.* **2017**, *137*, 165–172. <https://doi.org/10.1016/j.antiviral.2016.11.017>.
- (176) Gehring, G.; Rohrmann, K.; Atenchong, N.; Mittler, E.; Becker, S.; Dahlmann, F.; Pöhlmann, S.; Vondran, F. W. R.; David, S.; Manns, M. P.; et al. The Clinically Approved Drugs Amiodarone, Dronedarone and Verapamil Inhibit Filovirus Cell Entry. *J Antimicrob Chemother* **2014**, *69* (8), 2123–2131. <https://doi.org/10.1093/jac/dku091>.
- (177) Johansen, L. M.; DeWald, L. E.; Shoemaker, C. J.; Hoffstrom, B. G.; Lear-Rooney, C. M.; Stossel, A.; Nelson, E.; Delos, S. E.; Simmons, J. A.; Grenier, J. M.; et al. A Screen of Approved Drugs and Molecular Probes Identifies Therapeutics with Anti-Ebola Virus Activity. *Science Translational Medicine* **2015**, *7* (290), 290ra89–290ra89. <https://doi.org/10.1126/scitranslmed.aaa5597>.
- (178) Nishimura, H.; Yamaya, M. A Synthetic Serine Protease Inhibitor, Nafamostat Mesilate, Is a Drug Potentially Applicable to the Treatment of Ebola Virus Disease. *Tohoku J. Exp. Med.* **2015**, *237* (1), 45–50. <https://doi.org/10.1620/tjem.237.45>.
- (179) Moorthy, N. S. H. N.; Poongavanam, V.; Pratheepa, V. Viral M2 Ion Channel Protein: A Promising Target for Anti-Influenza Drug Discovery. *Mini Rev Med Chem* **2014**, *14* (10), 819–830.
- (180) Müller, K. H.; Kainov, D. E.; El Bakkouri, K.; Saelens, X.; De Brabander, J. K.; Kittel, C.; Samm, E.; Muller, C. P. The Proton Translocation Domain of Cellular Vacuolar ATPase Provides a Target for the Treatment of Influenza A Virus Infections. *Br. J. Pharmacol.* **2011**, *164* (2), 344–357. <https://doi.org/10.1111/j.1476-5381.2011.01346.x>.
- (181) Prchla, E.; Kuechler, E.; Blaas, D.; Fuchs, R. Uncoating of Human Rhinovirus Serotype 2 from Late Endosomes. *J. Virol.* **1994**, *68* (6), 3713–3723.
- (182) Persaud, M.; Martinez-Lopez, A.; Buffone, C.; Porcelli, S. A.; Diaz-Griffero, F. Infection by Zika Viruses Requires the Transmembrane Protein AXL, Endocytosis and Low PH. *Virology* **2018**, *518*, 301–312. <https://doi.org/10.1016/j.virol.2018.03.009>.
- (183) Cheng, H.; Lear-Rooney, C. M.; Johansen, L.; Varhegyi, E.; Chen, Z. W.; Olinger, G. G.; Rong, L. Inhibition of Ebola and Marburg Virus Entry by G Protein-Coupled Receptor Antagonists. *J Virol* **2015**, *89* (19), 9932–9938. <https://doi.org/10.1128/JVI.01337-15>.
- (184) Glomb-Reinmund, S.; Kielian, M. The Role of Low PH and Disulfide Shuffling in the Entry and Fusion of Semliki Forest Virus and Sindbis Virus. *Virology* **1998**, *248* (2), 372–381. <https://doi.org/10.1006/viro.1998.9275>.

- (185) Müller, K. H.; Spoden, G. A.; Scheffer, K. D.; Brunnhöfer, R.; Brabander, J. K. D.; Maier, M. E.; Florin, L.; Muller, C. P. Inhibition by Cellular Vacuolar ATPase Impairs Human Papillomavirus Uncoating and Infection. *Antimicrob. Agents Chemother.* **2014**, 58 (5), 2905–2911. <https://doi.org/10.1128/AAC.02284-13>.
- (186) Pavelin, J.; McCormick, D.; Chiweshe, S.; Ramachandran, S.; Lin, Y.-T.; Grey, F. Cellular V-ATPase Is Required for Virion Assembly Compartment Formation in Human Cytomegalovirus Infection. *Open Biol* **2017**, 7 (11). <https://doi.org/10.1098/rsob.160298>.
- (187) Zheng, A.; Umashankar, M.; Kielian, M. In Vitro and in Vivo Studies Identify Important Features of Dengue Virus Pr-E Protein Interactions. *PLoS Pathog.* **2010**, 6 (10), e1001157. <https://doi.org/10.1371/journal.ppat.1001157>.
- (188) Cotter, K.; Stransky, L.; McGuire, C.; Forgac, M. Recent Insights into the Structure, Regulation, and Function of the V-ATPases. *Trends in Biochemical Sciences* **2015**, 40 (10), 611–622. <https://doi.org/10.1016/j.tibs.2015.08.005>.
- (189) Marshansky, V.; Rubinstein, J. L.; Grüber, G. Eukaryotic V-ATPase: Novel Structural Findings and Functional Insights. *Biochim. Biophys. Acta* **2014**, 1837 (6), 857–879. <https://doi.org/10.1016/j.bbabi.2014.01.018>.
- (190) Pedersen, P. L.; Ko, Y. H.; Hong, S. ATP Synthases in the Year 2000: Evolving Views about the Structures of These Remarkable Enzyme Complexes. *J Bioenerg Biomembr* **2000**, 32 (4), 325–332. <https://doi.org/10.1023/A:1005594800983>.
- (191) Nelson, N. A Journey from Mammals to Yeast with Vacuolar H⁺-ATPase (V-ATPase). *J Bioenerg Biomembr* **2003**, 35 (4), 281–289. <https://doi.org/10.1023/A:1025768529677>.
- (192) Mazhab-Jafari, M. T.; Rubinstein, J. L. Cryo-EM Studies of the Structure and Dynamics of Vacuolar-Type ATPases. *Sci Adv* **2016**, 2 (7), e1600725. <https://doi.org/10.1126/sciadv.1600725>.
- (193) Kane, P. M. The Where, When, and How of Organelle Acidification by the Yeast Vacuolar H⁺-ATPase. *Microbiol. Mol. Biol. Rev.* **2006**, 70 (1), 177–191. <https://doi.org/10.1128/MMBR.70.1.177-191.2006>.
- (194) Toei, M.; Saum, R.; Forgac, M. Regulation and Isoform Function of the V-ATPases. *Biochemistry* **2010**, 49 (23), 4715–4723. <https://doi.org/10.1021/bi100397s>.
- (195) Forgac, M. Vacuolar ATPases: Rotary Proton Pumps in Physiology and Pathophysiology. *Nat Rev Mol Cell Biol* **2007**, 8 (11), 917–929. <https://doi.org/10.1038/nrm2272>.
- (196) Smith, G. A.; Howell, G. J.; Phillips, C.; Muench, S. P.; Ponnambalam, S.; Harrison, M. A. Extracellular and Luminal PH Regulation by Vacuolar H⁺-ATPase Isoform Expression and Targeting to the Plasma Membrane and Endosomes. *J Biol Chem* **2016**, 291 (16), 8500–8515. <https://doi.org/10.1074/jbc.M116.723395>.
- (197) Lau, W. C. Y.; Rubinstein, J. L. Structure of Intact *Thermus Thermophilus* V-ATPase by Cryo-EM Reveals Organization of the Membrane-Bound VO Motor. *Proc Natl Acad Sci U S A* **2010**, 107 (4), 1367–1372. <https://doi.org/10.1073/pnas.0911085107>.
- (198) Stam, N. J.; Wilkens, S. Structure of the Lipid Nanodisc-Reconstituted Vacuolar ATPase Proton Channel: DEFINITION OF THE INTERACTION OF ROTOR AND STATOR AND IMPLICATIONS FOR ENZYME REGULATION BY REVERSIBLE DISSOCIATION. *J. Biol. Chem.* **2017**, 292 (5), 1749–1761. <https://doi.org/10.1074/jbc.M116.766790>.

- (199) Shao, E.; Forgac, M. Involvement of the Nonhomologous Region of Subunit A of the Yeast V-ATPase in Coupling and in Vivo Dissociation. *J. Biol. Chem.* **2004**, 279 (47), 48663–48670. <https://doi.org/10.1074/jbc.M408278200>.
- (200) Vasilyeva, E.; Forgac, M. 3'-O-(4-Benzoyl)Benzoyladenosine 5'-Triphosphate Inhibits Activity of the Vacuolar (H⁺)-ATPase from Bovine Brain Clathrin-Coated Vesicles by Modification of a Rapidly Exchangeable, Noncatalytic Nucleotide Binding Site on the B Subunit. *J. Biol. Chem.* **1996**, 271 (22), 12775–12782. <https://doi.org/10.1074/jbc.271.22.12775>.
- (201) Chen, Y.-C.; Backus, K. M.; Merkulova, M.; Yang, C.; Brown, D.; Cravatt, B. F.; Zhang, C. Covalent Modulators of the Vacuolar ATPase. *J. Am. Chem. Soc.* **2017**, 139 (2), 639–642. <https://doi.org/10.1021/jacs.6b12511>.
- (202) Paunescu, T. G.; Da Silva, N.; Marshansky, V.; McKee, M.; Breton, S.; Brown, D. Expression of the 56-KDa B2 Subunit Isoform of the Vacuolar H⁺-ATPase in Proton-Secreting Cells of the Kidney and Epididymis. *Am. J. Physiol., Cell Physiol.* **2004**, 287 (1), C149–162. <https://doi.org/10.1152/ajpcell.00464.2003>.
- (203) Holliday, L. S.; Lu, M.; Lee, B. S.; Nelson, R. D.; Solivan, S.; Zhang, L.; Gluck, S. L. The Amino-Terminal Domain of the B Subunit of Vacuolar H⁺-ATPase Contains a Filamentous Actin Binding Site. *J. Biol. Chem.* **2000**, 275 (41), 32331–32337. <https://doi.org/10.1074/jbc.M004795200>.
- (204) Drory, O.; Frolow, F.; Nelson, N. Crystal Structure of Yeast V-ATPase Subunit C Reveals Its Stator Function. *EMBO Rep.* **2004**, 5 (12), 1148–1152. <https://doi.org/10.1038/sj.embor.7400294>.
- (205) Voss, M.; Vitavska, O.; Walz, B.; Wiczorek, H.; Baumann, O. Stimulus-Induced Phosphorylation of Vacuolar H⁺-ATPase by Protein Kinase A. *J. Biol. Chem.* **2007**, 282 (46), 33735–33742. <https://doi.org/10.1074/jbc.M703368200>.
- (206) Imamura, H.; Nakano, M.; Noji, H.; Muneyuki, E.; Ohkuma, S.; Yoshida, M.; Yokoyama, K. Evidence for Rotation of V1-ATPase. *Proc. Natl. Acad. Sci. U.S.A.* **2003**, 100 (5), 2312–2315. <https://doi.org/10.1073/pnas.0436796100>.
- (207) Sun-Wada, G.-H.; Imai-Senga, Y.; Yamamoto, A.; Murata, Y.; Hirata, T.; Wada, Y.; Futai, M. A Proton Pump ATPase with Testis-Specific E1-Subunit Isoform Required for Acrosome Acidification. *J. Biol. Chem.* **2002**, 277 (20), 18098–18105. <https://doi.org/10.1074/jbc.M111567200>.
- (208) Makyio, H.; Iino, R.; Ikeda, C.; Imamura, H.; Tamakoshi, M.; Iwata, M.; Stock, D.; Bernal, R. A.; Carpenter, E. P.; Yoshida, M.; et al. Structure of a Central Stalk Subunit F of Prokaryotic V-Type ATPase/Synthase from *Thermus Thermophilus*. *EMBO J.* **2005**, 24 (22), 3974–3983. <https://doi.org/10.1038/sj.emboj.7600859>.
- (209) Muench, S. P.; Scheres, S. H. W.; Huss, M.; Phillips, C.; Vitavska, O.; Wiczorek, H.; Trinick, J.; Harrison, M. A. Subunit Positioning and Stator Filament Stiffness in Regulation and Power Transmission in the V1 Motor of the *Manduca Sexta* V-ATPase. *J. Mol. Biol.* **2014**, 426 (2), 286–300. <https://doi.org/10.1016/j.jmb.2013.09.018>.
- (210) Jefferies, K. C.; Forgac, M. Subunit H of the V-ATPase Inhibits ATP Hydrolysis by the Free V1 Domain by Interaction with the Rotary Subunit F. *J Biol Chem* **2008**, 283 (8), 4512–4519. <https://doi.org/10.1074/jbc.M707144200>.
- (211) Liu, M.; Tarsio, M.; Charsky, C. M. H.; Kane, P. M. Structural and Functional Separation of the N- and C-Terminal Domains of the Yeast V-ATPase Subunit H. *J. Biol. Chem.* **2005**, 280 (44), 36978–36985. <https://doi.org/10.1074/jbc.M505296200>.

- (212) Nishi, T.; Kawasaki-Nishi, S.; Forgac, M. Expression and Function of the Mouse V-ATPase d Subunit Isoforms. *J. Biol. Chem.* **2003**, 278 (47), 46396–46402. <https://doi.org/10.1074/jbc.M303924200>.
- (213) Lee, S.-H.; Rho, J.; Jeong, D.; Sul, J.-Y.; Kim, T.; Kim, N.; Kang, J.-S.; Miyamoto, T.; Suda, T.; Lee, S.-K.; et al. V-ATPase V0 Subunit D2-Deficient Mice Exhibit Impaired Osteoclast Fusion and Increased Bone Formation. *Nat Med* **2006**, 12 (12), 1403–1409. <https://doi.org/10.1038/nm1514>.
- (214) Smith, A. N.; Jouret, F.; Bord, S.; Borthwick, K. J.; Al-Lamki, R. S.; Wagner, C. A.; Ireland, D. C.; Cormier-Daire, V.; Frattini, A.; Villa, A.; et al. Vacuolar H⁺-ATPase D2 Subunit: Molecular Characterization, Developmental Regulation, and Localization to Specialized Proton Pumps in Kidney and Bone. *J. Am. Soc. Nephrol.* **2005**, 16 (5), 1245–1256. <https://doi.org/10.1681/ASN.2004090761>.
- (215) Esmail, S.; Kartner, N.; Yao, Y.; Kim, J. W.; Reithmeier, R. A. F.; Manolson, M. F. N-Linked Glycosylation of a Subunit Isoforms Is Critical for Vertebrate Vacuolar H⁺ -ATPase (V-ATPase) Biosynthesis. *J. Cell. Biochem.* **2018**, 119 (1), 861–875. <https://doi.org/10.1002/jcb.26250>.
- (216) Jansen, E. J. R.; Timal, S.; Ryan, M.; Ashikov, A.; Scherpenzeel, M. van; Graham, L. A.; Mandel, H.; Hoischen, A.; Iancu, T. C.; Raymond, K.; et al. ATP6AP1 Deficiency Causes an Immunodeficiency with Hepatopathy, Cognitive Impairment and Abnormal Protein Glycosylation. *Nature Communications* **2016**, 7. <https://doi.org/10.1038/ncomms11600>.
- (217) Jansen, E. J. R.; van Bakel, N. H. M.; Olde Loohuis, N. F. M.; Hafmans, T. G. M.; Arentsen, T.; Coenen, A. J. M.; Scheenen, W. J. J. M.; Martens, G. J. M. Identification of Domains within the V-ATPase Accessory Subunit Ac45 Involved in V-ATPase Transport and Ca²⁺-Dependent Exocytosis. *J. Biol. Chem.* **2012**, 287 (33), 27537–27546. <https://doi.org/10.1074/jbc.M112.356105>.
- (218) Zhao, J.; Benlekbi, S.; Rubinstein, J. L. Electron Cryomicroscopy Observation of Rotational States in a Eukaryotic V-ATPase. *Nature* **2015**, 521 (7551), 241–245. <https://doi.org/10.1038/nature14365>.
- (219) Păunescu, T. G.; Jones, A. C.; Tyszkowski, R.; Brown, D. V-ATPase Expression in the Mouse Olfactory Epithelium. *Am J Physiol Cell Physiol* **2008**, 295 (4), C923–C930. <https://doi.org/10.1152/ajpcell.00237.2008>.
- (220) Smith, A. N.; Borthwick, K. J.; Karet, F. E. Molecular Cloning and Characterization of Novel Tissue-Specific Isoforms of the Human Vacuolar H⁽⁺⁾-ATPase C, G and d Subunits, and Their Evaluation in Autosomal Recessive Distal Renal Tubular Acidosis. *Gene* **2002**, 297 (1–2), 169–177.
- (221) Morel, N.; Dedieu, J.-C.; Philippe, J.-M. Specific Sorting of the A1 Isoform of the V-H⁺ATPase a Subunit to Nerve Terminals Where It Associates with Both Synaptic Vesicles and the Presynaptic Plasma Membrane. *J. Cell. Sci.* **2003**, 116 (Pt 23), 4751–4762. <https://doi.org/10.1242/jcs.00791>.
- (222) Toyomura, T.; Murata, Y.; Yamamoto, A.; Oka, T.; Sun-Wada, G.-H.; Wada, Y.; Futai, M. From Lysosomes to the Plasma Membrane: Localization of Vacuolar-Type H⁺ -ATPase with the A3 Isoform during Osteoclast Differentiation. *J. Biol. Chem.* **2003**, 278 (24), 22023–22030. <https://doi.org/10.1074/jbc.M302436200>.

- (223) Hurtado-Lorenzo, A.; Skinner, M.; Annan, J. E.; Futai, M.; Sun-Wada, G.-H.; Bourgoïn, S.; Casanova, J.; Wildeman, A.; Bechoua, S.; Ausiello, D. A.; et al. V-ATPase Interacts with ARNO and Arf6 in Early Endosomes and Regulates the Protein Degradative Pathway. *Nature Cell Biology* **2006**, 8 (2), 124–136. <https://doi.org/10.1038/ncb1348>.
- (224) Sun-Wada, G.-H.; Tabata, H.; Kawamura, N.; Futai, M.; Wada, Y. Differential Expression of a Subunit Isoforms of the Vacuolar-Type Proton Pump ATPase in Mouse Endocrine Tissues. *Cell Tissue Res.* **2007**, 329 (2), 239–248. <https://doi.org/10.1007/s00441-007-0421-7>.
- (225) McGuire, C.; Cotter, K.; Stransky, L.; Forgac, M. Regulation of V-ATPase Assembly and Function of V-ATPases in Tumor Cell Invasiveness. *Biochim. Biophys. Acta* **2016**, 1857 (8), 1213–1218. <https://doi.org/10.1016/j.bbabbio.2016.02.010>.
- (226) Capecci, J.; Forgac, M. The Function of Vacuolar ATPase (V-ATPase) a Subunit Isoforms in Invasiveness of MCF10a and MCF10CA1a Human Breast Cancer Cells. *J. Biol. Chem.* **2013**, 288 (45), 32731–32741. <https://doi.org/10.1074/jbc.M113.503771>.
- (227) Wagner, C. A.; Finberg, K. E.; Breton, S.; Marshansky, V.; Brown, D.; Geibel, J. P. Renal Vacuolar H⁺-ATPase. *Physiological Reviews* **2004**, 84 (4), 1263–1314. <https://doi.org/10.1152/physrev.00045.2003>.
- (228) Kane, P. M.; Parra, K. J. Assembly and Regulation of the Yeast Vacuolar H⁽⁺⁾-ATPase. *Journal of Experimental Biology* **2000**, 203 (1), 81–87.
- (229) Stransky, L. A.; Forgac, M. Amino Acid Availability Modulates Vacuolar H⁺-ATPase Assembly. *J. Biol. Chem.* **2015**, 290 (45), 27360–27369. <https://doi.org/10.1074/jbc.M115.659128>.
- (230) Dechant, R.; Binda, M.; Lee, S. S.; Pelet, S.; Winderickx, J.; Peter, M. Cytosolic PH Is a Second Messenger for Glucose and Regulates the PKA Pathway through V-ATPase. *EMBO J.* **2010**, 29 (15), 2515–2526. <https://doi.org/10.1038/emboj.2010.138>.
- (231) Sautin, Y. Y.; Lu, M.; Gaugler, A.; Zhang, L.; Gluck, S. L. Phosphatidylinositol 3-Kinase-Mediated Effects of Glucose on Vacuolar H⁺-ATPase Assembly, Translocation, and Acidification of Intracellular Compartments in Renal Epithelial Cells. *Mol. Cell. Biol.* **2005**, 25 (2), 575–589. <https://doi.org/10.1128/MCB.25.2.575-589.2005>.
- (232) Chen, S.-H.; Bubbs, M. R.; Yarmola, E. G.; Zuo, J.; Jiang, J.; Lee, B. S.; Lu, M.; Gluck, S. L.; Hurst, I. R.; Holliday, L. S. Vacuolar H⁺-ATPase Binding to Microfilaments: Regulation in Response to Phosphatidylinositol 3-Kinase Activity and Detailed Characterization of the Actin-Binding Site in Subunit B. *J. Biol. Chem.* **2004**, 279 (9), 7988–7998. <https://doi.org/10.1074/jbc.M305351200>.
- (233) Trombetta, E. S.; Ebersold, M.; Garrett, W.; Pypaert, M.; Mellman, I. Activation of Lysosomal Function During Dendritic Cell Maturation. *Science* **2003**, 299 (5611), 1400–1403. <https://doi.org/10.1126/science.1080106>.
- (234) McGuire, C. M.; Forgac, M. Glucose Starvation Increases V-ATPase Assembly and Activity in Mammalian Cells through AMP Kinase and Phosphatidylinositide 3-Kinase/Akt Signaling. *J Biol Chem* **2018**, 293 (23), 9113–9123. <https://doi.org/10.1074/jbc.RA117.001327>.
- (235) Xu, Y.; Parmar, A.; Roux, E.; Balbis, A.; Dumas, V.; Chevalier, S.; Posner, B. I. Epidermal Growth Factor-Induced Vacuolar (H⁺)-Atpase Assembly: A Role in Signaling via MTORC1 Activation. *J. Biol. Chem.* **2012**, 287 (31), 26409–26422. <https://doi.org/10.1074/jbc.M112.352229>.

- (236) Marjuki, H.; Gornitzky, A.; Marathe, B. M.; Ilyushina, N. A.; Aldridge, J. R.; Desai, G.; Webby, R. J.; Webster, R. G. Influenza A Virus-Induced Early Activation of ERK and PI3K Mediates V-ATPase-Dependent Intracellular pH Change Required for Fusion. *Cell. Microbiol.* **2011**, *13* (4), 587–601. <https://doi.org/10.1111/j.1462-5822.2010.01556.x>.
- (237) Alzamora, R.; Thali, R. F.; Gong, F.; Smolak, C.; Li, H.; Baty, C. J.; Bertrand, C. A.; Auchli, Y.; Brunisholz, R. A.; Neumann, D.; et al. PKA Regulates Vacuolar H⁺-ATPase Localization and Activity via Direct Phosphorylation of the α Subunit in Kidney Cells. *J. Biol. Chem.* **2010**, *285* (32), 24676–24685. <https://doi.org/10.1074/jbc.M110.106278>.
- (238) Alzamora, R.; Al-Bataineh, M. M.; Liu, W.; Gong, F.; Li, H.; Thali, R. F.; Joho-Auchli, Y.; Brunisholz, R. A.; Satlin, L. M.; Neumann, D.; et al. AMP-Activated Protein Kinase Regulates the Vacuolar H⁺-ATPase via Direct Phosphorylation of the α Subunit (ATP6V1A) in the Kidney. *Am. J. Physiol. Renal Physiol.* **2013**, *305* (7), F943–956. <https://doi.org/10.1152/ajprenal.00303.2013>.
- (239) Shum, W. W.; Da Silva, N.; Belleannée, C.; McKee, M.; Brown, D.; Breton, S. Regulation of V-ATPase Recycling via a RhoA- and ROCKII-Dependent Pathway in Epididymal Clear Cells. *Am. J. Physiol., Cell Physiol.* **2011**, *301* (1), C31–43. <https://doi.org/10.1152/ajpcell.00198.2010>.
- (240) Cruciat, C.-M.; Ohkawara, B.; Acebron, S. P.; Karaulanov, E.; Reinhard, C.; Ingelfinger, D.; Boutros, M.; Niehrs, C. Requirement of Prorenin Receptor and Vacuolar H⁺-ATPase-Mediated Acidification for Wnt Signaling. *Science* **2010**, *327* (5964), 459–463. <https://doi.org/10.1126/science.1179802>.
- (241) Hermle, T.; Saltukoglu, D.; Grünwald, J.; Walz, G.; Simons, M. Regulation of Frizzled-Dependent Planar Polarity Signaling by a V-ATPase Subunit. *Curr. Biol.* **2010**, *20* (14), 1269–1276. <https://doi.org/10.1016/j.cub.2010.05.057>.
- (242) Yan, Y.; Deneff, N.; Schüpbach, T. The Vacuolar Proton Pump, V-ATPase, Is Required for Notch Signaling and Endosomal Trafficking in *Drosophila*. *Dev. Cell* **2009**, *17* (3), 387–402. <https://doi.org/10.1016/j.devcel.2009.07.001>.
- (243) Zoncu, R.; Bar-Peled, L.; Efeyan, A.; Wang, S.; Sancak, Y.; Sabatini, D. M. mTORC1 Senses Lysosomal Amino Acids through an Inside-out Mechanism That Requires the Vacuolar H⁽⁺⁾-ATPase. *Science* **2011**, *334* (6056), 678–683. <https://doi.org/10.1126/science.1207056>.
- (244) Uhlman, A.; Folkers, K.; Liston, J.; Pancholi, H.; Hinton, A. Effects of Vacuolar H⁺-ATPase Inhibition on Activation of Cathepsin B and Cathepsin L Secreted from MDA-MB231 Breast Cancer Cells. *Cancer Microenviron* **2017**, *10* (1–3), 49–56. <https://doi.org/10.1007/s12307-017-0196-7>.
- (245) Kubisch, R.; Fröhlich, T.; Arnold, G. J.; Schreiner, L.; von Schwarzenberg, K.; Roidl, A.; Vollmar, A. M.; Wagner, E. V-ATPase Inhibition by Archazolid Leads to Lysosomal Dysfunction Resulting in Impaired Cathepsin B Activation in Vivo. *Int. J. Cancer* **2014**, *134* (10), 2478–2488. <https://doi.org/10.1002/ijc.28562>.
- (246) Pungercar, J. R.; Caglic, D.; Sajid, M.; Dolinar, M.; Vasiljeva, O.; Pozgan, U.; Turk, D.; Bogyo, M.; Turk, V.; Turk, B. Autocatalytic Processing of Procathepsin B Is Triggered by Proenzyme Activity. *FEBS J.* **2009**, *276* (3), 660–668. <https://doi.org/10.1111/j.1742-4658.2008.06815.x>.

- (247) Mauvezin, C.; Neufeld, T. P. Bafilomycin A1 Disrupts Autophagic Flux by Inhibiting Both V-ATPase-Dependent Acidification and Ca-P60A/SERCA-Dependent Autophagosome-Lysosome Fusion. *Autophagy* **2015**, *11* (8), 1437–1438. <https://doi.org/10.1080/15548627.2015.1066957>.
- (248) Mauvezin, C.; Nagy, P.; Juhász, G.; Neufeld, T. P. Autophagosome-Lysosome Fusion Is Independent of V-ATPase-Mediated Acidification. *Nat Commun* **2015**, *6*, 7007. <https://doi.org/10.1038/ncomms8007>.
- (249) El Mestikawy, S.; Wallén-Mackenzie, A.; Fortin, G. M.; Descarries, L.; Trudeau, L.-E. From Glutamate Co-Release to Vesicular Synergy: Vesicular Glutamate Transporters. *Nat. Rev. Neurosci.* **2011**, *12* (4), 204–216. <https://doi.org/10.1038/nrn2969>.
- (250) Fisher, J. M.; Scheller, R. H. Prohormone Processing and the Secretory Pathway. *J. Biol. Chem.* **1988**, *263* (32), 16515–16518.
- (251) Sun-Wada, G.-H.; Toyomura, T.; Murata, Y.; Yamamoto, A.; Futai, M.; Wada, Y. The A3 Isoform of V-ATPase Regulates Insulin Secretion from Pancreatic Beta-Cells. *J. Cell. Sci.* **2006**, *119* (Pt 21), 4531–4540. <https://doi.org/10.1242/jcs.03234>.
- (252) Sun-Wada, G.-H.; Wada, Y. Vacuolar-Type Proton Pump ATPases: Acidification and Pathological Relationships. *Histol. Histopathol.* **2013**, *28* (7), 805–815. <https://doi.org/10.14670/HH-28.805>.
- (253) Breton, S.; Brown, D. Regulation of Luminal Acidification by the V-ATPase. *Physiology (Bethesda)* **2013**, *28* (5), 318–329. <https://doi.org/10.1152/physiol.00007.2013>.
- (254) Brown, D.; Breton, S. H(+)V-ATPase-Dependent Luminal Acidification in the Kidney Collecting Duct and the Epididymis/Vas Deferens: Vesicle Recycling and Transcytotic Pathways. *Journal of Experimental Biology* **2000**, *203* (1), 137–145.
- (255) Smith, A. N.; Skaug, J.; Choate, K. A.; Nayir, A.; Bakkaloglu, A.; Ozen, S.; Hulton, S. A.; Sanjad, S. A.; Al-Sabban, E. A.; Lifton, R. P.; et al. Mutations in *ATP6N1B*, Encoding a New Kidney Vacuolar Proton Pump 116-KD Subunit, Cause Recessive Distal Renal Tubular Acidosis with Preserved Hearing. *Nature Genetics* **2000**, *26* (1), 71–75. <https://doi.org/10.1038/79208>.
- (256) Hennings, J. C.; Picard, N.; Huebner, A. K.; Stauber, T.; Maier, H.; Brown, D.; Jentsch, T. J.; Vargas-Poussou, R.; Eladari, D.; Hübner, C. A. A Mouse Model for Distal Renal Tubular Acidosis Reveals a Previously Unrecognized Role of the V-ATPase A4 Subunit in the Proximal Tubule. *EMBO Mol Med* **2012**, *4* (10), 1057–1071. <https://doi.org/10.1002/emmm.201201527>.
- (257) Da Silva, N.; Shum, W. W. C.; El-Annan, J.; Păunescu, T. G.; McKee, M.; Smith, P. J. S.; Brown, D.; Breton, S. Relocalization of the V-ATPase B2 Subunit to the Apical Membrane of Epididymal Clear Cells of Mice Deficient in the B1 Subunit. *American Journal of Physiology-Cell Physiology* **2007**, *293* (1), C199–C210. <https://doi.org/10.1152/ajpcell.00596.2006>.
- (258) Frattini, A.; Orchard, P. J.; Sobacchi, C.; Giliani, S.; Abinun, M.; Mattsson, J. P.; Keeling, D. J.; Andersson, A. K.; Wallbrandt, P.; Zecca, L.; et al. Defects in TCIRG1 Subunit of the Vacuolar Proton Pump Are Responsible for a Subset of Human Autosomal Recessive Osteopetrosis. *Nat. Genet.* **2000**, *25* (3), 343–346. <https://doi.org/10.1038/77131>.

- (259) Zhang, Y.; Huang, H.; Zhao, G.; Yokoyama, T.; Vega, H.; Huang, Y.; Sood, R.; Bishop, K.; Maduro, V.; Accardi, J.; et al. ATP6V1H Deficiency Impairs Bone Development through Activation of MMP9 and MMP13. *PLoS Genet* **2017**, *13* (2). <https://doi.org/10.1371/journal.pgen.1006481>.
- (260) Qin, A.; Cheng, T. S.; Pavlos, N. J.; Lin, Z.; Dai, K. R.; Zheng, M. H. V-ATPases in Osteoclasts: Structure, Function and Potential Inhibitors of Bone Resorption. *The International Journal of Biochemistry & Cell Biology* **2012**, *44* (9), 1422–1435. <https://doi.org/10.1016/j.biocel.2012.05.014>.
- (261) Sasazawa, Y.; Futamura, Y.; Tashiro, E.; Imoto, M. Vacuolar H⁺-ATPase Inhibitors Overcome Bcl-XL-Mediated Chemoresistance through Restoration of a Caspase-Independent Apoptotic Pathway. *Cancer Sci.* **2009**, *100* (8), 1460–1467. <https://doi.org/10.1111/j.1349-7006.2009.01194.x>.
- (262) Niikura, K.; Takeshita, N.; Takano, M. A Vacuolar ATPase Inhibitor, FR167356, Prevents Bone Resorption in Ovariectomized Rats With High Potency and Specificity: Potential for Clinical Application. *Journal of Bone and Mineral Research* **2005**, *20* (9), 1579–1588. <https://doi.org/10.1359/JBMR.050517>.
- (263) Cotter, K.; Capecci, J.; Sennoune, S.; Huss, M.; Maier, M.; Martinez-Zaguilan, R.; Forgac, M. Activity of Plasma Membrane V-ATPases Is Critical for the Invasion of MDA-MB231 Breast Cancer Cells. *J Biol Chem* **2015**, *290* (6), 3680–3692. <https://doi.org/10.1074/jbc.M114.611210>.
- (264) Merk, H.; Messer, P.; Ardelt, M. A.; Lamb, D. C.; Zahler, S.; Müller, R.; Vollmar, A. M.; Pachmayr, J. Inhibition of the V-ATPase by Archazolid A: A New Strategy to Inhibit EMT. *Mol Cancer Ther* **2017**, *16* (11), 2329–2339. <https://doi.org/10.1158/1535-7163.MCT-17-0129>.
- (265) König, R.; Stertz, S.; Zhou, Y.; Inoue, A.; Hoffmann, H.-H.; Bhattacharyya, S.; Alamares, J. G.; Tscherne, D. M.; Ortigoza, M. B.; Liang, Y.; et al. Human Host Factors Required for Influenza Virus Replication. *Nature* **2010**, *463* (7282), 813–817. <https://doi.org/10.1038/nature08699>.
- (266) Müller, K. H.; Kainov, D. E.; El Bakkouri, K.; Saelens, X.; De Brabander, J. K.; Kittel, C.; Samm, E.; Muller, C. P. The Proton Translocation Domain of Cellular Vacuolar ATPase Provides a Target for the Treatment of Influenza A Virus Infections. *Br. J. Pharmacol.* **2011**, *164* (2), 344–357. <https://doi.org/10.1111/j.1476-5381.2011.01346.x>.
- (267) Xu, L.; Shen, X.; Bryan, A.; Banga, S.; Swanson, M. S.; Luo, Z.-Q. Inhibition of Host Vacuolar H⁺-ATPase Activity by a Legionella Pneumophila Effector. *PLoS Pathog.* **2010**, *6* (3), e1000822. <https://doi.org/10.1371/journal.ppat.1000822>.
- (268) Dai, W.-M.; Guan, Y.; Jin, J. Structures and Total Syntheses of the Plecomacrolides. *Curr. Med. Chem.* **2005**, *12* (17), 1947–1993.
- (269) Bowman, E. J.; Siebers, A.; Altendorf, K. Bafilomycins: A Class of Inhibitors of Membrane ATPases from Microorganisms, Animal Cells, and Plant Cells. *PNAS* **1988**, *85* (21), 7972–7976. <https://doi.org/10.1073/pnas.85.21.7972>.
- (270) Bowman, E. J.; Graham, L. A.; Stevens, T. H.; Bowman, B. J. The Bafilomycin/Concanamycin Binding Site in Subunit c of the V-ATPases from Neurospora Crassa and Saccharomyces Cerevisiae. *J. Biol. Chem.* **2004**, *279* (32), 33131–33138. <https://doi.org/10.1074/jbc.M404638200>.

- (271) Bowman, B. J.; Bowman, E. J. Mutations in Subunit c of the Vacuolar ATPase Confer Resistance to Bafilomycin and Identify a Conserved Antibiotic Binding Site. *J. Biol. Chem.* **2002**, 277 (6), 3965–3972. <https://doi.org/10.1074/jbc.M109756200>.
- (272) Yamamoto, A.; Tagawa, Y.; Yoshimori, T.; Moriyama, Y.; Masaki, R.; Tashiro, Y. Bafilomycin A1 Prevents Maturation of Autophagic Vacuoles by Inhibiting Fusion between Autophagosomes and Lysosomes in Rat Hepatoma Cell Line, H-4-II-E Cells. *Cell Struct. Funct.* **1998**, 23 (1), 33–42.
- (273) Bhat, P.; Kriel, J.; Shubha Priya, B.; Basappa; Shivananju, N. S.; Loos, B. Modulating Autophagy in Cancer Therapy: Advancements and Challenges for Cancer Cell Death Sensitization. *Biochemical Pharmacology* **2018**, 147, 170–182. <https://doi.org/10.1016/j.bcp.2017.11.021>.
- (274) Pérez, L.; Carrasco, L. Involvement of the Vacuolar H(+)-ATPase in Animal Virus Entry. *J. Gen. Virol.* **1994**, 75 (Pt 10), 2595–2606. <https://doi.org/10.1099/0022-1317-75-10-2595>.
- (275) Gagliardi, S.; Gatti, P. A.; Belfiore, P.; Zocchetti, A.; Clarke, G. D.; Farina, C. Synthesis and Structure–Activity Relationships of Bafilomycin A1 Derivatives as Inhibitors of Vacuolar H⁺-ATPase. *J. Med. Chem.* **1998**, 41 (11), 1883–1893. <https://doi.org/10.1021/jm9707838>.
- (276) Teplova, V. V.; Tonshin, A. A.; Grigoriev, P. A.; Saris, N.-E. L.; Salkinoja-Salonen, M. S. Bafilomycin A1 Is a Potassium Ionophore That Impairs Mitochondrial Functions. *J Bioenerg Biomembr* **2007**, 39 (4), 321–329. <https://doi.org/10.1007/s10863-007-9095-9>.
- (277) Keeling, D. J.; Herslöf, M.; Ryberg, B.; Sjögren, S.; Sölvell, L. Vacuolar H⁺-ATPases Targets for Drug Discovery? *Annals of the New York Academy of Sciences* **1997**, 834 (1), 600–608. <https://doi.org/10.1111/j.1749-6632.1997.tb52329.x>.
- (278) Sasse, F.; Steinmetz, H.; Höfle, G.; Reichenbach, H. Archazolids, New Cytotoxic Macrolactones from Archangium Gephyra (Myxobacteria). Production, Isolation, Physico-Chemical and Biological Properties. *J. Antibiot.* **2003**, 56 (6), 520–525.
- (279) Huss, M.; Sasse, F.; Kunze, B.; Jansen, R.; Steinmetz, H.; Ingenhorst, G.; Zeeck, A.; Wieczorek, H. Archazolid and Apicularen: Novel Specific V-ATPase Inhibitors. *BMC Biochem.* **2005**, 6, 13. <https://doi.org/10.1186/1471-2091-6-13>.
- (280) Gözl, J. P.; Bockelmann, S.; Mayer, K.; Steinhoff, H.-J.; Wieczorek, H.; Huss, M.; Klare, J. P.; Menche, D. EPR Studies of V-ATPase with Spin-Labeled Inhibitors DCC and Archazolid: Interaction Dynamics with Proton Translocating Subunit C. *ChemMedChem* **2015**, n/a-n/a. <https://doi.org/10.1002/cmdc.201500500>.
- (281) Bockelmann, S.; Menche, D.; Rudolph, S.; Bender, T.; Grond, S.; von Zezschwitz, P.; Muench, S. P.; Wieczorek, H.; Huss, M. Archazolid A Binds to the Equatorial Region of the C-Ring of the Vacuolar H⁺-ATPase. *J. Biol. Chem.* **2010**, 285 (49), 38304–38314. <https://doi.org/10.1074/jbc.M110.137539>.
- (282) Wiedmann, R. M.; von Schwarzenberg, K.; Palamidessi, A.; Schreiner, L.; Kubisch, R.; Liebl, J.; Schempp, C.; Trauner, D.; Vereb, G.; Zahler, S.; et al. The V-ATPase-Inhibitor Archazolid Abrogates Tumor Metastasis via Inhibition of Endocytic Activation of the Rho-GTPase Rac1. *Cancer Res.* **2012**, 72 (22), 5976–5987. <https://doi.org/10.1158/0008-5472.CAN-12-1772>.

- (283) Bartel, K.; Winzi, M.; Ulrich, M.; Koeberle, A.; Menche, D.; Werz, O.; Müller, R.; Guck, J.; Vollmar, A. M.; von Schwarzenberg, K. V-ATPase Inhibition Increases Cancer Cell Stiffness and Blocks Membrane Related Ras Signaling - a New Option for HCC Therapy. *Oncotarget* **2016**, 8 (6), 9476–9487. <https://doi.org/10.18632/oncotarget.14339>.
- (284) Thomas, L.; Rao, Z.; Gerstmeier, J.; Raasch, M.; Weinigel, C.; Rummeler, S.; Menche, D.; Müller, R.; Pergola, C.; Mosig, A.; et al. Selective Upregulation of TNF α Expression in Classically-Activated Human Monocyte-Derived Macrophages (M1) through Pharmacological Interference with V-ATPase. *Biochemical Pharmacology* **2017**, 130, 71–82. <https://doi.org/10.1016/j.bcp.2017.02.004>.
- (285) Kobayashi, J.; Cheng, J.; Ohta, T.; Nakamura, H.; Nozoe, S.; Hirata, Y.; Ohizumi, Y.; Sasaki, T. Iejimalides A and B, Novel 24-Membered Macrolides with Potent Antileukemic Activity from the Okinawan Tunicate Eudistoma Cf. Rigida. *J. Org. Chem.* **1988**, 53 (26), 6147–6150. <https://doi.org/10.1021/jo00261a040>.
- (286) Kikuchi, Y.; Ishibashi, M.; Sasaki, T.; Kobayashi, J. Iejimalides C and D, New Antineoplastic 24-Membered Macrolide Sulfates from the Okinawan Marine Tunicate Eudistoma Cf. Rigida. *Tetrahedron Letters* **1991**, 32 (6), 797–798. [https://doi.org/10.1016/S0040-4039\(00\)74889-1](https://doi.org/10.1016/S0040-4039(00)74889-1).
- (287) Fürstner, A.; Nevado, C.; Waser, M.; Tremblay, M.; Chevrier, C.; Teplý, F.; Aïssa, C.; Moulin, E.; Müller, O. Total Synthesis of Iejimalide A-D and Assessment of the Remarkable Actin-Depolymerizing Capacity of These Polyene Macrolides. *J. Am. Chem. Soc.* **2007**, 129 (29), 9150–9161. <https://doi.org/10.1021/ja072334v>.
- (288) McHenry, P.; Wang, W.-L. W.; Devitt, E.; Kluesner, N.; Davisson, V. J.; McKee, E.; Schweitzer, D.; Helquist, P.; Tenniswood, M. Iejimalides A and B Inhibit Lysosomal Vacuolar H⁺-ATPase (V-ATPase) Activity and Induce S-Phase Arrest and Apoptosis in MCF-7 Cells. *J. Cell. Biochem.* **2010**, 109 (4), 634–642. <https://doi.org/10.1002/jcb.22438>.
- (289) Wang, W.-L. W.; McHenry, P.; Jeffrey, R.; Schweitzer, D.; Helquist, P.; Tenniswood, M. Effects of Iejimalide B, a Marine Macrolide, on Growth and Apoptosis in Prostate Cancer Cell Lines. *J. Cell. Biochem.* **2008**, 105 (4), 998–1007. <https://doi.org/10.1002/jcb.21898>.
- (290) Schweitzer, D.; Zhu, J.; Jarori, G.; Tanaka, J.; Higa, T.; Davisson, V. J.; Helquist, P. Synthesis of Carbamate Derivatives of Iejimalides. Retention of Normal Antiproliferative Activity and Localization of Binding in Cancer Cells. *Bioorg. Med. Chem.* **2007**, 15 (9), 3208–3216. <https://doi.org/10.1016/j.bmc.2007.02.046>.
- (291) Moulin, E.; Nevado, C.; Gagnepain, J.; Kelter, G.; Fiebig, H.-H.; Fürstner, A. Synthesis and Evaluation of an Iejimalide-Archazolid Chimera. *Tetrahedron* **2010**, 66 (33), 6421–6428. <https://doi.org/10.1016/j.tet.2010.05.043>.
- (292) Gagnepain, J.; Moulin, E.; Nevado, C.; Waser, M.; Maier, A.; Kelter, G.; Fiebig, H.-H.; Fürstner, A. Molecular Editing and Assessment of the Cytotoxic Properties of Iejimalide and Progeny. *Chem. Eur. J.* **2011**, 17 (25), 6973–6984. <https://doi.org/10.1002/chem.201100180>.
- (293) Huss, M.; Wiczorek, H. Inhibitors of V-ATPases: Old and New Players. *J Exp Biol* **2009**, 212 (3), 341–346. <https://doi.org/10.1242/jeb.024067>.

- (294) Boyd, M. R.; Farina, C.; Belfiore, P.; Gagliardi, S.; Kim, J. W.; Hayakawa, Y.; Beutler, J. A.; McKee, T. C.; Bowman, B. J.; Bowman, E. J. Discovery of a Novel Antitumor Benzolactone Enamide Class That Selectively Inhibits Mammalian Vacuolar-Type (H⁺)-ATPases. *J Pharmacol Exp Ther* **2001**, 297 (1), 114–120.
- (295) Xie, X.-S.; Padron, D.; Liao, X.; Wang, J.; Roth, M. G.; De Brabander, J. K. Salicylilalamide A Inhibits the V0 Sector of the V-ATPase through a Mechanism Distinct from Bafilomycin A1. *J. Biol. Chem.* **2004**, 279 (19), 19755–19763. <https://doi.org/10.1074/jbc.M313796200>.
- (296) Osteresch, C.; Bender, T.; Grond, S.; von Zezschwitz, P.; Kunze, B.; Jansen, R.; Huss, M.; Wieczorek, H. The Binding Site of the V-ATPase Inhibitor Apicularen Is in the Vicinity of Those for Bafilomycin and Archazolid. *J Biol Chem* **2012**, 287 (38), 31866–31876. <https://doi.org/10.1074/jbc.M112.372169>.
- (297) Kim, J.-S.; Lee, Y.-C.; Nam, H.-T.; Li, G.; Yun, E.-J.; Song, K.-S.; Seo, K.-S.; Park, J.-H.; Ahn, J.-W.; Zee, O.; et al. Apicularen A Induces Cell Death through Fas Ligand Up-Regulation and Microtubule Disruption by Tubulin down-Regulation in HM7 Human Colon Cancer Cells. *Clin. Cancer Res.* **2007**, 13 (21), 6509–6517. <https://doi.org/10.1158/1078-0432.CCR-07-1428>.
- (298) Seo, K.-S.; Kim, H.; Hong, T.-H.; Kim, J.-S.; Song, K.-S.; Yun, E.-J.; Park, J.-H.; Jung, Y.-H.; Park, J.-I.; Kweon, G. R.; et al. Apicularen A Acetate Induces Cell Death via AIF Translocation and Disrupts the Microtubule Network by Down-Regulating Tubulin in HM7 Human Colon Cancer Cells. *Biochem. Biophys. Res. Commun.* **2013**, 434 (3), 634–640. <https://doi.org/10.1016/j.bbrc.2013.03.133>.
- (299) Scherer, O.; Steinmetz, H.; Kaether, C.; Weinigel, C.; Barz, D.; Kleinert, H.; Menche, D.; Müller, R.; Pergola, C.; Werz, O. Targeting V-ATPase in Primary Human Monocytes by Archazolid Potently Represses the Classical Secretion of Cytokines Due to Accumulation at the Endoplasmic Reticulum. *Biochemical Pharmacology* **2014**, 91 (4), 490–500. <https://doi.org/10.1016/j.bcp.2014.07.028>.
- (300) Lebreton, S.; Jaunbergs, J.; Roth, M. G.; Ferguson, D. A.; De Brabander, J. K. Evaluating the Potential of Vacuolar ATPase Inhibitors as Anticancer Agents and Multigram Synthesis of the Potent Salicylilalamide Analog Saliphenylalamide. *Bioorganic & Medicinal Chemistry Letters* **2008**, 18 (22), 5879–5883. <https://doi.org/10.1016/j.bmcl.2008.07.003>.
- (301) Saurin, A. J.; Hamlett, J.; Clague, M. J.; Pennington, S. R. Inhibition of Mitogen-Induced DNA Synthesis by Bafilomycin A1 in Swiss 3T3 Fibroblasts. *Biochemical Journal* **1996**, 313 (1), 65–70. <https://doi.org/10.1042/bj3130065>.
- (302) Nakagawa, H.; Takami, M.; Udagawa, N.; Sawae, Y.; Suda, K.; Sasaki, T.; Takahashi, N.; Wachi, M.; Nagai, K.; Woo, J. T. Destruixins, Cyclodepsipeptides, Block the Formation of Actin Rings and Prominent Clear Zones and Ruffled Borders in Osteoclasts. *Bone* **2003**, 33 (3), 443–455. [https://doi.org/10.1016/S8756-3282\(03\)00201-1](https://doi.org/10.1016/S8756-3282(03)00201-1).
- (303) Woo, J.-T.; Yonezawa, T.; Cha, B.-Y.; Teruya, T.; Nagai, K. Pharmacological Topics of Bone Metabolism: Antiresorptive Microbial Compounds That Inhibit Osteoclast Differentiation, Function, and Survival. *Journal of Pharmacological Sciences* **2008**, 106 (4), 547–554. <https://doi.org/10.1254/jphs.FM0070288>.

- (304) Murata, T.; Takase, K.; Yamato, I.; Igarashi, K.; Kakinuma, Y. Purification and Reconstitution of Na⁺-Translocating Vacuolar ATPase from *Enterococcus Hirae*. *J. Biol. Chem.* **1997**, 272 (40), 24885–24890. <https://doi.org/10.1074/jbc.272.40.24885>.
- (305) Vázquez, M. J.; Albarrán, M. I.; Espada, A.; Rivera-Sagredo, A.; Díez, E.; Hueso-Rodríguez, J. A. A New Destruxin as Inhibitor of Vacuolar-Type H⁺-ATPase of *Saccharomyces Cerevisiae*. *Chemistry & Biodiversity* **2005**, 2 (1), 123–130. <https://doi.org/10.1002/cbdv.200490163>.
- (306) Yoshida, M.; Takeuchi, H.; Ishida, Y.; Yashiroda, Y.; Yoshida, M.; Takagi, M.; Shin-ya, K.; Doi, T. Synthesis, Structure Determination, and Biological Evaluation of Destruxin E. *Org. Lett.* **2010**, 12 (17), 3792–3795. <https://doi.org/10.1021/ol101449x>.
- (307) Zhao, J.; Beyrakhova, K.; Liu, Y.; Alvarez, C. P.; Bueler, S. A.; Xu, L.; Xu, C.; Boniecki, M. T.; Kanelis, V.; Luo, Z.-Q.; et al. Molecular Basis for the Binding and Modulation of V-ATPase by a Bacterial Effector Protein. *PLoS Pathog.* **2017**, 13 (6), e1006394. <https://doi.org/10.1371/journal.ppat.1006394>.
- (308) Prevost, M. S.; Pinotsis, N.; Dumoux, M.; Hayward, R. D.; Waksman, G. The *Legionella* Effector WipB Is a Translocated Ser/Thr Phosphatase That Targets the Host Lysosomal Nutrient Sensing Machinery. *Sci Rep* **2017**, 7. <https://doi.org/10.1038/s41598-017-10249-6>.
- (309) Rahioui, I.; Eyraud, V.; Karaki, L.; Sasse, F.; Carre-Pierrat, M.; Qin, A.; Zheng, M. H.; Toepfer, S.; Sivignon, C.; Royer, C.; et al. Host Range of the Potential Biopesticide Pea Albumin 1b (PA1b) Is Limited to Insects. *Toxicon* **2014**, 89, 67–76. <https://doi.org/10.1016/j.toxicon.2014.07.004>.
- (310) Muench, S. P.; Rawson, S.; Eyraud, V.; Delmas, A. F.; Da Silva, P.; Phillips, C.; Trinick, J.; Harrison, M. A.; Gressent, F.; Huss, M. PA1b Inhibitor Binding to Subunits c and e of the Vacuolar ATPase Reveals Its Insecticidal Mechanism. *J. Biol. Chem.* **2014**, 289 (23), 16399–16408. <https://doi.org/10.1074/jbc.M113.541250>.
- (311) Gagliardi, S.; Nadler, G.; Consolandi, E.; Parini, C.; Morvan, M.; Legave, M.-N.; Belfiore, P.; Zocchetti, A.; Clarke, G. D.; James, I.; et al. 5-(5,6-Dichloro-2-Indolyl)-2-Methoxy-2,4-Pentadienamides: Novel and Selective Inhibitors of the Vacuolar H⁺-ATPase of Osteoclasts with Bone Antiresorptive Activity. *J. Med. Chem.* **1998**, 41 (10), 1568–1573. <https://doi.org/10.1021/jm9800144>.
- (312) Nadler, G.; Morvan, M.; Delimoge, I.; Belfiore, P.; Zocchetti, A.; James, I.; Zembryki, D.; Lee-Rycakzewski, E.; Parini, C.; Consolandi, E.; et al. (2Z,4E)-5-(5,6-Dichloro-2-Indolyl)-2-Methoxy-N-(1,2,2,6,6-Pentamethylpiperidin-4-Yl)-2,4-Pentadienamide, a Novel, Potent and Selective Inhibitor of the Osteoclast V-ATPase. *Bioorganic & Medicinal Chemistry Letters* **1998**, 8 (24), 3621–3626. [https://doi.org/10.1016/S0960-894X\(98\)00660-X](https://doi.org/10.1016/S0960-894X(98)00660-X).
- (313) Dixon, N.; Páli, T.; Kee, T. P.; Ball, S.; Harrison, M. A.; Findlay, J. B. C.; Nyman, J.; Väänänen, K.; Finbow, M. E.; Marsh, D. Interaction of Spin-Labeled Inhibitors of the Vacuolar H⁺-ATPase with the Transmembrane Vo-Sector. *Biophys J* **2008**, 94 (2), 506–514. <https://doi.org/10.1529/biophysj.107.111781>.
- (314) Visentin, L.; Dodds, R. A.; Valente, M.; Misiano, P.; Bradbeer, J. N.; Oneta, S.; Liang, X.; Gowen, M.; Farina, C. A Selective Inhibitor of the Osteoclastic V-H⁺-ATPase Prevents Bone Loss in Both Thyroparathyroidectomized and Ovariectomized Rats. *J Clin Invest* **2000**, 106 (2), 309–318.

- (315) Nyman, J. K. E.; Väänänen, H. K. A Rationale for Osteoclast Selectivity of Inhibiting the Lysosomal V-ATPase A3 Isoform. *Calcif. Tissue Int.* **2010**, *87* (3), 273–283. <https://doi.org/10.1007/s00223-010-9395-7>.
- (316) Farina, C.; Gagliardi, S.; Nadler, G.; Morvan, M.; Parini, C.; Belfiore, P.; Visentin, L.; Gowen, M. Novel Bone Antiresorptive Agents That Selectively Inhibit the Osteoclast V-H⁺-ATPase. *Farmaco* **2001**, *56* (1–2), 113–116.
- (317) Farina, C.; Gagliardi, S. Selective Inhibition of Osteoclast Vacuolar H(+)-ATPase. *Curr. Pharm. Des.* **2002**, *8* (23), 2033–2048.
- (318) Petrangolini, G.; Supino, R.; Pratesi, G.; Dal Bo, L.; Tortoreto, M.; Croce, A. C.; Misiano, P.; Belfiore, P.; Farina, C.; Zunino, F. Effect of a Novel Vacuolar-H⁺-ATPase Inhibitor on Cell and Tumor Response to Camptothecins. *J. Pharmacol. Exp. Ther.* **2006**, *318* (3), 939–946. <https://doi.org/10.1124/jpet.106.103481>.
- (319) Supino, R.; Petrangolini, G.; Pratesi, G.; Tortoreto, M.; Favini, E.; Bo, L. D.; Casalini, P.; Radaelli, E.; Croce, A. C.; Bottiroli, G.; et al. Antimetastatic Effect of a Small-Molecule Vacuolar H⁺-ATPase Inhibitor in in Vitro and in Vivo Preclinical Studies. *J. Pharmacol. Exp. Ther.* **2008**, *324* (1), 15–22. <https://doi.org/10.1124/jpet.107.128587>.
- (320) Supino, R.; Petrangolini, G.; Croce, A. C.; Bo, L. D.; Tortoreto, M.; Pratesi, G.; Misiano, P.; Farina, C.; Zunino, F. A Novel Inhibitor of Vacuolar H⁺-ATPase, NIK-12192, Potentiates the Antitumor Effect of Topotecan in BCRP-Expressing Tumor Systems. *Cancer Res* **2006**, *66* (8 Supplement), 1273–1273.
- (321) Supino, R.; Scovassi, A. I.; Croce, A. C.; Bo, L. D.; Favini, E.; Corbelli, A.; Farina, C.; Misiano, P.; Zunino, F. Biological Effects of a New Vacuolar-H⁺-ATPase Inhibitor in Colon Carcinoma Cell Lines. *Annals of the New York Academy of Sciences* **2009**, *1171* (1), 606–616. <https://doi.org/10.1111/j.1749-6632.2009.04705.x>.
- (322) Niikura, K.; Takano, M.; Sawada, M. A Novel Inhibitor of Vacuolar ATPase, FR167356, Which Can Discriminate between Osteoclast Vacuolar ATPase and Lysosomal Vacuolar ATPase. *Br. J. Pharmacol.* **2004**, *142* (3), 558–566. <https://doi.org/10.1038/sj.bjp.0705812>.
- (323) Nishisho, T.; Hata, K.; Nakanishi, M.; Morita, Y.; Sun-Wada, G.-H.; Wada, Y.; Yasui, N.; Yoneda, T. The A3 Isoform Vacuolar Type H⁺-ATPase Promotes Distant Metastasis in the Mouse B16 Melanoma Cells. *Mol Cancer Res* **2011**, *9* (7), 845–855. <https://doi.org/10.1158/1541-7786.MCR-10-0449>.
- (324) Niikura, K.; Nakajima, S.; Takano, M.; Yamazaki, H. FR177995, a Novel Vacuolar ATPase Inhibitor, Exerts Not Only an Inhibitory Effect on Bone Destruction but Also Anti-Immunoinflammatory Effects in Adjuvant-Induced Arthritic Rats. *Bone* **2007**, *40* (4), 888–894. <https://doi.org/10.1016/j.bone.2006.10.015>.
- (325) Niikura, K. Effect of a V-ATPase Inhibitor, FR202126, in Syngeneic Mouse Model of Experimental Bone Metastasis. *Cancer Chemother. Pharmacol.* **2007**, *60* (4), 555–562. <https://doi.org/10.1007/s00280-006-0401-8>.
- (326) Niikura, K. Comparative Analysis of the Effects of a Novel Vacuolar Adenosine 5'-Triphosphatase Inhibitor, FR202126, and Doxycycline on Bone Loss Caused by Experimental Periodontitis in Rats. *Journal of Periodontology* **2006**, *77* (7), 1211–1216. <https://doi.org/10.1902/jop.2006.050344>.
- (327) Niikura, K.; Takeshita, N.; Chida, N. A Novel Inhibitor of Vacuolar ATPase, FR202126, Prevents Alveolar Bone Destruction in Experimental Periodontitis in Rats. *J Toxicol Sci* **2005**, *30* (4), 297–304.

- (328) Kartner, N.; Yao, Y.; Li, K.; Crasto, G. J.; Datti, A.; Manolson, M. F. Inhibition of Osteoclast Bone Resorption by Disrupting Vacuolar H⁺-ATPase A3-B2 Subunit Interaction. *J Biol Chem* **2010**, 285 (48), 37476–37490. <https://doi.org/10.1074/jbc.M110.123281>.
- (329) Marrone, G.; De Chiara, F.; Böttcher, K.; Levi, A.; Dhar, D.; Longato, L.; Mazza, G.; Zhang, Z.; Marrali, M.; Fernández-Iglesias, A.; et al. The Adenosine Monophosphate-Activated Protein Kinase-Vacuolar Adenosine Triphosphatase-PH Axis: A Key Regulator of the Profibrogenic Phenotype of Human Hepatic Stellate Cells. *Hepatology* **2018**, 68 (3), 1140–1153. <https://doi.org/10.1002/hep.30029>.
- (330) Kissing, S.; Hermesen, C.; Repnik, U.; Nasset, C. K.; von Bargen, K.; Griffiths, G.; Ichihara, A.; Lee, B. S.; Schwake, M.; De Brabander, J.; et al. Vacuolar ATPase in Phagosome-Lysosome Fusion. *J. Biol. Chem.* **2015**, 290 (22), 14166–14180. <https://doi.org/10.1074/jbc.M114.628891>.
- (331) Bodzęta, A.; Kahms, M.; Klingauf, J. The Presynaptic V-ATPase Reversibly Disassembles and Thereby Modulates Exocytosis but Is Not Part of the Fusion Machinery. *Cell Reports* **2017**, 20 (6), 1348–1359. <https://doi.org/10.1016/j.celrep.2017.07.040>.
- (332) Denisova, O. V.; Kakkola, L.; Feng, L.; Stenman, J.; Nagaraj, A.; Lampe, J.; Yadav, B.; Aittokallio, T.; Kaukinen, P.; Ahola, T.; et al. Obatoclax, Saliphenylhalamide, and Gemcitabine Inhibit Influenza A Virus Infection. *J. Biol. Chem.* **2012**, 287 (42), 35324–35332. <https://doi.org/10.1074/jbc.M112.392142>.
- (333) Müller, K. H.; Spoden, G. A.; Scheffer, K. D.; Brunnhöfer, R.; Brabander, J. K. D.; Maier, M. E.; Florin, L.; Muller, C. P. Inhibition by Cellular Vacuolar ATPase Impairs Human Papillomavirus Uncoating and Infection. *Antimicrob. Agents Chemother.* **2014**, 58 (5), 2905–2911. <https://doi.org/10.1128/AAC.02284-13>.
- (334) Kuivanen, S.; Beshpalov, M. M.; Nandania, J.; Ianevski, A.; Velagapudi, V.; De Brabander, J. K.; Kainov, D. E.; Vapalahti, O. Obatoclax, Saliphenylhalamide and Gemcitabine Inhibit Zika Virus Infection in Vitro and Differentially Affect Cellular Signaling, Transcription and Metabolism. *Antiviral Research* **2017**, 139, 117–128. <https://doi.org/10.1016/j.antiviral.2016.12.022>.
- (335) Söderholm, S.; Anastasina, M.; Islam, M. M.; Tynell, J.; Poranen, M. M.; Bamford, D. H.; Stenman, J.; Julkunen, I.; Šaulienė, I.; De Brabander, J. K.; et al. Immuno-Modulating Properties of Saliphenylhalamide, SNS-032, Obatoclax, and Gemcitabine. *Antiviral Research* **2016**, 126, 69–80. <https://doi.org/10.1016/j.antiviral.2015.12.011>.
- (336) Dell'Antone, P. Inactivation of H⁺-Vacuolar ATPase by the Energy Blocker 3-Bromopyruvate, a New Antitumour Agent. *Life Sci.* **2006**, 79 (21), 2049–2055. <https://doi.org/10.1016/j.lfs.2006.06.043>.
- (337) Aldrich, L. N.; Kuo, S.-Y.; Castoreno, A. B.; Goel, G.; Kuballa, P.; Rees, M. G.; Seashore-Ludlow, B. A.; Cheah, J. H.; Latorre, I. J.; Schreiber, S. L.; et al. Discovery of a Small-Molecule Probe for V-ATPase Function. *J. Am. Chem. Soc.* **2015**, 137 (16), 5563–5568. <https://doi.org/10.1021/jacs.5b02150>.
- (338) Giorgio, C. D.; Delmas, F.; Akhmedjanova, V.; Ollivier, E.; Bessonova, I.; Riad, E.; Timon-David, P. In Vitro Antileishmanial Activity of Diphyllin Isolated from *Haplophyllum Bucharicum*. *Planta Med* **2005**, 71 (04), 366–369. <https://doi.org/10.1055/s-2005-864106>.

- (339) Asano, J.; Chiba, K.; Tada, M.; Yoshii, T. Antiviral Activity of Lignans and Their Glycosides from *Justicia Procumbens*. *Phytochemistry* **1996**, *42* (3), 713–717.
- (340) Lim, S.; Grassi, J.; Akhmedjanova, V.; Debiton, E.; Balansard, G.; Beliveau, R.; Barthomeuf, C. Reversal of P-Glycoprotein-Mediated Drug Efflux by Eudesmin from *Haplophyllum Perforatum* and Cytotoxicity Pattern versus Diphyllin, Podophyllotoxin and Etoposide. *Planta Med.* **2007**, *73* (15), 1563–1567. <https://doi.org/10.1055/s-2007-993754>.
- (341) Fukamiya, N.; Lee, K.-H. Antitumor Agents, 81. Justicidin-A and Diphyllin, Two Cytotoxic Principles from *Justicia Procumbens*. *J. Nat. Prod.* **1986**, *49* (2), 348–350. <https://doi.org/10.1021/np50044a030>.
- (342) Sørensen, M. G.; Henriksen, K.; Neutzsky-Wulff, A. V.; Dziegiel, M. H.; Karsdal, M. A. Diphyllin, a Novel and Naturally Potent V-ATPase Inhibitor, Abrogates Acidification of the Osteoclastic Resorption Lacunae and Bone Resorption. *J. Bone Miner. Res.* **2007**, *22* (10), 1640–1648. <https://doi.org/10.1359/jbmr.070613>.
- (343) Shen, W.; Zou, X.; Chen, M.; Liu, P.; Shen, Y.; Huang, S.; Guo, H.; Zhang, L. Effects of Diphyllin as a Novel V-ATPase Inhibitor on Gastric Adenocarcinoma. *European Journal of Pharmacology* **2011**, *667* (1–3), 330–338. <https://doi.org/10.1016/j.ejphar.2011.05.042>.
- (344) Chen, H.; Liu, P.; Zhang, T.; Gao, Y.; Zhang, Y.; Shen, X.; Li, X.; Shen, W. Effects of Diphyllin as a Novel V-ATPase Inhibitor on TE-1 and ECA-109 Cells. *Oncol. Rep.* **2018**, *39* (3), 921–928. <https://doi.org/10.3892/or.2018.6191>.
- (345) Chen, H.-W.; Cheng, J. X.; Liu, M.-T.; King, K.; Peng, J.-Y.; Zhang, X.-Q.; Wang, C.-H.; Shrestha, S.; Schooley, R. T.; Liu, Y.-T. Inhibitory and Combinatorial Effect of Diphyllin, a v-ATPase Blocker, on Influenza Viruses. *Antiviral Research* **2013**, *99* (3), 371–382. <https://doi.org/10.1016/j.antiviral.2013.06.014>.
- (346) Hu, C.-M. J.; Chang, W.-S.; Fang, Z.-S.; Chen, Y.-T.; Wang, W.-L.; Tsai, H.-H.; Chueh, L.-L.; Takano, T.; Hohdatsu, T.; Chen, H.-W. Nanoparticulate Vacuolar ATPase Blocker Exhibits Potent Host-Targeted Antiviral Activity against Feline Coronavirus. *Scientific Reports* **2017**, *7* (1), 13043. <https://doi.org/10.1038/s41598-017-13316-0>.
- (347) Thummar, V. R.; Parasuraman, S.; Basu, D.; Raveendran, R. Evaluation of in Vivo Antitumor Activity of Cleistanthin B in Swiss Albino Mice. *Journal of Traditional and Complementary Medicine* **2016**, *6* (4), 383–388. <https://doi.org/10.1016/j.jtcme.2015.08.004>.
- (348) Meenakshi Jayaraman; Shanmugam Govindaswamy. Cleistanthin A, a Diphyllin Glycoside from *Cleistanthus Collinus*, Is Cytotoxic to PHA-stimulated (Proliferating) Human Lymphocytes. *Drug Development Research* **2001**, *51* (3), 187–190. [https://doi.org/10.1002/1098-2299\(200011\)51:3<187::AID-DDR7>3.0.CO;2-6](https://doi.org/10.1002/1098-2299(200011)51:3<187::AID-DDR7>3.0.CO;2-6).
- (349) Pan, S.; Pan, S.; Cai, H.; Cai, H.; Gu, L.; Gu, L.; Cao, S.; Cao, S. Cleistanthin A Inhibits the Invasion and Metastasis of Human Melanoma Cells by Inhibiting the Expression of Matrix Metalloproteinase-2 and -9. *Oncology Letters* **2017**, *14* (5), 6217–6223.
- (350) Zhang, Z.; Ma, J.; Zhu, L.; Zhao, Y. Synthesis and Identification of Cytotoxic Diphyllin Glycosides as Vacuolar H⁺-ATPase Inhibitors. *European Journal of Medicinal Chemistry* **2014**, *82*, 466–471. <https://doi.org/10.1016/j.ejmech.2014.06.002>.
- (351) Zhao, Y.; Zhang, R.; Lu, Y.; Ma, J.; Zhu, L. Synthesis and Bioevaluation of Heterocyclic Derivatives of Cleistanthin-A. *Bioorganic & Medicinal Chemistry* **2015**, *23* (15), 4884–4890. <https://doi.org/10.1016/j.bmc.2015.05.033>.

- (352) Zhao, Y.; Lu, Y.; Ma, J.; Zhu, L. Synthesis and Evaluation of Cleistanthin A Derivatives as Potent Vacuolar H⁺-ATPase Inhibitors. *Chem Biol Drug Des* **2015**, 86 (4), 691–696. <https://doi.org/10.1111/cbdd.12538>.
- (353) Lu, Y.; Zhang, R.; Liu, S.; Zhao, Y.; Gao, J.; Zhu, L. ZT-25, a New Vacuolar H⁺-ATPase Inhibitor, Induces Apoptosis and Protective Autophagy through ROS Generation in HepG2 Cells. *European Journal of Pharmacology* **2016**, 771, 130–138. <https://doi.org/10.1016/j.ejphar.2015.12.026>.
- (354) Ren, Y.; Lantvit, D. D.; Deng, Y.; Kanagasabai, R.; Gallucci, J. C.; Ninh, T. N.; Chai, H.-B.; Soejarto, D. D.; Fuchs, J. R.; Yalowich, J. C.; et al. Potent Cytotoxic Arylnaphthalene Lignan Lactones from *Phyllanthus Poilanei*. *J. Nat. Prod.* **2014**, 77 (6), 1494–1504. <https://doi.org/10.1021/np5002785>.
- (355) Woodard, J. L.; Huntsman, A. C.; Patel, P. A.; Chai, H.-B.; Kanagasabai, R.; Karmahapatra, S.; Young, A. N.; Ren, Y.; Cole, M. S.; Herrera, D.; et al. Synthesis and Antiproliferative Activity of Derivatives of the *Phyllanthus*min Class of Arylnaphthalene Lignan Lactones. *Bioorganic & Medicinal Chemistry* **2018**, 26 (9), 2354–2364. <https://doi.org/10.1016/j.bmc.2018.03.033>.
- (356) 2014-2016 Ebola Outbreak in West Africa | Ebola Hemorrhagic Fever | CDC <http://www.cdc.gov/vhf/ebola/outbreaks/2014-west-africa/index.html> (accessed Nov 26, 2016).
- (357) Anantpadma, M.; Kouznetsova, J.; Wang, H.; Huang, R.; Kolokoltsov, A.; Guha, R.; Lindstrom, A. R.; Shtanko, O.; Simeonov, A.; Maloney, D. J.; et al. Large Scale Screening and Identification of Novel Ebolavirus and Marburgvirus Entry Inhibitors. *Antimicrob. Agents Chemother.* **2016**, AAC.00543-16. <https://doi.org/10.1128/AAC.00543-16>.
- (358) Basu, A.; Mills, D. M.; Mitchell, D.; Ndungo, E.; Williams, J. D.; Herbert, A. S.; Dye, J. M.; Moir, D. T.; Chandran, K.; Patterson, J. L.; et al. Novel Small Molecule Entry Inhibitors of Ebola Virus. *J Infect Dis.* **2015**, 212 (suppl 2), S425–S434. <https://doi.org/10.1093/infdis/jiv223>.
- (359) van der Linden, W. A.; Schulze, C. J.; Herbert, A. S.; Krause, T. B.; Wirchnianski, A. A.; Dye, J. M.; Chandran, K.; Bogyo, M. Cysteine Cathepsin Inhibitors as Anti-Ebola Agents. *ACS Infect. Dis.* **2016**, 2 (3), 173–179. <https://doi.org/10.1021/acsinfecdis.5b00130>.
- (360) Luthra, P.; Liang, J.; Pietzsch, C. A.; Khadka, S.; Edwards, M. R.; Wei, S.; De, S.; Posner, B.; Bukreyev, A.; Ready, J. M.; et al. A High Throughput Screen Identifies Benzoquinoline Compounds as Inhibitors of Ebola Virus Replication. *Antiviral Research* **2018**, 150, 193–201. <https://doi.org/10.1016/j.antiviral.2017.12.019>.
- (361) Yates, M. K.; Raje, M. R.; Chatterjee, P.; Spiropoulou, C. F.; Bavari, S.; Flint, M.; Soloveva, V.; Seley-Radtke, K. L. Flex-Nucleoside Analogues – Novel Therapeutics against Filoviruses. *Bioorganic & Medicinal Chemistry Letters* **2017**, 27 (12), 2800–2802. <https://doi.org/10.1016/j.bmcl.2017.04.069>.
- (362) Selaković, Ž.; Soloveva, V.; Gharaibeh, D. N.; Wells, J.; Šegan, S.; Panchal, R. G.; Šolaja, B. A. Anti-Ebola Activity of Diazachrysene Small Molecules. *ACS Infect. Dis.* **2015**, 1 (6), 264–271. <https://doi.org/10.1021/acsinfecdis.5b00028>.

- (363) Bixler, S. L.; Bocan, T. M.; Wells, J.; Wetzel, K. S.; Van Tongeren, S. A.; Dong, L.; Garza, N. L.; Donnelly, G.; Cazares, L. H.; Nuss, J.; et al. Efficacy of Favipiravir (T-705) in Nonhuman Primates Infected with Ebola Virus or Marburg Virus. *Antiviral Research* **2018**, *151*, 97–104. <https://doi.org/10.1016/j.antiviral.2017.12.021>.
- (364) Salata, C.; Baritussio, A.; Munegato, D.; Calistri, A.; Ha, H. R.; Bigler, L.; Fabris, F.; Parolin, C.; Palù, G.; Mirazimi, A. Amiodarone and Metabolite MDEA Inhibit Ebola Virus Infection by Interfering with the Viral Entry Process. *Pathog Dis* **2015**, *73* (5). <https://doi.org/10.1093/femspd/ftv032>.
- (365) Madrid, P. B.; Panchal, R. G.; Warren, T. K.; Shurtleff, A. C.; Endsley, A. N.; Green, C. E.; Kolokoltsov, A.; Davey, R.; Manger, I. D.; Gilfillan, L.; et al. Evaluation of Ebola Virus Inhibitors for Drug Repurposing. *ACS Infect. Dis.* **2015**, *1* (7), 317–326. <https://doi.org/10.1021/acsinfecdis.5b00030>.
- (366) Johansen, L. M.; DeWald, L. E.; Shoemaker, C. J.; Hoffstrom, B. G.; Lear-Rooney, C. M.; Stossel, A.; Nelson, E.; Delos, S. E.; Simmons, J. A.; Grenier, J. M.; et al. A Screen of Approved Drugs and Molecular Probes Identifies Therapeutics with Anti-Ebola Virus Activity. *Science Translational Medicine* **2015**, *7* (290), 290ra89-290ra89. <https://doi.org/10.1126/scitranslmed.aaa5597>.
- (367) Kouznetsova, J.; Sun, W.; Martínez-Romero, C.; Tawa, G.; Shinn, P.; Chen, C. Z.; Schimmer, A.; Sanderson, P.; McKew, J. C.; Zheng, W.; et al. Identification of 53 Compounds That Block Ebola Virus-like Particle Entry via a Repurposing Screen of Approved Drugs. *Emerg Microbes Infect* **2014**, *3* (12), e84. <https://doi.org/10.1038/emi.2014.88>.
- (368) Johansen, L. M.; Brannan, J. M.; Delos, S. E.; Shoemaker, C. J.; Stossel, A.; Lear, C.; Hoffstrom, B. G.; DeWald, L. E.; Schornberg, K. L.; Scully, C.; et al. FDA-Approved Selective Estrogen Receptor Modulators Inhibit Ebola Virus Infection. *Science Translational Medicine* **2013**, *5* (190), 190ra79-190ra79. <https://doi.org/10.1126/scitranslmed.3005471>.
- (369) Reynolds, P.; Marzi, A. Ebola and Marburg Virus Vaccines. *Virus Genes* **2017**, 1–15. <https://doi.org/10.1007/s11262-017-1455-x>.
- (370) Mire, C. E.; Matassov, D.; Geisbert, J. B.; Latham, T. E.; Agans, K. N.; Xu, R.; Ota-Setlik, A.; Egan, M. A.; Fenton, K. A.; Clarke, D. K.; et al. Single-Dose Attenuated Vesiculovax Vaccines Protect Primates against Ebola Makona Virus. *Nature* **2015**, *520* (7549), 688–691. <https://doi.org/10.1038/nature14428>.
- (371) Wolfe, D. N.; Zarrabian, A. G.; Disbrow, G. L.; Espeland, E. M. Progress towards a Vaccine against Ebola to Meet Emergency Medical Countermeasure Needs. *Vaccine* **2017**. <https://doi.org/10.1016/j.vaccine.2017.10.111>.
- (372) Qiu, X.; Wong, G.; Audet, J.; Bello, A.; Fernando, L.; Alimonti, J. B.; Fausther-Bovendo, H.; Wei, H.; Aviles, J.; Hiatt, E.; et al. Reversion of Advanced Ebola Virus Disease in Nonhuman Primates with ZMapp. *Nature* **2014**, *514* (7520), 47–53. <https://doi.org/10.1038/nature13777>.
- (373) Warren, T. K.; Jordan, R.; Lo, M. K.; Ray, A. S.; Mackman, R. L.; Soloveva, V.; Siegel, D.; Perron, M.; Bannister, R.; Hui, H. C.; et al. Therapeutic Efficacy of the Small Molecule GS-5734 against Ebola Virus in Rhesus Monkeys. *Nature* **2016**, *531* (7594), nature17180. <https://doi.org/10.1038/nature17180>.

- (374) Sanchez, A. Analysis of Filovirus Entry into Vero E6 Cells, Using Inhibitors of Endocytosis, Endosomal Acidification, Structural Integrity, and Cathepsin (B and L) Activity. *J. Infect. Dis.* **2007**, *196 Suppl 2*, S251-258. <https://doi.org/10.1086/520597>.
- (375) Mosso, C.; Galván-Mendoza, I. J.; Ludert, J. E.; del Angel, R. M. Endocytic Pathway Followed by Dengue Virus to Infect the Mosquito Cell Line C6/36 HT. *Virology* **2008**, *378* (1), 193–199. <https://doi.org/10.1016/j.virol.2008.05.012>.
- (376) Hunt, S. R.; Hernandez, R.; Brown, D. T. Role of the Vacuolar-ATPase in Sindbis Virus Infection. *J Virol* **2011**, *85* (3), 1257–1266. <https://doi.org/10.1128/JVI.01864-10>.
- (377) Chandran, K.; Sullivan, N. J.; Felbor, U.; Whelan, S. P.; Cunningham, J. M. Endosomal Proteolysis of the Ebola Virus Glycoprotein Is Necessary for Infection. *Science* **2005**, *308* (5728), 1643–1645. <https://doi.org/10.1126/science.1110656>.
- (378) Brown, D.; Paunescu, T. G.; Breton, S.; Marshansky, V. Regulation of the V-ATPase in Kidney Epithelial Cells: Dual Role in Acid-Base Homeostasis and Vesicle Trafficking. *J. Exp. Biol.* **2009**, *212* (Pt 11), 1762–1772. <https://doi.org/10.1242/jeb.028803>.
- (379) Rahman, S.; Yamato, I.; Murata, T. Function and Regulation of Mammalian V-ATPase Isoforms. In *Regulation of Ca²⁺-ATPases, V-ATPases and F-ATPases*; Advances in Biochemistry in Health and Disease; Springer, Cham, 2016; pp 283–299. https://doi.org/10.1007/978-3-319-24780-9_15.
- (380) Fordyce, C. A.; Grimes, M. M.; Licon-Munoz, Y.; Chan, C.-Y.; Parra, K. J. Vacuolar ATPase in Physiology and Pathology: Roles in Neurobiology, Infectious Disease, and Cancer. In *Regulation of Ca²⁺-ATPases, V-ATPases and F-ATPases*; Chakraborti, S., Dhalla, N. S., Eds.; Advances in Biochemistry in Health and Disease; Springer International Publishing, 2016; pp 337–369. https://doi.org/10.1007/978-3-319-24780-9_17.
- (381) Chen, H.-W.; Cheng, J. X.; Liu, M.-T.; King, K.; Peng, J.-Y.; Zhang, X.-Q.; Wang, C.-H.; Shrestha, S.; Schooley, R. T.; Liu, Y.-T. Inhibitory and Combinatorial Effect of Diphyllin, a v-ATPase Blocker, on Influenza Viruses. *Antiviral Research* **2013**, *99* (3), 371–382. <https://doi.org/10.1016/j.antiviral.2013.06.014>.
- (382) Rivera, A.; Messaoudi, I. Molecular Mechanisms of Ebola Pathogenesis. *J Leukoc Biol* **2016**, *100* (5), 889–904. <https://doi.org/10.1189/jlb.4RI0316-099RR>.
- (383) Aldrich, L. N.; Kuo, S.-Y.; Castoreno, A. B.; Goel, G.; Kuballa, P.; Rees, M. G.; Seashore-Ludlow, B. A.; Cheah, J. H.; Latorre, I. J.; Schreiber, S. L.; et al. Discovery of a Small-Molecule Probe for V-ATPase Function. *J. Am. Chem. Soc.* **2015**, *137* (16), 5563–5568. <https://doi.org/10.1021/jacs.5b02150>.
- (384) Zoncu, R.; Bar-Peled, L.; Efeyan, A.; Wang, S.; Sancak, Y.; Sabatini, D. M. MTORC1 Senses Lysosomal Amino Acids Through an Inside-Out Mechanism That Requires the Vacuolar H⁺-ATPase. *Science* **2011**, *334* (6056), 678–683. <https://doi.org/10.1126/science.1207056>.
- (385) Charlton, J. L. Antiviral Activity of Lignans. *J. Nat. Prod.* **1998**, *61* (11), 1447–1451. <https://doi.org/10.1021/np980136z>.
- (386) Daina, A.; Michielin, O.; Zoete, V. SwissADME: A Free Web Tool to Evaluate Pharmacokinetics, Drug-Likeness and Medicinal Chemistry Friendliness of Small Molecules. *Scientific Reports* **2017**, *7*, srep42717. <https://doi.org/10.1038/srep42717>.
- (387) Palmgren, M. G. Acridine Orange as a Probe for Measuring PH Gradients across Membranes: Mechanism and Limitations. *Analytical Biochemistry* **1991**, *192* (2), 316–321. [https://doi.org/10.1016/0003-2697\(91\)90542-2](https://doi.org/10.1016/0003-2697(91)90542-2).

- (388) Elshabrawy, H. A.; Fan, J.; Haddad, C. S.; Ratia, K.; Broder, C. C.; Caffrey, M.; Prabhakar, B. S. Identification of a Broad-Spectrum Antiviral Small Molecule against Severe Acute Respiratory Syndrome Coronavirus and Ebola, Hendra, and Nipah Viruses by Using a Novel High-Throughput Screening Assay. *J Virol* **2014**, *88* (8), 4353–4365. <https://doi.org/10.1128/JVI.03050-13>.
- (389) Basu, A.; Li, B.; Mills, D. M.; Panchal, R. G.; Cardinale, S. C.; Butler, M. M.; Peet, N. P.; Majgier-Baranowska, H.; Williams, J. D.; Patel, I.; et al. Identification of a Small-Molecule Entry Inhibitor for Filoviruses. *J. Virol.* **2011**, *85* (7), 3106–3119. <https://doi.org/10.1128/JVI.01456-10>.
- (390) Ruiz-Jarabo, C. M.; Arias, A.; Baranowski, E.; Escarmís, C.; Domingo, E. Memory in Viral Quasispecies. *Journal of Virology* **2000**, *74* (8), 3543–3547. <https://doi.org/10.1128/JVI.74.8.3543-3547.2000>.
- (391) Sanjuán, R.; Nebot, M. R.; Chirico, N.; Mansky, L. M.; Belshaw, R. Viral Mutation Rates. *J. Virol.* **2010**, *84* (19), 9733–9748. <https://doi.org/10.1128/JVI.00694-10>.
- (392) Vignuzzi, M.; Andino, R. Closing the Gap: The Challenges in Converging Theoretical, Computational, Experimental and Real-Life Studies in Virus Evolution. *Curr Opin Virol* **2012**, *2* (5), 515–518. <https://doi.org/10.1016/j.coviro.2012.09.008>.
- (393) Miura, M.; Maekawa, S.; Sato, M.; Komatsu, N.; Tatsumi, A.; Takano, S.; Amemiya, F.; Nakayama, Y.; Inoue, T.; Sakamoto, M.; et al. Deep Sequencing Analysis of Variants Resistant to the Non-Structural 5A Inhibitor Daclatasvir in Patients with Genotype 1b Hepatitis C Virus Infection. *Hepatol. Res.* **2014**, *44* (14), E360-367. <https://doi.org/10.1111/hepr.12316>.
- (394) Charpentier, C.; Dwyer, D. E.; Mammano, F.; Lecossier, D.; Clavel, F.; Hance, A. J. Role of Minority Populations of Human Immunodeficiency Virus Type 1 in the Evolution of Viral Resistance to Protease Inhibitors. *Journal of Virology* **2004**, *78* (8), 4234–4247. <https://doi.org/10.1128/JVI.78.8.4234-4247.2004>.
- (395) Hussain, M.; Galvin, H. D.; Haw, T. Y.; Nutsford, A. N.; Husain, M. Drug Resistance in Influenza A Virus: The Epidemiology and Management. *Infect Drug Resist* **2017**, *10*, 121–134. <https://doi.org/10.2147/IDR.S105473>.
- (396) Webster, R. G.; Govorkova, E. A. Continuing Challenges in Influenza. *Ann. N. Y. Acad. Sci.* **2014**, *1323*, 115–139. <https://doi.org/10.1111/nyas.12462>.
- (397) Stouffer, A. L.; Acharya, R.; Salom, D.; Levine, A. S.; Di Costanzo, L.; Soto, C. S.; Tereshko, V.; Nanda, V.; Stayrook, S.; DeGrado, W. F. Structural Basis for the Function and Inhibition of an Influenza Virus Proton Channel. *Nature* **2008**, *451* (7178), 596–599. <https://doi.org/10.1038/nature06528>.
- (398) Heider, H.; Adamczyk, B.; Presber, H. W.; Schroeder, C.; Feldblum, R.; Indulen, M. K. Occurrence of Amantadine- and Rimantadine-Resistant Influenza A Virus Strains during the 1980 Epidemic. *Acta Virol.* **1981**, *25* (6), 395–400.
- (399) Dong, G.; Peng, C.; Luo, J.; Wang, C.; Han, L.; Wu, B.; Ji, G.; He, H. Adamantane-Resistant Influenza A Viruses in the World (1902-2013): Frequency and Distribution of M2 Gene Mutations. *PLoS ONE* **2015**, *10* (3), e0119115. <https://doi.org/10.1371/journal.pone.0119115>.
- (400) Pielak, R. M.; Schnell, J. R.; Chou, J. J. Mechanism of Drug Inhibition and Drug Resistance of Influenza A M2 Channel. *Proc. Natl. Acad. Sci. U.S.A.* **2009**, *106* (18), 7379–7384. <https://doi.org/10.1073/pnas.0902548106>.

- (401) Iyidogan, P.; Anderson, K. S. Current Perspectives on HIV-1 Antiretroviral Drug Resistance. *Viruses* **2014**, *6* (10), 4095–4139. <https://doi.org/10.3390/v6104095>.
- (402) Matthew, A. N.; Leidner, F.; Newton, A.; Petropoulos, C. J.; Huang, W.; Ali, A.; KurtYilmaz, N.; Schiffer, C. A. Molecular Mechanism of Resistance in a Clinically Significant Double-Mutant Variant of HCV NS3/4A Protease. *Structure* **2018**. <https://doi.org/10.1016/j.str.2018.07.004>.
- (403) López-Labrador, F. X.; Berenguer, M.; Navarro, D. Overcoming Drug Resistance in HSV, CMV, HBV and HCV Infection. *Future Microbiol* **2015**, *10* (11), 1759–1766. <https://doi.org/10.2217/fmb.15.74>.
- (404) Kinashi, H.; Someno, K.; Sakaguchi, K. Isolation and Characterization of Concanamycins A, B and C. *J. Antibiot.* **1984**, *37* (11), 1333–1343.
- (405) Hu, C.-M. J.; Chang, W.-S.; Fang, Z.-S.; Chen, Y.-T.; Wang, W.-L.; Tsai, H.-H.; Chueh, L.-L.; Takano, T.; Hohdatsu, T.; Chen, H.-W. Nanoparticulate Vacuolar ATPase Blocker Exhibits Potent Host-Targeted Antiviral Activity against Feline Coronavirus. *Sci Rep* **2017**, *7*. <https://doi.org/10.1038/s41598-017-13316-0>.
- (406) Nath, A. K.; Roberts, L. D.; Liu, Y.; Mahon, S. B.; Kim, S.; Ryu, J. H.; Werdich, A.; Januzzi, J. L.; Boss, G. R.; Rockwood, G. A.; et al. Chemical and Metabolomic Screens Identify Novel Biomarkers and Antidotes for Cyanide Exposure. *FASEB J.* **2013**, *27* (5), 1928–1938. <https://doi.org/10.1096/fj.12-225037>.
- (407) Borzilleri, R. M.; Zheng, X.; Schmidt, R. J.; Johnson, J. A.; Kim, S.-H.; DiMarco, J. D.; Fairchild, C. R.; Gougoutas, J. Z.; Lee, F. Y. F.; Long, B. H.; et al. A Novel Application of a Pd(0)-Catalyzed Nucleophilic Substitution Reaction to the Regio- and Stereoselective Synthesis of Lactam Analogues of the Epothilone Natural Products. *J. Am. Chem. Soc.* **2000**, *122* (37), 8890–8897. <https://doi.org/10.1021/ja001899n>.
- (408) Stachel, S. J.; Lee, C. B.; Spassova, M.; Chappell, M. D.; Bornmann, W. G.; Danishefsky, S. J.; Chou, T.-C.; Guan, Y. On the Interactivity of Complex Synthesis and Tumor Pharmacology in the Drug Discovery Process: Total Synthesis and Comparative in Vivo Evaluations of the 15-Aza Epothilones. *J. Org. Chem.* **2001**, *66* (12), 4369–4378. <https://doi.org/10.1021/jo010275c>.
- (409) Gardner, R. A.; Delcros, J.-G.; Konate, F.; Breitbeil, F.; Martin, B.; Sigman, M.; Huang, M.; Phanstiel. N-Substituent Effects in the Selective Delivery of Polyamine Conjugates into Cells Containing Active Polyamine Transporters. *J. Med. Chem.* **2004**, *47* (24), 6055–6069. <https://doi.org/10.1021/jm0497040>.
- (410) Iv, O. P.; Kaur, N.; Delcros, J.-G. Structure-Activity Investigations of Polyamine-Anthracene Conjugates and Their Uptake via the Polyamine Transporter. *Amino Acids* **2007**, *33* (2), 305–313. <https://doi.org/10.1007/s00726-007-0527-y>.
- (411) Nowotarski, S. L.; Woster, P. M.; Casero, R. A. Polyamines and Cancer: Implications for Chemoprevention and Chemotherapy. *Expert Rev Mol Med* **2013**, *15*, e3. <https://doi.org/10.1017/erm.2013.3>.
- (412) Barret, J.-M.; Kruczynski, A.; Vispé, S.; Annereau, J.-P.; Brel, V.; Guminski, Y.; Delcros, J.-G.; Lansiaux, A.; Guilbaud, N.; Imbert, T.; et al. F14512, a Potent Antitumor Agent Targeting Topoisomerase II Vectored into Cancer Cells via the Polyamine Transport System. *Cancer Res* **2008**, *68* (23), 9845–9853. <https://doi.org/10.1158/0008-5472.CAN-08-2748>.

- (413) Yeo, H.; Li, Y.; Fu, L.; Zhu, J.-L.; Gullen, E. A.; Dutschman, G. E.; Lee, Y.; Chung, R.; Huang, E.-S.; Austin, D. J.; et al. Synthesis and Antiviral Activity of Helioxanthin Analogues. *J. Med. Chem.* **2005**, *48* (2), 534–546. <https://doi.org/10.1021/jm034265a>.
- (414) Charlton, J. L.; Oleschuk, C. J.; Chee, G.-L. Hindered Rotation in Arylnaphthalene Lignans. *J. Org. Chem.* **1996**, *61* (10), 3452–3457. <https://doi.org/10.1021/jo952048e>.
- (415) Zhao, Y.; Hui, J.; Zhu, L. Synthesis and Bioevaluation of Novel Arylnaphthalene Lignans as Anticancer Agents. *Med Chem Res* **2012**, *22* (5), 2505–2510. <https://doi.org/10.1007/s00044-012-0245-1>.
- (416) Naresh, G.; Kant, R.; Narender, T. Silver(I)-Catalyzed Regioselective Construction of Highly Substituted α -Naphthols and Its Application toward Expedient Synthesis of Lignan Natural Products. *Org. Lett.* **2015**, *17* (14), 3446–3449. <https://doi.org/10.1021/acs.orglett.5b01477>.
- (417) Kim, T.; Jeong, K. H.; Kang, K. S.; Nakata, M.; Ham, J. An Optimized and General Synthetic Strategy To Prepare Arylnaphthalene Lactone Natural Products from Cyanophthalides. *Eur. J. Org. Chem.* **2017**, *2017* (13), 1704–1712. <https://doi.org/10.1002/ejoc.201601611>.
- (418) Vasilyeva, E.; Liu, Q.; MacLeod, K. J.; Baleja, J. D.; Forgac, M. Cysteine Scanning Mutagenesis of the Noncatalytic Nucleotide Binding Site of the Yeast V-ATPase. *J. Biol. Chem.* **2000**, *275* (1), 255–260. <https://doi.org/10.1074/jbc.275.1.255>.
- (419) Benjamin, C. J.; Wright, K. J.; Hyun, S.-H.; Krynski, K.; Yu, G.; Bajaj, R.; Guo, F.; Stauffacher, C. V.; Jiang, W.; Thompson, D. H. Nonfouling NTA-PEG-Based TEM Grid Coatings for Selective Capture of Histidine-Tagged Protein Targets from Cell Lysates. *Langmuir* **2016**, *32* (2), 551–559. <https://doi.org/10.1021/acs.langmuir.5b03445>.
- (420) Stransky, L.; Cotter, K.; Forgac, M. The Function of V-ATPases in Cancer. *Physiol. Rev.* **2016**, *96* (3), 1071–1091. <https://doi.org/10.1152/physrev.00035.2015>.
- (421) Hamm, R.; Sugimoto, Y.; Steinmetz, H.; Efferth, T. Resistance Mechanisms of Cancer Cells to the Novel Vacuolar H(+)-ATPase Inhibitor Archazolid B. *Invest New Drugs* **2014**, *32* (5), 893–903. <https://doi.org/10.1007/s10637-014-0134-1>.
- (422) Holliday, L. S. Vacuolar H⁺-ATPases (V-ATPases) as Therapeutic Targets: A Brief Review and Recent Developments. *Biotarget* **2017**, *1* (8).
- (423) Forrester, N. L.; Wertheim, J. O.; Dugan, V. G.; Auguste, A. J.; Lin, D.; Adams, A. P.; Chen, R.; Gorchakov, R.; Leal, G.; Estrada-Franco, J. G.; et al. Evolution and Spread of Venezuelan Equine Encephalitis Complex Alphavirus in the Americas. *PLOS Neglected Tropical Diseases* **2017**, *11* (8), e0005693. <https://doi.org/10.1371/journal.pntd.0005693>.
- (424) Colacurcio, D. J.; Nixon, R. A. Disorders of Lysosomal Acidification-The Emerging Role of v-ATPase in Aging and Neurodegenerative Disease. *Ageing Res. Rev.* **2016**, *32*, 75–88. <https://doi.org/10.1016/j.arr.2016.05.004>.

VITA

Aaron Raymond Lindstrom was born to parent Jeff and Mavis on December 6th, 1990 in Minneapolis Minnesota. He attended Andover Elementary School and Oakview Middle School before entering Andover High School in 2005. Upon graduation from high school in 2009, Aaron attended the University of Nebraska-Lincoln and earned Bachelor of Science degrees in Chemistry and Biochemistry with minors in Math and History. During his undergraduate studies, Aaron studied the use of electrochemically plated metals on a carbon substrate as a novel supercapacitor design under the tutelage of Dr. Jody Redepenning. Following his graduation from the University of Nebraska-Lincoln in May of 2013, Aaron joined the Department of Medicinal Chemistry and Molecular Pharmacology at Purdue University. He joined the lab of Dr. Douglas LaCount in December of the same year studying interactions between host proteins and the NS5 proteins of West Nile Virus and Japanese Encephalitis Virus. In the spring of 2015, Aaron joined Dr. Vincent Jo Davisson's lab and began work on studying the role of Vacuolar-ATPase during Ebolavirus infection. From fall 2014 to spring 2018, he worked as a teaching assistant in MCMP 204/205 organic laboratory courses and was the head teaching assistant from fall 2015 until spring 2018. Aaron completed his graduate studies in October 2018 and graduated with his Ph.D. in December of that year.